SSCG METHODS OF EMI EMISSIONS REDUCTION APPLIED TO SWITCHING POWER CONVERTERS

A thesis presented by

José Alfonso Santolaria Lorenzo

to

The Department of Electronics Engineering

in partial fulfillment of the requirements for the degree of Doctor of Philosophy in the subject of

Electronic Engineering

This thesis was directed by

Ph.D. Josep Balcells i Sendra

UNIVERSITAT POLITÈCNICA DE CATALUNYA

June, 2004

ACKNOWLEDGEMENTS

Every task in our life is the sum of our own effort and the help and support of people around us. I'm sure both things share the same weight in the final result. For this reason, it's a pleasure for me to express my gratitude to all people without whom, I couldn't have finished successfully one of the most important periods of my life:

To my family, my wonderful family: my father José, my mother Concha, my sister MariCarmen, my brother-in-law Antonio and my niece María. There are no enough words to express my gratitude for the whole support received during all these years, but nothing would have been possible without them. Thanks again.

I must extend both my thanks and admiration to my thesis director, Josep Balcells. He was the wise sailor who knew to fix the navigation course in those moments of storm to, finally, reach a successful port.

I'm particularly grateful to David González and Javier Gago for the time dedicated to read my papers and the thesis itself and give me their valuable comments.

Lastly my thanks go to David Saltiveri for helping me with PSPICE simulations and the construction of the hardware prototype. He is the kind of people who only need few words to understand what you want, what is very worthy when you don't have time.

If I forget mentioning any persons who also gave me their help and support, from here, I express my excuses and I hope they don't take this mistake into consideration.

Thanks.

June, 2004 A.D.

INDEX OF CONTENTS

ANNEXES:

CHAPTER

1

INTRODUCTION

1. INTRODUCTION

1.1 Objectives of this thesis

Spread Spectrum Clock Generation (SSCG) techniques have been studied and implemented in digital systems ([RA-2] to [RA-6]), where a clock signal is normally one of the main sources of EMI emissions. Clock-related signals (port lines, serial communications and so on) are also an indirect way of emission of EMI. Although the presence of SSCG-techniques in digital systems is not a strange situation in some specific commercial applications, it is nearly unknown in the world of switching power converters. The main objective of this thesis deals with the worthy possibility of implementing such techniques in switching power converters in order to reduce EMI emissions due to the PWM signal controlling these converters.

Besides, it is very difficult to find bibliography directly related to SSCG and, when found, terms nearer to "feeling", "approximately", "rule of thumb" than to mathematical expressions are the commonest. It would be worthy to have these SSCG-techniques analytically expressed and systematized: this is another important objective of this thesis.

Finally, SSCG-techniques offer the capability of moving the modulation spectrum as desired (of course, with certain limitations); this fact can be profitable in order to avoid undesired interferences with other systems and will be studied in this thesis.

1.2 Motivation

Many methods for EMI suppression have been developed in the last fifty years, most of them, showing a hardly change in its implementation.

Traditional tools for EMI suppression are related to the use of filters, shielding techniques and new methods for layout improvement. A complete set or rules have been growing around these techniques just to take most profit of them when trying to reduce EMI emissions:

- Frequency and bandwidth of both signals used in a unit and their harmonics must be limited to the absolutely necessary minimum.
- Frequencies and their harmonics should differ from those reserved frequencies, normally, related to radio signals at their different bands: 455 kHz, 4.1 MHz, 4.6 MHz, 5.0 MHz, 5.5 MHz, 9.8 MHz, 10 MHz, 10.7 MHz, 21.4 MHz, 45 MHz and others.
- Frequencies and their harmonics used in different areas of the same circuit should be different to prevent interference interactions of several signals.
- Because of the narrow-band characteristics of suppressor components, frequency difference should be kept as small as possible in order to use the same filter for as many noise frequencies as possible. Anyway, frequency difference should be more than 0.2% of the related nominal frequencies to avoid several simultaneous disturbing frequencies from interfering with the same external device tuned to this frequency.

These hardware techniques are normally supported with waveform shapes having themselves a lower spectral content. Instead of using a "perfect square" waveform for transmission purposes, this having a significant spectral content at high frequencies, new procedures and standards started to propose finite rising and falling times for the signal flanks in order to obtain a reduction of high-frequency harmonics in the total spectral content of the signal. Figures 1-1 and 1-3 show a square and trapezoidal waveforms, respectively, the second one representing the evolution of the classical square signals just giving values higher than zero for rising and falling times, that is, $\tau_R > 0$ (risetime) and $\tau_F > 0$ (falltime). These two values are defined as the time required for the signal to transition from 0 to A, that is, from the 0% to the 100 % of the amplitude. Because actual pulses do not vary so sharply, it is common in industry to define the rise- and falltimes as being from 10% to 90% of the amplitude.

The spectral contents of both square and trapezoidal waveforms are shown in Figures 1-2 and 1-4, respectively. Both signals have the same characteristics except for the rising and falling times. A conventional Fourier analysis demonstrates that the spectral content of square waveforms at higher harmonic order is greater than for trapezoidal signals.

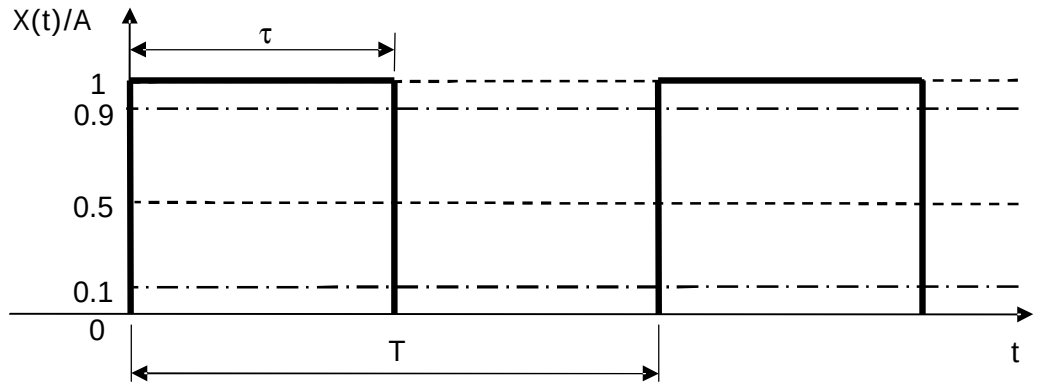

Figure 1-1. A periodic, square waveform

The corresponding Fourier analysis for a periodic, square waveform in the time domain yields a spectral content in the frequency domain expressed as follows [RD-3] (only harmonic amplitude c_h):

$$\left|c_h\right| = 2 \cdot \frac{A \cdot \tau}{T} \cdot \left| \frac{\sin\left(h \cdot \pi \cdot f_0 \cdot \tau\right)}{h \cdot \pi \cdot f_0 \cdot \tau} \right| \qquad (1\text{-}1)$$

where:

- h is the harmonic order where "0" represent the dc component.
- $f_0 = \frac{1}{T}$ is the frequency of the signal.

Amplitudes of the spectral components lie on an envelope as expressed in (1-2):

$$envelope = 2 \cdot \frac{A \cdot \tau}{T} \cdot \left| \frac{\sin\left(\pi \cdot \tau / T\right)}{\pi \cdot \tau / T} \right| \qquad (1\text{-}2)$$

Expression (1-2) goes to zero when $\pi \cdot \tau / T = m \cdot \pi$ or at multiples of $\frac{1}{\tau}$. Moreover, expression (1-2) can be easily represented taking into account that:

$$\left| \frac{\sin(x)}{x} \right| \leq \begin{cases} 1 & (\text{small } x) \\ \frac{1}{|x|} & (\text{large } x) \end{cases} \qquad (1\text{-}3)$$

This can be drawn in a logarithmic plot (Figure 1-2) as two straight lines, the first one, 0 dB/decade corresponding to small values of x and the second one, representing an asymptote decreasing linearly with x, that is, -20 dB/decade. A similar development

applied to the trapezoidal waveform in Figure 1-3 results in the spectral content envelope shown in Figure 1-4.

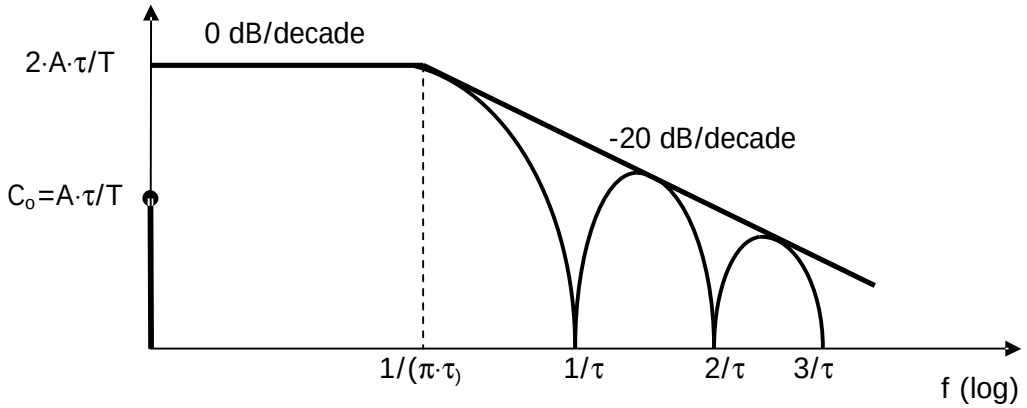

Figure 1-2. Spectral content of a periodic, square signal and the corresponding bounds

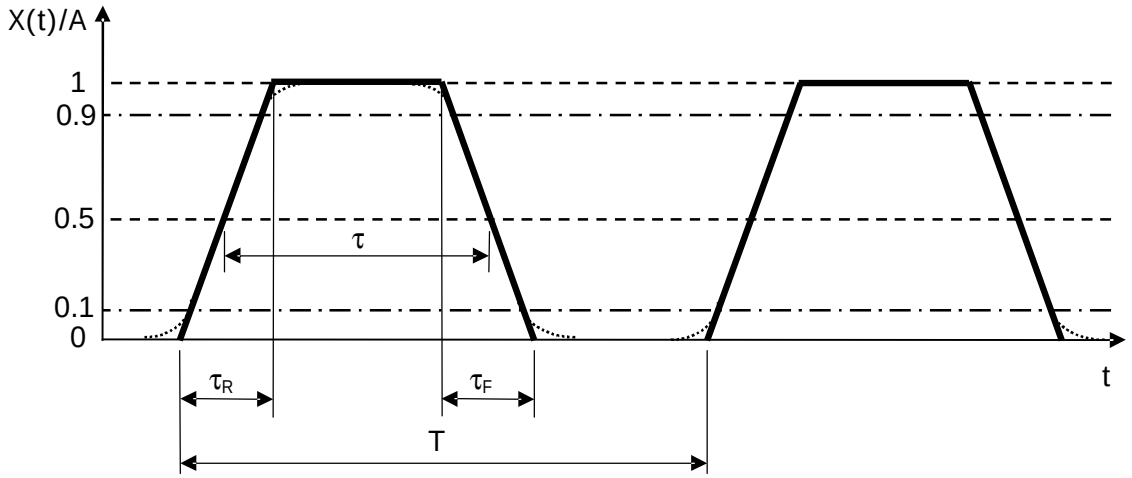

Figure 1-3. A periodic, trapezoidal waveform

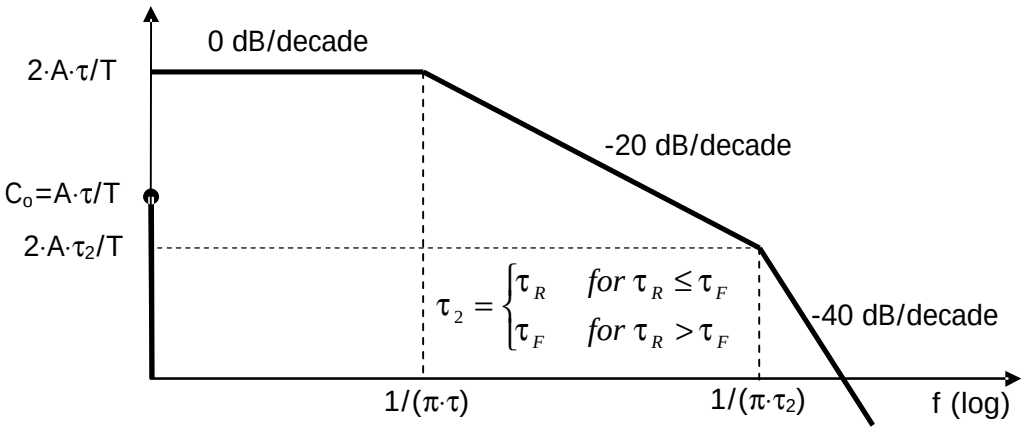

Figure 1-4. Bounds of the spectral content of a periodic, trapezoidal signal

From these spectral bounds it now becomes clear that the high-frequency content of a trapezoidal pulse train is primarily due to the rise/falltime of the pulse. Pulses having small rise/falltimes will have larger high-frequency spectral content than those having larger rise/falltimes. Thus, in order to reduce the high-frequency spectrum and, consequently, the emissions of a product, the rise/falltimes of the clock, data pulses or switching waveform should be increased as much as possible [RD-3].

This kind of signals makes part of a different concept of EMI suppression that consists of limiting the spectral content in the signal itself. When possible, just waveforms with a lower spectral content should be used, this way making easier, simpler and cheaper the use of filters and other suppression means, as explained above.

In this line, EMI-reduction techniques such a Spread Spectrum Clock Generation (SSCG) are contributing to eliminate or limit the problem at the root, that is, at the signal itself.

1.3 State of Art

It was only in the past decade when this new technique appeared. Instead of maintaining a constant frequency, SSCG systems modulate the clock frequency following certain modulation profiles, thereby spreading the harmonic energy into an amount of side-band harmonics having the same energy but smaller amplitude ([RB-1] and [RB-2]), which normally corresponds to spreading conducted and radiated energy over a wider frequency range.

At any frequency, the detected emissions are lower. To its proponents, SSCG held the promise of EMI suppression by way of a clock replacement.

The history of SSCG is quite interesting. It is normally accepted that the parents of these modulation techniques are George Antheil and the actress Hedy Lamarr. With the help of an electrical engineering professor from the California Institute of Technology they worked in order to become the idea in a patent, which was finally granted on August 11th, 1942. The patent disclosed a method of frequency hopping used to immunize radio-controlled torpedoes against jamming. In the last two decades, the technique has become a mainstay of the communications revolutions because of its advantages in range, immunity and security.

The first published work (or, at least, it is normally said to be the first one) on the use of Spread Spectrum Clock Generation applied to reduce EMI emissions in power converters was a paper presented at the Virginia Power Electronics Center, Tenth Annual Power Electronics Seminar in 1992 [RA-1]. The intention of the author was to present how a modulation of the initially constant switching frequency controlling a switching power supply contributed to a significant reduction of EMI emissions. In this paper, author Lin presents a forward converter circuit and the related PWM controller based on the Unitrode circuit UC3823. With an ingenious modification of the frequency control of this UC3823 in order to inject not a constant but a variable frequency, it generates a variable-frequency PWM, not affecting the duty cycle of this PWM. The experimental verification was tested at a power supply's nominal switching frequency of 90 kHz by following a sinusoidal modulation profile generating a frequency peak deviation lower than 10 kHz and an adjustable modulating frequency. Anyway, some results are also shown at frequency peak deviation of 15 kHz and modulating frequency of 400 Hz showing a substantial reduction in emissions.

At the 1994 IEEE International Symposium on Electromagnetic Compatibility, authors Keith B. Hardin, John T. Fessler and Donald R. Bush presented the results of their work [RA-2]. As a difference with the previous paper [RA-1], the application field was related to the higher frequencies world of CPU clocks in digital devices, thus giving the fundamental jump into the area where it shows currently the biggest development. The wide modulation frequency proposed by Lin was impractical for use as a clock generator. The authors proposed to vary the frequency of the clock only slightly, deviating a 20 MHz clock by a frequency peak deviation of 125 kHz (that is, ± 125 kHz from the nominal frequency of 20 MHz), thus resulting in a variation of only 0.625% instead of the 16.67% used by Lin. It must be kept in mind that SSCG applied to power converters and CPU clocks have different exigencies. Anyway, this technique resulted in a measured attenuation of the third harmonic, 60 MHz, of only 2 dB. However, as the harmonic number increased so did the attenuation. At the 20^{th} harmonic, 400 MHz, the measured attenuation was 10 dB.

Lexmark International (formerly IBM's Office Products Division) performed this research. Early on, it was observed that the sinusoidal waveform used by Lin to frequency modulate the clock in his power supply did not produce optimal EMI suppression. As shown in Figure 1-5, modulation of a sinusoidal carrier by following a

sinusoidal modulating profile (Figure 1-5(a)) generates a spectrum which tends to concentrate side-band harmonics around the two frequencies defining the bandwidth generated during the frequency modulation process, that is, a spectrum peaked at its extremities (Figure 1-5(b)). The reason for this effect has to do with the rate of change, or derivative, of the sine wave. Its rate of change slows as the sine wave reaches its peak values. That happens at the ends of the spectra in Figure 1-5(b) and it is there that the oscillator "hangs out" a little longer than it does elsewhere. Better results were achieved when a triangular wave was used to modulate the clock [Figures 1-5(c) and 1-5(d)]. But the engineers at Lexmark found that an optimal waveform was that shown in Figure 1-5(e) which produced a nearly flat spectra across the deviated range, results presented in [RA-2]. The waveform of Figure 1-5(e) has become known as the "Lexmark Shape". Lexmark filed for, and received a patent on optimal waveforms for use in producing a spread spectrum clock generator like that used in the SC501AXB integrated circuit [RA-2].

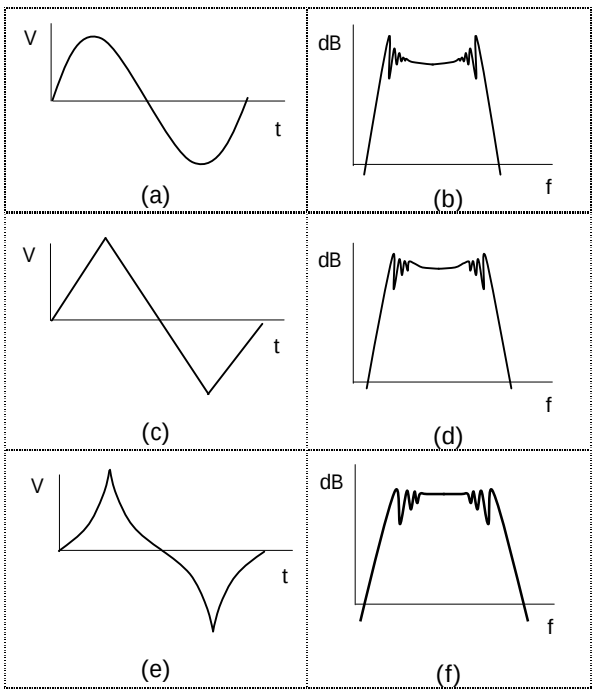

Figure 1-5. Different modulation profiles (left) produce different frequency spreading effects (right)

Anyway, some points in [RA-2] are to be reconsidered in order to clarify some dark aspects in this paper mainly related to the shape of the generated spectrum after modulation depending on the modulation profile. A quantification of the spectrum resulting from the modulation is also given further in the thesis.

It is known this paper [RA-2] was greeted with a mixture of accolades and unusually harsh criticism but no one questioned the effect was real. Emissions detected by an EMI receiver used in accordance with CISPR Publications 16 and 22 ([RE-1], [RE-2] and [RE-3]) would be significantly less at the higher harmonics when SSCG was used in place of a traditional clock. However, some engineers claimed that the technique did not really reduce emissions, but simply "fooled" the quasi-peak detector in the EMI receiver. That criticism, however, was unfair. A close (narrow band) look at the spectra produced by a SSCG will reveal individual harmonics at the modulating clock frequency, usually chosen to be between 20 and 100 kHz. Each one of the harmonics is stationary and, therefore, will measure the same whether measured on a peak, average or a quasi peak detector. The reason that emissions fall is that only a few of these modulations products fall within the bandpass filter of the receiver (120 kHz) at the higher harmonics.

Others argued that spreading the energy does not reduce it, and that receivers which were sensitive to the total energy emitted by a digital device would not see any improvement in their immunity due to the use of spread spectrum clock generators. Also, receivers using bandwidths wider than 120 kHz, such as TV receivers, could be adversely affected. The FCC rules intended to protect a wide variety of devices but fixing a 120 kHz measuring bandwidth might be an inappropriate way to measure the interference potential of devices employing this new technology.

The current FCC rules, and the voluntary standards upon which they are based, specify receiver bandwidths and detectors that were developed decades ago. Anyway, the FCC, which has already reviewed this issue once, does not see an interference threat from SSCGs as currently implemented.

In addition, Hardin, Fessler and Bush reported on a detailed Philips Consumer Electronics study on the effects of the use of spread spectrum clock generation in place of fixed frequency clock on television reception ([RA-3] and [RA-11]). They concluded that most televisions are, more or less, indifferent to the interference caused by either a narrow band or a spread spectrum generated clock, both set to the FCC Class B limits and centered on the same frequency. To avoid interference, the authors did point out that the modulation frequency used should be greater than 20 kHz in order to be beyond the audible range of the human ear. Use of a modulating frequency above 20 kHz helps to ensure that any signals working their way through to the audio

system are at frequencies high enough to be filtered out by the receiver, speaker or to be undetectable by the human ear.

No timing considerations have been made until now. Certain applications simply cannot tolerate a wandering clock. Video displays, for example, may shiver noticeably unless the horizontal sweep is synchronized with the SSCG. Many forms of communications require a synchronous clock in line with tight specifications. According to [RD-4], the technique should not be used for timing on Ethernet, Fiber Channel, FDDI, ATM, SONET or ADSL applications. Unless the clock is highly stable, these applications can suffer from poor locking, failure to lock or data errors.

In order to evaluate the suitability of a spread spectrum generated clock, at least three timing specifications should be reviewed (see Figure 1-6):

- peak-to-peak jitter (ΔT_c)
- cycle-to-cycle jitter
- setup/hold times

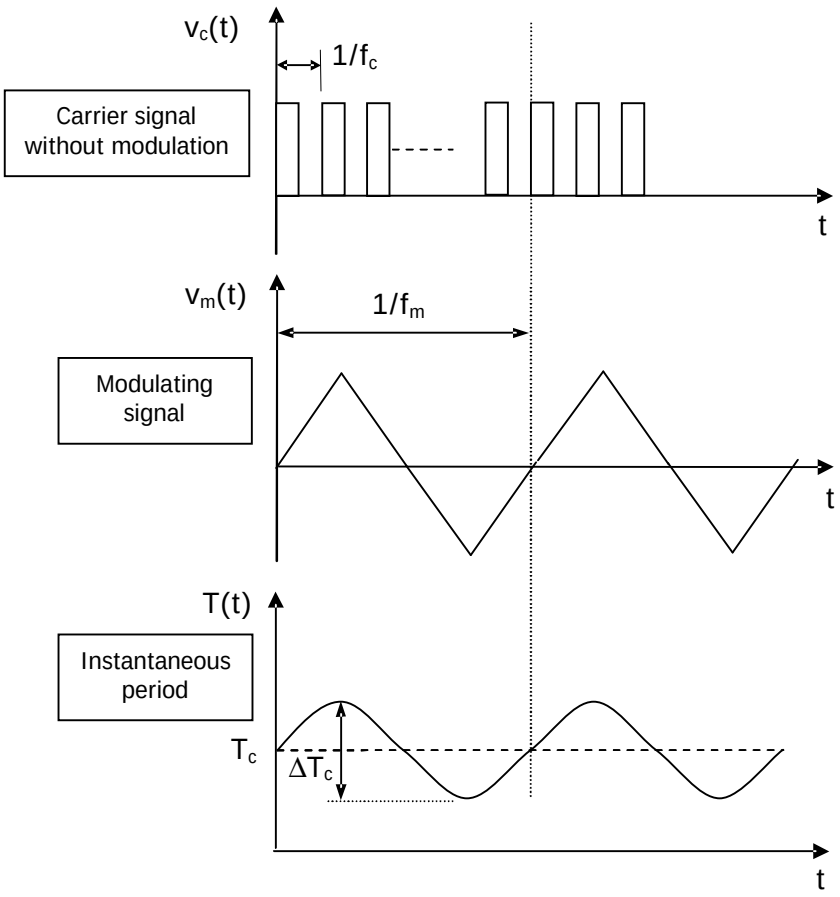

Figure 1-6. Timing specifications of a modulation process: peak-to-peak and cycle-to-cycle jitters

Peak-to-peak jitter ΔT_c is defined as the total percentage of spreading divided by the center frequency f_c and is usually specified in nanoseconds. For example, a f_c=50 MHz (T_c=20ns) clock undergoing a spread of ± 0.625% would produce a peak-to-peak variation of ΔT_c=0.25 nanoseconds (20 ns · 0.625% · 2). Cycle-to-cycle jitter is the amount of variation in picoseconds per cycle and depends on the waveform and frequency used for modulation. It can be calculated as $2 \cdot \frac{T_c \cdot \Delta T_c}{T_m}$. For example in Figure 1-6, where a triangular modulating signal (f_m=50 kHz, T_m=20 µs) is used, the cycle-to-cycle jitter would be calculated as follows. The +0.625% or -0.625% frequency change would occur over half cycle of the triangular waveform, that is, $\frac{1}{2 \cdot f_m}$ =10 µs. But 10 µs corresponds to 500 cycles of the 50 MHz clock. Since the peak-to-peak jitter ΔT_c was 0.25 ns, the cycle-to-cycle variation is $\frac{0.25 ns}{500}$ = 0.5 ps.

In most applications, neither the peak-to-peak jitter nor the cycle-to-cycle jitter of a SSCG is of significant concern. That is not true, however, for set up and hold times illustrated in Figure 1-7. As the frequency is increased, set up and hold margins decrease. Some designs use such tight set up and hold margins that any frequency increase cannot be tolerated.

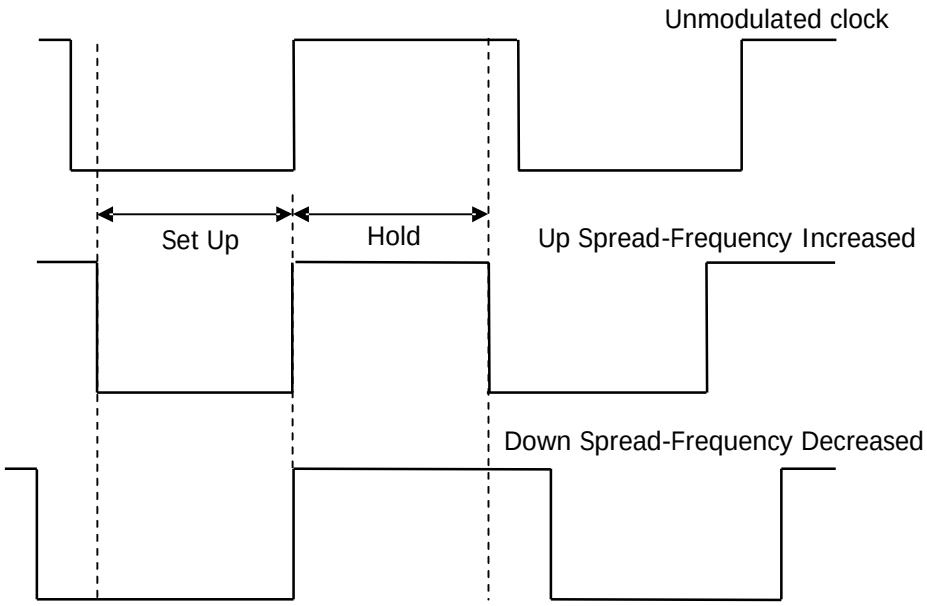

Figure 1-7. Set up and hold times must be considered when the clock speed is to be changed

For this reason, spread spectrum clock generation is sometimes implemented using a "down spreading" only technique. Instead of shifting the clock frequency above or below around the narrow band carrier, the frequency is only shifted downwards, which should only increase the setup and hold margins. One of the most challenging applications for spread spectrum clock generation is its use in Pentium based machines. Techniques such as down spreading can resolve most timing concerns. However, use of a spread spectrum clock generator in these high performance designs is not easy. The reason for this is the internal multiplication that is used to increase clock speed. As mentioned, this internal multiplication is done by way of a phase locked loop (PLL). A PLL uses a feedback system to compare a frequency-divided version of the output signal to the input signal, thereby locking the two in frequency. Like most feedback systems, however, an instantaneous change at the input does not result in an instantaneous proportional change at the output. Rather, the output can approach its final value asymptotically (as in a single pole, "overdamped" feedback system) or bounce around its final value (as in the case of a multiple order, "underdamped" system). Most phase locked loops used for frequency multiplication in CPUs are third order, making predictions as to how the output frequency will change with changes to the input frequency non trivial [RA-5].

1.4 Generic structure of the thesis

This thesis is developed logically in several parts, corresponding to different chapters. A summary of these chapters is presented onwards:

- In chapter 2, a wide theoretical development of the modulation and related concepts are presented. It is explained generically all aspects related to the modulation and particularly, to the frequency modulation. Main parameters of frequency modulation are presented and explained in detail and how practical considerations may affect to the theoretical behaviour of these parameters. Because the theoretical part of this thesis is completely based on the fundaments of the Fourier Transform, a sufficient explanation was thought to include for a right understanding of this thesis (Annex 3). Finally, all this knowledge is summarized in a computational algorithm (MATLAB environment), capable of generating any frequency modulation of a sinusoidal carrier and the corresponding spectral components resulting from the modulation process.

- Chapter 3 takes profit of the results obtained in Chapter 2 where it is possible to obtain the theoretical behaviour of the different modulation profiles of interest: sinusoidal, triangular, exponential and mixed waveforms. This way, chapter 3 is intended to completely understand and analyze the theoretical behaviour of these modulation profiles and be quantified according to several significant measure parameters. Afterwards, a comparison of these modulation profiles is carried out by means of the measure parameters defined previously. A proposal of control for a real power converter and theoretical considerations to apply a certain SSCG method to switching power converters are also included in this chapter.
- After all aspects of frequency modulation by means of SSCG methods have been theoretically developed, it is mandatory the verification of the theoretical conclusions through an experimental test plant. Chapter 4 starts with the description, theoretical calculation and physical implementation of this test plant. Most practical considerations are here dealt with, like the influence of the Spectrum Analyzer's Resolution Bandwidth (RBW) on the measured EMI, a proposal of a practical method to select a valuable SSCG technique applied to Switching Power Converters, comparative measurements of conducted EMI within the range of conducted emissions (0 Hz ÷ 30 MHz) and a proposal about SSCG as a method to avoid interfering a certain signal.
- Chapter 5 summarizes the whole conclusions gathered through the previous chapters and, finally, chapter 6 lists references related to the thesis, separated into different thematic groups.
- Several annexes have been included at the end of this document. Some of them are direct references to the thesis and the rest are included because they were considered to be of interest, like the one entitled "CONSIDERATIONS ABOUT EMC UNITS EXPRESSED IN DECIBELS".

1.5 Experimental considerations and operative guideline

Diagram in Figure 1-8 summarizes the operative guideline of this thesis:

1. Development of a mathematical model and working environment. It will gather the whole concepts, parameters and expressions related to frequency modulation and its particular focus on SSCG. Further, this model is to be concretized in a

computational algorithm, this one generating both modulated waveforms to be introduced into an arbitrary function generator and the theoretical results of the different frequency modulations under test.

Profile modulations to be applied include sinusoidal, triangular and exponential modulating waveforms as analytical expressions but also sampled modulating waveforms and other specific modulating waveforms will be an available option.

2. The waveform resulting from the selected mathematical modulation will be introduced into an arbitrary signal generator. Special care must be taken when selecting the characteristics and performance of this equipment.

3. The modulated signal coming out from the signal generator is then introduced either into a specific switching power converter (in order to control it) or directly into the spectrum analyzer. In the first case, the EMI emissions are measured by using a compliant LISN (Line Impedance Stabilization Network), whose output is directed to the input of the spectrum analyzer. A detailed explanation of how a spectrum analyzer works is mandatory for a perfect understanding of the further experimental results (Annex 1). A broad explanation of measurement normative requirements will be also exposed (Annex 2) in order to show that true EMI emissions reduction can be faded by regulatory exigencies.

4. The two different types of experimental results (those generated by the measurement of modulation directly from the output of the signal generator and those coming from the LISN) can be useful to decide whether their differences are due to the modulation processes themselves or just because of the experimental plant being used. In a first approach, experimental results from measurements taken directly from the output of the signal generator should be nearly the same as those obtained in theoretical calculations; however, those results from measurements through a switching power converter and the corresponding LISN should be affected by the plant's characteristics as component behaviour (recovery time of diodes, switching of the power transistor ON $\leftrightarrow$ OFF, coupled capacitances and so on). A description of the experimental plant is to be presented in detail in chapter 4.

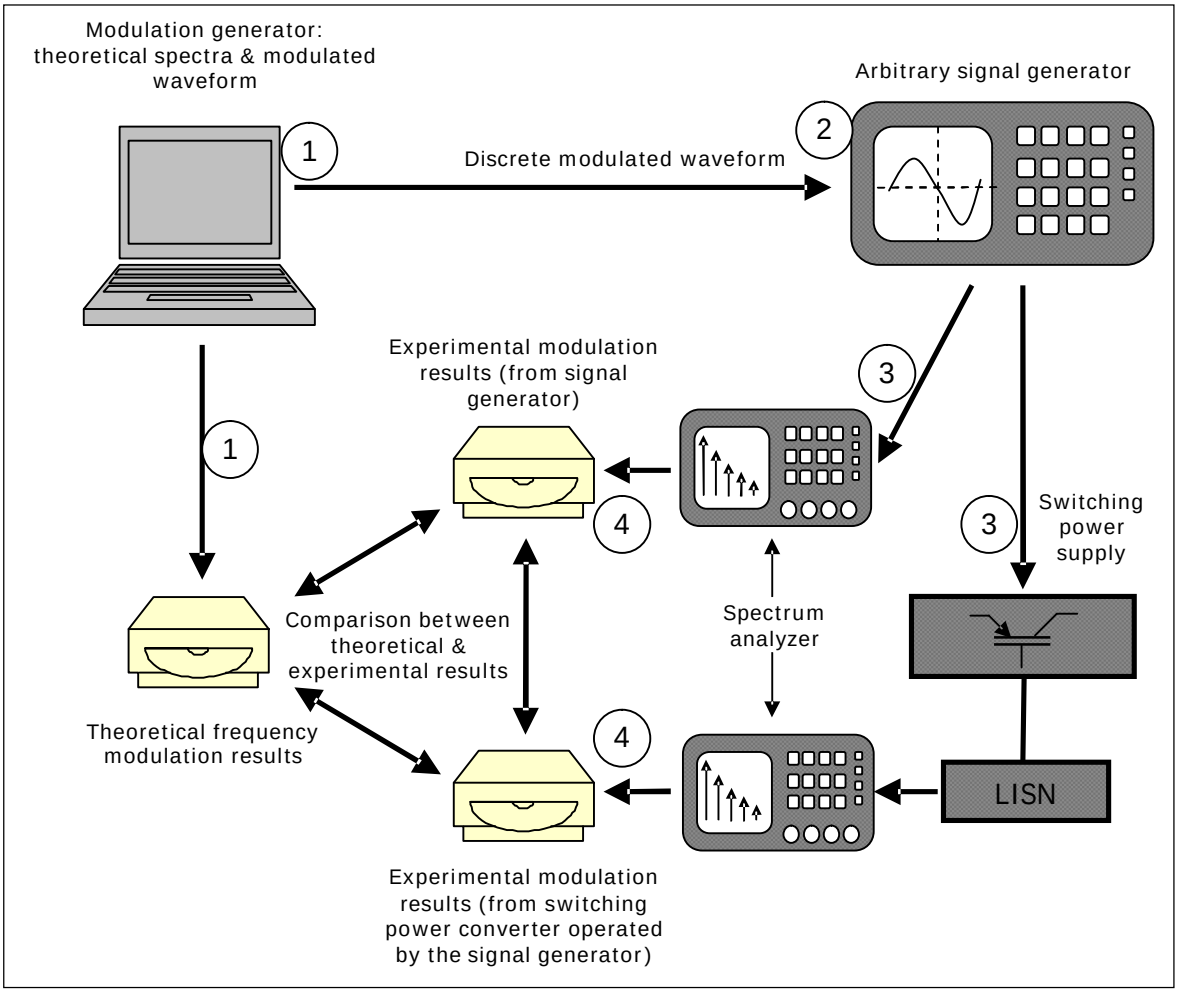

Figure 1-8. Diagram representing the basic guidelines of the thesis's development. Inside the circles, a number representing the step of development

In order to cover the first objective of this thesis, the four points above are to be applied mainly to switching power converters. A particular investigation related to switching power supplies is to be carried out managing the whole information together (normative regulations, theoretical & experimental results, spectrum analyzer limitations ...). This study will be of interest in order to decide whether a particular modulation (a set of modulation profile, carrier and modulating frequencies, peak frequency deviation, index modulation and normative regulatory requirements) is of profit for EMI emissions reduction or is just not worthy.

CHAPTER 2

THEORETICAL BASIS

2. THEORETICAL BASIS

This chapter is intended to introduce all aspects related to the modulation and particularly, to the frequency modulation, because this is the kind of modulation used to generate SSCG (Spread Spectrum Clock Generation) methods in this thesis. A wide theoretical development of the modulation and related concepts are presented as well as the main parameters of frequency modulation and how practical considerations may affect to the theoretical behaviour of these parameters. Although the theoretical development here presented considers only the modulation of a sinusoidal waveform, it is also demonstrated the validity and extension of these results to a generic signal. Because the theoretical part of this thesis is completely based on the fundaments of the Fourier Transform, a sufficient explanation was included for a right understanding of the thesis (Annex 3). Finally, all this knowledge is summarized in a computational algorithm (MATLAB environment), capable of generating any frequency modulation of a sinusoidal carrier and the corresponding spectral components resulting from the modulation process. A verification procedure for this algorithm is also presented in order to validate one of the most important parts of the thesis.

2.1 Modulation

Modulation is the process by which some characteristics of a carrier waveform are modified by another signal in order to obtain some benefits [RD-1]. This process of modulation is widely used in telecommunications (both video and audio signals) where the information of a signal is transferred to the carrier before transmission.

The characteristics of the carrier being modulated are normally amplitude and/or frequency. In its simplest way, a modulator can vary such characteristics of the carrier proportionally to the modulating waveform: this is called analogical modulation. More complicated modulators make first a conversion to digital and codify the modulating signal before modulation; this is known as a digital modulation.

In order to understand the process of modulation, it is a good procedure to present a modulator as a black box with two inputs and one output (Figure 2-1):

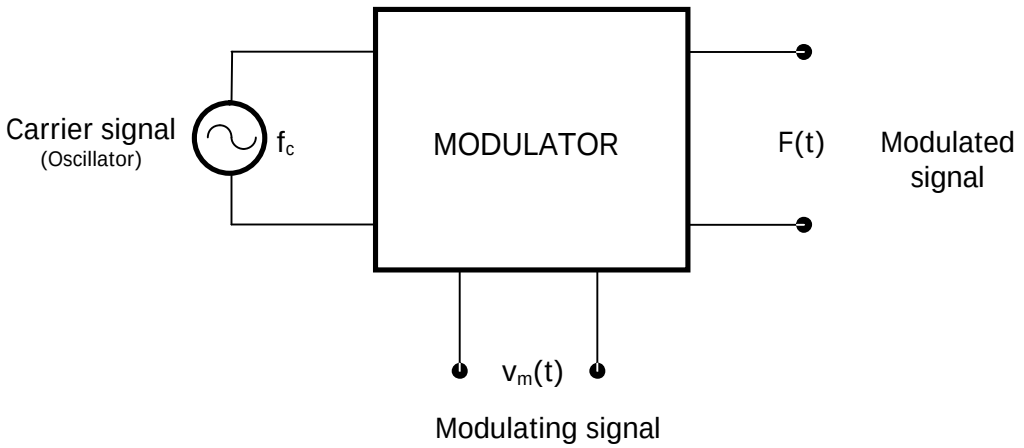

Figure 2-1. Black box modelling a modulator

Three signals are taking part in a modulation process:

- Carrier signal: periodic waveform of constant frequency (f_c) and constant amplitude profile.
- Modulating signal è $v_m(t)$: waveform responsible for changing (modulating) the initially constant characteristics of the carrier signal. It can be either periodical or non-periodical signal.
- Modulated signal è F(t): waveform resulting from the modulation process.

The output of the modulation process can be expressed as follows:

$$F(t) = A(t) \cdot \cos[\omega_c \cdot t + \Theta(t)] = A(t) \cdot \cos(\phi(t)) \qquad (2\text{-}1)$$

where:

- A(t) is a time-dependent amplitude
- f_c ($\omega_c=2\pi f_c$) is the carrier frequency
- $\Theta(t)$ is a time-dependent phase angle
- $\phi(t)$ is the angle of the modulated signal

The modulating signal $v_m(t)$ controls either the amplitude A(t) or the angle $\phi(t)$ or both together. There are normally two techniques of modulation:

- Amplitude modulation (AM): the carrier envelope A(t) is changed according to the modulating signal $v_m(t)$ while $\Theta(t)$ stays constant.

- Angle modulation: A(t) is a constant value A but the angle $\phi(t)$ is controlled by the modulating signal $v_m(t)$. This angle modulation has two variants depending on the close relationship between the angle $\phi(t)$ and the modulating signal:
    - Phase modulation (PM)
    - Frequency modulation (FM)

Because frequency modulation is the base of this thesis, a more detailed explanation of it is required.

2.1.1 Frequency Modulation (FM)

Systems based on angle modulation show a very good insensitiveness to fluctuations due to noise, particularly, impulse noise when used in communications. Onwards, some concepts related to FM are presented in order to frame further developments. A more detailed explanation can be found in reference [RD-1] and others.

2.1.1.1 Generic Formulation of Frequency Modulation

In frequency modulation, the deviation ($\delta\omega$) of instantaneous frequency $\omega(t)$ respect to the constant carrier frequency ω_c is directly proportional to the instantaneous amplitude of the modulating signal voltage $v_m(t)$ as shown in Figure 2-2.

The instantaneous frequency of the resulting FM waveform can be expressed as follows (2-2):

$$\omega(t) = \frac{d\phi}{dt} = \omega_c + \frac{d\Theta(t)}{dt} \tag{2-2}$$

According to expression (2-2), instantaneous deviation $\delta\omega(t)$ of $\omega(t)$ is given by (2-3):

$$\delta\omega(t) = \omega(t) - \omega_c = \frac{d\Theta(t)}{dt} \tag{2-3}$$

In frequency modulation, deviation $\delta\omega(t)$ is supposed to be proportional to the modulating signal voltage $v_m(t)$, that is:

$$\delta\omega(t) = k_\omega \cdot v_m(t) \tag{2-4}$$

where k_ω is a sensitivity factor of the modulator expressed in rad/sec/V or Hz/V.

From (2-3) and (2-4), the following expression arises:

$$\Theta(t) = \int_0^t k_\omega \cdot v_m(t) \cdot dt + \Theta(0) \qquad (2\text{-}5)$$

where Θ(0) is the initial value of phase and it is commonly taken as zero.

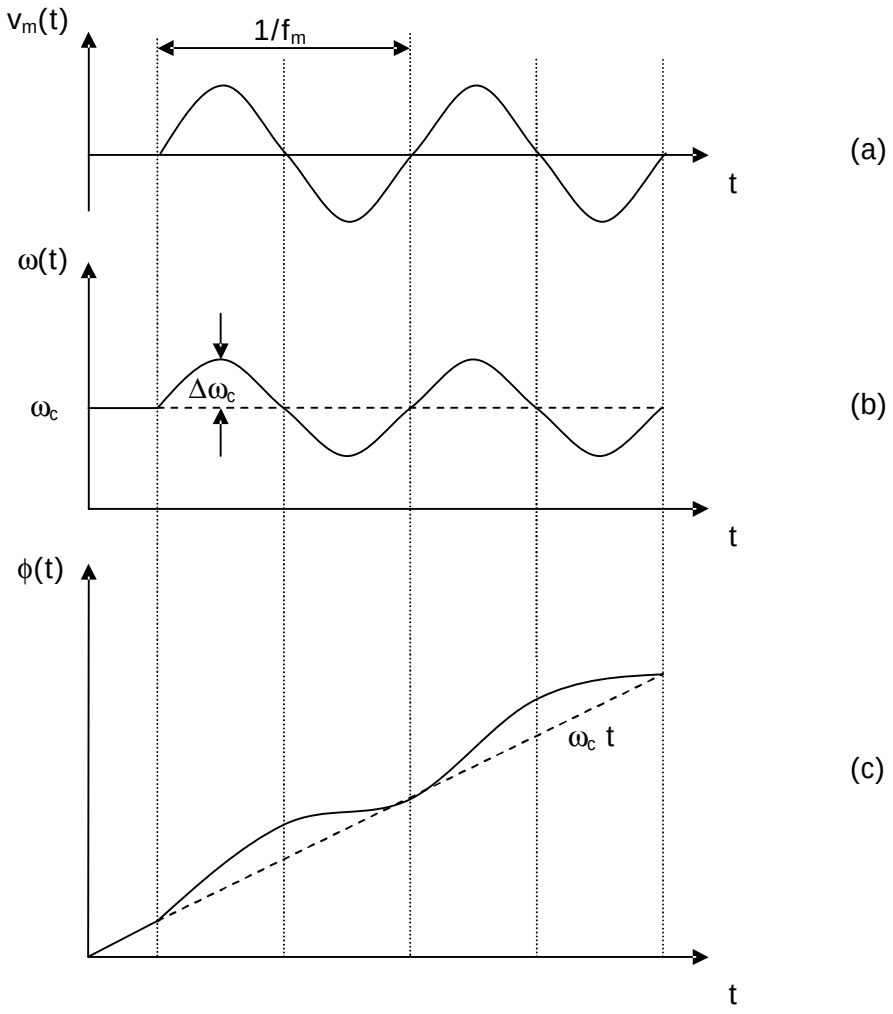

Figure 2-2. Effect of sinusoidal frequency modulation. (a) modulating wave; (b) instantaneous frequency of the FM waveform; (c) instantaneous angle of the FM waveform.

From (2-1) and (2-5), the generic expression of a frequency modulated sinusoidal waveform F(t) takes this aspect:

$$F(t) = A \cdot \cos\left[\omega_c \cdot t + k_\omega \cdot \int_0^t v_m(t) \cdot dt\right] \qquad (2\text{-}6)$$

A very important ratio in frequency modulation is known as modulation index m_f and is expressed this way:

$$m_f = \frac{\Delta\omega_c}{\omega_m} = \frac{\Delta f_c}{f_m} \tag{2-7}$$

where (according to Figure 2-2(b)):

- Δf_c is the peak deviation of the carrier frequency.
- f_m is the frequency of the modulating signal $v_m(t)$, assuming it is a periodic waveform.

2.1.1.2 Other important parameters

Some other parameters and concepts are to be used along the thesis. The following ones are the most important:

2.1.1.2.1 Modulation ratio δ

The modulation ratio denotes the peak excursion of the switching or carrier frequency referred to itself, that is:

$$\delta = \frac{\Delta f_c}{f_c} \tag{2-8}$$

When the modulation ratio is expressed in %, it is more usually known as percentage of modulation δ%:

$$\delta\% = \frac{\Delta f_c}{f_c} \cdot 100 \tag{2-9}$$

This percentage of modulation normally ranges between 1% and 2.5% for the commercial applications [RC-5] at higher frequencies (in order to conserve the minimum-period requirements for control system timing). In the case of switching power converters, where timing requirements are much less important, this percentage can be larger, much more than 2.5%. This will be studied in the thesis later on.

2.1.1.2.2 Modulation profiles

The most important parameter defining the shape of the resulting modulated wave spectrum is strongly related to the modulation profile, that is, the shape of the waveform used to modulate but these profiles also influence the displacement of the central frequency up- or down-wards respect to the original signal, as shown in Figure 2-3.

Instead of shifting the carrier frequency above and below symmetrically, the frequency is only shifted up or downwards respect to the carrier.

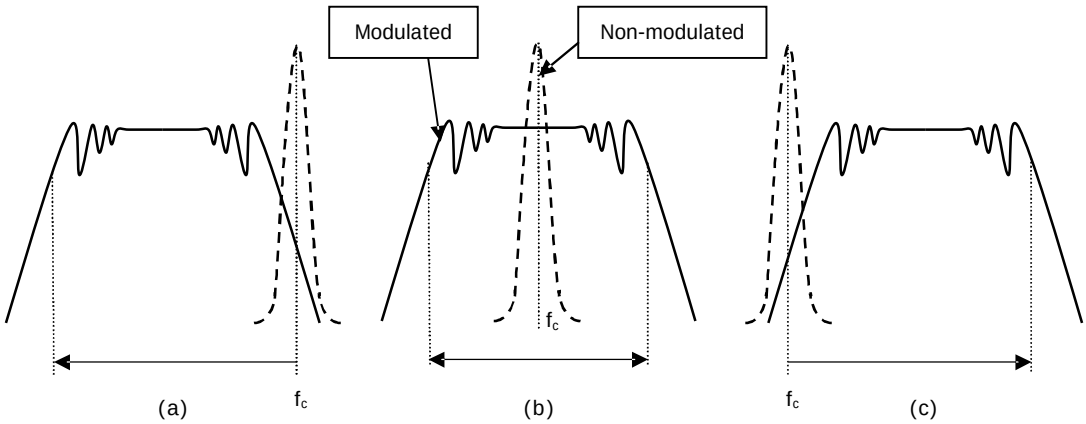

Figure 2-3. a) Down-spreading, b) symmetrical and c) up-spreading SSCG techniques

Where setup and hold time margins are critical, down spreading technique is preferred.

In practice, there are three profiles used for modulation purposes: sinusoidal, triangular and exponential, which are shown in Figure 2-4. As seen later on, exponential profile is very easy to be parameterized then giving different aspects ranging from nearly-peaks to nearly-square waveforms. Each modulation profile shows different advantages depending on the system characteristics where it is to be implemented and, at this stage, it is not right to say that a profile is much better than the others.

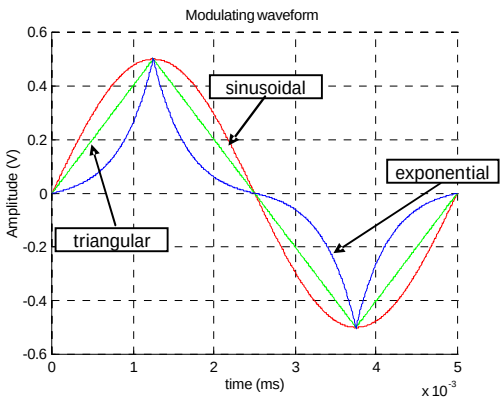

Figure 2-4. Sinusoidal, triangular and exponential modulation profiles

A line of investigation in this area points necessarily to study how a profile should be in order to obtain the maximum benefits when using SSCG and it will be developed later on.

2.1.2 Bandwidth of the FM waveform

Bandwidth is defined as the difference between the limiting frequencies within which performance of a device, in respect to some characteristic, falls within specified limits or the difference between the limiting frequencies of a continuous frequency band.

An FM signal actually contains an infinite number of side frequencies besides the carrier and therefore occupies infinite bandwidth. However, the side frequencies quickly decrease in strength and can be considered negligible at some point. In practice, a tradeoff between bandwidth and distortion must be considered.

The bandwidth of a frequency modulated waveform is approximately given by the Carson's rule (valid for any angle-modulated signal) and can be summarized as follows [RD-3]:

- Total energy of the original signal keeps unaffected
- The 98% of the total energy is contained inside a bandwidth B calculated as follows:

$$B = 2 \cdot f_m \cdot (1 + m_f) = 2 \cdot (\Delta f_c + f_m) \tag{2-10}$$

where:

- f_m represents the highest modulating frequency.
- Δf_c is the peak deviation of the carrier frequency.
- Modulation index is defined as $m_f = \frac{\Delta f_c}{f_m}$.

2.1.3 Sinusoidal carrier vs. a generic carrier: validity of modulation results

Until this point, all considerations and developments have taken into account the fact of modulating a sinusoidal carrier. Most of the carriers (even those intended to be sinusoidal) are not a pure sine wave but a set of harmonics. In switching power converters, a PWM signal is to be found; microprocessor systems will be activated by a square clock signal and communication standards define normally trapezoidal waveforms in order to reduce the high-frequency spectral components [see Figures 1-3 and 1-4 in clause 1.2]. The question now is how to deal with these generic waveforms consisting of infinity of harmonics.

2.1.3.1 Spectral content of a signal [RD-3] & [RD-8]

As an example, consider the periodic square waveform shown in Figure 2-5, with period T, amplitude A and pulse duration of τ. The complete spectral content is to be calculated analytically and displayed graphically onwards.

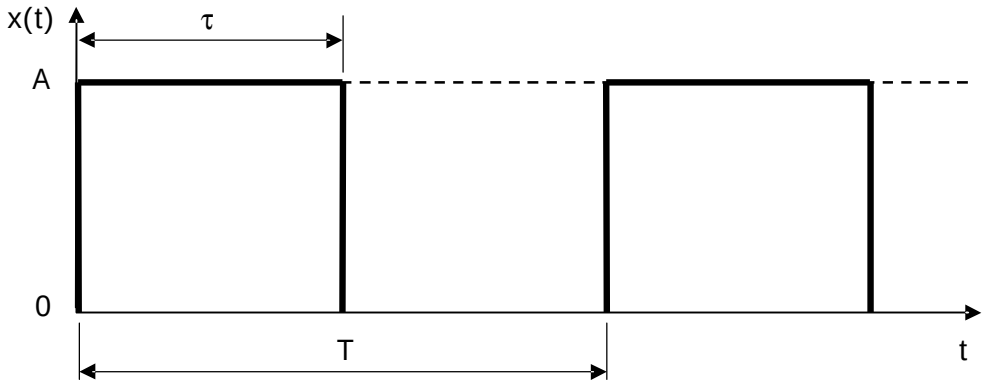

Figure 2-5. A periodic, square waveform

The complex-exponential expansion coefficients are usually more easily computed than the coefficients in the trigonometric form $\left(\omega_c = 2\cdot\pi/T\right)$.

$$c_n = \frac{1}{T}\int_0^T x(t)\cdot e^{-jn\omega_c t}dt \qquad (2\text{-}11.a)$$

$$= \frac{1}{T}\left[\int_0^\tau A\cdot e^{-jn\omega_c t} + \int_\tau^T 0\cdot e^{-jn\omega_c t}\right] \qquad (2\text{-}11.b)$$

$$c_n = \frac{A}{jn\omega_c T}\left(1-e^{-jn\omega_c\tau}\right) \qquad (2\text{-}11)$$

In calculation of this type is often desirable to put the result into a sine or cosine form of function as shown below:

$$c_n = \frac{A}{jn\omega_c T}e^{-jn\omega_c\tau/2}\left(e^{jn\omega_c\tau/2}-e^{-jn\omega_c\tau/2}\right) \qquad (2\text{-}12.a)$$

$$= \frac{A}{jn\omega_c T}e^{-jn\omega_c\tau/2}\cdot 2j\sin\left(\tfrac{1}{2}n\omega_c\tau\right) \qquad (2\text{-}12.b)$$

$$c_n = \frac{A\tau}{T}\cdot e^{-jn\omega_c\tau/2}\frac{\sin\left(\frac{1}{2}n\omega_c\tau\right)}{\frac{1}{2}n\omega_c\tau} \qquad (2\text{-}12)$$

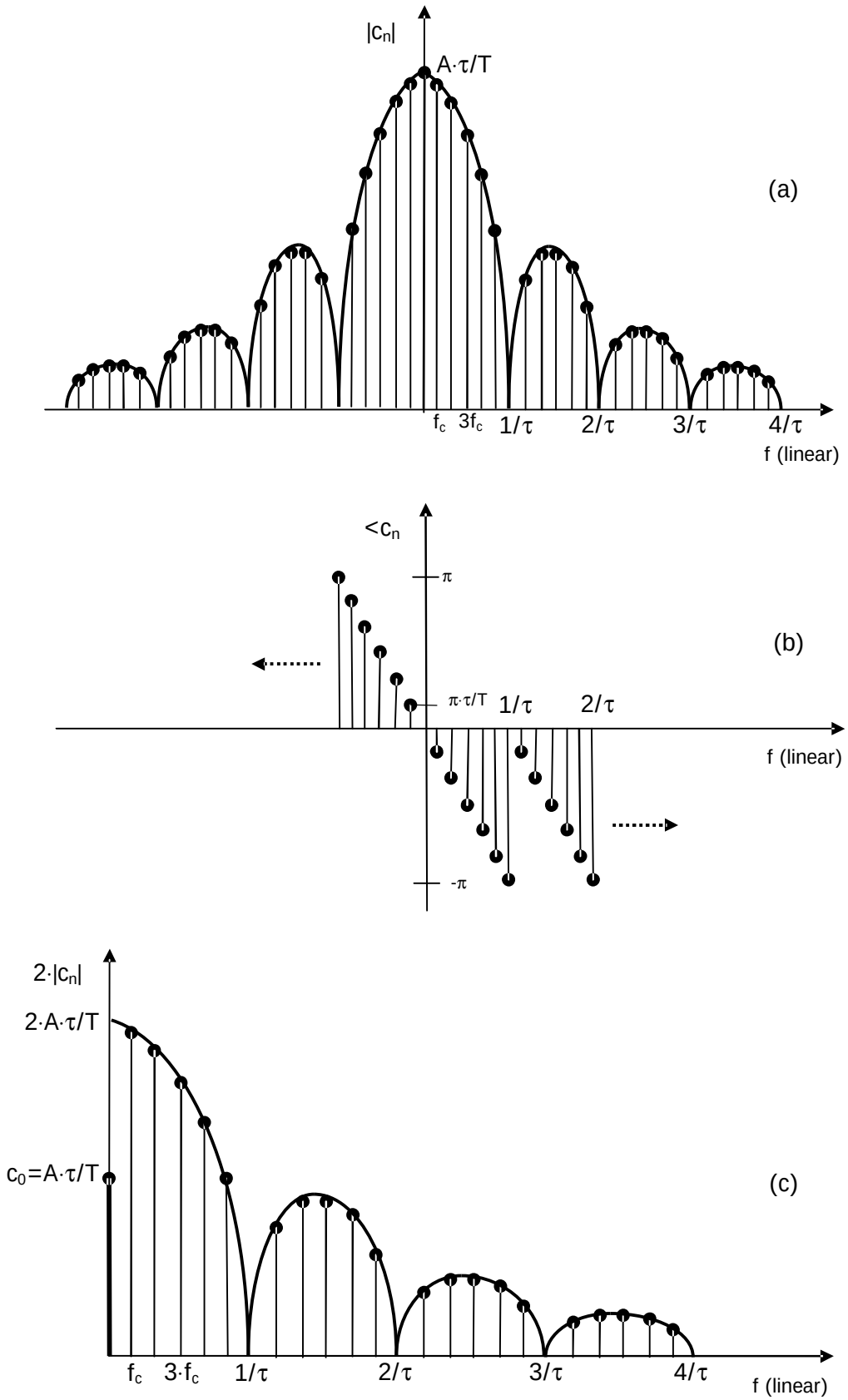

Figure 2-6. Frequency-domain representation of a square wave: (a) the two-sided magnitude spectrum; (b) the phase spectrum; (c) the one-sided magnitude spectrum

From the result above, the following two expressions corresponding to the module and phase of the n-harmonic can be derived:

$$|c_n| = \frac{A\tau}{T} \cdot \left| \frac{\sin\left(\frac{1}{2} n\omega_c \tau\right)}{\frac{1}{2} n\omega_c \tau} \right| \quad (2\text{-}13)$$

$$\angle c_n = \pm \tfrac{1}{2} n\omega_c \tau \quad (2\text{-}14)$$

or, in terms of period T ($\omega_c = 2\pi/T$):

$$|c_n| = \frac{A\tau}{T} \cdot \left| \frac{\sin\left(n\pi\tau / T\right)}{n\pi\tau / T} \right| \quad (2\text{-}15)$$

$$\angle c_n = \pm \frac{n\pi\tau}{T} \quad (2\text{-}16)$$

The ± sign of the angle comes about because the $\sin\left(\frac{1}{2} n\omega_c \tau\right)$ term may be positive or negative (an angle of 180º). This is added to the angle of $e^{-jn\omega_c \tau/2}$.

A usual convention is displaying both positive and negative frequency sinusoids for each frequency and halving the amplitude accordingly, as in Figure 2-6(a). A more intuitive convention is related to represent only positive frequency sinusoids, which is achieved by doubling the amplitude of each individual component, as shown in Figure 2-6(c).

How every spectral component is affected by the modulation process is clarified in the next clause.

2.1.3.2 Impact of modulation on every spectral component

The distance in frequency between two consecutives harmonics is given by the frequency f_c of the original signal (supposing to be periodic). The frequency f_h of the harmonic F_h is expressed this way:

$$f_h = h \cdot f_c \quad (2\text{-}17)$$

where h is the harmonic order varying from 0 to ∞.

Each harmonic component is represented as a pair amplitude-phase (A_h-θ_h) at a frequency position f_h and is equivalent to a pure sinusoidal waveform with the only consideration of not being independent but making part of a "bigger" signal (see Figure 2-6):

$$F_h(t) = A_h \cdot \cos\left(h \cdot \omega_c \cdot t + \theta_h\right) \quad (2\text{-}18)$$

If the same frequency modulation is applied to each harmonic component, expressions (2-1), (2-3) and (2-4) can be generalized as follows, respectively:

$$F_h^{\text{mod}}(t) = A_h(t) \cdot \cos\left[h \cdot \omega_c \cdot t + \Theta_h(t)\right] = A_h(t) \cdot \cos\left(\phi_h(t)\right) \quad (2\text{-}19)$$

$$\delta\omega_h(t) = \omega_h(t) - h \cdot \omega_c = \frac{d\Theta_h(t)}{dt} \quad (2\text{-}20)$$

$$\delta\omega_h(t) = k_\omega^h \cdot v_m(t) = h \cdot k_\omega \cdot v_m(t) \quad (2\text{-}21)$$

where k_ω^h in (2-21) was defined for similarity with expression (2-4) .

From (2-19), (2-20) and (2-21), the generic expression of a frequency modulated harmonic component is:

$$F_h^{\text{mod}}(t) = A_h \cdot \cos\left[h \cdot \omega_c \cdot t + \theta_h + k_\omega^h \cdot \int_0^t v_m(t) \cdot dt\right] \quad (2\text{-}22)$$

and

$$\Theta_h(t) = \theta_h + k_\omega^h \cdot \int_0^t v_m(t) \cdot dt \quad (2\text{-}23)$$

Some conclusions can be obtained from the expressions above:

- From (2-20) and (2-23), the particular harmonic phase θ_h does not affect the results of frequency modulation because of the derivative behaviour of the frequency deviation as expressed in (2-20) and demonstrated further in clause 2.2.3.3.
- From (2-17), the peak frequency deviation affecting each harmonic component increases linearly with the harmonic order, that is, $\Delta f_h = h \cdot \Delta f_c$. In other words, the modulation index related to each harmonic component m_f^h will also increase linearly with the harmonic order:

$$m_f^h = \frac{\Delta f_h}{f_m} = h \cdot \frac{\Delta f_c}{f_m} = h \cdot m_f \quad (2\text{-}24)$$

- The bandwidth B_h of the frequency modulated harmonic component h increases also linearly with the harmonic order:

$$B_h = 2 \cdot f_m \cdot (1 + m_f^h) = 2 \cdot (\Delta f_h + f_m) \quad (2\text{-}25)$$

that is,

$$B_h = B + 2 \cdot \Delta f_c \cdot (h-1) \quad (2\text{-}26)$$

$$B_h = B + 2 \cdot f_m \cdot m_f \cdot (h-1) \quad (2\text{-}27)$$

where B is the bandwidth corresponding to modulation of a sinusoidal waveform of frequency f_c, equivalent to the 1st harmonic of the generic waveform.

2.2 Practical considerations related to FM parameters

It is important to distinguish between a phenomenon itself and the way it is measured. Although theoretical results show a good performance of frequency modulation regarding to EMI emissions reduction in every case (as demonstrated in chapter 3), measurements procedures (normally related to practical limitations of measure equipment or normative aspects) can fade such a good behaviour even making it negligible. In other words, a good theoretical SSCG system is not a guarantee of a good experimental result when measuring; it should be only taken as a start point which, after some modifications, could work properly. Onwards, some practical considerations related to each FM parameter together with its theoretical implication are to be exposed.

2.2.1 Carrier (Switching) & modulating frequencies

As exposed previously, the carrier (switching) signal is the constant frequency (f_c) wave to be modulated, while the modulating signal (normally a constant frequency [f_m] wave) is the waveform used to do the modulation.

Fourier series is a common way to express any waveform:

$$F(t) = F_0 + \sum_{h=1}^{\infty} F_h(t) \quad (2\text{-}28)$$

where F_0 represents the average (dc) component of the original signal and F_h, each one of the infinity of harmonics.

When talking about modulation of a base frequency (no matter the kind of modulation: square, triangular, sinusoidal, exponential, random, etc), a common way to operate is modulating each individual component F_h of the base waveform (onwards, main harmonics) and, then, obtaining a window of sub-harmonics (onwards, side-band harmonics) for each main harmonic (see Figure 2-7).

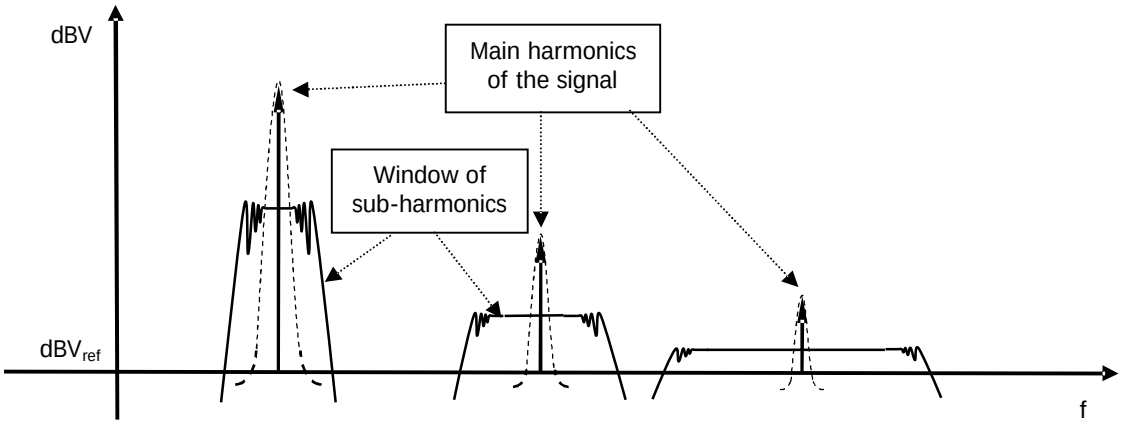

Figure 2-7. Only one modulating signal modulates every harmonic of the original signal.

As expressed in (2-10), the bandwidth of the side-band harmonics increases linearly with the carrier frequency f_c, the modulation ratio δ and the modulating frequency f_m. For frequency modulation, the distance between two consecutive side-band harmonics is given by the modulating frequency f_m (see Figure 2-8). This frequency is usually selected to be larger than 30 kHz in order to be above the audio band.

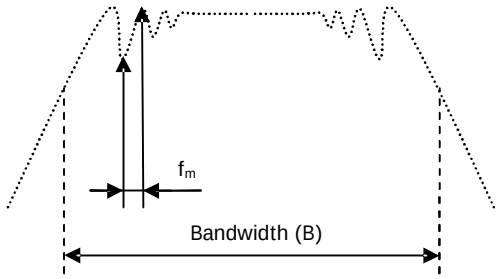

Figure 2-8. Distance between two consecutive side-band harmonics (FM modulation)

Common values for the modulating frequency f_m range from 50 kHz to 250 kHz [RC-5] (for system clocks). No commercial information is available for power converters related to modulating frequency but it is advisable to use smaller modulating frequencies depending on the application ([RB-1] & [RB-2]). In the same way, CISPR 16-1 specifies several RBWs (6 dB) for the different frequency ranges and

measurement modes. This way, a RBW of 220 Hz is intended for measurements in the band A (9 kHz-150 kHz); 9 kHz for the band B (150 kHz-30MHz); 120 kHz for the bands C (30 MHz-300 MHz) and D (300 MHz-1GHz) and 1 MHz for frequencies higher than 1 GHz (valid for quasi-peak, peak and average measurement mode).

The spectrum analyzer band-pass filter (commonly known as Resolution Bandwidth-RBW) is adjustable, for instance, to accomplish the value defined in a regulatory norm.

Two main cases are of significance (see clauses 4.2 and 4.3):

- f_m < RBW: It is not possible to distinguish individual side-band harmonics, so the measured value will be higher than expected in theoretical calculations but it can still be worthy if RBW < B (see Figure 2-8).
- f_m > RBW: Considering no overlap exists, the measured value corresponds to the actual individual side-band harmonic amplitude.

For the second case (f_m > RBW) to be reached for the different frequency ranges expressed above, special care must be taken when selecting the modulating frequency.

As the sum of the several side-band harmonics inside this RBW is done by just adding amplitudes (this represents the way a spectrum analyzer actually adds signals in its bandwidth {according to [RD-3] and Annex 1}), it is expected to obtain (for the first case) a value higher than the actual one. The larger RBW, the larger the measured value for each side-band harmonic too.

2.2.2 Carrier frequency peak deviation Δf_c (Overlap)

Carrier frequency peak deviation Δf_c denotes the peak excursion of the switching frequency f_c and it is normally expressed as $\Delta f_c = \delta \cdot f_c$, where the factor δ is the modulation ratio. The resulting window bandwidth B (already presented in expression (2-10)) depends on the modulation ratio δ and it is desired that the side-band frequencies do not fall into the audible range. It is important to remind that the bandwidth resulting from modulation process is wider than two times the carrier frequency peak deviation, the first one given by the Carson's rule.

According to Figure 2-9 and expression (2-25), derived in clause 2.1.3.2 and reproduced below,

$$B_h = 2 \cdot f_m \cdot (1 + m_f^h) = 2 \cdot (\Delta f_h + f_m) \qquad (2\text{-}25)$$

and taking into account that audio problems occur normally at h=1, the following sequence of expressions can be derived (note that $f_c=f_1$):

$$f_c - \frac{B_1}{2} > f_{aud,\max} \tag{2-29}$$

$$f_c - (\Delta f_c + f_m) > f_{aud,\max} \tag{2-30}$$

$$f_c - (\delta \cdot f_c + f_m) > f_{aud,\max} \tag{2-31}$$

$$f_c \cdot (1-\delta) > f_{aud,\max} + f_m \tag{2-32}$$

where $f_{aud,max}$ represents the higher limit of the human audible frequencies.

Expression (2-32) should be accomplished in order to avoid undesirable audio interferences. Note that switching frequencies of power converters are usually low (f_c < 1MHz) and special care must be taken to avoid harmonics into the audible band ($f_{aud,min}$=20 Hz < f_{aud} < $f_{aud,max}$=20 kHz).

However, the main influence of the parameter Δf_c is related to the possibility of overlap between the side-band harmonics of two consecutive main harmonics. Overlap can be an important aspect at higher harmonic components because benefits are only obtained only when the sum of side-band harmonics belonging to several main harmonic windows is lower than the related-carrier harmonic.

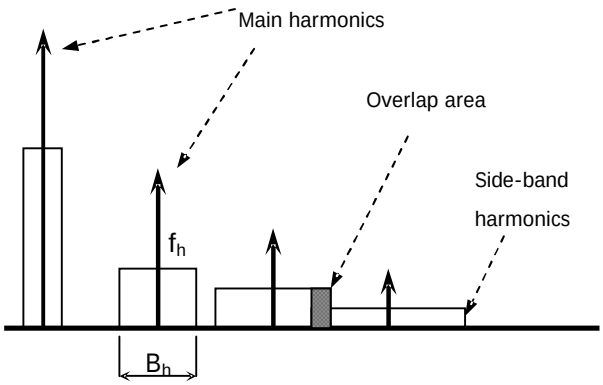

Figure 2-9. Side-band windows overlap

Of course, the side-band harmonic window is not a perfect square box as shown in Figure 2-9. Moreover, the spectra resulting from a modulating process contains infinity of harmonics which extends over the whole frequency axis. But the Carson's rule

establishes that a 98% of the total energy of the modulated signal is contained inside a bandwidth given by the expression (2-25). No information related to the shape of the side-band harmonic window is given by the Carson's rule because this one only depends on the shape of the modulation profile.

The square approximation of the window is valid for the purpose of finding the harmonic order at which the overlap effect is starting to appear.

Approximately, overlap effect occurs when (see Figure 2-9):

$$f_h + \frac{B_h}{2} = f_{h+1} - \frac{B_{h+1}}{2} \tag{2-33}$$

Substituting (2-25) into (2-33), the following sequence is derived (keeping in mind that $f_h = h \cdot f_c$):

$$h \cdot f_c + \Delta f_h + f_m = (h+1) \cdot f_c - \Delta f_{h+1} - f_m \tag{2-34}$$

$$h \cdot f_c + h \cdot \delta \cdot f_c + f_m = (h+1) \cdot f_c - (h+1) \cdot \delta \cdot f_c - f_m \tag{2-35}$$

and, finally:

$$f_c = \frac{2}{1 - \delta \cdot (1 + 2 \cdot h_{overlap})} \cdot f_m \tag{2-36}$$

where:

- f_c is the carrier frequency.
- f_m is the modulating frequency.
- δ is the modulation ratio.
- $h_{overlap}$ is the harmonic number at which the overlap effect starts to occur.

Or, in other terms:

$$h_{overlap} = \frac{1}{\delta} \cdot \left(\frac{1}{2} - \frac{f_m}{f_c} \right) - \frac{1}{2} \tag{2-37}$$

Although expression (2-37) is completely generic and valid for any modulation parameters and types, some approximations may be done.

As it can be derived from (2-37), the smaller f_c (or the larger f_m and δ), the smaller $h_{overlap}$ is to be found, but not significant differences arise because f_c is commonly much larger than f_m, then the expression (2-37) can also be written in the following way:

$$h_{overlap} \approx \frac{1}{\delta} \cdot \left(\frac{1}{2} \right) - \frac{1}{2} \tag{2-38}$$

Moreover, the modulation ratio δ is usually small enough (for instance, not larger than 2.5% for clock systems) as to simplify the expression (2-38), obtaining the following reduced equation:

$$h_{overlap} \approx \frac{1}{2 \cdot \delta} \tag{2-39}$$

In other words, larger values of frequency deviation (for a defined f_c) are to produce overlap at lower main harmonic numbers. Influence of modulating frequency f_m in this overlap effect is significantly smaller and, in a first step, is negligible.

2.2.3 Influence of the modulation profile parameters

Modulation profiles are of great importance in the final results when a modulation process is present. They are mainly responsible for the shape of the resulting spectrum after the modulation process, but they also influence the displacement of the central frequency up- or down-wards respect to the original signal. The following points deal with these important aspects in more detail.

2.2.3.1 Influence on the power converter output voltage of the modulation profile

It is of great interest to find out the influence of modulation profiles on the output voltage of the converter. In order to answer this question, a finer development is carried out onwards.

As in a real power converter, a square waveform is being frequency-modulated following a certain modulation profile (e.g., Figure 2-10(a)), which means that the instantaneous frequency of the signal is changing constantly (Figure 2-10(b)). However, a condition must be guaranteed: the initial and the final frequencies inside a modulating signal period (T_m) must be exactly the same. This way, a new more complicated signal appears, but showing a constant periodT_m (Figure 2-10(b)) which repeats indefinitely in time.

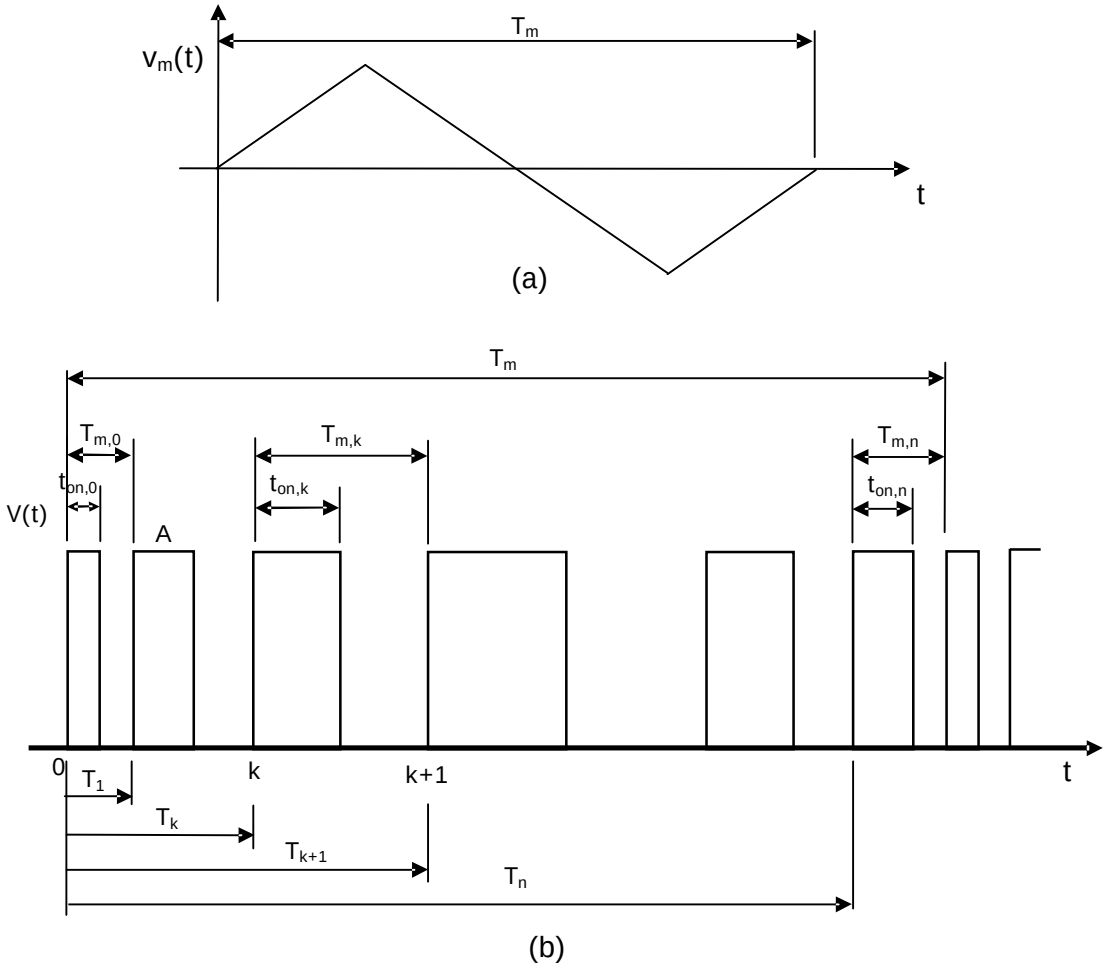

Figure 2-10. (a) A typical triangular modulation profile and (b) a frequency-modulated square waveform

Calculating the average voltage of the modulated square waveform in Figure 2-10(b) yields:

$$V_{average} = \frac{1}{T_m} \cdot \int_0^{T_m} V(t) \cdot dt \qquad (2\text{ -}40)$$

Separating integral (2-40) into different partial integrals yields:

$$V_{average} = \frac{1}{T_m} \cdot \left[\int_0^{T_1} V(t) \cdot dt + \int_{T_1}^{T_2} V(t) \cdot dt + \cdots + \int_{T_k}^{T_{k+1}} V(t) \cdot dt + \cdots + \int_{T_n}^{T_m} V(t) \cdot dt \right] \qquad (2\text{-}41)$$

with k from 0 to a generic n.

A generic partial integral in expression (2-41) can also be expressed as follows:

$$\int_{T_k}^{T_{k+1}} V(t)\cdot dt = \int_{T_k}^{T_k+T_{m,k}} V(t)\cdot dt \qquad (2\text{-}42)$$

But V(t) is zero outside the $t_{on,k}$ period, which yields:

$$\int_{T_k}^{T_{k+1}} V(t)\cdot dt = \int_{T_k}^{T_k+T_{m,k}} V(t)\cdot dt = \int_{T_k}^{T_k+t_{on,k}} A\cdot dt = A\cdot \int_{T_k}^{T_k+t_{on,k}} dt = A\cdot t_{on,k} \qquad (2\text{-}43)$$

Duty-cycle D is constant through the whole period T_m, that is, $D=\frac{t_{on,k}}{T_{m,k}}$, thus the generic partial integral in expression (2-43) can be rewritten as follows:

$$\int_{T_k}^{T_{k+1}} V(t)\cdot dt = A\cdot D\cdot T_{m,k} \qquad (2\text{-}44)$$

Thus, expression (2-41) can take this more profitable aspect:

$$V_{average}=\frac{1}{T_m}\cdot\left[A\cdot D\cdot\sum_{k=0}^{n}T_{m,k}\right] \qquad (2\text{-}45)$$

but the sum inside the integral is exactly the modulating period T_m; therefore a final expression is derived:

$$V_{average}=\frac{1}{T_m}\cdot\left[A\cdot D\cdot T_m\right]=A\cdot D \qquad (2\text{-}46)$$

Therefore, no influence of the modulation profile on the output voltage is expected, at least theoretically, with the condition of guaranteeing a constant instantaneous duty-cycle D during the modulating period T_m.

2.2.3.2 Influence on the final spectrum of a voltage offset in the modulation profile

For convenience, a modulating waveform can be expressed as a normalized profile $\bar{v}_m(t)$ instead of the nominal one (see Figure 2-11),

$$v_m(t)=V_m\cdot\bar{v}_m(t)+V_{offset} \qquad (2\text{-}57)$$

where V_m contains the actual amplitude of the modulation profile and V_{offset} is the displacement of the whole modulation profile along with the vertical axis.

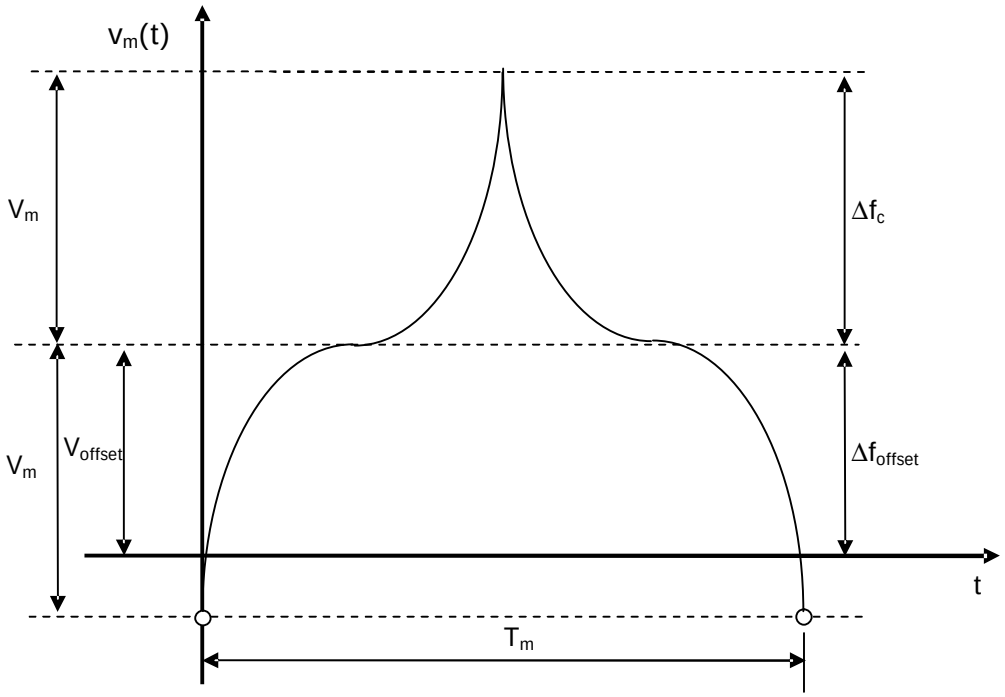

Figure 2-11. A generic modulation profile with vertical offset

Substitution of expression (2-57) into the generic expression of the time-dependant phase yields the following sequence of results:

$$\Theta(t) = \int_0^t k_\omega \cdot v_m(t) \cdot dt + \Theta(0) \tag{2-58}$$

$$\Theta(t) = \int_0^t k_\omega \cdot \left(V_m \cdot \bar{v}_m(t) + V_{offset}\right) \cdot dt + \Theta(0) \tag{2-59}$$

$$\Theta(t) = k_\omega \cdot V_m \cdot \int_0^t \bar{v}_m(t) \cdot dt + k_\omega \cdot V_{offset} \cdot \int_0^t dt + \Theta(0) \tag{2-60}$$

The two next definitions in (2-61.a and b) allow the expression (2-60) to be expressed as shown in (2-62):

$$\text{(a)}\ \Delta f_c = \frac{k_\omega \cdot V_m}{2\pi} \qquad \text{(b)}\ \Delta f_{offset} = \frac{k_\omega \cdot V_{offset}}{2\pi} \tag{2-61}$$

$$\Theta(t) = 2\pi \cdot \Delta f_c \cdot \int_0^t \bar{v}_m(t) \cdot dt + 2\pi \cdot \Delta f_{offset} \cdot t + \Theta(0) \tag{2-62}$$

Substituting (2-62) into the generic expression (2-1) of a frequency modulated sinusoidal signal, the following expressions are found ($\Theta(0) = 0$):

$$F(t) = A \cdot \cos\left[\left(\omega_c + 2\pi \cdot \Delta f_{offset}\right) \cdot t + 2\pi \cdot \Delta f_c \cdot \int_0^t \bar{v}_m(t) \cdot dt\right] \qquad (2\text{-}63.1)$$

$$F(t) = A \cdot \cos\left[\left(\omega_c + 2\pi \cdot \Delta f_{offset}\right) \cdot t + k_\omega \cdot \int_0^t V_m \cdot \bar{v}_m(t) \cdot dt\right] \qquad (2\text{-}63)$$

In summary, it is a direct conclusion from (2-63) that a frequency offset (coming from the modulation profile) does not produce any effects on the spectral components resulting from a modulation process because they only depend on the modulation profile characteristics $\bar{v}_m(t)$. But this feature gives the possibility of an easy generation of down- and up-spreading the central frequency. Defining the resulting carrier frequency as ω_c^*:

$$\omega_c^* = \omega_c + 2\pi \cdot \Delta f_{offset} \qquad (2\text{-}64)$$

then, positive values of Δf_{offset} will generate up-spreading of the carrier frequency, negative values of Δf_{offset} will generate down-spreading of the carrier frequency and a null value of Δf_{offset} will keep the carrier frequency at its original value, as shown in Figure 2-12.

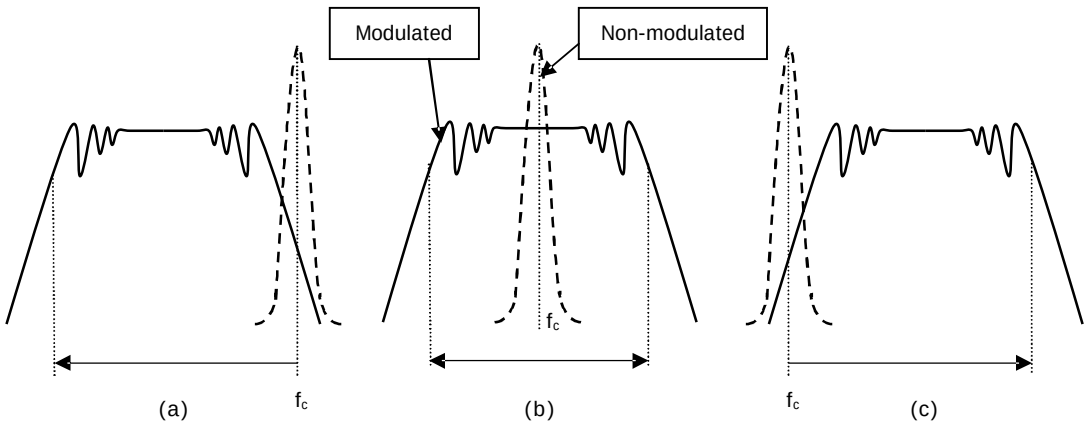

Figure 2-12. a) Down-spreading, b) symmetrical and c) up-spreading SSCG techniques

2.2.3.3 Influence of the modulation profile phase-shift on the spectrum resulting from the modulation process

Consider now the initial phase value $\Theta(0) \neq 0$ or a modulation profile which has been shifted a time t_0, as shown in Figure 2-13:

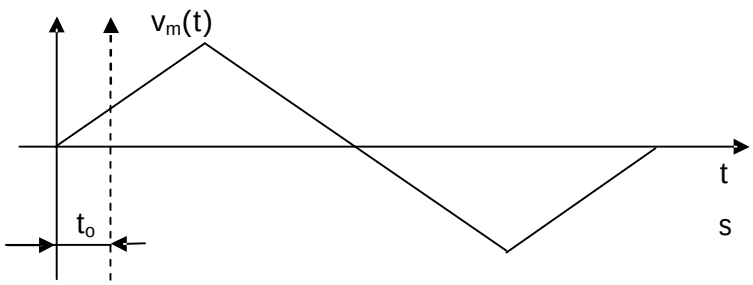

Figure 2-13. Modulation profile shifted in time

The equation describing the modulation process, earlier presented, is the following one:

$$F(t) = A \cdot \cos\left[\omega_c \cdot t + k_\omega \cdot \int_0^t v_m(t) \cdot dt\right] \tag{2-65}$$

For the time-shifted modulation profile, expression (2-65) changes slightly (note the relationship $s = t - t_0$ applied to the modulation profile):

$$F(t - t_0) = F(s) = A \cdot \cos\left[\omega_c \cdot [s + t_0] + k_\omega \cdot \int_{-t_0}^{s} v_m(s) \cdot ds\right] = \tag{2-66}$$

$$= A \cdot \cos\left[\omega_c \cdot s + k_\omega \cdot \int_0^s v_m(s) \cdot ds + \omega_c \cdot t_0 + k_\omega \cdot \int_{-t_0}^{0} v_m(s) \cdot ds\right] = \tag{2-67}$$

$$F(s) = A \cdot \cos\left[\omega_c \cdot s + k_\omega \cdot \int_0^s v_m(s) \cdot ds + \Theta(t_0)\right] \tag{2-68}$$

where two new variables are defined to make further developments easier:

– $\Theta(t_0) = \omega_c \cdot t_0 + k_\omega \cdot \int_{-t_0}^{0} v_m(s) \cdot ds$ (2-69)

– $b(s) = \omega_c \cdot s + k_\omega \cdot \int_0^s v_m(s) \cdot ds$ (2-70)

Expression (2-68) may then be written in the following way:

$$F(s) = A \cdot \cos[b(s) + \Theta(t_0)] \tag{2-71}$$

Defining $H_{SHIFT}(f)$ as the Fourier transform (see Annex 3) of the time-shifted waveform and $H_{ORI}(f)$ as the original Fourier transform, then:

$$H_{SHIFT}(f) = \int_{-\infty}^{+\infty} F(t - t_0) \cdot e^{-j2\pi \cdot f \cdot t} \cdot dt = \tag{2-72}$$

$$= \int_{-\infty}^{+\infty} F(s) \cdot e^{-j2\pi \cdot f \cdot (s + t_0)} \cdot ds = e^{-j2\pi \cdot f \cdot t_0} \cdot \int_{-\infty}^{+\infty} F(s) \cdot e^{-j2\pi \cdot f \cdot s} \cdot ds = \tag{2-73}$$

$$H_{SHIFT}(f) = e^{-j2\pi \cdot f \cdot t_0} \cdot H_{ORI}(f) \tag{2-74}$$

In summary, expression (2-74) shows that a phase shift in the modulation profile does not change the harmonic amplitudes but the harmonic phases. In other words, spectral power distribution of a frequency modulated waveform is independent on the absolute phase of the modulating waveform. As it is only of interest the magnitude of the harmonics, no care must be taken respect to the modulation profile phase.

2.2.3.4 Influence of the frequency peak deviation Δf_c defined by the modulation profile

As exposed later on, a step-down power converter was selected for experimental measurements (see Figure 2-14). Although the following comments are of general application, a focus on this topology is preferred in order to make the concept understanding easier.

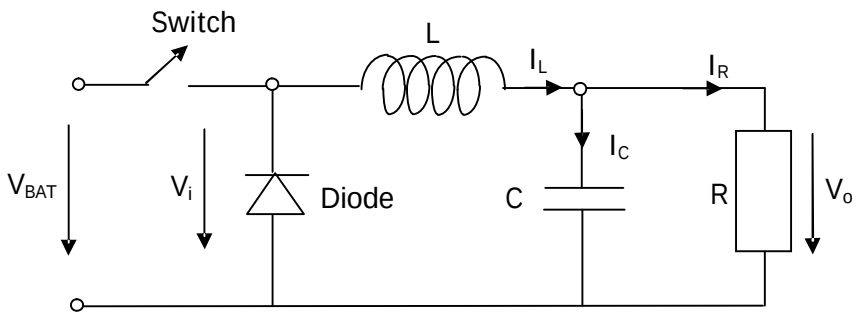

Figure 2-14. Step-down power converter

Anyway, one important influence of the modulation profile is related to the maximum peak excursion of the switching frequency Δf_c respect to the initially constant carrier

frequency. As a general asseveration, a power converter consists of a low-pass filter whose function is to filter out the whole ac components coming after the switch, thus allowing only the dc component to flow across the load resistor. For a step-down power converter, a LC filter is implemented. The cut-off frequency of this filter establishes approximately the minimum high-frequency being rejected. For a constant switching frequency, no problem is normally found and only the dc component flows across the load resistor but, during the frequency modulation process, switching frequency can fall beyond the cut-off frequency, then transmitting this low frequency immediately to the load resistor, making the output voltage V_o oscillate, which is unacceptable.

For the following analysis of converter in Figure 2-14, phasorial magnitudes are to be considered:

$$\vec{V_i} - \vec{V_o} = j \cdot \omega \cdot L \cdot \vec{I_L} \tag{2 -52}$$

$$\vec{I_L} = \vec{I_C} + \frac{\vec{V_o}}{R} \tag{2 -53}$$

$$\vec{V_o} = \frac{1}{j \cdot \omega \cdot C} \cdot \vec{I_C} \tag{2 -54}$$

From the previous equations, the following gain is obtained:

$$\frac{\vec{V_o}}{\vec{V_i}} = \frac{1}{1 - \omega^2 \cdot L \cdot C + j \cdot \omega \cdot \frac{L}{R}} \tag{2 -55}$$

It is only of interest the module of these phasorial magnitudes, what it is obtained by extracting the module of the previous expression, yielding the following relationship:

$$\frac{V_o}{V_i} = \frac{1}{\sqrt{\left(1 - \omega^2 \cdot L \cdot C\right)^2 + \left(\omega \cdot \frac{L}{R}\right)^2}} \tag{2 -56}$$

The following inductor, capacitor and resistor values (the ones finally defined in point 4.1 after the power converter design considerations) are assumed: L = 350 μH; C= 2.2 μF and R = 20 Ω. The graphical representation of expression (2-56) is shown in Figure 2-15.

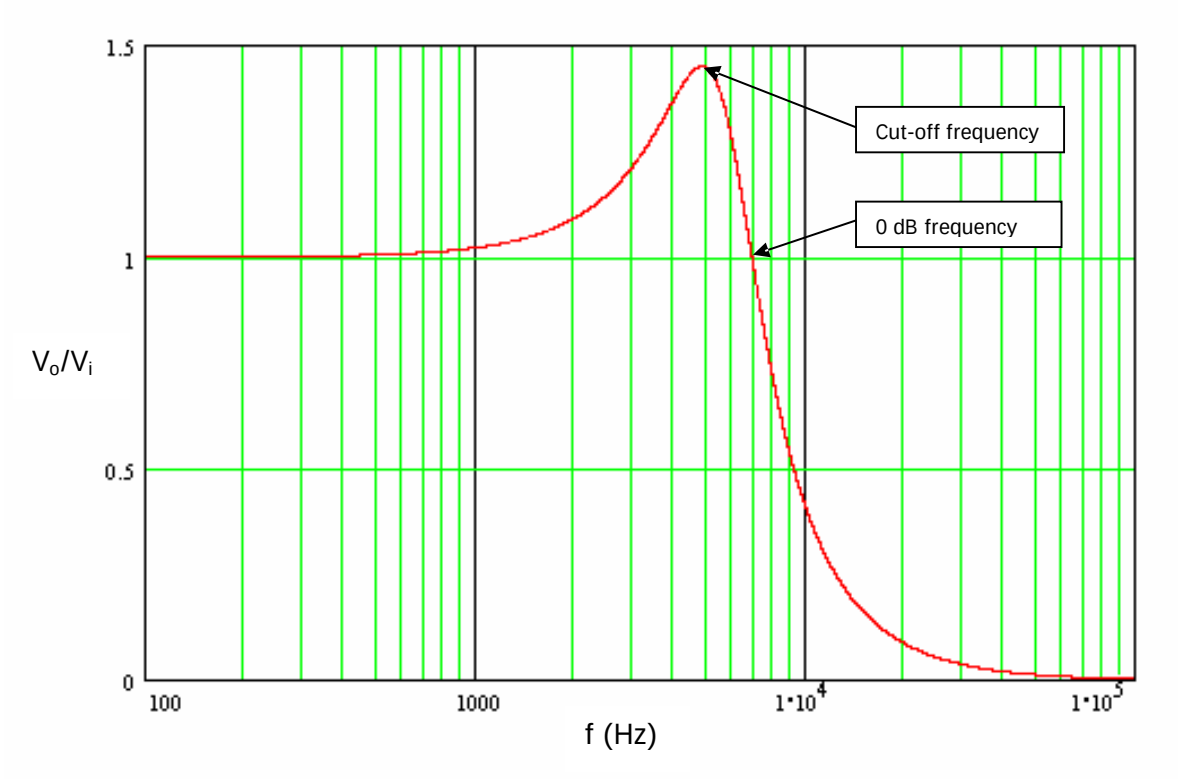

Figure 2-15. Bode diagram of a LC filter

The damping rate of the ideal LC filter is 40 dB and the cut-off frequency becomes $f_{cut-off} = \frac{1}{2 \cdot \pi \cdot \sqrt{L \cdot C}}$. For the selected component values above, the cut-off frequency is $f_{cut-off} = 5.736\, kHz$. Frequencies higher than ≈30 kHz are completely filtered out while those frequencies lower than the cut-off frequency go across the system with no attenuation. And this is really the problem. If a modulation system itself is able to generate switching frequencies lower than the cut-off frequency, oscillations are to appear at the output voltage. Frequencies inside the side-band harmonics bandwidth resulting from the modulation process must be filtered out by the low-pass filter. Normally, this bandwidth (given by the Carson's rule) is approximated to $2 \cdot \Delta f_c$ around the carrier (switching) frequency f_c and the minimum frequency present is given by $f_c - \Delta f_c$. Therefore, inferior limit of the peak switching frequency deviation (respect to the central frequency) is given by the cut-off frequency of the LC filter, that is, $f_c - \Delta f_c > f_{cut-off}$, what must be taken into account when selecting a certain modulation profile and its related parameters.

2.2.3.5 Influence of a modulation profile with a certain average value

Another point of interest is related to the symmetrical aspect of the modulating waveform $\bar{v}_m(t)$. If the modulation profile $\bar{v}_m(t)$ is an odd function, a symmetrical side-band harmonics distribution is expected (for instance, as in Figure 2-12). But what happens when $\bar{v}_m(t)$ is not an odd function thus giving an average value of $\bar{v}_m(t) \neq 0$ during the modulating period T_m? It is clear that the final aspect of the side-band harmonics can take whichever distribution depending on the shape of the modulating waveform because it is this last which establishes the final shape of the side-band harmonics. But which average frequency, equivalent to a constant switching frequency, is to be found when the average value of the modulating waveform is not zero?

In frequency modulation, deviation $\delta\omega(t)$ is supposed to be proportional to the modulating signal voltage $v_m(t)$, that is:

$$\delta\omega(t) = \omega(t) - \omega_c = k_\omega \cdot v_m(t) \tag{2-57}$$

where k_ω is a sensitivity factor of the modulator expressed in rad/sec/V or Hz/V, ω_c is the carrier pulsation and $\omega(t)$ is the instantaneous pulsation. Instantaneous frequency of the modulated signal is derived directly from expression (2-57), yielding the following equation (2-58):

$$f(t) = f_c + \frac{k_\omega}{2 \cdot \pi} \cdot v_m(t) \tag{2 -58}$$

Once obtained the instantaneous frequency f(t), the instantaneous period T(t) is the inverse of f(t), that is,

$$T(t) \cdot f(t) = 1 \tag{2 -59}$$

The average value of instantaneous frequency f(t) is directly related to the average value of the modulation profile, shown in expression (2-58). The relationship between average frequency $\bar{f}$ and average period $\overline{T}$ is developed onwards:

$$\overline{T} \cdot \bar{f} = \overline{T} \cdot \frac{1}{T_m} \cdot \int_0^{T_m} f(t)dt = \tag{2 -60}$$

Average period $\overline{T}$ is a constant value which can be introduced into the integral:

$$= \frac{1}{T_m} \cdot \int_0^{T_m} \overline{T} \cdot f(t) \cdot dt = \quad (2\text{-}61)$$

But $\overline{T}$ also has its own expression similar to $\bar{f}$ in expression (2-60):

$$= \frac{1}{T_m} \cdot \int_0^{T_m} \left(\frac{1}{T_m} \cdot \int_0^{T_m} T(t) \cdot dt \right) \cdot f(t) \cdot dt = \quad (2\text{-}62)$$

Applying the properties of the double integral, expression (2-62) can be also expressed as follows:

$$\overline{T} \cdot \bar{f} = \frac{1}{T_m^2} \cdot \int_0^{T_m} \int_0^{T_m} T(t) \cdot f(t) \cdot dt \cdot dt = \quad (2\text{-}63)$$

Direct application of expression (2-59) in equation (2-63) yields the following result:

$$= \frac{1}{T_m^2} \cdot \int_0^{T_m} \int_0^{T_m} 1 \cdot dt \cdot dt = \frac{1}{T_m^2} \cdot T_m \cdot T_m = 1 \quad (2\text{-}64)$$

In other words,

$$\overline{T} \cdot \bar{f} = 1 \quad (2\text{-}65)$$

Thus, the average period of a modulated waveform is exactly the inverse of the average frequency and, therefore, depends inversely on the average value of the modulation profile.

If the average voltage of the modulation profile is zero, the average value of instantaneous frequency is f_c (according to expression (2-58)) and, therefore, the average period is $T_c = 1/f_c$ or, in other words, this is the expected value if no modulation is present and a constant switching frequency $f_c = 1/ T_c$ rules the system.

In the case of an average voltage of the modulation profile different of zero, it corresponds to an equivalent constant switching frequency higher or lower than the central frequency f_c.

Just as an example, let's consider a half-sinusoidal modulation profile $v_m(t)$ in Figure 2-16 and the following parameters of modulations: f_c = 200 kHz, T_m = 50 µs, $k_\omega = 2 \cdot \pi \cdot 20$ kHz/V, V_m = 1 V.

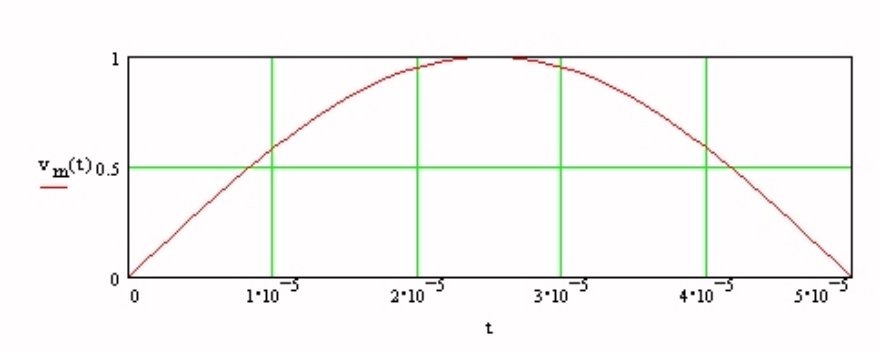

Figure 2-16. Half-sinusoidal modulation profile

The instantaneous frequency corresponding to the modulated waveform is calculated by using expression (2-58) and the resulting plot is shown in Figure 2-17.

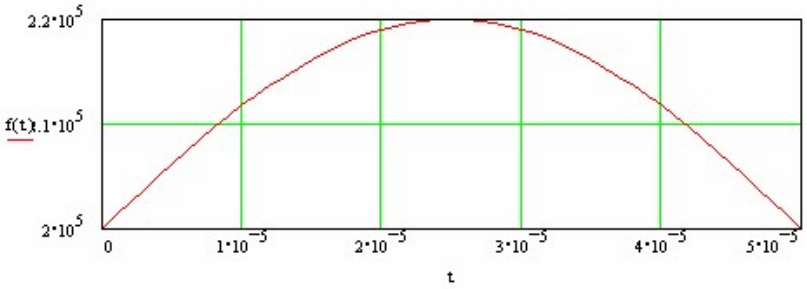

Figure 2-17. Instantaneous frequency of the modulated waveform

The average value of this instantaneous frequency is 212.732 kHz, that is, 12.732 kHz over the carrier frequency.

Finally, the instantaneous period T(t) = 1/ f(t) is plotted in Figure 2-18.

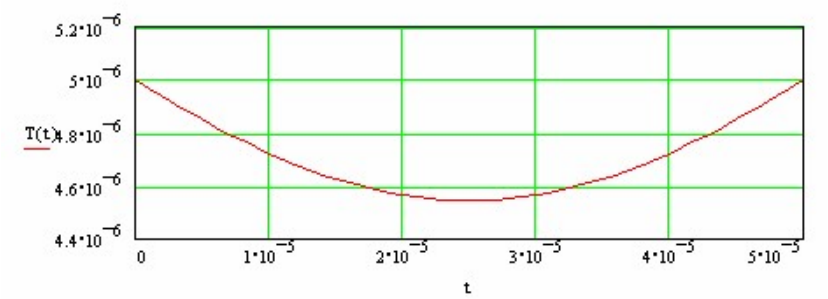

Figure 2-18. Instantaneous period of the modulated waveform

The average value of this instantaneous period is 4.7075 μs, that is, 0.293 μs under the carrier signal period. Of course, the relationship $\overline{T} \cdot \overline{f} = 1$ is accomplished (4.7075 μs · 212.732 kHz = 1).

2.3 Computation of Frequency Modulation (SSCG) by means of a MATLAB algorithm

Theoretical basis of the thesis is completely based on the fundaments of the Fourier Transform and the related computational algorithm is a particular implementation of the Fast Fourier Transform (FFT). Readers are kindly referred to Annex 3, where main concepts of the Fourier Transform are explained.

The computational algorithm hereby developed is intended to carry out two main functions:

- Generating any frequency modulation of a sinusoidal carrier. These results are also valid for any generic carrier, as square clocks signals in digital devices, PWM signals controlling the switching power converters or trapezoidal signals in digital communication systems, as explained in clause 2.1.3. This modulation data are not only valid for the theoretical calculation of the resulting spectra after modulation but also for obtaining a data set to be introduced into the arbitrary function generator, as presented in chapter 1.
- Obtaining the theoretical spectral components resulting from the frequency modulation process.

This algorithm was developed for a MATLAB environment, thus, some particularities more must also been taken into account.

2.3.1 Considerations to apply FFT correctly to the MATLAB algorithm

The mathematical calculation of the frequency spectra by means of the FFT shows some difficulties to obtain accurate and correct results. Although some of them have been already presented, a complete view of the exigencies are shown onwards. The Matlab algorithm here developed matches all these points.

1. As exposed in A.3.2 (Annex 3), the discrete Fourier transform is expressed as follows:

$$H(\frac{n}{NT}) = T \cdot \sum_{k=0}^{N-1} h(kT) \cdot e^{-j \cdot 2 \cdot \pi \cdot n \cdot k / N} \qquad n = 0, 1, \text{L}, N-1 \qquad \text{(2-66)}$$

where T is the sampling period (time domain) and N is the number of equidistant samples inside the truncation interval T_0, equated to the modulating period $T_m = 1/f_m$.

The key-point of the discrete Fourier transform (DFT) (and, consequently, of the FFT) is that the result matches exactly the one given by the continuous Fourier transform just preserving the following conditions:

- The time function h(t) must be periodic.
- h(t) must be band-limited. An FM signal actually contains an infinite number of side frequencies besides the carrier and therefore occupies infinite bandwidth. However, the side frequencies quickly decrease in strength and can be considered negligible at some point. In practice, a tradeoff between bandwidth and distortion must be considered. The bandwidth of a frequency modulated waveform is approximately given by the Carson's rule.
- the sampling rate must be at least two times the largest frequency component of h(t) è Nyquist's theorem.
- the truncation function x(t) must be non-zero over exactly one period (or integer multiple period) of h(t).

DFT assumes that the waveform sampled during this sampling time of T (the period of the signal) repeats itself down- and upwards indefinitely.

2. SSCG techniques are based on modulating the frequency of a carrier signal by following a selected modulation profile. The waveform resulting from this modulation process is a periodic signal whose frequency equates the frequency of the modulating signal (f_m), that is, the modulation profile. This is easy to understand taking into account that the carrier signal frequency is constantly varying, following the modulation profile, but showing the same value of frequency (normally the carrier signal frequency) both at the beginning and at the end of the complete cycle of variation through the modulation profile. This way, it is obtained a modulated waveform which repeats itself indefinitely with a period of$1/f_m$.

   Expressed in equation form:

   - Carrier signal è $F_c(t) = F_c^0 \cdot \sin(2 \cdot \pi \cdot f_c \cdot t)$

- Modulating signal è $F_m(t) = f\left(F_m^0, f_m, t\right)$
- Modulated signal è $F(t) = f(F_c, F_m, t)$

3. As exposed in point 1) above, the way of working corresponding to the FFT algorithm consists of selecting a truncation window and supposing that the data contained inside this window repeats itself indefinitely in time, thus becoming this window the period of the signal. If this truncation window is not selected in a proper way, for instance, choosing a window a little larger or shorter than the period of the original signal (or an integer value of it), a discontinuity is to be appear between the adjacent periods. This discontinuity in the time domain is also shown in the frequency domain, where fine theoretical spectral lines (representing the true harmonics of the signal) spread over a series of wider lobes. This effect is known in the technical literature as spectral leakage. These frequencies or lobes do not exist in the original signal; they are just the result of either an incorrect application of the analysis methods or the own limitations of these methods. Regarding the Matlab algorithm here developed, as the period of the modulated signal is perfectly known and equal to the modulating frequency fm, a truncation window of T_0 = 1/fm is to be selected in order not to have any problems and it is a condition included in the Matlab algorithm. Resolution or distance F in frequency domain between two consecutive samples is given by the following expression (directly derived form equation 2-66):

$$F = \frac{1}{N \cdot T} = \frac{1}{T_0} \tag{2-67}$$

where T is the sampling period (time domain) and N is the number of equidistant samples inside the truncation interval T_0.

The selected resolution F will be therefore f_m, that is, $F = f_m = \frac{1}{N \cdot T} = f_s \cdot N$

where f_s is the sampling frequency.

4. In order to rebuild a sampled waveform without losing any information, the Nyquist's theorem establishes that the sampling frequency must be, at least, twice the largest frequency composing the original waveform. Besides, the Carson's rule (valid for any angle modulated waveform) specifies that the harmonic spectra resulting from modulating a sinusoidal signal are included inside a bandwidth B_h

given by de following expression (for the 98% of the total energy of the original signal):

$$B_h = 2 \cdot f_m \cdot (1 + h \cdot m_f) \quad (2\text{-}68)$$

$$m_f = \frac{\Delta f_c}{f_m} \quad (2\text{-}69)$$

where:

- h is the harmonic order of the non-modulated signal
- f_m is the frequency of the modulating waveform
- m_f is the modulation index
- Δf_c is the peak frequency deviation of the modulated signal

Supposing this bandwidth to be symmetrically distributed around the non-modulated harmonic f_h, the maximum frequency f_{max} of the modulated waveform can be approximately expressed as follows:

$$f_{\max} = f_h + \frac{B_h}{2} \quad (2\text{-}70)$$

Thus, the sampling frequency f_s must meet the following expression:

$$f_s \geq 2 \cdot f_{\max} = 2 \cdot f_h + B_h = 2 \cdot (f_h + f_m + h \cdot \Delta f_c) \quad (2\text{-}71)$$

(Substitute h=1 and $f_h=f_c$ for the first harmonic of the non-modulated signal)

5. The number of samples N must be a power of 2, that is, $N = 2^k$ where k is a natural number. This aspect improves the efficiency of the FFT which is normally expressed in terms of number of complex multiplications. As said before, a conventional DFT needs approximately a number of N^2 complex multiplications, while for a FFT, a number of $N \cdot \log_2 N$ is typical. As an example, a sampling process with N = 1024 leads to 10,240 multiplications for FFT in front of the 1,048,576 multiplications necessaries when computing a conventional DFT.
6. The FFT algorithm returns a total number of N points but only the N/2 first ones are of interest because the rest N/2 points are symmetrical respect to the first ones.

7. The particular frequency of a generic point k from the FFT algorithm is expressed as follows:

$$f_k = k \cdot \frac{f_s}{N} \qquad (2\text{-}72)$$

From the last point 6), it can be derived that the maximum generic frequency f_k which is able to be displayed corresponds to $k = N/2$ or, in other terms, to a frequency of $f_s/2$.

2.3.2 Mathematical formulation of FM applied to different modulation profiles

The generic expression of an angle modulated sinusoidal signal responds to the following equation:

$$F(t) = A(t) \cdot \cos[\omega_c \cdot t + \Theta(t)] \qquad (2\text{-}73)$$

where:

- A(t) is a time-dependant amplitude.
- f_c (or, ω_c) is the frequency of the unmodulated signal (or carrier).
- Θ(t) is the time-dependant phase.

In the particular case of a frequency modulation, the amplitude A(t) is a constant value A in the time domain while the phase value varies in the following way:

$$\Theta(t) = \int_0^t k_\omega \cdot v_m(t) \cdot dt + \Theta(0) \qquad (2\text{-}74)$$

where:

- $v_m(t)$ is the modulating signal (normally, a periodic wave of frequency f_m)
- k_ω is a sensibility factor controlling the carrier frequency deviation as follows: $\delta\omega(t) = k_\omega \cdot v_m(t)$
- Θ(0) is the initial variable-phase value (normally, it is taken as zero).

Thus, once the profile or modulating signal equation $v_m(t)$ is selected, its integration, according to expression (2-74), yields a variable angle $\Theta(t)$ which, in summary, produces the variation of the instantaneous carrier frequency

Two working hypotheses are of application in the whole further calculations:

- $\Theta(0) = 0$. This particularity does not subtract any generality to the resulting expression because it would only affect the absolute position of the window generated by the modulation of the original carrier but not to the relative distribution of the side-band harmonics inside this window (as demonstrated in clause 2.2.3.3).
- Defining V_m as the peak value of the modulating signal $v_m(t)$, the product $k_\omega \cdot V_m$ expresses the maximum peak deviation of the pulsation $\omega(t)$ respect to the central pulsation ω_c, that is:

$$k_\omega \cdot V_m = 2 \cdot \pi \cdot \Delta f_c = \Delta \omega_c \tag{2-75}$$

2.3.2.1 Sinusoidal modulation profile

In this kind of modulation, the expression that rules this profile is:

$$v_m(t) = V_m \cdot sin(2 \cdot \pi \cdot f_m \cdot t) \tag{2-76}$$

Applying the profile (2-76) into the equation (2-74), it is obtained:

$$\Theta(t) = \int_0^t k_\omega \cdot v_m(t) \cdot dt \tag{2-77}$$

$$\Theta(t) = \int_0^t k_\omega \cdot V_m \cdot sin(2 \cdot \pi \cdot f_m \cdot t) \cdot dt \tag{2-78}$$

Integration of the equation (2-78) yields the following result:

$$\Theta(t) = \frac{k_\omega \cdot V_m}{2 \cdot \pi \cdot f_m} \cdot [1 - \cos(2 \cdot \pi \cdot f_m \cdot t)] \tag{2-79}$$

Applying expression (2-75) into the equation (2-79), a more useful equation is to be obtained:

$$\Theta(t) = \frac{\Delta f_c}{f_m} \cdot [1 - \cos(2 \cdot \pi \cdot f_m \cdot t)] \tag{2-80}$$

In most bibliographic references, the following definition can be found:

$$m_f = \frac{\Delta f_c}{f_m} \tag{2-81}$$

where m_f is called as frequency modulation index, and applied to (2-80) yields the well-known expression (2-82):

$$\Theta(t) = m_f \cdot \left[1 - \cos\left(2 \cdot \pi \cdot f_m \cdot t\right)\right] \tag{2-82}$$

The modulating profile (2-76) responds to a sine function. In case of using the cosine profile in (2-83), equation (2-82) would take the following aspect (2-84):

$$v_m(t) = V_m \cdot \cos(2 \cdot \pi \cdot f_m \cdot t) \tag{2-83}$$

$$\Theta(t) = m_f \cdot sin\left(2 \cdot \pi \cdot f_m \cdot t\right) \tag{2-84}$$

It is important to notice that power distribution of the spectra corresponding to an angle-modulated waveform (both frequency and phase modulation) is independent on the absolute phase of the modulating signal. Thus, and apart from the apparent difference between (2-82) and (2-84), the result of modulation will be absolutely the same independently on using a sine or cosine function for $v_m(t)$.

As an example, Figure 2-19 is included, representing a sine modulation profile $v_m(t)$ and its time integral $\Theta(t)$ (A = 0.5 V, f_c = 120 kHz, δ = 1, f_m = 20 kHz).

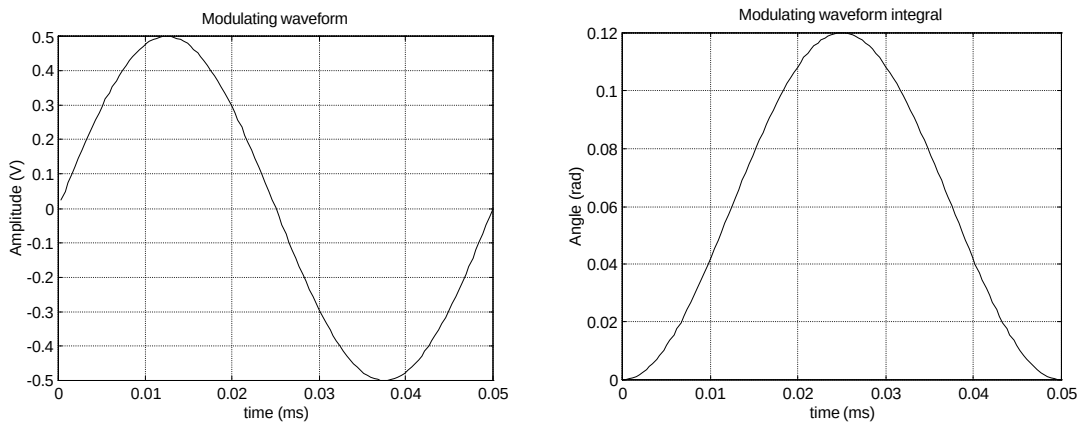

(a) (b)

Figure 2-19. (a) Sinusoidal modulating profile and (b) its variable-phase angle

2.3.2.2 Triangular modulation profile

The triangular modulation profile consists of three trams, each one defined by an equation as shown below (Figure 2-20):

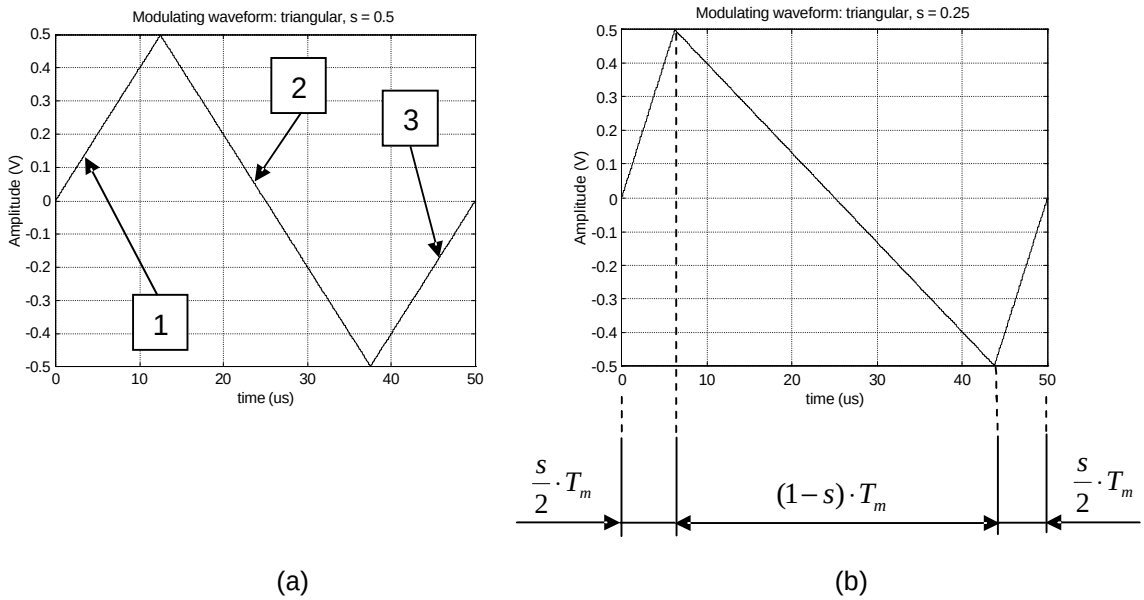

Figure 2-20. (a) Triangular modulating profiles: (a) symmetrical and (b) sawtooth type

Parameter s controls the position of the vertex of the triangular waveform from 0 to $T_m/2$, thus making the implementation of profiles such a sawtooth waveform very easy. Parameter s can range from 0 to 1, and, for a classical triangular profile, s = 0.5.

TRAM 1: Valid for t where $0 \le t < s \cdot \frac{T_m}{2}$

The expression for the modulating profile along this tram 1 is:

$$v_m(t) = V_m \cdot f_m \cdot \frac{2}{s} \cdot t \qquad (2\text{-}85)$$

Applying the profile (2-85) to the equation (2-74) and making the integration, the following result is obtained:

$$\Theta^{(1)}(t) = 2 \cdot \pi \cdot \Delta f_c \cdot \frac{f_m}{s} \cdot t^2 \qquad (2\text{-}86)$$

TRAM 2: Valid for t where $s \cdot \frac{T_m}{2} \le t < \left(1 - \frac{s}{2}\right) \cdot T_m$

Again, the expression for the modulating profile along this tram 2 is:

$$v_m(t) = \frac{V_m}{(1-s)} \cdot (1 - 2 \cdot f_m \cdot t) \tag{2-87}$$

Just for convenience, equation (2-74) is presented in such a way that it also reflects the previous trams:

$$\Theta(t) = \int_0^t k_\omega \cdot v_m(t) \cdot dt \tag{2-88}$$

$$\Theta(t) = \int_0^{s \cdot T_m/2} k_\omega \cdot v_m(t) \cdot dt + \int_{s \cdot T_m/2}^{t} k_\omega \cdot v_m(t) \cdot dt \tag{2-89}$$

or, in other terms:

$$\Theta(t) = \Theta^{(1)}\left(s \cdot \frac{T_m}{2} \right) + \int_{s \cdot T_m/2}^{t} k_\omega \cdot v_m(t) \cdot dt \tag{2-90}$$

Resolving the integral in (2-90), the following result is obtained:

$$\Theta^{(2)}(t) = \Theta^{(1)}\left(s \cdot \frac{T_m}{2} \right) + 2 \cdot \pi \cdot \Delta f_c \cdot \frac{1}{(1-s)} \cdot \left[- f_m \cdot t^2 + t + \frac{s}{2 \cdot f_m} \cdot \left(\frac{s}{2} - 1 \right) \right] \tag{2-91}$$

TRAM 3: Valid for t where $\left(1 - \frac{s}{2}\right) \cdot T_m \le t < T_m$

Finally, the expression for the modulating profile along this tram 3 is:

$$v_m(t) = \frac{2}{s} \cdot V_m \cdot \left(f_m \cdot t - 1 \right) \tag{2-92}$$

As in (2-89) and after integration, the expression of the variable-phase angle is as follows:

$$\Theta^{(3)}(t) = \Theta^{(2)}\left(\left[1 - s/2 \right] \cdot T_m \right) + 2 \cdot \pi \cdot \Delta f_c \cdot \frac{1}{s} \cdot \left[f_m \cdot t^2 - 2 \cdot t + \left(1 - \left(\frac{s}{2} \right)^2 \right) \cdot \frac{1}{f_m} \right] \tag{2-93}$$

As an example, integrals Θ(t) (A = 0.5 V, f_c = 120 kHz, δ = 1, f_m = 20 kHz) are included in Figure 2-21, corresponding to the triangular profiles in Figure 2-20.

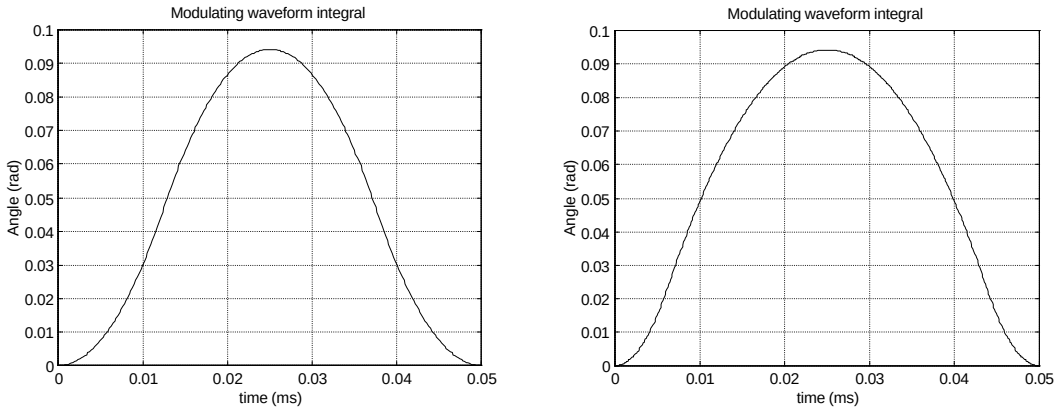

(a) s = 0.5 (b) s = 0.25

Figure 2-21. Variable-phase angle of waveforms in Fig. 2-20(a) and (b), respectively

2.3.2.3 Exponential modulation profile

The exponential modulation can be expressed as a waveform consisting of four trams, each one defined by its corresponding analytical equation. The four trams are shown in Figure 2-22.

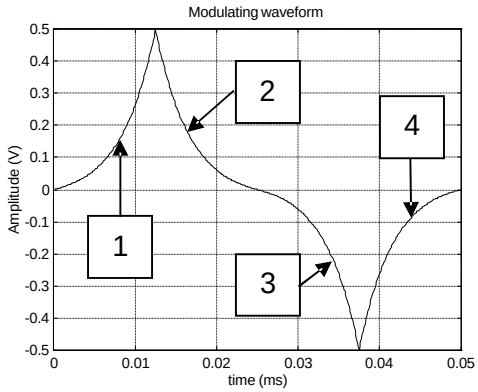

Figure 2-22. Exponential modulating profiles

Onwards, a more detailed description of each tram is to be developed, focusing specific attention on the different parameters describing this profile.

TRAM 1: Valid for t where $0 \le t < \frac{T_m}{4}$

Analytical expression for this tram can be expressed by means of the following equation:

$$v_m(t) = V_m \cdot \frac{1}{e^{\frac{p}{4 \cdot f_m}} - 1} \cdot \left(e^{p \cdot t} - 1\right) \qquad (2\text{-}94)$$

Parameter p is a very helpful factor because it defines exactly not only the higher or lower curvature of the exponential profile but also its concavity or convexity. In summary, the following behaviour is derived from (2-94) and it is shown in Figure 2-23:

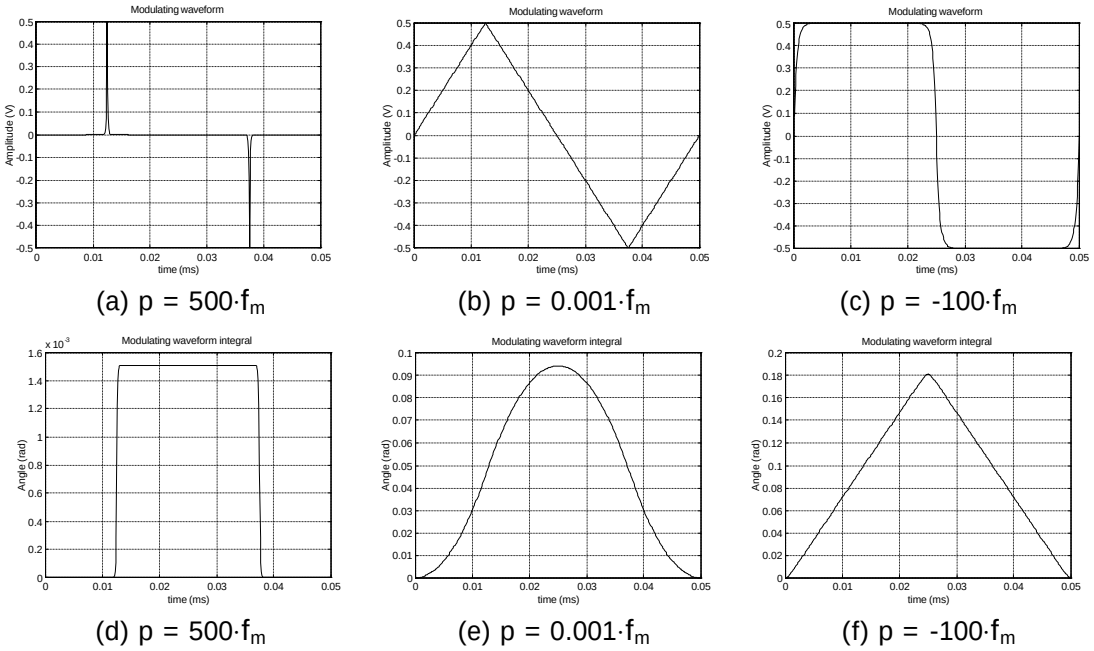

(a) p = 500·f_m (b) p = 0.001·f_m (c) p = -100·f_m

(d) p = 500·f_m (e) p = 0.001·f_m (f) p = -100·f_m

Figure 2-23. (a), (b) and (c): Different representations of an exponential profile as a function of parameter p and its corresponding variable-phase angle (d), (e) and (f), respectively. (f_c = 120 kHz, δ% = 1%, f_m = 20 kHz)

It is more useful to declare this parameter as a function of the modulating frequency, that is, $p = k \cdot f_m$, where k is the concavity factor. Three combinations of k are possible:

- k > 0 è Exponential profile with concave curvature. Graphically, the curve line is always placed below the one corresponding to the triangular profile (with s = 0.5). Its larger or smaller curvature is defined by the value of k, in such a way that values nearer to zero are to produce practically triangular profiles, while higher values (k >> 100) are to produce narrower and narrower pulses (see Figure 2-23 (a)).
- k = 0 è Exponential profile with zero curvature, that is, the curve line matches exactly the one corresponding the triangular profile (see Figure 2-23 (b)).
- k < 0 è Exponential profile with convex curvature. Graphically, the curve keeps always placed above the one corresponding to the triangular profile (with s = 0.5).

In the same way as in k > 0, larger or smaller curvatures are defined by the value k, where values nearer to zero are to produce again practically triangular profiles and higher values (|k| >> 100) are to produce nearly rectangular profiles, as shown in Figure 2-23 (c).

Substituting profile equation (2-94) into expression (2-74) and integrating yields the following result

$$\Theta^{(1)}(t) = 2 \cdot \pi \cdot \Delta f_c \cdot \frac{1}{p \cdot \left(e^{p/4 \cdot f_m} - 1 \right)} \cdot \left(e^{p \cdot t} - p \cdot t - 1 \right) \tag{2-95}$$

TRAM 2: Valid for t where $\frac{T_m}{4} \le t < \frac{T_m}{2}$

The modulating profile equation corresponding to this tram 2 can be expressed as follows:

$$v_m(t) = V_m \cdot \frac{1}{\left(e^{p/4 \cdot f_m} - 1 \right)} \cdot \left(e^{p/2 \cdot f_m} e^{-p \cdot t} - 1 \right) \tag{2-96}$$

Again, making the integration of the modulating profile expressed in (2-96) following the expression (2-74) and applying the separation of the total integral into two partial ones (as it was done with the triangular profile), the following expression (2-99) results:

$$\Theta(t) = \int_0^t k_\omega \cdot v_m(t) \cdot dt \tag{2-97}$$

$$\Theta(t) = \int_0^{T_m/4} k_\omega \cdot v_m(t) \cdot dt + \int_{T_m/4}^t k_\omega \cdot v_m(t) \cdot dt \tag{2-98}$$

$$\Theta^{(2)}(t) = \Theta^{(1)}\left(T_m/4 \right) + 2 \cdot \pi \cdot \Delta f_c \cdot \frac{1}{p \cdot \left(e^{p/4 \cdot f_m} - 1 \right)} \left\{ -e^{-p \cdot t} \cdot e^{p/2 \cdot f_m} + e^{p/4 \cdot f_m} - p \cdot t + \frac{p}{4 \cdot f_m} \right\}$$

(2-99)

TRAM 3: Valid for t where $\frac{T_m}{2} \le t < 3 \cdot \frac{T_m}{4}$

The modulating profile equation corresponding to this tram 3 can be expressed as follows:

$$v_m(t) = V_m \cdot \frac{1}{e^{p/4 \cdot f_m} - 1} \cdot \left(1 - e^{-p/2 \cdot f_m} e^{p \cdot t}\right) \quad (2\text{-}100)$$

Again, integrating the modulating profile expressed in (2-100) following the expression (2-74) and applying the separation of the total integral into two partial ones, the following expression (2-103) is obtained:

$$\Theta(t) = \int_0^t k_\omega \cdot v_m(t) \cdot dt \quad (2\text{ -}101)$$

$$\Theta(t) = \int_0^{T_m/2} k_\omega \cdot v_m(t) \cdot dt + \int_{T_m/2}^t k_\omega \cdot v_m(t) \cdot dt \quad (2\text{ -}102)$$

$$\Theta^{(3)}(t) = \Theta^{(2)}\left(T_m/2\right) + 2 \cdot \pi \cdot \Delta f_c \cdot \frac{1}{p \cdot \left(e^{p/4 \cdot f_m} - 1\right)} \left\{ -e^{p \cdot t} \cdot e^{-p/2 \cdot f_m} + p \cdot t - \frac{p}{2 \cdot f_m} + 1 \right\}$$

(2-103)

TRAM 4: Valid for t where $3 \cdot \frac{T_m}{4} \le t < T_m$

The modulating profile equation corresponding to this tram 4 can be expressed as follows:

$$v_m(t) = V_m \cdot \frac{1}{\left(e^{p/4 \cdot f_m} - 1\right)} \cdot \left(1 - e^{p/f_m} e^{-p \cdot t}\right) \quad (2\text{ -}104)$$

As above, the integration of the modulating profile expressed in (2-104) following the expression (2-74) and the separation of the total integral into two partial ones yields the following expression (2-107):

$$\Theta(t) = \int_0^t k_\omega \cdot v_m(t) \cdot dt \quad (2\text{ -}105)$$

$$\Theta(t) = \int_0^{3 \cdot T_m/4} k_\omega \cdot v_m(t) \cdot dt + \int_{3 \cdot T_m/4}^t k_\omega \cdot v_m(t) \cdot dt \quad (2\text{ -}106)$$

$$\Theta^{(4)}(t) = \Theta^{(3)}\left(3 \cdot {T_m}/{4}\right) + 2 \cdot \pi \cdot \Delta f_c \cdot \frac{1}{p \cdot \left(e^{{p}/{4 \cdot f_m}} - 1\right)} \left\{ e^{-p \cdot t} \cdot e^{{p}/{f_m}} - e^{{p}/{4 \cdot f_m}} + p \cdot t - \frac{3}{4} \cdot \frac{p}{f_m} \right\}$$

(2-107)

The final results of these time-varying angles are shown graphically in Figure 2-23 (d), (e) and (f) corresponding to their respective modulating waveforms in Figure 2-23 (a), (b) and (c) (carrier and modulating signal values are f_c = 120 kHz, δ% = 1%, f_m = 20 kHz).

2.3.2.4 Discrete modulation profile

Apart from those modulation profiles which are likely to be expressed in an analytical way, as the previous sinusoidal, triangular and exponential waveforms, it is very appreciated to have the possibility to test any modulating waveforms, even those which are difficult, when not impossible, to be expressed into an equation.

Figure 2-24 shows a modulating waveform and the whole parameters defining the discretization process. Although the waveform below represents a symmetrical profile, expressions and conclusions hereby developed are of generic validity; the only condition is that the modulation profile in Figure 2-24 must be a complete period of the modulating signal.

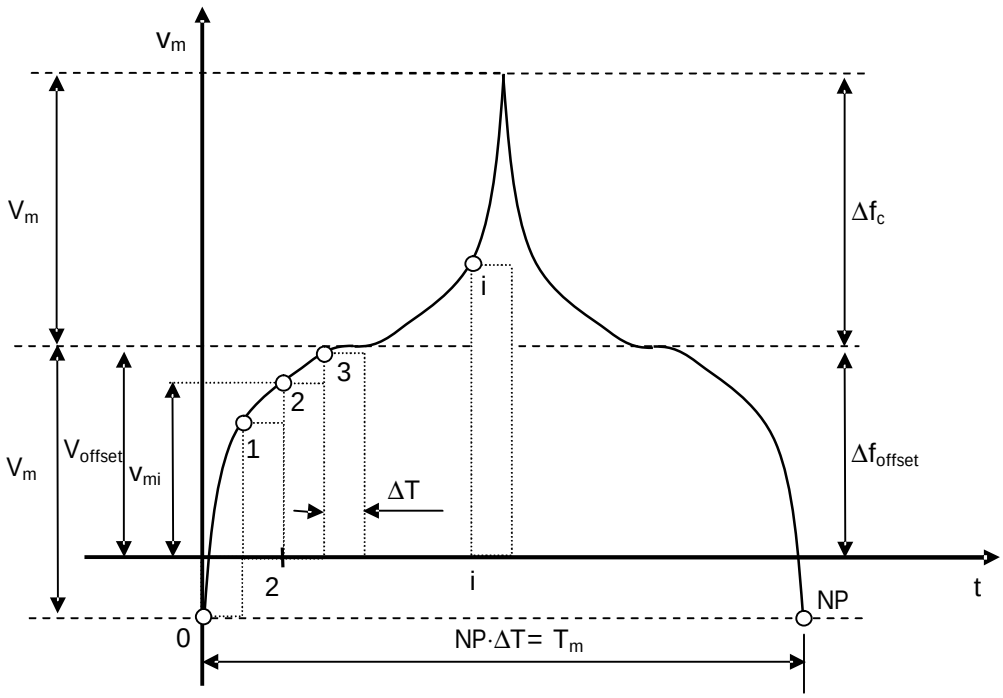

Figure 2-24. Discretization of a modulation profile

Obviously, the discrete modulation profile will be a set of couples (v_{mi} , i) resulting from a sampling process. A more detailed description of these parameters comes below:

- NP is the total number of points or samples corresponding to a period T_m (or $1/f_m$) of the modulating waveform $v_m(t)$.
- ΔT is the spacing in the time domain between two consecutive samples and corresponds to the period of the sampling signal of frequency f_s, that is, $\Delta T = \frac{1}{f_s}$.

  Another useful expression can be derived from the NP definition:

$$\Delta T = \frac{T_m}{NP} \tag{2-108}$$

- The couple (v_{mi}, i) represents the sampled value of the modulating profile [v_{mi}] at the time corresponding to i. Pay attention to the fact that i is not a time value but a sample number, ranging from 0 to NP-1.
- V_{offset}, V_m è V_{offset} represents a reference position of the whole waveform referred to the horizontal axis and it is normally used to generate down- or up-spreading modulation techniques. V_{offset} is selected in such a way that the same signal excursion down and upwards is obtained. For a symmetrical shifting of the carrier frequency above and below, V_{offset} must be zero with V_m giving the maximum peak deviation carrier frequency as follows (from clause 2.1.1.1):

$$\delta\omega(t) = k_\omega \cdot v_m(t) \tag{2-109}$$

  and then,

$$\Delta\omega_c = k_\omega \cdot V_m \tag{2-110}$$

As defined in clause 2.1.1.1, the time-varying angle Θ(t) is expressed as follows:

$$\Theta(t) = \int_0^t k_\omega \cdot v_m(t) \cdot dt \tag{2-111}$$

Expression (2-111) can be easily translated in order to accept a sampled waveform (from Figure 2-24):

$$\Theta(i) = k_\omega \cdot \sum_{j=0}^{i-1} v_{mj} \cdot \Delta T \tag{2-112}$$

For convenience, a normalized profile $\bar{v}_{mi}$ is to be used instead of the nominal one,

$$v_{mi} = V_m \cdot \bar{v}_{mi} + V_{offset} \tag{2-113}$$

where a symmetrical profile ($V_m = V_{m1} = V_{m2}$) has been used. This mathematical simplification resulting from applying a symmetrical profile does not eliminate the generality of this discussion but makes the analytical expressions easier to understand. Thus, substituting expression (2-113) into the equation (2-112) yields the following result:

$$\Theta(i) = k_\omega \cdot \sum_{j=0}^{i-1} V_m \cdot \bar{v}_{mj} \cdot \Delta T + k_\omega \cdot \sum_{j=0}^{i-1} V_{offset} \cdot \Delta T = \tag{2-114}$$

$$= k_\omega \cdot V_m \cdot \Delta T \cdot \sum_{j=0}^{i-1} \bar{v}_{mj} + k_\omega \cdot V_{offset} \cdot \Delta T \cdot i \tag{2-115}$$

In a similar way as in (2-110), these two relationships are obtained (see Figure 2-24):

$$\text{(a)}\ \Delta f_c = \frac{k_\omega \cdot V_m}{2\pi} \qquad \text{(b)}\ \Delta f_{offset} = \frac{k_\omega \cdot V_{offset}}{2\pi} \tag{2-116}$$

where:

- Δf_c is the frequency peak deviation respect to the V_{offset} level.
- Δf_{offset} is the constant frequency deviation related to the horizontal axis.

From expression (2-108) and substituting the relationships 2-116(a) and (b) into the equation (2-115), a final expression is derived ($f_m = 1/T_m$):

$$\Theta(i) = \frac{2\pi}{NP} \cdot \frac{\Delta f_c}{f_m} \cdot \sum_{j=0}^{i-1} \bar{v}_{mj} + \frac{2\pi}{NP} \cdot \frac{\Delta f_{offset}}{f_m} \cdot i \qquad \text{i = 0 ... NP-1} \tag{2-117}$$

Anyway, the total number of points NP describing the discrete modulation profile does not have to match the total number of points N describing the modulated waveform. Moreover, a normal situation can be summarized in an inequality: NP < N. This situation must be taken into account at the time of writing the MATLAB algorithm.

As shown in Figure 2-25, several time-points corresponding to the sampling of the modulated signal will have the same discrete modulation profile value, that is, time-points between two consecutives samples of the discrete modulation profile i and i+1 will expose exactly the same value (of course, a linear interpolation between i and i+1

is possible; this situation is not taken into account in this development and can result in an improvement of the algorithm).

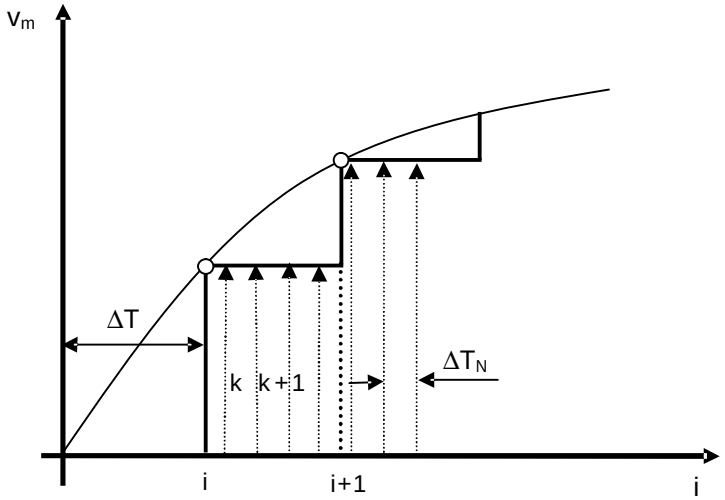

Figure 2-25. Sampling frequency of the modulated waveform ($1/\Delta T_N$) and the modulation profile ($1/\Delta T$)

As shown in Figure 2-25, several time-points corresponding to the sampling of the modulated signal will have the same discrete modulation profile value, that is, time-points between two consecutives samples of the discrete modulation profile i and i+1 will expose exactly the same value (of course, a linear interpolation between i and i+1 is possible; this situation is not taken into account in this development and can result in an improvement of the algorithm).

This way, modulated waveform samples from 0 to ΔT get the same value; samples from $1 \cdot \Delta T$ to $2 \cdot \Delta T$ have the same value and different from the previous one and so on.

Expressing $i \cdot \Delta T$ as a function of the sample number i (from expression (2-108),

$$i \cdot \Delta T = i \cdot \frac{T_m}{NP} \qquad \text{i = 0 .. NP-1} \qquad (2\text{-}118)$$

and $k \cdot \Delta T_N$ as a function of the sample number k,

$$k \cdot \Delta T_N = k \cdot \frac{T_m}{N} \qquad \text{k = 0 .. N-1} \qquad (2\text{-}119)$$

a k-sample will have the same value while $k \cdot \Delta T_N < i \cdot \Delta T$ or, in other terms, $NP \cdot k < N \cdot i$ (from the last i-1 index and to the next i+1 index, of course). Note that the following relationship can be derived from (2-118) and (2-119):

$$NP \cdot \Delta T = N \cdot \Delta T_N = T_m \qquad (2\text{-}120)$$

Thus, k-samples between the i- and (i+1)-samples are to be calculated by following this procedure (a V_{offset} = 0 was considered):

1. Let k = 0, i = 1, Θ(0) = 0, F(0) = 0
2. while NP·k < N·i, then
   2.1. Let k=k+1
   2.2. Calculation of F(k) [modulated waveform]
3. endwhile
4. if NP·k ≥ N·i, then
   4.1. let i=i+1
   4.2. Calculation of Θ(i) [new values only when increasing the i-index]
5. endif
6. Continue at point 2 till i=NP-1 (inclusive)

2.3.3 Structure of the algorithm

In order to make easier the readability of the MATLAB algorithm, an overview of its internal structure was considered to be exposed. The following points make the skeleton of this algorithm:

– First of all, a re-initialization of the environment is mandatory in order to avoid an undesirable influence of previous calculations in the current one.

– Once the environment is ready, a complete list of definitions and parameters to be used along this algorithm is to be done. Please keep in mind that V_{offset} = 0 is to be considered in these computations, then simplifying the expressions obtained previously. Main parameters hereby described are: switching (carrier) and modulating frequencies (fc and fm), peak amplitudes of both signals (amp_c and amp_m), parameter s for triangular modulation, percentage of modulation (delta), initial values for modulating profile (vm=0) and phase value (theta = 0), peak deviation of the carrier frequency (delta_fc), modulation index (mf), bandwidth of the modulated waveform (bandwidth) from the Carson's rule and a final calculation of the sampling frequency (fsampling).

– After these definitions, computation of modulated waveform is now possible. To do this, a 6-option menu is available in order to select the desired modulation:

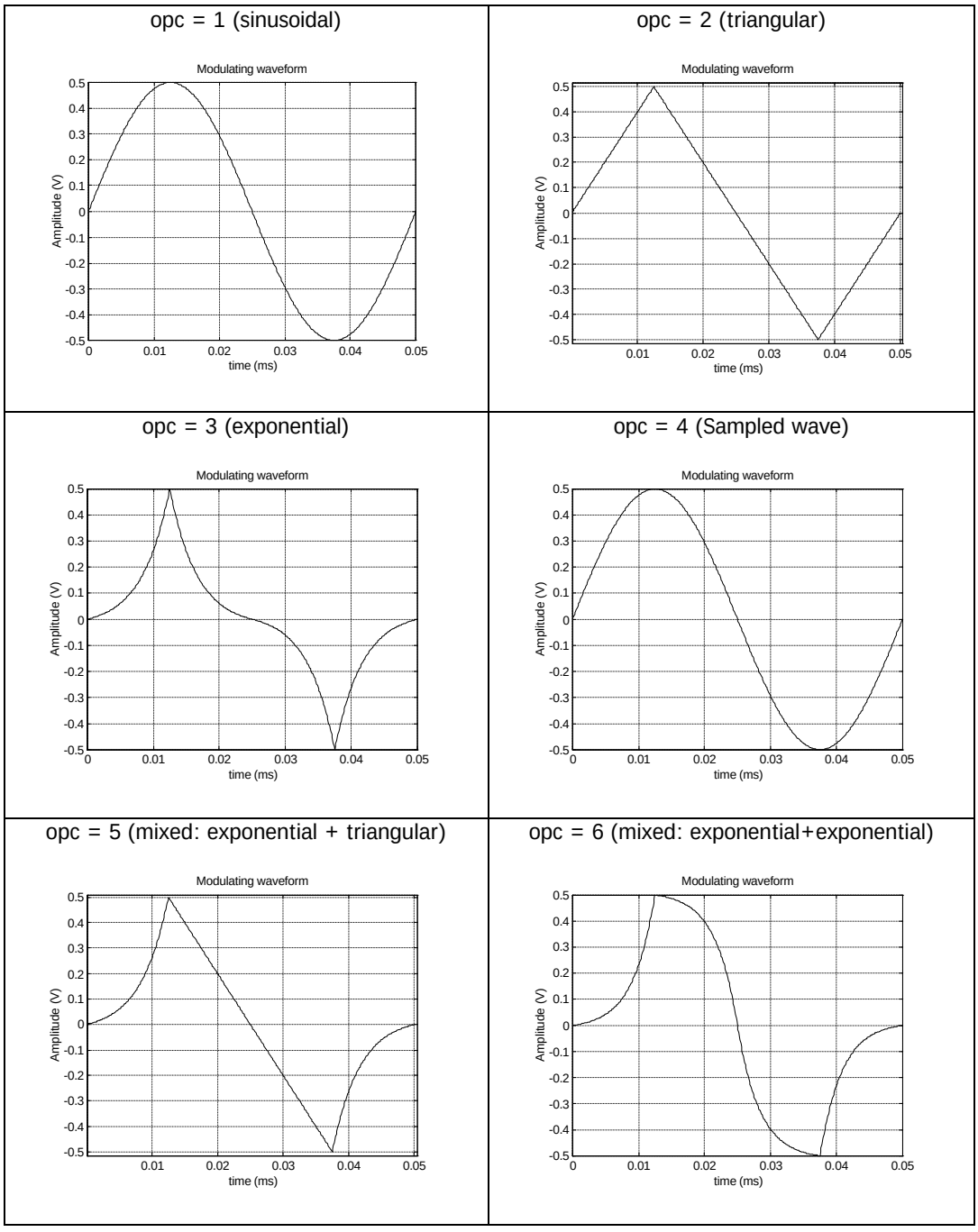

Figure 2-26. Different options of modulation profiles available in the algorithm through a menu

– Each of these 6 modulations are analytically described, obtaining finally the resulting modulated waveform f(k).

– A computation of the spectral components related to the modulated signal is carried out by using the MATLAB function fft (f, N). A special mention has to be

done now related to fft: to obtain the rms values of the spectral components (MOD_FFT, in the algorithm), the following steps must be followed, (please refer to manuals of MATLAB for a detailed information):

$$Y = fft(f, N) \tag{2-121}$$

$$Y = Y\left(1{:}1+\frac{N}{2}\right) \tag{2-122}$$

$$MOD\_FFT = \frac{2}{N}\cdot abs\left(\frac{Y}{\sqrt{2}}\right) \tag{2-123}$$

where Y(1) represents the dc component and Y(1+N/2) contains the Nyquist component of the modulated waveform. Only the 1+N/2 first points contain the spectra information.

– Afterwards, a graphical representation of the modulating signal, the time-varying phase and the spectral content is displayed.

– Finally, both modulated waveform and its related spectra are stored into two different files, just in order to be post-processed by other tools.

2.3.4 The MATLAB algorithm code lines

Please refer to Annex 4.

2.3.5 Verification of the algorithm

No algorithm must be accepted as a computing tool before a rigorous verification. A best practice consists of verifying every step or routine inside the algorithm by comparison with theoretical or, at least, reliable demonstrable values.

Onwards, the following schema will be followed:

a) Sinusoidal modulation: Comparison of the MATLAB algorithm results versus the analytical results.

b) Discrete modulation profile: the idea is to sample a sinusoidal modulation profile with both the same and lower sampling frequency than the one used to sample the modulated signal, and compare such results to the theoretical sinusoidal ones.

c) Rest of modulation profiles: Unlike the sinusoidal modulation, no theoretical expression for the spectral content of the modulated waveforms (mainly, regarding to triangular and exponential modulations) is easy to derive because of its great complexity. However, if the verification for an analytically described sinusoidal modulation profile is properly accomplished, it makes sense to think that this is also extensible to the rest of modulation profiles also expressed into an analytical form, really the case of triangular and exponential profiles. Anyway, and in order to test the equations in the MATLAB algorithm, a second verification will be made, consisting of sampling these modulation profiles in order to use them as an input for the discrete calculation at the MATLAB algorithm (opc=4 in point 2.3.3). These results will be then compared to the ones obtained with several opc options (see Figure 2-26), particularly, triangular and exponential modulation profiles.

   There are some other modulation profiles (opc = 5, 6) available in the MATLAB algorithm. They are usually just a combination of the first three ones, that is, sinusoidal, triangular and exponential profiles. Because verification must be done for these three profiles, further combination of them has not to be validated just paying attention to the right writing of the equations describing the waveforms in the algorithm.

In every case, the discrete modulation profile to be used must match the one calculated by the MATLAB algorithm. Test discretized profiles can be obtained, for instance, by means of commercial software like MathCad or MATLAB itself and they must guarantee that the same modulation profile is running in the MATLAB algorithm.

a) Sinusoidal carrier modulated by a sinusoidal signal [RD-1]

First of all, theoretical development of this modulation is mandatory to derive.

The theoretical expression of a sinusoidal carrier modulated by another sinusoidal waveform is usually expressed as follows:

$$F(t) = V_c \cdot \cos\left[\omega_c t + m_f \sin \omega_m t\right] \tag{2-124}$$

From a trigonometric equality

$$F(t) = V_c \cdot \left(\cos \omega_c t \cdot \cos\left(m_f \sin \omega_m t\right) - \sin \omega_c t \cdot \sin\left(m_f \sin \omega_m t\right)\right) \tag{2-125}$$

In order to establish a relationship between $\cos\left(m_f \sin\omega_m t\right)$ and $\sin\left(m_f \sin\omega_m t\right)$, let consider the function

$$g(t) = e^{jm_f \sin\omega_m t} \tag{2-126}$$

Fourier's exponential series is represented by

$$g(t) = \sum_{n=-\infty}^{\infty} c_n \cdot e^{jn\omega t} \tag{2-127}$$

with

$$c_n = \frac{1}{2\pi}\int_0^{2\pi} g(t)\cdot e^{-jn\omega t}\, d(\omega t) \tag{2-128}$$

The Bessel's function of first specie is defined by

$$J_n(m_f) = \frac{1}{2\pi}\int_0^{2\pi} e^{jm_f \sin\omega_m t}\cdot e^{-jn\omega t}\, d(\omega t) \tag{2-129}$$

which is similar to (2-128) with ω_m replaced by ω and $g(t) = e^{jm_f \sin\omega_m t}$. Thus, the following equalities can be exposed:

$$c_n = J_n(m_f) \tag{2-130}$$

$$g(t) = \sum_{n=-\infty}^{\infty} J_n(m_f)\cdot e^{jn\omega_m t} \tag{2-131}$$

Adding the components +n and –n of g(t), it can be demonstrated that:

$$J_{-n}(m_f) = (-1)^n \cdot J_n(m_f) \tag{2-132}$$

Thus, for n even,

$$\begin{aligned} J_{-n}(m_f)\cdot e^{-jn\omega_m t} + J_n(m_f)\cdot e^{jn\omega_m t} &= \\ = J_n(m_f)\cdot\left(e^{jn\omega_m t} + e^{-jn\omega_m t}\right) &\\ = 2\cdot J_n(m_f)\cdot\cos\left(n\cdot\omega_m\cdot t\right) & \end{aligned} \tag{2 -133}$$

For n odd,

$$J_{-n}(m_f)\cdot e^{-jn\omega_m t} + J_n(m_f)\cdot e^{jn\omega_m t} =$$

$$= J_n(m_f) \cdot \left(e^{jn\omega_m t} - e^{-jn\omega_m t}\right)$$

$$= j \cdot 2 \cdot J_n(m_f) \cdot \sin\left(n \cdot \omega_m \cdot t\right) \quad (2\text{-}134)$$

Thus, expression (2-131) is also expressed as follows:

$$g(t) = J_0(m_f) + 2\sum_{n\ even} J_n(m_f) \cdot \cos(n\omega_m t) + j2\sum_{n\ odd} J_n(m_f) \cdot \sin(n\omega_m t) \quad (2\text{-}135)$$

Applying the Euler's theorem to (2-126),

$$g(t) = \cos\left(m_f \sin\omega_m t\right) + j\sin\left(m_f \sin\omega_m t\right) \quad (2\text{-}136)$$

A comparison among (2-135) and (2-136) yields:

$$\cos(m_f \sin\omega_m t) = J_0(m_f) + 2\sum_{n\ even} J_n(m_f) \cdot \cos(n\omega_m t) \quad (2\text{-}137)$$

$$\sin(m_f \sin\omega_m t) = 2\sum_{n\ odd} J_n(m_f) \cdot \sin(n\omega_m t) \quad (2\text{-}138)$$

Substitution of (2-137) and (2-138) into (2-135) yields:

$$\begin{aligned} F(t) = V_c \{ & J_0(m_f)\cos\omega_c t \\ & - 2J_1(m_f) \cdot \sin\omega_c t \cdot \sin\omega_m t \\ & + 2J_2(m_f) \cdot \cos\omega_c t \cdot \cos 2\omega_m t \\ & - 2J_3(m_f) \cdot \sin\omega_c t \cdot \sin 3\omega_m t \\ & + 2J_4(m_f) \cdot \cos\omega_c t \cdot \cos 4\omega_m t \\ & + \ldots \} \end{aligned} \quad (2\text{ -}139)$$

Or, in other more interesting terms,

$$\begin{aligned} F(t) = V_c \{ & J_0(m_f)\cos\omega_c t \\ & + J_1(m_f) \cdot \left[\cos\left(\omega_c + \omega_m\right) \cdot t - \cos\left(\omega_c - \omega_m\right) \cdot t\right] \\ & + J_2(m_f) \cdot \left[\cos\left(\omega_c + 2\omega_m\right) \cdot t + \cos\left(\omega_c - 2\omega_m\right) \cdot t\right] \\ & + J_3(m_f) \cdot \left[\cos\left(\omega_c + 3\omega_m\right) \cdot t - \cos\left(\omega_c - 3\omega_m\right) \cdot t\right] \end{aligned}$$

$$+ J_4(m_f)\cdot\left[\cos\left(\omega_c + 4\omega_m\right)\cdot t + \cos\left(\omega_c - 4\omega_m\right)\cdot t\right]$$

$$+ \ldots \Big\} \qquad (2\text{-}140)$$

Once obtained the theoretical expression for sinusoidal modulation, verification was performed by using the following parameters:

- f_c = 200 kHz (carrier frequency)
- f_m = 20 kHz (modulating frequency)
- V_c = 0.5 V (peak amplitude of the switching-carrier frequency)
- m_f =1 (modulation index)

Side-band harmonics resulting from the sinusoidal modulation are presented below (Table 2-1):

Theoretical value		MATLAB algorithm value	At right harmonic frequency (kHz)	MATLAB algorithm value	At left harmonic frequency (kHz)
$V_c \cdot J_0(m_f)/\sqrt{2}$	0.2705382	0.27053824	200	0.27053824	200
$V_c \cdot J_1(m_f)/\sqrt{2}$	0.1555814	0.15558139	220	0.15558136	180
$V_c \cdot J_2(m_f)/\sqrt{2}$	0.0406245	0.04062450	240	0.04062454	160
$V_c \cdot J_3(m_f)/\sqrt{2}$	0.0069167	0.00691667	260	0.00691671	140
$V_c \cdot J_4(m_f)/\sqrt{2}$	$8.756241\cdot10^{-4}$	$8.7563\cdot10^{-4}$	280	$8.7562\cdot10^{-4}$	120
$V_c \cdot J_5(m_f)/\sqrt{2}$	$8.8302692\cdot10^{-5}$	$8.831\cdot10^{-5}$	300	$8.830\cdot10^{-5}$	100

Table 2-1. Sinusoidal modulation: Comparison of theoretical and computational results

A second verification was performed additionally (Table 2-2):

- f_c = 200 kHz (carrier frequency)
- f_m = 20 kHz (modulating frequency)
- V_c = 0.5 V (peak amplitude of the switching-carrier frequency)
- m_f =0.1 (modulation index)

Theoretical value		MATLAB algorithm value	At right harmonic frequency (kHz)	MATLAB algorithm value	At left harmonic frequency (kHz)
$V_c \cdot J_0(m_f)/\sqrt{2}$	0.3526701	0.35267006	200	0.35267006	200
$V_c \cdot J_1(m_f)/\sqrt{2}$	0.0176556	0.01765558	220	0.01765558	180
$V_c \cdot J_2(m_f)/\sqrt{2}$	0.00044157356	0.00044154	240	0.00044160	160
$V_c \cdot J_3(m_f)/\sqrt{2}$	0.00000736109	0.00000736	260	0.00000736	140

Table 2-2. Sinusoidal modulation: Comparison of theoretical and computational results

Conclusion is very clear: algorithm results matches exactly the theoretical ones, just a negligible and unavoidable divergence is found beyond the 6^{th} or 7^{th} significant position.

b) Discrete modulation profile

As exposed before, a sinusoidal modulation profile will be sampled at both the same (b.1) and lower sampling frequency (b.2) than the one used to sample the modulated signal, and compare such results to the theoretical sinusoidal ones. The discrete samples were obtained by using the sinus function in MATLAB and stored in the corresponding file to be called further in the algorithm through option opc = 4.

b.1) Modulation profile sampling frequency=modulated signal sampling frequency

Verification was performed by using the following parameters:

- f_c = 200 kHz (carrier frequency)
- f_m = 20 kHz (modulating frequency)
- V_c = 0.5 V (peak amplitude of the switching-carrier frequency)
- m_f =1 (modulation index)
- N = 128 and NP = 128

In this case, N=NP and the results are shown below (opc=4 in Matlab algorithm) in Table 2-4:

Theoretical value		MATLAB algorithm value	At right harmonic frequency (kHz)	MATLAB algorithm value	At left harmonic frequency (kHz)
$V_c \cdot J_0(m_f)/\sqrt{2}$	0.2705382	0.27052262	200	0.27052262	200
$V_c \cdot J_1(m_f)/\sqrt{2}$	0.1555814	0.15559294	220	0.15559292	180
$V_c \cdot J_2(m_f)/\sqrt{2}$	0.0406245	0.04063196	240	0.04063200	160
$V_c \cdot J_3(m_f)/\sqrt{2}$	0.0069167	0.00691865	260	0.00691869	140
$V_c \cdot J_4(m_f)/\sqrt{2}$	$8.756241 \cdot 10^{-4}$	$8.7597 \cdot 10^{-4}$	280	$8.7597 \cdot 10^{-4}$	120
$V_c \cdot J_5(m_f)/\sqrt{2}$	$8.8302692 \cdot 10^{-5}$	$8.837 \cdot 10^{-5}$	300	$8.835 \cdot 10^{-5}$	100

Table 2-3. Discrete modulation profile: Comparison of theoretical and computational results (N=NP)

For the side-band harmonics with significant amplitude, differences between theoretical and computed values are lower than 0.1%, even for those near to zero (non-significant harmonic amplitudes), where computing inaccuracies are expected. This way, this part of the MATLAB algorithm can be accepted.

b.2) Modulation profile sampling frequency < modulated signal sampling frequency

Verification was performed by using the following parameters:

- f_c = 200 kHz (carrier frequency)
- f_m = 20 kHz (modulating frequency)
- V_c = 0.5 V
- m_f =1 (modulation index)
- N = 128 and NP = 64

In this case, N > NP and the results are shown below (opc=4 in Matlab algorithm) in Table 2-4.

Of course, some differences are expected in the final results because of the lower resolution of the sampled modulation profile with NP = 64 respect to the previous situation in b.1) with NP = 128.

Theoretical value		MATLAB algorithm value	At right harmonic frequency (kHz)	MATLAB algorithm value	At left harmonic frequency (kHz)
$V_c \cdot J_0(m_f)/\sqrt{2}$	0.2705382	0.27047790	200	0.27047790	200
$V_c \cdot J_1(m_f)/\sqrt{2}$	0.1555814	0.15560610	220	0.15560534	180
$V_c \cdot J_2(m_f)/\sqrt{2}$	0.0406245	0.04061189	240	0.04059485	160
$V_c \cdot J_3(m_f)/\sqrt{2}$	0.0069167	0.00688272	260	0.00688487	140
$V_c \cdot J_4(m_f)/\sqrt{2}$	$8.756241 \cdot 10^{-4}$	$8.5864 \cdot 10^{-4}$	280	0.00089073	120
$V_c \cdot J_5(m_f)/\sqrt{2}$	$8.8302692 \cdot 10^{-5}$	$10.756 \cdot 10^{-5}$	300	$10.487 \cdot 10^{-5}$	100

Table 2-4. Discrete modulation profile: Comparison of theoretical and computational results (N>NP)

Equally as exposed in b.1), those side-band harmonics with a significant amplitude show differences between theoretical and computed values lower than 0.1%. For those ones near to zero (non-significant harmonic amplitudes), these differences increase due to computing inaccuracies and lower modulation profile sampling frequency. Again, this part of the MATLAB algorithm can also be accepted.

c) Rest of modulation profiles

c.1) Triangular modulation profile

As exposed before, a sampled triangular modulation profile with N points must be obtained. This set of samples will be used to compute this triangular modulation by means of a discretized profile (opc=4 in Matlab algorithm). A final comparison between the results from the discretized modulation profile (opc=4) and those from a direct computation (opc=2) will validate this part of algorithm.

Verification (Table 2-5) was performed by using the following parameters:

- f_c = 200 kHz (carrier frequency)
- f_m = 20 kHz (modulating frequency)
- V_c = 0.5 V
- m_f =1 (modulation index)

– NP = N = 128 and s = 0.5

Triangular direct calculation (opc = 2)				Discrete triangular modulation profile (opc = 4)			
Value	kHz	Value	kHz	Value	kHz	Value	kHz
0.29763500	200	0.29763500	200	0.2976043	200	0. 2976043	200
0.13222291	220	0.13222289	180	0.13223932	220	0.13228067	180
0.02546458	240	0.02546463	160	0.02547591	240	0.02547829	160
0.00831795	260	0.00831803	140	0.00831970	260	0.00836593	140
0.00192682	280	0.00192681	120	0.00193096	280	0.00193635	120
0.00142526	300	0.00142588	100	0.00142312	300	0.00148062	100

Table 2-5. Triangular modulation: Verification by comparison with a discrete triangular profile

Those side-band harmonics with a significant amplitude show differences between direct and discrete calculation lower than 0.05%. For those ones near to zero (non-significant harmonic amplitudes), these differences increase till a 4% due to computing inaccuracies. Again, this part of the MATLAB algorithm can also be accepted.

c.2) Exponential modulation profile

In a similar way as in c.1), a sampled exponential modulation profile with N points must be obtained. This set of samples will be used to compute this exponential modulation by means of a discrete profile (opc=4 in Matlab algorithm). A final comparison between the results from the discrete modulation profile (opc=4) and those from a direct computing (opc=3) will validate this part of algorithm.

Verification (Table 2-6) was performed by using the following parameters:

– f_c = 200 kHz (carrier frequency)

– f_m = 20 kHz (modulating frequency)

– V_c = 0.5 V

– m_f =1 (modulation index)

– NP = N = 128 and p=12*f_m

Exponential direct calculation (opc = 3)				Discrete exponential modulation profile (opc = 4)			
Value	kHz	Value	kHz	Value	kHz	Value	kHz
0.33144977	200	0.33144977	200	0.33139960	200	0.33139960	200
0.08563651	220	0.08570948	180	0.08571305	220	0.08582111	180
0.00764433	240	0.00764858	160	0.00765442	240	0.00766008	160
0.01249041	260	0.01257255	140	0.01251852	260	0.01263869	140
0.00223175	280	0.00224173	120	0.00223788	280	0.00225115	120
0.00324281	300	0.00334848	100	0.00325820	300	0.00316919	100

Table 2-6. Exponential modulation: Verification by comparison with an discrete exponential profile

Those side-band harmonics with a significant amplitude show differences between direct and discrete calculation lower than 0.1%. For those ones near to zero (non-significant harmonic amplitudes), these differences increase till a 5.5% due to computing inaccuracies. Again, this part of the MATLAB algorithm can also be accepted.

In summary, a successful verification of the MATLAB algorithm has been obtained, thus validating its use for further developments.

2.4 Summary

In this chapter, all concepts of interest related to the modulation were introduced. Because frequency modulation is used to generate SSCG methods in this thesis, a wide theoretical development of this kind of modulation and related concepts were also presented as well as its main parameters: 1) carrier (or switching) frequency f_c, 2) modulating frequency f_m (defines the distance in frequency between two consecutive side-band harmonics), 3) modulation index m_f (together with f_m, defines the bandwidth of the FM waveform), 4) carrier frequency peak deviation Δf_c (defines the peak frequency excursion around f_c), 5) modulation ratio δ and 6) modulation profiles (define the shape of the resulting modulated waveform spectrum and the possibility of up- and down-spreading SSCG techniques).

Practical considerations were also introduced in order to show possible deviations of these parameters respect to their theoretical behaviour. This way, 1) and 2) are of interest when measuring with spectrum analyzers: their RBW (Resolution Bandwidth) and measure mode (peak, quasy-peak and average) are responsible for giving different measured values of the same physical fact of modulation; as a general asseveration, the larger the selected RBW, the higher the obtained measure because more side-band harmonics can fall inside this RBW, adding their amplitudes. Parameters 3), 4) and 5) are responsible for the spectrum overlap at higher harmonics orders because of the growing side-band harmonics bandwidth resulting from the modulation process. Parameters 2) and 4) define the side-band harmonics bandwidth around the carrier (or switching) frequency, thus giving the lowest working frequency present in the system ($\approx f_c - \Delta f_c$) which must be higher than the cut-off frequency of the low-pass filter integrated in the power converter in order to avoid frequencies under cut-off to be present on the output voltage. Regarding to 6), it was also demonstrated there was no influence of the modulation profile on the output voltage of a power converter; a voltage offset in the modulation profile does not modify the final modulation spectrum but only the central frequency of the side-band harmonics window, thus being an easy way to implement up- and down-spreading modulation techniques; in a similar way, resulting modulated wave spectrum is independent on a possible phase-shift in the modulation profile.

Although the theoretical development considered only the modulation of a sinusoidal waveform, it was also demonstrated the validity of these results when a generic signal is present, just paying attention to the right use of the harmonic order h in every expression derived for the modulation of a sinusoidal waveform.

Because the theoretical part of this thesis is completely based on the fundaments of the Fourier Transform, a sufficient explanation was included for a right understanding of the thesis (Annex 3); conclusions of interest for this thesis are related to the exigencies of FFT to implement correctly the computational algorithm (MATLAB environment): modulated signal must be periodic and band-limited (Carson's rule considerations), sampling rate must be at least two times the largest frequency component (Nyquist's theorem), the truncation function must be non-zero over exactly one period of the modulated signal and the number of samples must be a power of 2. This algorithm is capable of generating any frequency modulation of a sinusoidal

carrier and the corresponding spectral components resulting from the modulation process; three special modulation profiles were studied: sinusoidal, triangular and exponential waveforms. A specific development was also carried out for a generic discrete modulation profile. A verification procedure for the algorithm was also presented in order to validate one of the most important parts of the thesis.

CHAPTER

3

THEORETICAL ANALYSIS OF EMI WITH DIFFERENT MODULATION PARAMETERS

3. THEORETICAL ANALYSIS OF EMI WITH DIFFERENT MODULATION PARAMETERS

Chapter 3 takes profit of the results obtained in Chapter 2 and assumes them in order to completely understand and analyze the theoretical behaviour of the modulation profiles, providing simultaneously a quantification of the modulation process according to several significant measure parameters. In order to systematize the theoretical analysis of EMI, the following points are considered:

1. Evolution of significant parameters shown in Figures 3-1 and 3-2 is to be studied as a function of the modulation index m_f. A further demonstration will show that side-band harmonic amplitudes resulting from the modulation process (and, therefore, the shape or outline of the side-band harmonics window) only depends on the modulation index m_f.

   This study must be accomplished for a significant range of modulation indexes. The idea is to obtain a graphical behaviour of the attenuation for the specified range of modulation indexes.

2. After the theoretical analysis in point 1 for the three modulation profiles of interest (sinusoidal, triangular and exponential waveforms), a comparison of these profiles is to be carried out according to the measure parameters defined in Figure 3-2.

3. It is also presented a theoretical proposal of control for a switching power converter and derived some considerations to apply a certain SSCG method in power converters in order to reduce EMI emissions.

The two first previous points are to be developed for every modulation profile under study, that is, sinusoidal, triangular, exponential and mixed profiles.

Figure 3-1 shows the main parameters describing the harmonic spectrum resulting from the modulation process at which a sinusoidal carrier has been subjected. A definition of these parameters is done onwards:

– f_c is the carrier frequency. When no modulation is present, a single harmonic (dot line) appears in the whole spectra.

– F (or $V_{rms,carrier}$) is the RMS-amplitude (in volts) of the harmonic corresponding to the non-modulated carrier waveform at a frequency f_c. This value is fixed at $0.5/\sqrt{2}$ =0.354 volts.

– F_1 is the RMS-amplitude (in volts) of the harmonic corresponding to the modulated waveform at a frequency f_c.

– $F_{env,peak}$ is the maximum RMS-amplitude (in volts) of the side-band harmonic envelope corresponding to the modulated waveform.

– B is the side-band harmonic window bandwidth resulting from the modulation process. It can be estimated by using the Carson's rule (see considerations in clause 2.1.2).

– Δf_{peak} is the distance in frequency between the two envelope peaks of value $F_{env,peak}$.

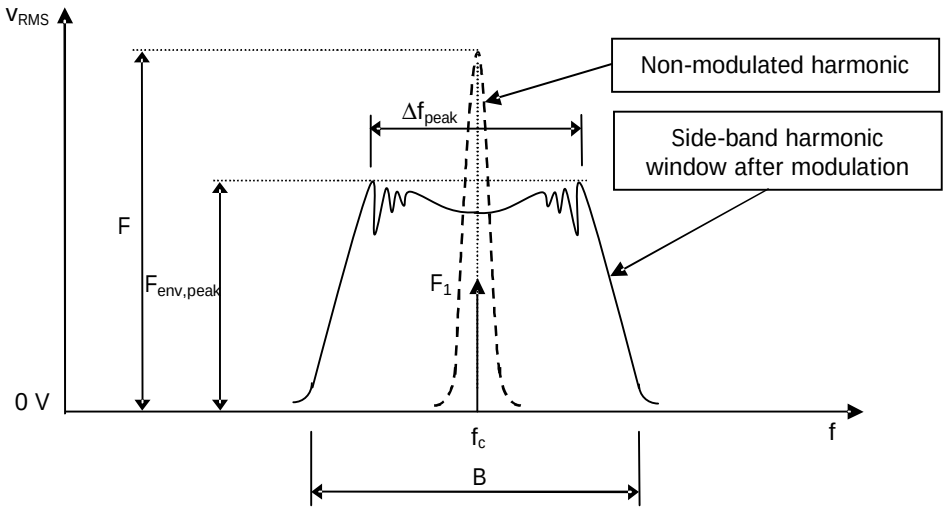

Figure 3-1. Definition of parameters to use in further analysis

However, theoretical results are to be presented as relative values respect to the non-modulated harmonic amplitude (carrier) and expressed in dB (the commonest units in EMC/EMI). Conversion of previous values to accomplish this exigency is done as follows:

$$V_{rel} = \frac{V_{rms,parameter}}{V_{rms,carrier}} = \frac{V_{rms,parameter}}{F} \text{ è} \qquad (3\text{-}1)$$

$$20 \cdot \log_{10}(V_{rel}) = 20 \cdot \log_{10}(V_{rms,parameter}) - 20 \cdot \log_{10}(V_{rms,carrier}) \quad (3\text{-}2)$$

$$dBV_{rel} = dBV_{parameter} - (-9.0309\ dBV) \quad (3\text{-}3)$$

In other words, parameters presented in Figure 3-1 are finally displayed following the schema exposed in Figure 3-2. All parameters and expressions regarding amplitudes (mainly, F_1 and $F_{env,peak}$) are to be expressed along this chapter as relative values respect to the non-modulated signal amplitude, that is, according to Figure 3-2.

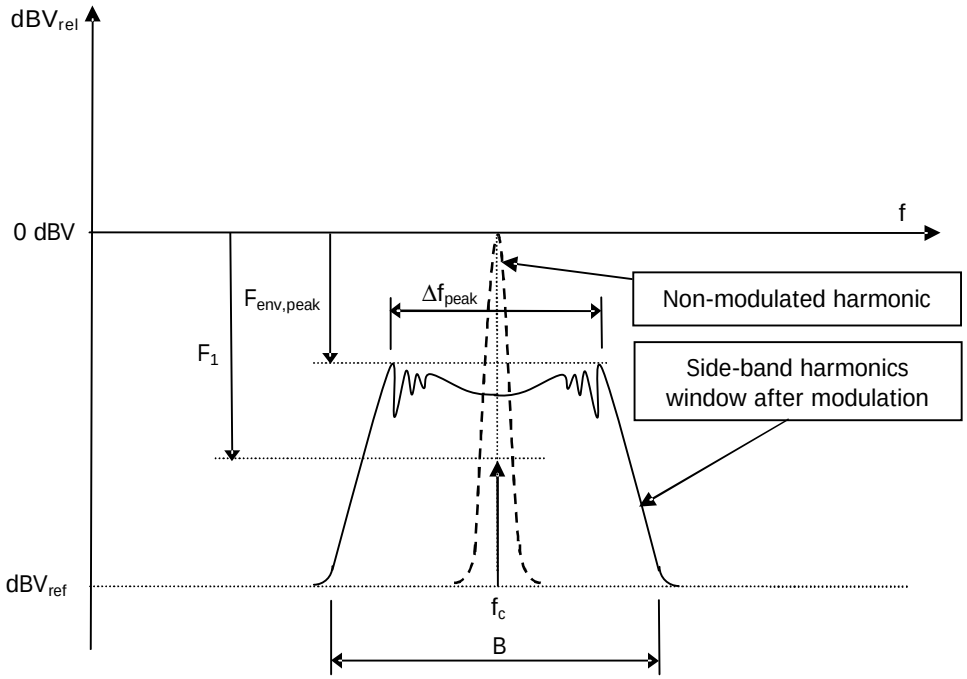

Figure 3-2. Re-definition of parameters to be finally used in further graphical representations

Next points are dedicated to the theoretical study of sinusoidal, triangular and exponential modulation profile.

3.1 Sinusoidal modulation profile

This is a very accurate starting point because analytical expressions are available for this modulation profile, thus conclusions from experimental results by means of a right theoretical interpretation can be derived. Afterwards, this procedure will be applied to the rest of modulation profiles, of which no analytical expressions have been developed.

Just to remember, in point 2.3.5, the analytical expression of a sinusoidal carrier modulated by a sinusoidal modulation profile was derived:

$$\begin{aligned} F(t) = V_c \{ & J_0(m_f)\cos\omega_c t \\ & + J_1(m_f)\cdot\left[\cos(\omega_c+\omega_m)\cdot t - \cos(\omega_c-\omega_m)\cdot t\right] \\ & + J_2(m_f)\cdot\left[\cos(\omega_c+2\omega_m)\cdot t + \cos(\omega_c-2\omega_m)\cdot t\right] \\ & + J_3(m_f)\cdot\left[\cos(\omega_c+3\omega_m)\cdot t - \cos(\omega_c-3\omega_m)\cdot t\right] \\ & + J_4(m_f)\cdot\left[\cos(\omega_c+4\omega_m)\cdot t + \cos(\omega_c-4\omega_m)\cdot t\right] \\ & + \ldots \} \end{aligned} \quad (3\text{-}4)$$

In other words, amplitudes of side-band harmonics depend only on the modulation index as the argument of the Bessel functions.

This is the main reason for the graphical results in the next sections to be presented as a function of the modulation index, mainly applying to all parameters in Figure 3-2 related to amplitude values. Because the modulation index m_f is a ratio between the product of the modulation ratio δ and the carrier frequency f_c and the modulating frequency f_m ($m_f = \frac{\delta \cdot f_c}{f_m}$), it can be derived that different combinations of these three parameters are to produce the same amplitude results of the side-band harmonics resulting from the modulation process. This way, the modulation index becomes a very helpful figure of merit because it summarizes the complete behaviour of three different parameters (δ, f_c and f_m) working together in just one variable, that is, the modulation index.

Although the side-band harmonics amplitudes are only depending on the modulation index for a sinusoidal modulation, this behaviour must be firstly verified for the rest of modulation profiles in order to apply the same analysis which is to be carried out for the sinusoidal modulation profile, making the comparison between different modulation profiles easier to display and the related conclusions to derive, one of the main objectives of this thesis.

As shown in the following pictures (Figures 3-3 and 3-4), Bessel functions decrease in amplitude at higher values of modulation index m_f.

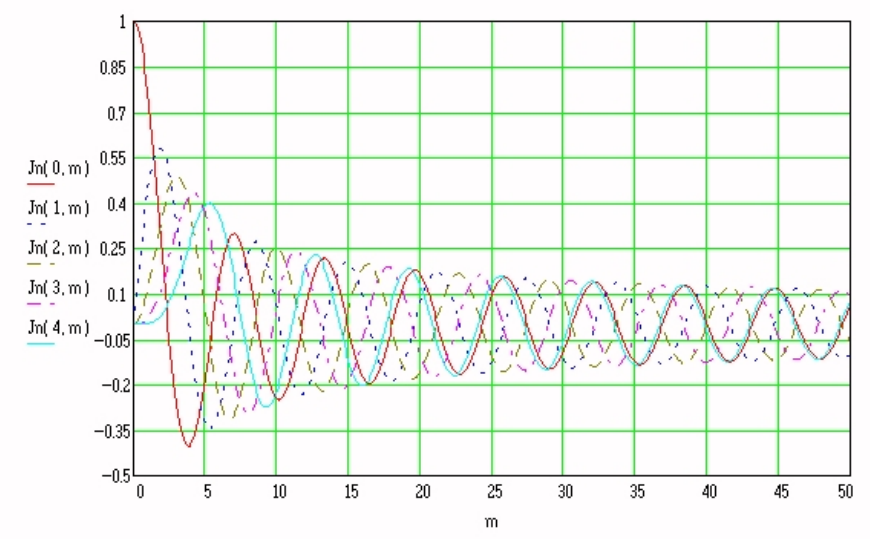

Figure 3-3. Bessel functions of several orders (up to $m_f = 50$)

(NOTE: Expression in Figures 3-3 and 3-4 related to Bessel functions must be understood this way è $J_n(k,m) \equiv J_k(m)$)

Figure 3-4 shows the amplitude evolution of Bessel functions for a larger value of modulation index ($m_f = 1000$). Up to $m_f \approx 200$, peak amplitude is decreasing considerably for Bessel functions of any order.

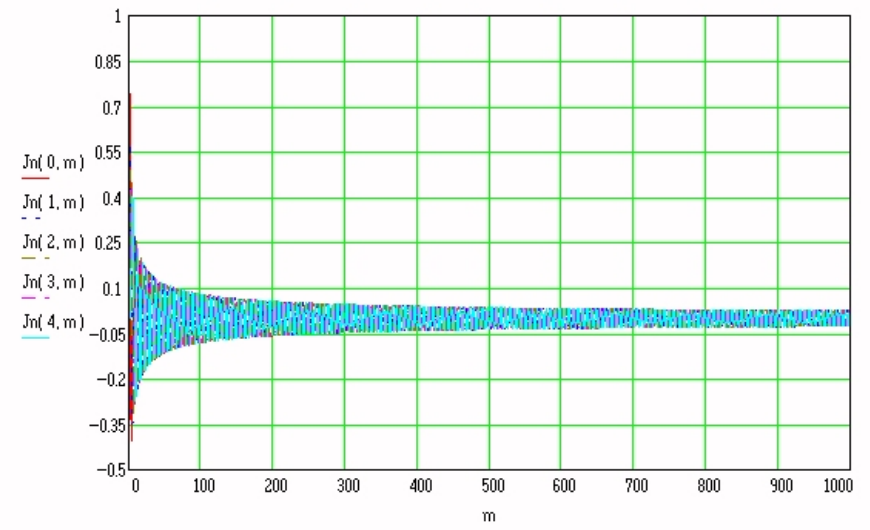

Figure 3-4. Bessel functions of several orders (up to $m_f = 1000$)

From the Bessel functions plot above, it must be concluded that amplitudes of the side-band harmonics are to decrease as the modulation index m_f gets higher. Anyway, from $m_f \approx 200$ onwards, only slightly differences in amplitude should be expected. This is an important point to be observed in the following analysis.

Figures 3-5 and 3-6 contain MATLAB plots corresponding to the shape evolution of the side-band harmonics resulting from the sinusoidal modulation of a sinusoidal carrier.

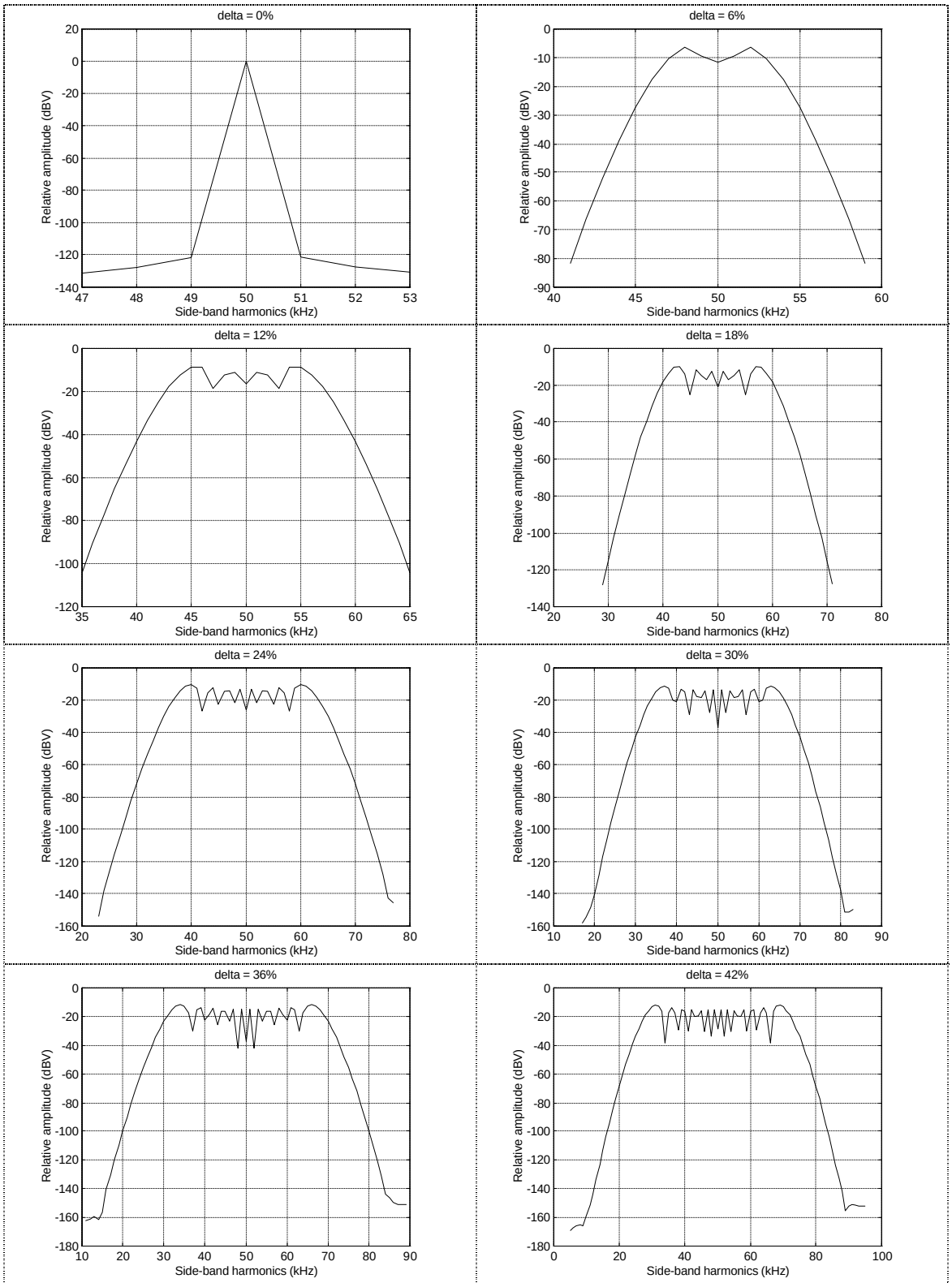

Figure 3-5. Evolution of side-band harmonics envelope: sinusoidal modulation (f_c = 50 kHz, f_m = 1 kHz)

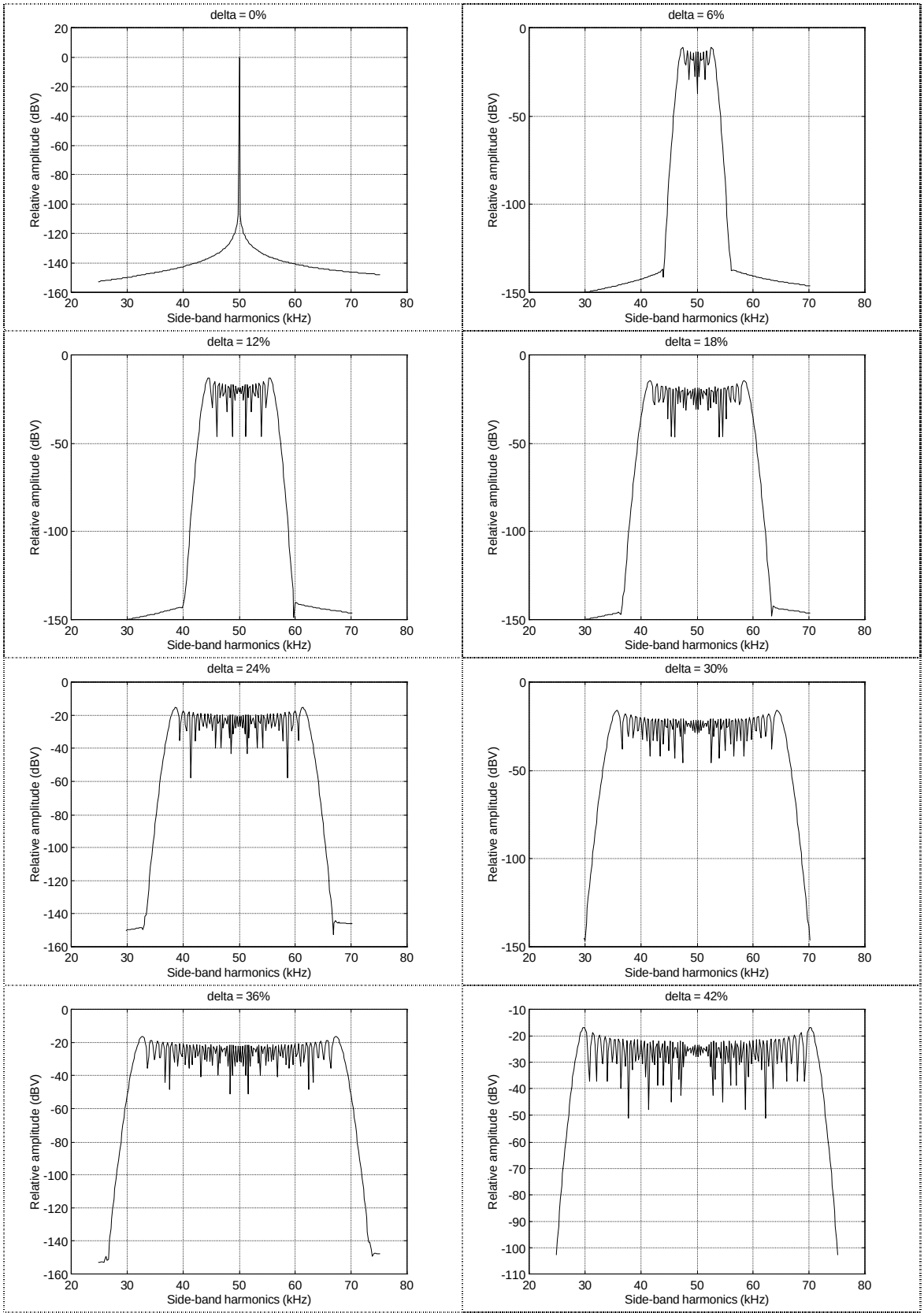

Figure 3-6. Evolution of side-band harmonics envelope: sinusoidal modulation (f_c = 50 kHz, f_m = 200 Hz)

Observe the shape change as the window bandwidth increases as a function of the modulation ratio δ: two peaks at both ends of the window tend to consolidate while the envelope of the side-band harmonic between these two peaks gets a larger concavity. The reason for this fact is to be found in the Bessel's functions behaviour (see Figure 3-7).

As shown in Figure 3-7, amplitude of Bessel's function remains zero up to nearly the modulation index equalling the function order value (≈100 in Figure 3-7). From this value upwards, an attenuated sinusoidal oscillation appears, showing an initial peak near to the function order value (≈105 in Figure 3-7).

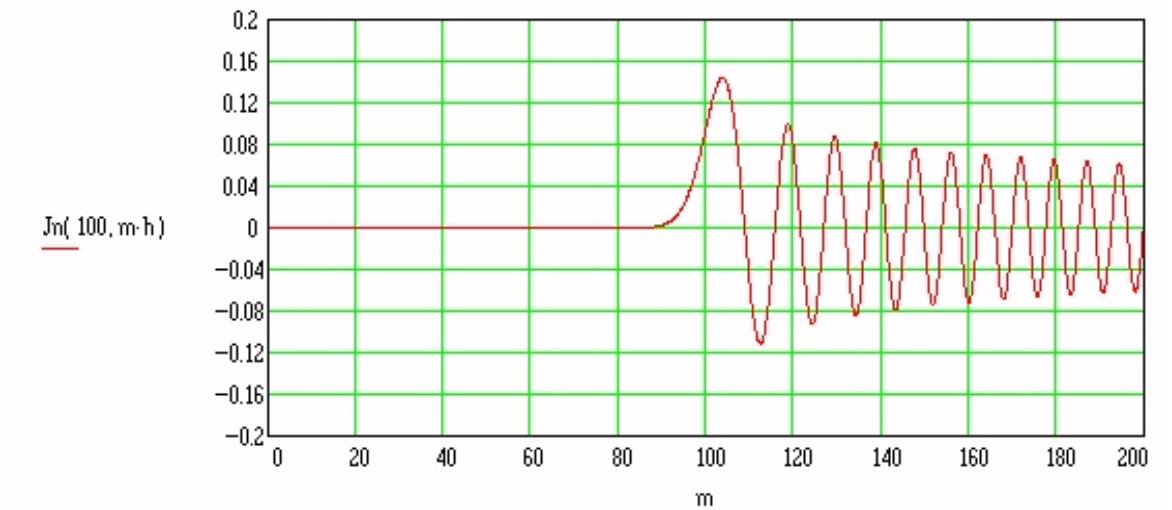

Figure 3-7. Bessel's function of 100th order (h=1)

As presented in expression (3-4), side-band harmonics amplitudes are given by the n-order Bessel function $J_n(m_f)$, where n represents the harmonic order (up- and down-wards respect to the carrier frequency) and m_f the modulation index. This way, harmonic orders n higher than the modulation index ($n>m_f$) must be zero. In other words, the peak-to-peak bandwidth (in the modulated waveform spectra) to be reached (approximately) is $B = 2 \cdot m_f \cdot f_m$ which is an approximation to the Carson's rule [$B_{Carson} = 2 \cdot f_m \cdot (1 + m_f)$]. This is developed in this chapter 3 under the title "Evolution of the peak-to-peak envelope bandwidth Δf_{peak}".

Another important conclusion is related to the proper modulation index to use. The higher the modulation index, the wider the peak-to-peak bandwidth, and then, a larger attenuation of the side-band harmonics.

3.1.1 Evolution of the central harmonic amplitude F_1

In the following Figures 3-8(a) and 3-8(b), F_1 (relative amplitude of the harmonic corresponding to the modulated waveform at a frequency f_c) is displayed (blue line) as a function of the modulation index m_f. Figure 3-8(a) consists of four graphs, each one at a different range of modulation indexes, till m_f = 500; Figure 3-8(b) shows the same values till a modulation index m_f = 2000. This way, a wide range of modulation indexes is covered for a complete variety of parameters values, as shown in Table 3-1.

f_c (kHz) Carrier frequency	f_m (kHz) Modulating frequency	δ% (%) Percentage of modulation	$m_f = \frac{\delta \cdot f_c}{f_m}$
50 ÷1000	0.25 ÷20	0 ÷50	$\frac{0.5 \cdot 1000}{0.25} = 2000$

Table 3-1.Values of the different parameters and maximum value expected for m_f

Besides, the maximum amplitude of the harmonics envelope ($F_{env,peak}$) is also included in these figures (red line) in order to compare visually the different attenuation of these two parameters.

In every case, an oscillation of the amplitude F_1 is present; however, an envelope can be defined, consisting of a logarithmic curve joining the local maximum points of every individual oscillation. This logarithmic curve gives the maximum attenuation possible with the selected parameters: δ%, f_c and f_m. However, a larger attenuation is also possible, just selecting the proper point where the oscillation reaches a minimum value. For instance, for m_f > 4 (see Figure 3-8(a)), an attenuation larger than -8 dBV is always to be obtained; however, for m_f = 5.52, an attenuation larger than -90 dBV is available. In other words, a special profit of this individual behaviour can be taken just tuning the system to a concrete modulation index in order, for instance, to eliminate the harmonic at the carrier frequency.

As the sinusoidal frequency modulation of a sinusoidal carrier was derived theoretically and an analytical expression (3-4) was obtained, a specific profit of this fact is to be taken in order to analyse and interpret the MATLAB-algorithm results (shown in Figures 3-8(a) and 3-8(b)) to justify them by comparing them to the theoretical ones.

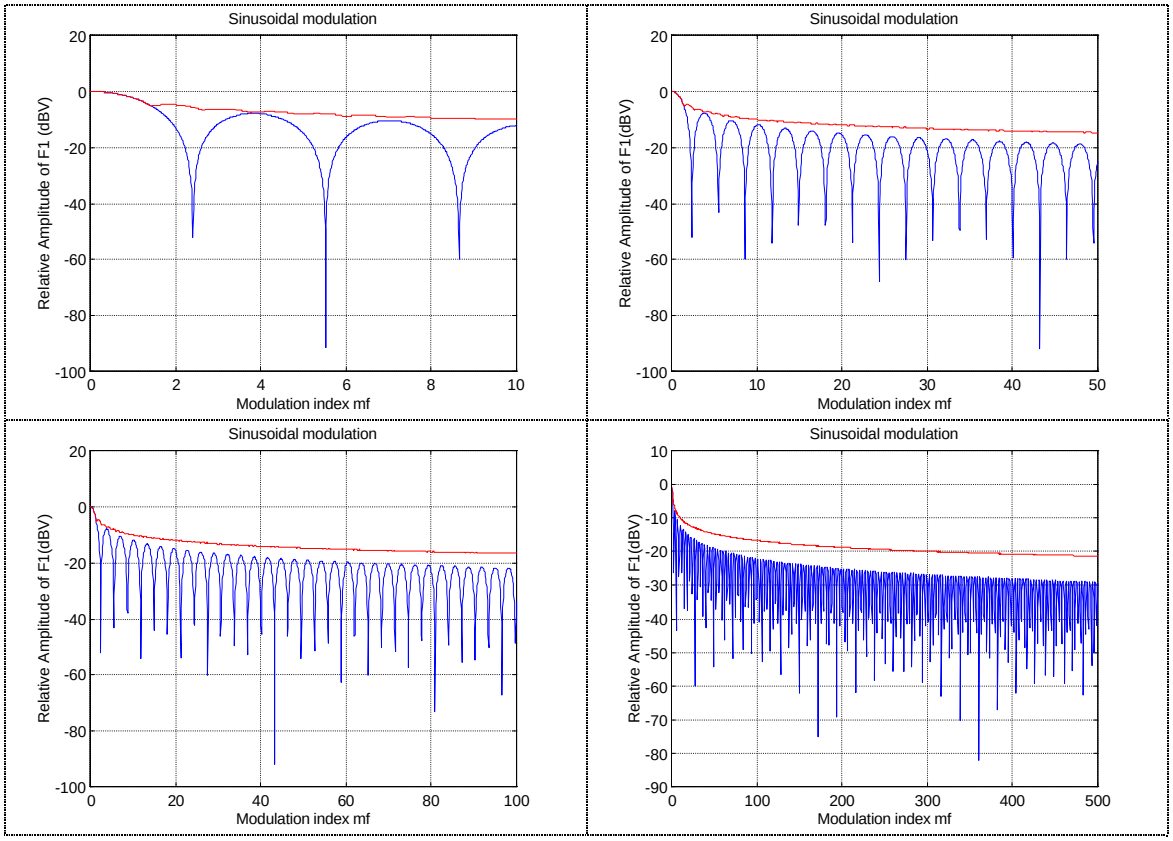

Figure 3-8(a). Rms-amplitude (F_1) of the carrier harmonic (blue line) and the maximum rms-amplitude ($F_{env,peak}$) of the harmonic envelope (red line) for different zooms of m_f. (Note: relative values respect to the non-modulated harmonic)

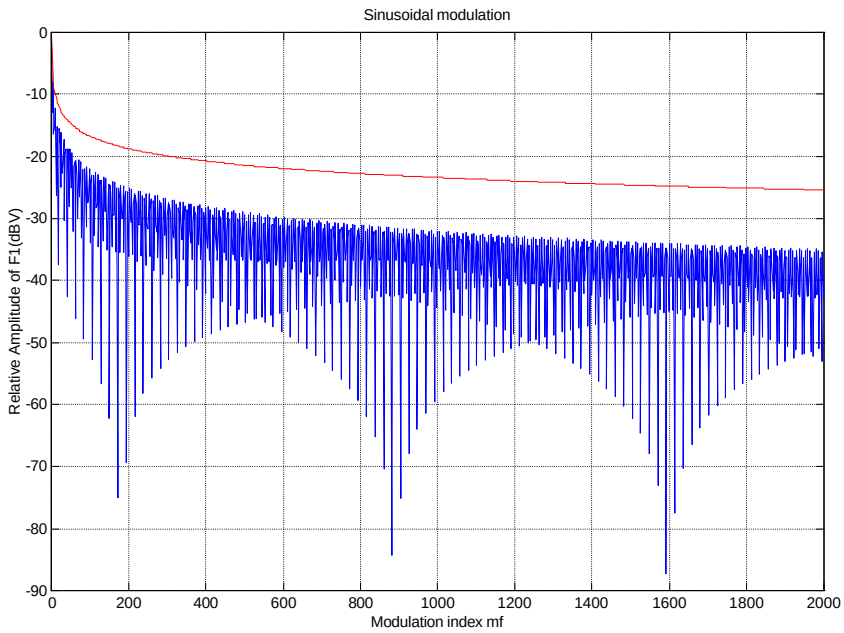

Figure 3-8(b). Rms-amplitude (F_1) of the carrier harmonic (blue line) and the maximum rms-amplitude ($F_{env,peak}$) of the harmonic envelope (red line) up to m_f = 2000 (Note: relative values respect to the non-modulated harmonic)

Focus now on the Bessel function $J_0(m_f)$ [in Figures 3-3 and 3-4, this function is described as Jn(0,mf)] because this is the responsible for the value of the harmonic corresponding to the carrier frequency, that is, parameter F_1. This function is individually represented in Figure 3-9(a).

(Please note that values displayed in Figures 3-8(a) and 3-8(b) are expressed in dBV; however, values in Figure 3-9(a) are expressed in a linear scale).

Values in Figure 3-8(a) represents the module of the parameter F1 and are expressed in dBV. In order to compare computational results in Figure 3-8(a), expressed in dBV, with those analytical in Figure 3-9(a), expressed in volts, a new graph must be obtained just rectifying (extracting the module) of the Bessel function $J_0(m_f)$ and expressing the module in dBV by applying the equation $20\cdot\log_{10}\left(\left|J_0\left(m_f\right)\right|\right)$. Figure 3-9(b) is then obtained.

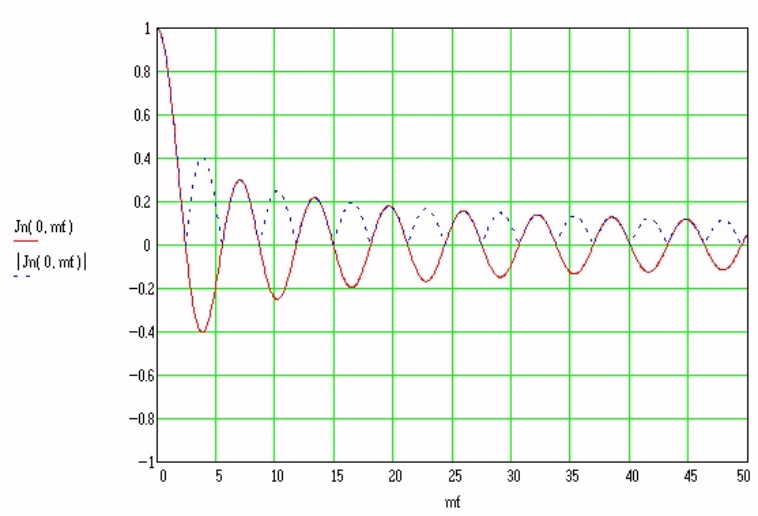

(a)

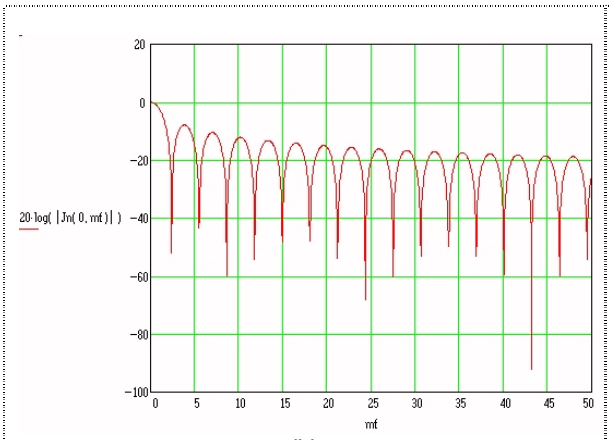

(b)

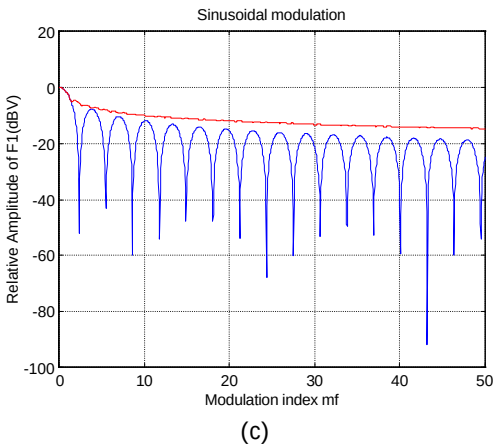

(c)

Figure 3-9. Bessel's function $J_0(m_f)$

Figure 3-8(a) is presented again in Figure 3-9(c) for convenience. It is easy to see that the shape of the F1 parameter in Figure 3-9(c) [range m_f =0 to 50] matches exactly the one in Figure 3-9(b).

Other important conclusions are listed below:

- As expected from expression (3-4), higher modulation indexes m_f are to produce higher attenuation (regarding the envelope of F_1). For instance, for m_f = 4, attenuation of F_1 –envelope is -8 dBV while for m_f = 20, attenuation is -15 dBV.
- Difference between the F_1 -envelope and the parameter $F_{env,peak}$ increases with the modulation index m_f, that is, the larger m_f, the larger the difference between F_1 -envelope and $F_{env,peak}$, and, thus, the larger concavity of the side-band spectra envelope.
- Because of the logarithmic behaviour, it is observed that attenuation remains approximately constant for modulation indexes higher than ≈200; in other words, it is not worthy to design modulation processes with higher modulation indexes.

Therefore, higher modulation indexes should be selected and, through its definition $m_f = \frac{\delta \cdot f_c}{f_m}$, this can be done by increasing the modulation ratio δ or the carrier frequency f_c or decreasing the modulating frequency f_m.

3.1.2 Evolution of the maximum envelope amplitude $F_{env,peak}$

Another important parameter to be analysed corresponds to the maximum rms-amplitude of the side-band harmonic envelope corresponding to the modulated waveform, $F_{env,peak}$. The Matlab algorithm presented in clause 2.3 calculates these values just storing the maximum value at each modulation index or iteration. Figures 3-10(a) and 3-10(b) show the behaviour of this parameter versus the modulation index. Figure 3-10(a) consists of four graphs, each one at a different range of modulation indexes, till m_f = 500; Figure 3-10(b) shows the same values till a modulation index m_f = 2000. This way, the complete range of modulation indexes is covered for the complete variety of parameters values (see Table 3-1).

In every case, an oscillation of the amplitudes $F_{env,peak}$ is present; however, a logarithmic envelope defined by joining the local maximum points of every individual oscillation is found.

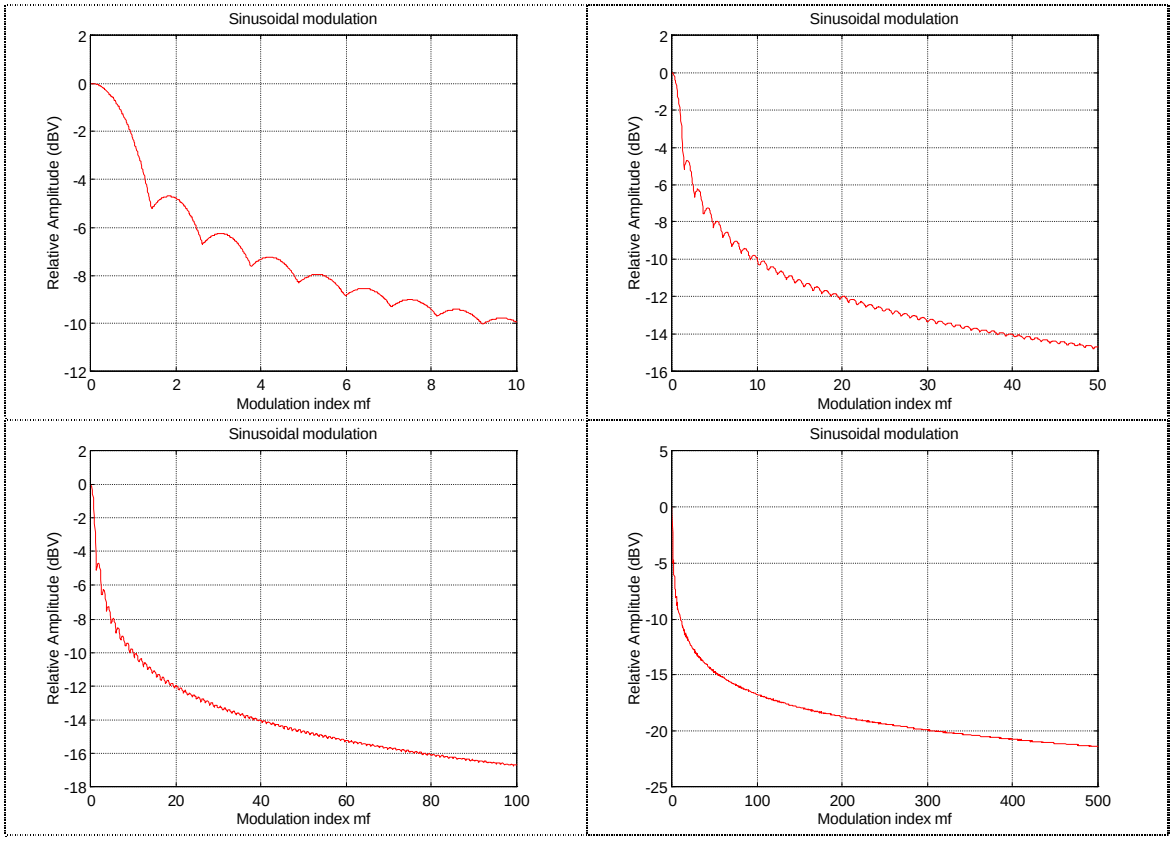

Figure 3-10(a). Maximum rms-amplitude ($F_{env,peak}$) of the harmonics envelope for different zooms of m_f. (Note: relative values respect to the non-modulated harmonic).

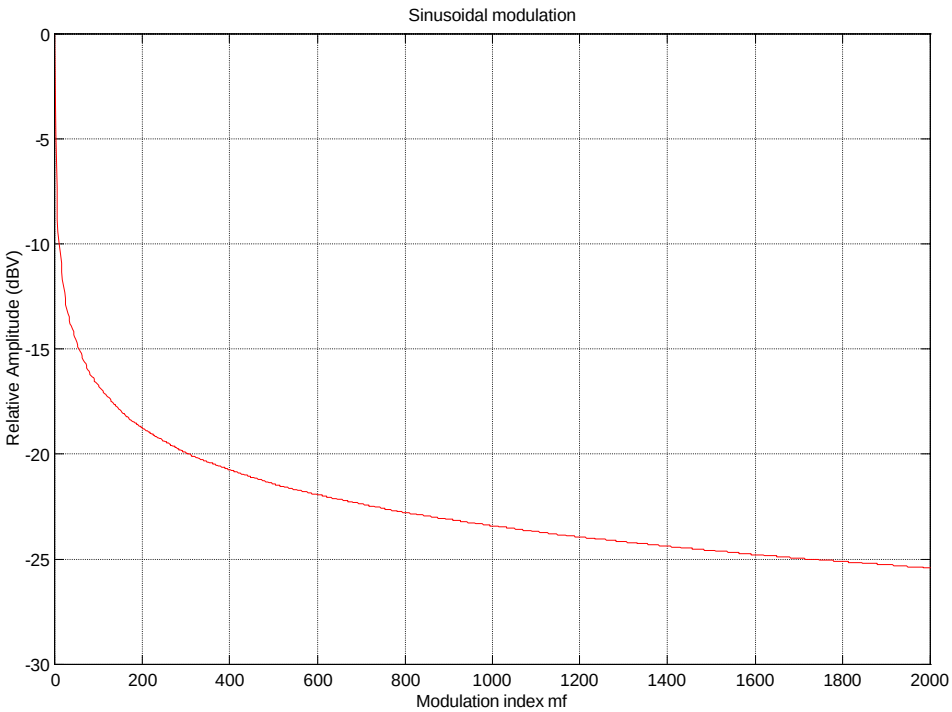

Figure 3-10(b). Maximum rms-amplitude ($F_{env,peak}$) of the harmonics envelope up to m_f. = 2000 (Note: relative values respect to the non-modulated harmonic).

This logarithmic curve produces the maximum attenuation reachable at any frequency for the selected parameters: δ%, f_c and f_m. For instance, for m_f = 5.32, an attenuation of -8 dBV is obtained. However, a larger attenuation is also possible, just selecting the proper point where the oscillation reaches a minimum value; this way, for m_f = 5.98, attenuation is -8.85 dBV. Again, a special profit of this individual behaviour can be taken just tuning the system to a concrete modulation index. Anyway, differences between minimum local values and the generic logarithmic envelope are nearly negligible compared to the differences obtained for F1.

Because of the analytical formulation of the sinusoidal modulation, behaviour shown in Figures 3-10(a) and 3-10(b) can be completely explained. To do this, it is worthy a careful sight to Figure 3-11(a).

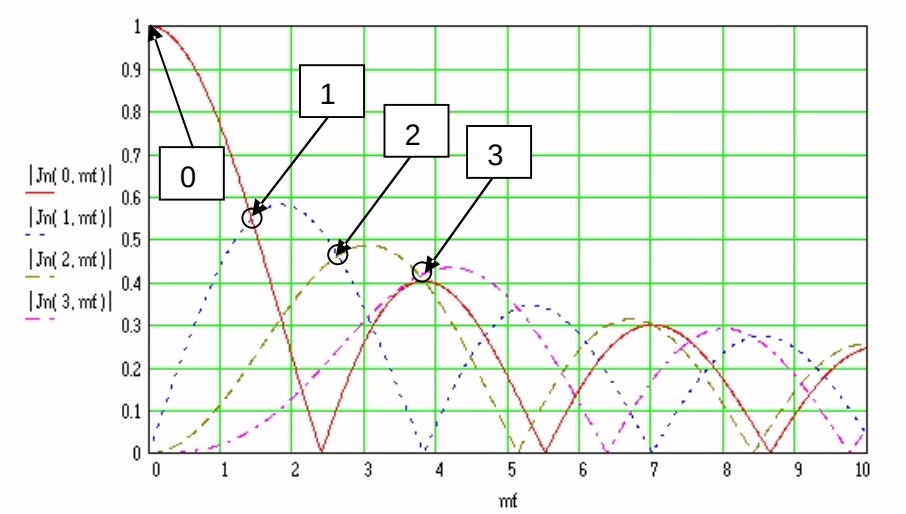

(a)

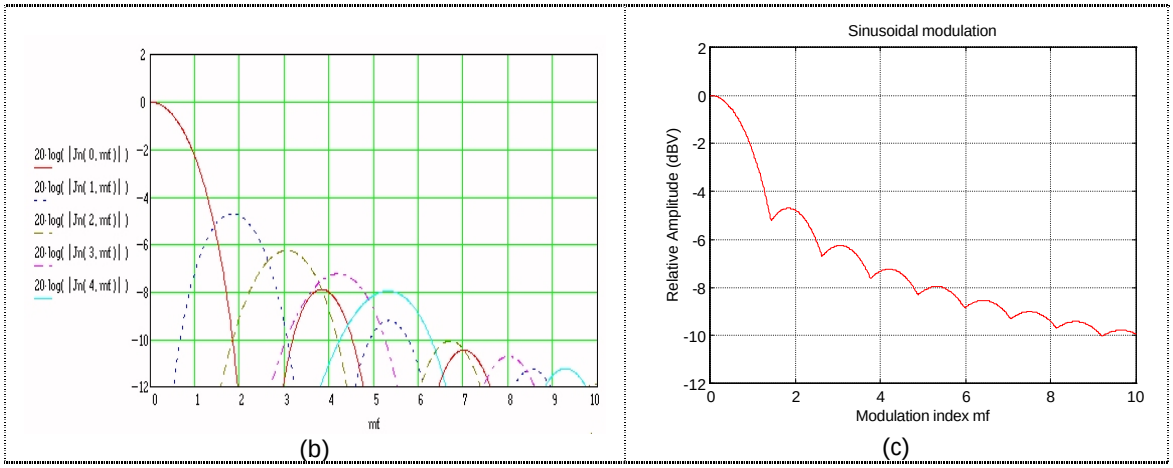

(b) (c)

Figure 3-11. Bessel functions (absolute value) of several orders (up to m_f = 10)

The absolute value of the first four Bessel functions is shown in the same picture in a vertical linear scale. From Point 0 in Figure 3-11(a) to Point 1, the amplitude corresponding to the harmonic at the carrier frequency is the largest one [$J_0(m_f)$ from expression (4-1)] and because of this, values F_1 and $F_{env,peak}$ are exactly the same. But from Point 1 (or better said, from the modulation index corresponding to Point 1) to Point 2, the amplitude corresponding to the first two side-band harmonics [$J_1(m_f)$] is now the largest one, then $F_{env,peak}$ must follow now the shape of the $J_1(m_f)$ curve. And this is the situation till Point 2, where amplitude corresponding to the two second side-band harmonics becomes the largest one [$J_2(m_f)$]. Then, from Point 2 to Point 3, $F_{env,peak}$ follows the shape of the $J_2(m_f)$ curve and so on. To sum up, $F_{env,peak}$ corresponds itself to the instantaneous maximum value of $J_n(m_f)$ (with n=0··∞).

Figure 3-11(b) corresponds exactly to Figure 3-11(a) where amplitude values are now expressed in dBV, according to expression $20 \cdot \log_{10}\left(\left|J_n\left(m_f\right)\right|\right)$. For convenience, Figure 3-10(a) for range m_f = 0..10 is reproduced again in Figure 3-11(c). This way, a direct comparison can be done between theoretical values (in Figure 3-11(b)) and computational results (in Figure 3-11(c)), observing exactly the same values in both plots.

Some important conclusions are listed below respect to the parameter $F_{env,peak}$:

- $F_{env,peak}$ shows a logarithmic trend of attenuation corresponding to the maximum value of the side-band harmonics envelope. Opposite to F_1 amplitude, a very low oscillation in the values is found, which is expected from the previous explanation.
- The larger the modulation index m_f, the more the attenuation. As an example, for m_f = 40, attenuation of $F_{env,peak}$ is -14 dBV while for m_f = 800, attenuation is -23 dBV.
- Because this logarithmic behaviour, it is observed that attenuation remains approximately constant for modulation indexes higher than ≈400.

As in clause 3.1.1, it is worthy to work with higher modulation indexes and, through its definition $m_f = \frac{\delta \cdot f_c}{f_m}$, this can be done by increasing the modulation ratio δ or the carrier frequency f_c or decreasing the modulating frequency f_m.

CONSIDERATIONS ABOUT THE LOGARITHMIC BEHAVIOUR OF PARAMETERS $F_{env,peak}$ and F1

In previous Figures, it is observed that the evolution of the relatives amplitudes F1 and $F_{env,peak}$ shows a logarithmic trend. In order to quantify this behaviour, significant Figure 3-8(b) is to be displayed in a logarithmic scale for the m_f-axis and the result plotted in Figure 3-12.

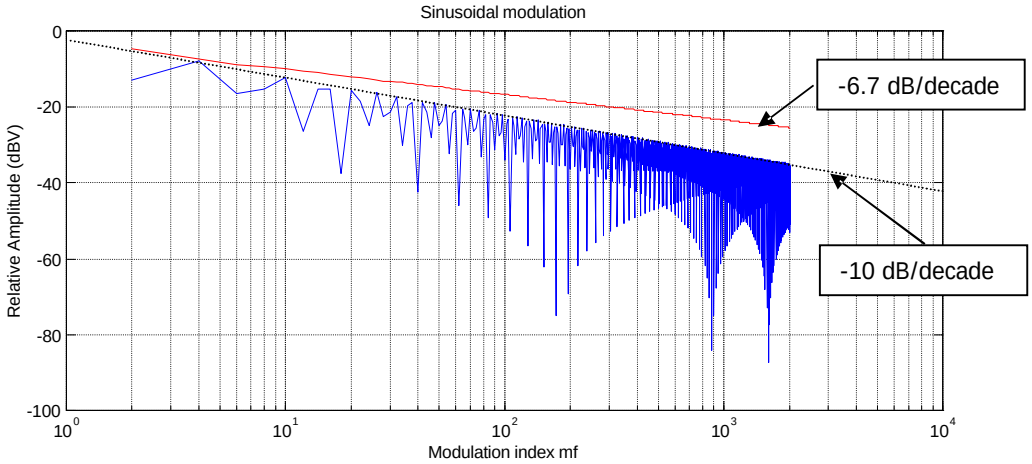

Figure 3-12. Figure 3-8(b) with m_f-axis in logarithmic scale: $F_{env,peak}$ (red line), F1 (blue line)

Envelopes of both parameters have a clear logarithmic behaviour because of its linear representation when the x-axis is displayed in logarithmic scale (Bode diagrams). In the case of parameter F1, an auxiliary dotted line was drawn, representing the envelope; this was not necessary for $F_{env,peak}$ because of its direct linear representation. The only difference is related to the slope: -6.7 dB/decade for the parameter $F_{env,peak}$ and -10 dB/decade for the parameter F1.

3.1.3 Evolution of the peak-to-peak envelope bandwidth Δf_{peak}

Another important parameter to be analysed corresponds to the peak-to-peak bandwidth Δf_{peak} of the side-band harmonics envelope corresponding to the modulated waveform. Figures 3-13(a) and 3-13(b) show the behaviour of this parameter versus the modulation index. Figure 3-13(a) displays four graphs at different ranges of modulation indexes, till m_f = 500; Figure 3-13(b) shows the same values till a modulation index m_f = 2000. This way, the complete range of modulation indexes is covered for the complete variety of parameter values (see Table 3-1).

A consecution of steps seems to be the behaviour of this parameter Δf_{peak} vs. the modulation index m_f. Again and due to the analytical results obtained for a sinusoidal modulation, this amusing behaviour can be derived. To do this, pay attention to Figure 3-11(a). Although infinity of side-band harmonics are always present in the modulated waveform spectra, from Point 0 to Point 1, the harmonic corresponding to the carrier frequency is the largest one, then yielding a null value for Δf_{peak}. From Point 1 to Point 2, the amplitude corresponding to the first two side-band harmonics [$J_1(m_f)$] is now the largest one; this means this range (Point 1-Point 2) is characterised for two harmonics of largest amplitude, each one separated in frequency a quantity of f_m from the carrier frequency, that is, a total distance of $2 \cdot f_m$ which corresponds to Δf_{peak}. In the same way, From Point 2 to Point 3, the amplitude corresponding to the second two side-band harmonics [$J_2(m_f)$] becomes now the largest one which means that the range Point 2-Point 3 is now characterised for two harmonics of largest amplitude, each one separated in frequency a quantity of $2 \cdot f_m$ from the carrier frequency, that is, a total distance of $2 \cdot 2 \cdot f_m = 4 \cdot f_m$ and so on. To sum up, From Point n to Point n+1, the amplitude corresponding to the n^{th} two side-band harmonics [$J_n(m_f)$] becomes the largest one which means that the range (Point n-Point n+1) is now characterised for two harmonics of largest amplitude, each one separated in frequency a quantity of $n \cdot f_m$ from the carrier frequency, that is, a total distance of $2 \cdot n \cdot f_m$. For instance, the first picture in Figure 3-13(a) shows steps 20 kHz-high, due to the modulating frequency of 10 kHz.

Some important conclusions are listed below:

- Envelope of Δf_{peak} shows a linear trend respect to m_f, which confirms the related analysis in point 3.1 where it was derived the expression $B = \Delta f_{peak} \approx 2 \cdot m_f \cdot f_m$. As an example, in Figure 3-13(b), for a modulation index m_f = 200 and a modulating frequency f_m = 250 Hz, Δf_{peak} is equal to 97.5 kHz, value which can be estimated by $B = \Delta f_{peak} \approx 2 \cdot m_f \cdot f_m$ = 100 kHz.
- Higher modulation indexes m_f are to produce wider bandwidths in a linear ratio.
- The step width remains practically constant through m_f and equal to $2 \cdot f_m$.

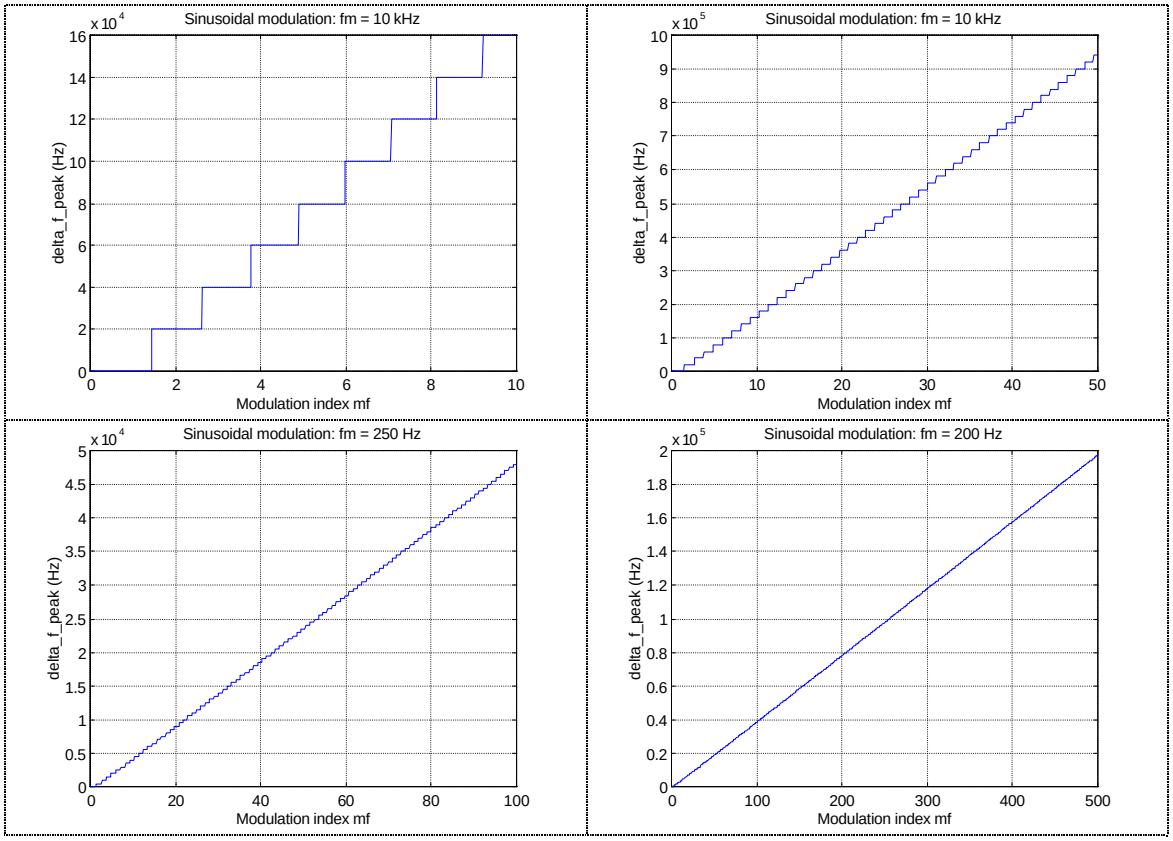

Figure 3-13(a). Peak-to-peak envelope bandwidth (Δf_{peak}) for different zooms of m_f..

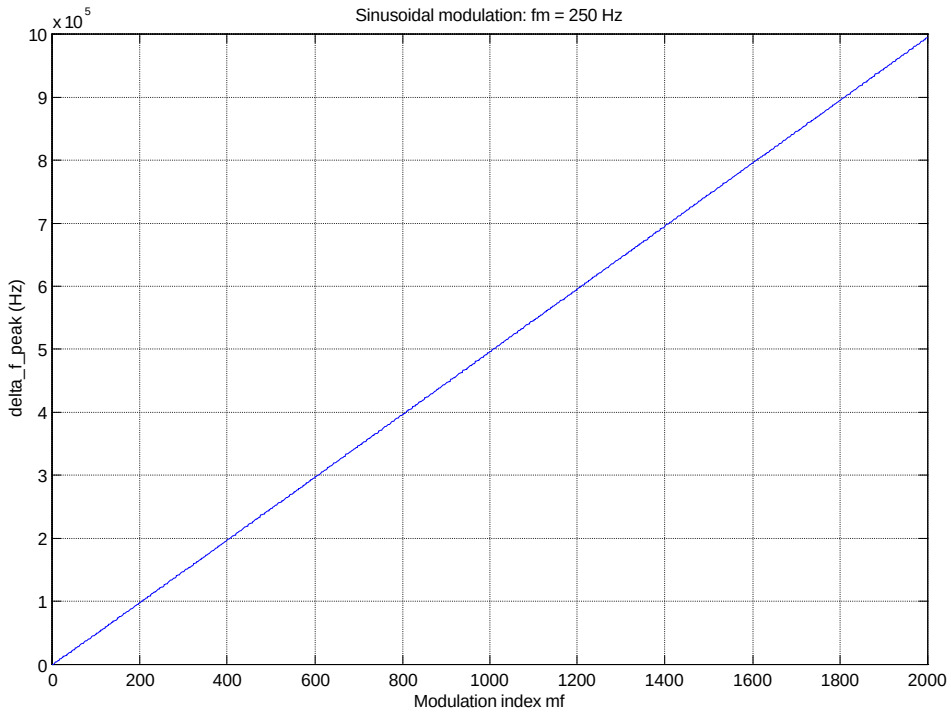

Figure 3-13(b). Peak-to-peak envelope bandwidth (Δf_{peak}) up to m_f. = 2000

3.2 Triangular modulation profile

Another typical modulation profile is that related to a triangular waveform. As presented in 2.3.2.2, parameter s controls the position of the triangular waveform vertex from 0 to $T_m/2$; therefore, modulation profiles from the typical triangular waveform to sawtooth waveforms are available. In Figure 3-14, three different triangular modulation profiles are shown, each one corresponding to a particular value of s (0.125, 0.25 and 0.5).

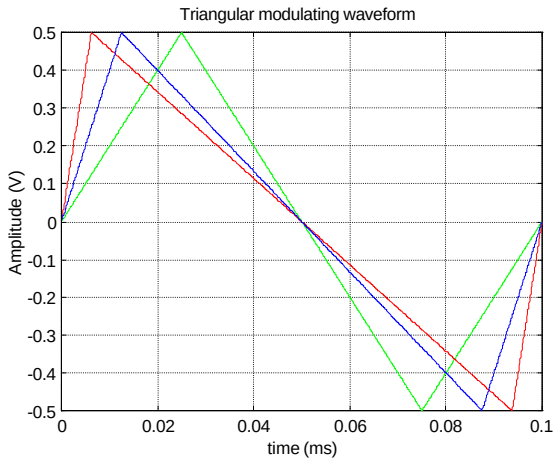

Figure 3-14. Triangular modulation profiles: s = 0.5 (green), s = 0.25 (blue), s = 0.125 (red)

An important point to study is related to the influence of the parameter s on the modulated waveform spectra, that is, how the more or less slope influences the resulting spectra. An important key to keep in mind is that a pure triangular modulation profile maintains a constant slope (in absolute value) during the whole period (except at the maximum and minimum peaks where the slope sign changes).

Figure 3-15 contains plots (obtained from the MATLAB algorithm) corresponding to the shape evolution of the side-band harmonics resulting from the pure triangular modulation (s = 0.5) of a sinusoidal carrier. A very important difference compared to the sinusoidal modulation is clearly observed: for a triangular modulation, the envelope of the side-band harmonics corresponds to a nearly straight, horizontal line, very opposite to the sinusoidal modulation behaviour where a concavity between two extreme peaks is the most impacting visual aspect. And this "pure" triangular behaviour is extensive to the sawtooth waveforms as it can be derived of Figure 3-16, where four triangular modulation profiles with the unique difference of the parameter s are compared.

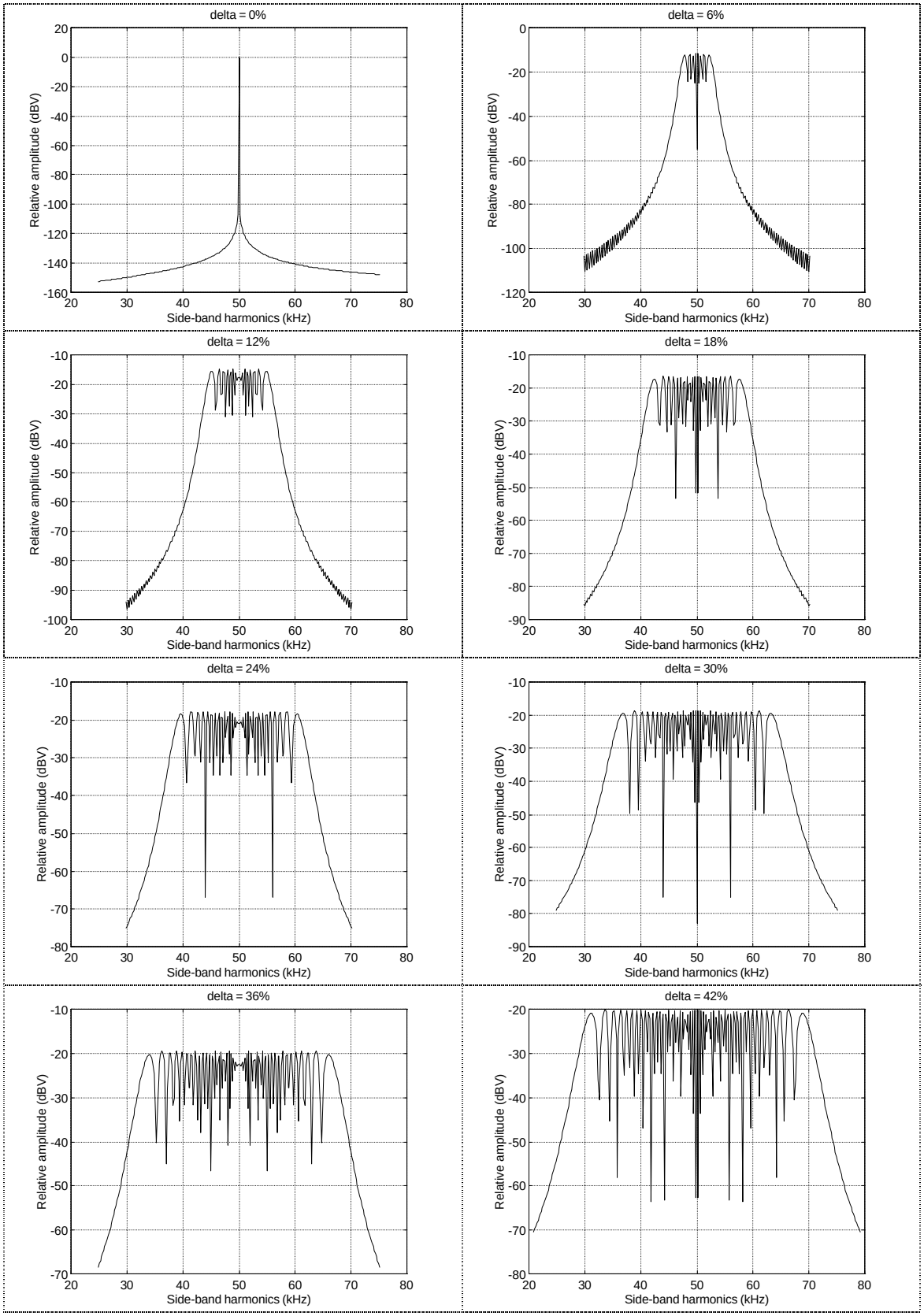

Figure 3-15. Evolution of side-band harmonics envelope: triangular modulation

($s = 0.5$, $f_c = 50$ kHz, $f_m = 200$ Hz)

Another important conclusion can be derived from plots in Figure 3-16. The lower the parameter s, the lower the variation band of the side-band harmonic amplitudes. For s = 0.5, amplitudes ranges from ≈-20 dBV to ≈-65 dBV; however, for s = 0.0625, harmonic amplitudes vary from ≈-21.5 dBV to ≈-26 dBV.

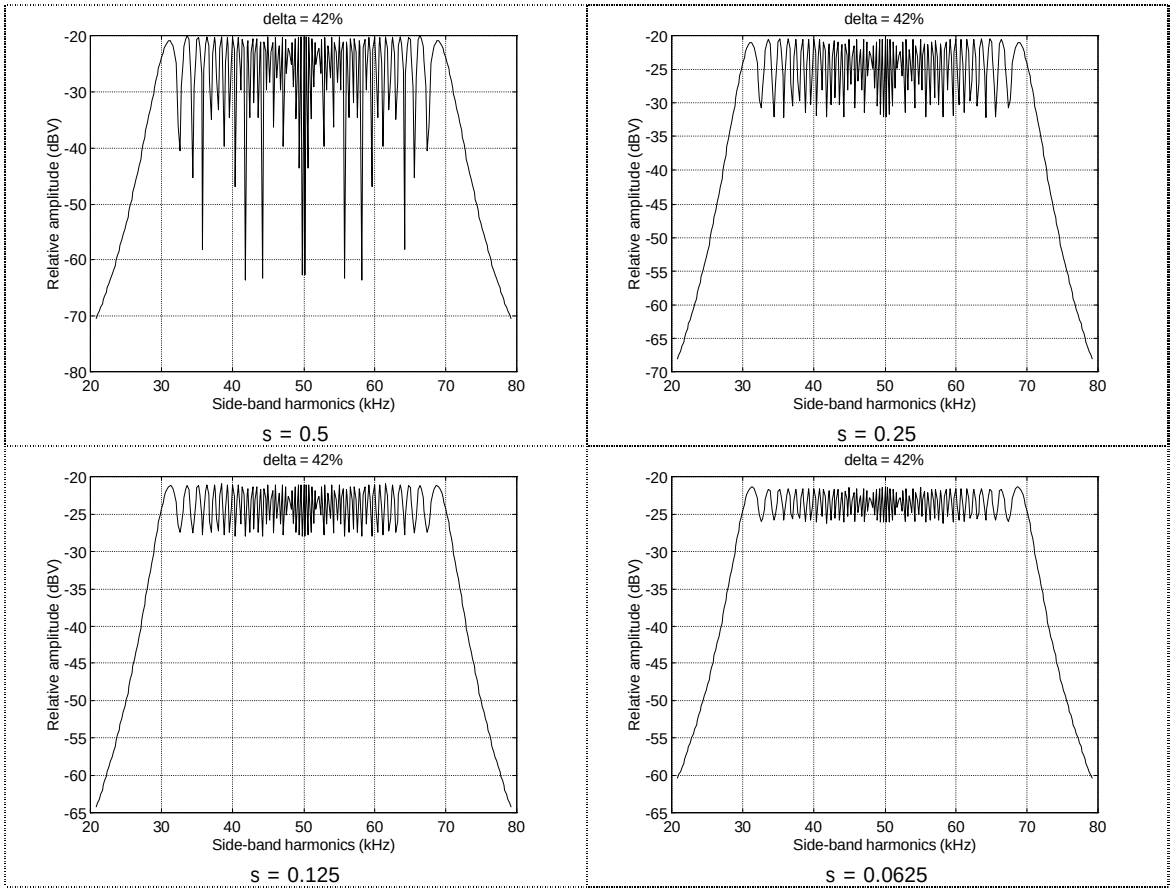

Figure 3-16. Evolution of side-band harmonics envelope: triangular modulation (f_c = 50 kHz, f_m = 200 Hz) at different values of s.

In other words, sawtooth modulation profiles are to produce a flat distribution of side-band harmonics along the complete modulation bandwidth, keeping them inside a narrower band of amplitude variation than the one corresponding to a "pure" triangular modulation profile. This is a logical behaviour: as the total energy of the modulated waveform must be maintained, the whole side-band harmonics can be either distributed inside a very narrow amplitude variation band (sawtooth waveforms) obtaining an approximate constant value of harmonic amplitude or distributed in such a way that some or many of them to be cancelled (-60 dBV in "pure" triangular profile) while the rest must be a few larger than the approximate constant value obtained for

the sawtooth case, in order to conserve the total energy of the modulated waveform, as expressed before.

This way, a triangular modulation profile may be used to cancel some harmonics while increasing a few more the amplitude of the rest ones; opposite to it, a sawtooth modulation profile is not intended to cancel harmonic but to keep all of them inside a narrow variation band. This will be studied in more detail in the following clauses 3.2.1 to 3.2.3.

3.2.1 Dependence on the modulation index

When the sinusoidal modulation was developed in detail (see clause 3.1), it was demonstrated that side-band harmonic amplitudes only depended on the modulation index m_f. This aspect facilitates the representation of the different parameters under study (F_1, $F_{env,peak}$ and Δf_{peak}) along the modulation index m_f, which means a complete generalization of the plots. It is now time to verify if this behaviour is also present in triangular modulation. To do this, some calculations are to be carried out with different combinations of modulation ratioδ, modulating frequency f_m and carrier frequency f_c, but yielding the same modulation index $m_f = \frac{\delta \cdot f_c}{f_m}$. If the results match exactly each other, it can be assured that, for triangular modulations, the amplitudes of the side-band harmonics only depend on the modulation index too.

Table 3-2 summarizes the different combinations intended to verify the dependence on the harmonic amplitude of a triangular modulation with the modulation index. This verification was tested for two different values of the parameter s and the different combinations were named from mf_1 to mf_8.

m_f	s	δ% (%)	f_c (kHz)	f_m (kHz)	File name
10	0.5	10	100	1	mf_1
10	0.5	8	250	2	mf_2
10	0.5	10	500	5	mf_3
10	0.5	1	200	0.2	mf_4
10	0.25	10	100	1	mf_5
10	0.25	8	250	2	mf_6
10	0.25	10	500	5	mf_7
10	0.25	1	200	0.2	mf_8

Table 3-2. Four combinations of δ%, f_c, f_m for the same modulation index m_f and different values of s

Results (expressed in V) are shown in Table 3-3, whose values were calculated by using the MATLAB algorithm. In this table, figures in bold represent the F1 value of the modulated waveform spectra, just surrounded by the left- and right side-band harmonics.

s = 0.5				s = 0.25			
mf_1	mf_2	mf_3	mf_4	mf_5	mf_6	mf_7	mf_8
0.00033990	0.00033952	0.00033990	0.00033987	0.00041363	0.00041370	0.00041363	0.00041380
0.00038185	0.00038179	0.00038185	0.00038181	0.00055045	0.00055047	0.00055045	0.00055035
0.00054312	0.00054273	0.00054312	0.00054260	0.00067022	0.00067004	0.00067022	0.00066987
0.00065401	0.00065395	0.00065401	0.00065397	0.00082732	0.00082717	0.00082732	0.00082711
0.00094254	0.00094218	0.00094254	0.00094258	0.00113321	0.00113328	0.00113321	0.00113334
0.00122354	0.00122348	0.00122354	0.00122350	0.00158376	0.00158383	0.00158376	0.00158401
0.00181355	0.00181319	0.00181355	0.00181300	0.00214708	0.00214696	0.00214708	0.00214733
0.00254899	0.00254894	0.00254899	0.00254898	0.00298032	0.00298021	0.00298032	0.00298065
0.00393666	0.00393633	0.00393666	0.00393681	0.00440822	0.00440831	0.00440822	0.00440853
0.00596608	0.00596603	0.00596608	0.00596608	0.00670845	0.00670855	0.00670845	0.00670844
0.00960035	0.00960001	0.00960035	0.00959978	0.01025036	0.01025026	0.01025036	0.01025000
0.01531108	0.01531103	0.01531108	0.01531117	0.01594444	0.01594432	0.01594444	0.01594418
0.02493679	0.02493649	0.02493679	0.02493725	0.02528284	0.02528291	0.02528284	0.02528306
0.03943931	0.03943927	0.03943931	0.03943951	0.03964441	0.03964448	0.03964441	0.03964506
0.06026075	0.06026043	0.06026075	0.06026030	0.05942704	0.05942690	0.05942704	0.05942787
0.08411734	0.08411731	0.08411734	0.08411773	0.08254799	0.08254787	0.08254799	0.08254866
0.10206243	0.10206215	0.10206243	0.10206311	0.10043350	0.10043349	0.10043350	0.10043327
0.09342640	0.09342635	0.09342640	0.09342580	0.09476005	0.09475982	0.09476005	0.09475872
0.03910452	0.03910416	0.03910452	0.03910212	0.05062800	0.05062779	0.05062800	0.05062730
0.05360463	0.05360471	0.05360463	0.05360580	0.05658498	0.05658511	0.05658498	0.05658567
0.11291572	0.11291598	0.11291572	0.11291470	0.10607621	0.10607629	0.10607621	0.10607560
0.05241729	0.05241730	0.05241729	0.05241614	0.05438447	0.05438449	0.05438447	0.05438428
0.08462207	0.08462179	0.08462207	0.08462167	0.08537532	0.08537545	0.08537532	0.08537527
0.0776960	0.0776959	0.0776960	0.0776959	0.0796256	0.0796257	0.0796256	0.0796256
0.08462175	0.08462203	0.08462175	0.08462215	0.08537554	0.08537547	0.08537554	0.08537554
0.05241756	0.05241763	0.05241756	0.05241877	0.05438459	0.05438458	0.05438459	0.05438479
0.11291636	0.11291613	0.11291636	0.11291740	0.10607669	0.10607650	0.10607669	0.10607734
0.05360439	0.05360439	0.05360439	0.05360328	0.05658484	0.05658493	0.05658484	0.05658422
0.03910464	0.03910496	0.03910464	0.03910701	0.05062789	0.05062793	0.05062789	0.05062853
0.09342652	0.09342651	0.09342652	0.09342707	0.09475995	0.09476015	0.09475995	0.09476124
0.10206187	0.10206209	0.10206187	0.10206115	0.10043368	0.10043359	0.10043368	0.10043386
0.08411724	0.08411719	0.08411724	0.08411680	0.08254784	0.08254771	0.08254784	0.08254717
0.06026043	0.06026068	0.06026043	0.06026083	0.05942662	0.05942667	0.05942662	0.05942580
0.03943924	0.03943921	0.03943924	0.03943898	0.03964441	0.03964435	0.03964441	0.03964378
0.02493627	0.02493649	0.02493627	0.02493576	0.02528314	0.02528293	0.02528314	0.02528295
0.01531103	0.01531100	0.01531103	0.01531088	0.01594451	0.01594443	0.01594451	0.01594480
0.00960006	0.00960030	0.00960006	0.00960056	0.01025031	0.01025037	0.01025031	0.01025070
0.00596606	0.00596603	0.00596606	0.00596601	0.00670867	0.00670861	0.00670867	0.00670873
0.00393619	0.00393641	0.00393619	0.00393595	0.00440851	0.00440831	0.00440851	0.00440825
0.00254897	0.00254894	0.00254897	0.00254892	0.00298026	0.00298016	0.00298026	0.00297996
0.00181324	0.00181347	0.00181324	0.00181369	0.00214687	0.00214691	0.00214687	0.00214662
0.00122351	0.00122349	0.00122351	0.00122350	0.00158385	0.00158381	0.00158385	0.00158363
0.00094209	0.00094229	0.00094209	0.00094194	0.00113351	0.00113334	0.00113351	0.00113344
0.00065398	0.00065395	0.00065398	0.00065396	0.00082737	0.00082729	0.00082737	0.00082760
0.00054278	0.00054300	0.00054278	0.00054317	0.00067010	0.00067015	0.00067010	0.00067043
0.00038183	0.00038180	0.00038183	0.00038181	0.00055056	0.00055055	0.00055056	0.00055068
0.00033945	0.00033965	0.00033945	0.00033935	0.00041389	0.00041375	0.00041389	0.00041378

Table 3-3. MATLAB algorithm results (in volts) for the different combinations in Table 3-2.

From the direct analysis of data in Table 3-3, it must be concluded that the amplitude of the harmonics generated during a triangular modulation process only depend on the modulation index. As expected, parameter s does not have any influence over the studied behaviour.

This way, and as in the sinusoidal modulation case, the following analysis will be carried out by studying the behaviour of the several parameters defined at the beginning of chapter 3 along the modulation index m_f.

3.2.2 Evolution of the central harmonic amplitude F_1

In the following Figures 3-17(a) to (d), F_1 (relative amplitude of the harmonic corresponding to the modulated waveform at a frequency f_c) is displayed as a function of the modulation index m_f. Each figure consists of three graphs corresponding to three different values of parameter s, i.e., 0.5 (blue line), 0.25 (red line) and 0.125 (green line), and a certain range of modulation indexes, trying to cover a very wide range of modulation indexes.

Just a consideration to indicate that exactly the same figures are to be obtained for values of s symmetrical to s = 0.5, that is, the same spectra is to be found for s = 0.25 and for s = 0.75 because it is only a matter of phases and it was derived in 2.2.3.3 that phase does not affect the resulting amplitude spectra at all.

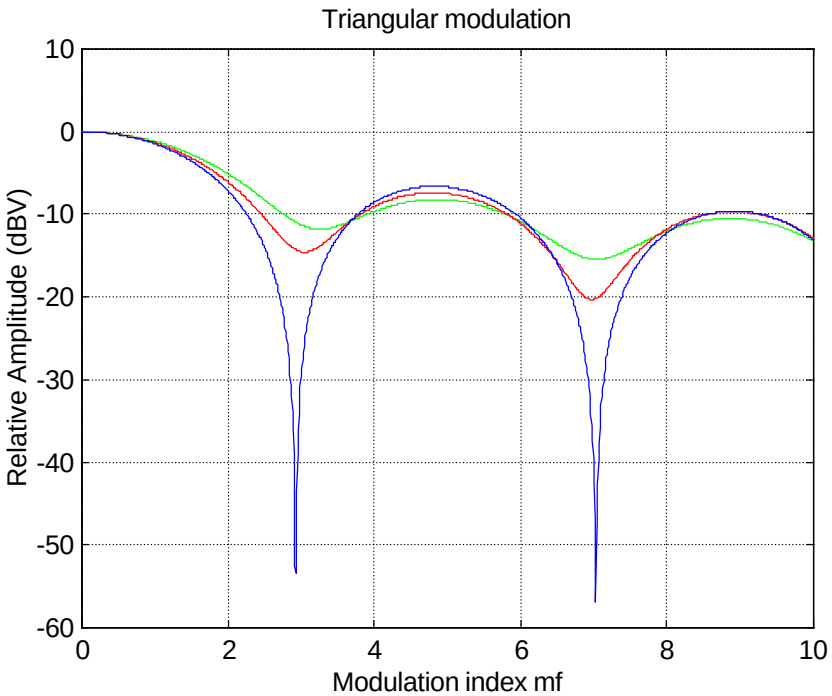

Figure 3-17(a). Relative rms-amplitude (F_1) of harmonic at the carrier frequency for different values of parameter s: s = 0.125 (green line), s = 0.25 (red), s = 0.5 (blue) till m_f = 10

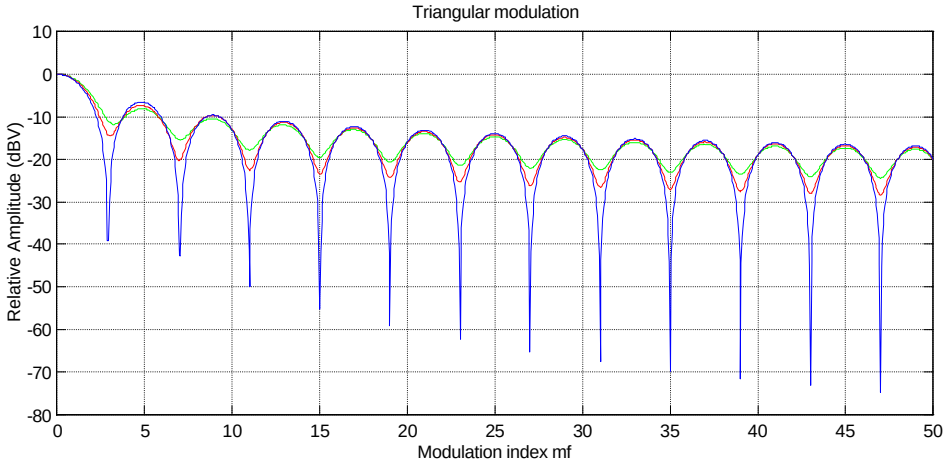

Figure 3-17(b). Relative rms-amplitude (F_1) of harmonic at the carrier frequency for different values of parameter s: s = 0.125 (green line), s = 0.25 (red), s = 0.5 (blue) till m_f = 50

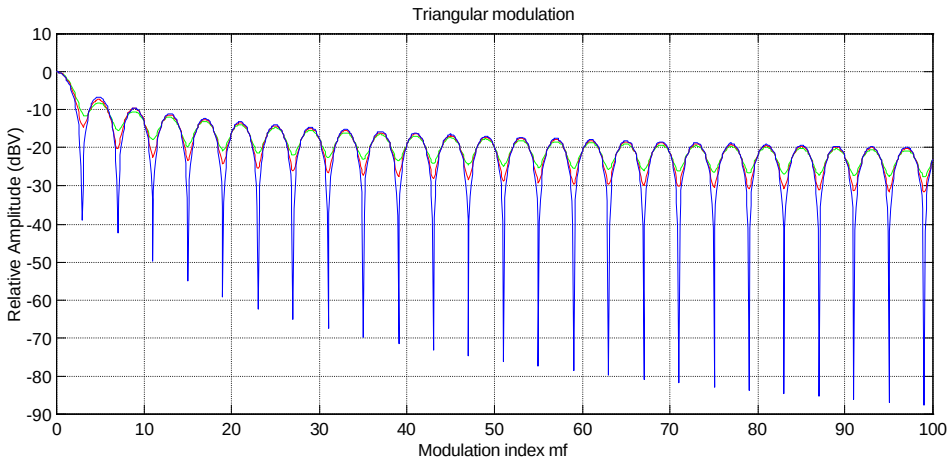

Figure 3-17(c). Relative rms-amplitude (F_1) of harmonic at the carrier frequency for different values of parameter s: s = 0.125 (green line), s = 0.25 (red), s = 0.5 (blue) till m_f = 100

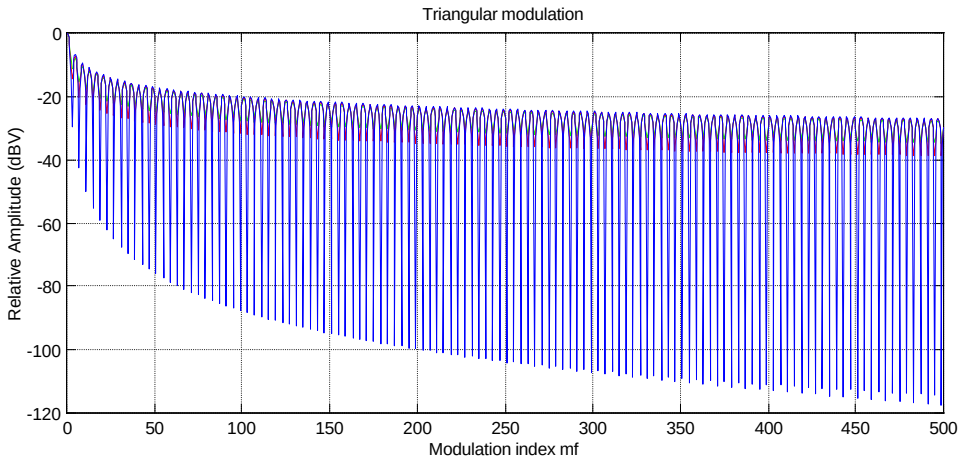

Figure 3-17(d). Relative rms-amplitude (F_1) of harmonic at the carrier frequency for different values of parameter s: s = 0.125 (green line), s = 0.25 (red), s = 0.5 (blue) till m_f = 500

Several conclusions can be extracted from the observation of these figures:

- The larger m_f, the larger the attenuation (regarding the envelope of F_1). However, for $m_f > 200$, attenuation remains nearly constant; therefore, it is not worthy to work at higher modulation indexes than 200.
- As anticipated at the beginning of clause 3.2, values of s higher or lower than 0.5 are not to produce a cancellation of the harmonic at the carrier frequency, i.e., cancellation of F1, for any modulation indexes. However, for s = 0.5, a special profit of this individual behaviour can be taken just tuning thet system to a concrete modulation index in order, for instance, to eliminate the harmonic at the carrier frequency.
- The lower s, the lower the oscillation band of F1. And even more significant, oscillation period along m_f is equal independently on the parameter s.
- Maximum value of the F1-envelope (a logarithmic curve joining the local maximum points of every individual oscillation) at any modulation indexes corresponds to the blue line, that is, to s = 0.5.

3.2.3 Evolution of the maximum envelope amplitude $F_{env,peak}$

Next important parameter to be analysed corresponds to the maximum rms-amplitude of the side-band harmonic envelope corresponding to the modulated waveform. In the following Figures 3-18(a) to 3-18(d), $F_{env,peak}$ is displayed as a function of the modulation index m_f. Each figure consists of three graphs corresponding to three different values of parameter s, i.e., 0.5 (blue line), 0.25 (red line) and 0.125 (green line), and a certain range of modulation indexes, trying to cover a very wide range of modulation indexes.

Some conclusions are to be extracted from the analysis of the plots in Figure 3-18:

- A very narrow oscillation band is present at any modulation index m_f and s. For $m_f > 2$, the lower s, the higher the attenuation of $F_{env,peak.}$ Although amplitude differences of $F_{env,peak}$ for the different values of s increase along m_f, only slightly differences are to be found. For instance, at $m_f = 500$, $F_{env,peak} = -26.86$ dBV for s = 0.5 and , $F_{env,peak} = -27.77$ dBV for s = 0.125.

The larger m_f, the larger the attenuation of $F_{env,peak}$ (referred to the envelope). However, for $m_f > 200$, attenuation remains nearly constant; therefore, it is not worthy to work at higher modulation indexes than 200.

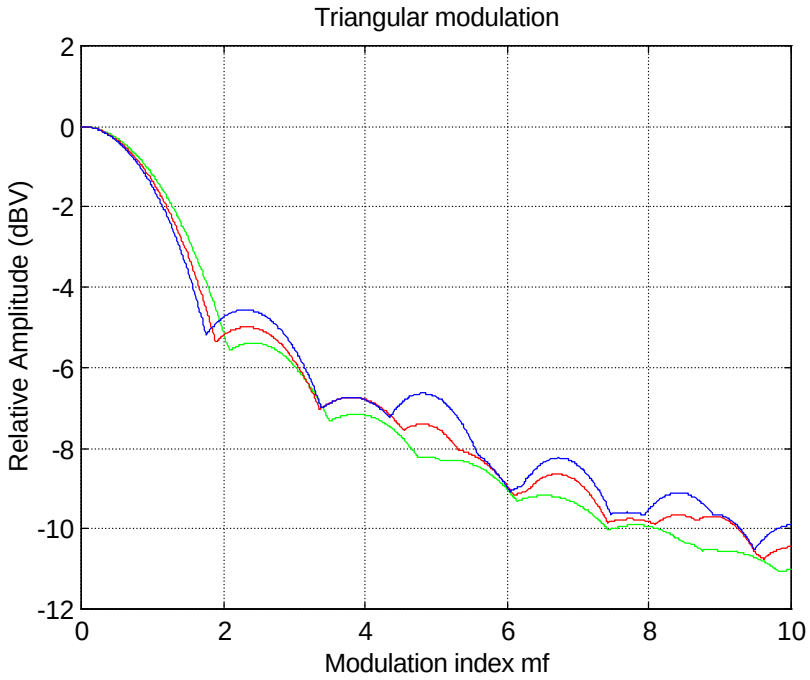

Figure 3-18(a). Maximum relative rms-amplitude ($F_{env,peak}$) of the harmonics envelope for different values of parameter s: s = 0.125 (green line), s = 0.25 (red), s = 0.5 (blue) till $m_f = 10$

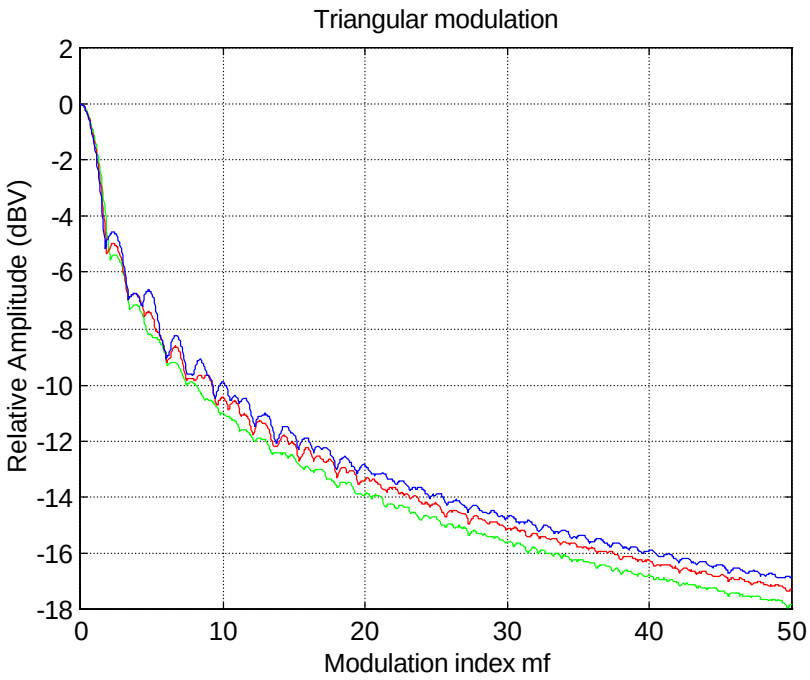

Figure 3-18(b). Maximum relative rms-amplitude ($F_{env,peak}$) of the harmonics envelope for different values of parameter s: s = 0.125 (green line), s = 0.25 (red), s = 0.5 (blue) till $m_f = 50$

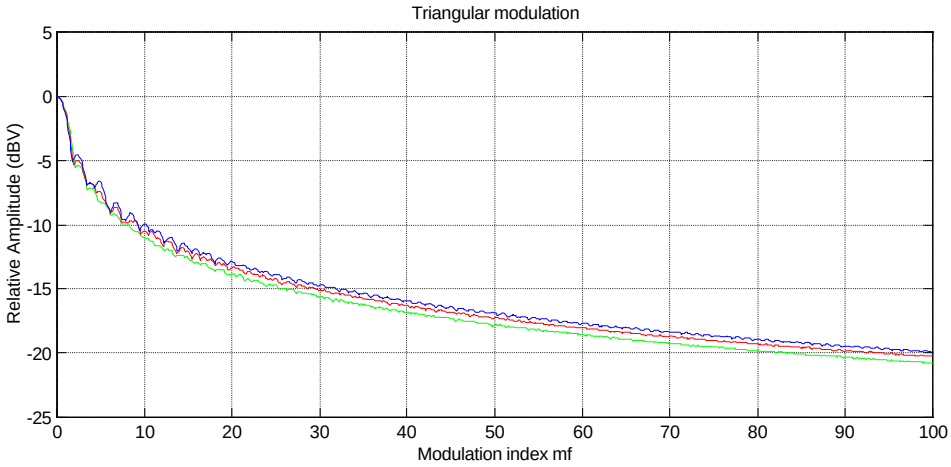

Figure 3-18(c). Maximum relative rms-amplitude ($F_{env,peak}$) of the harmonics envelope for different values of parameter s: s = 0.125 (green line), s = 0.25 (red), s = 0.5 (blue) till m_f = 100

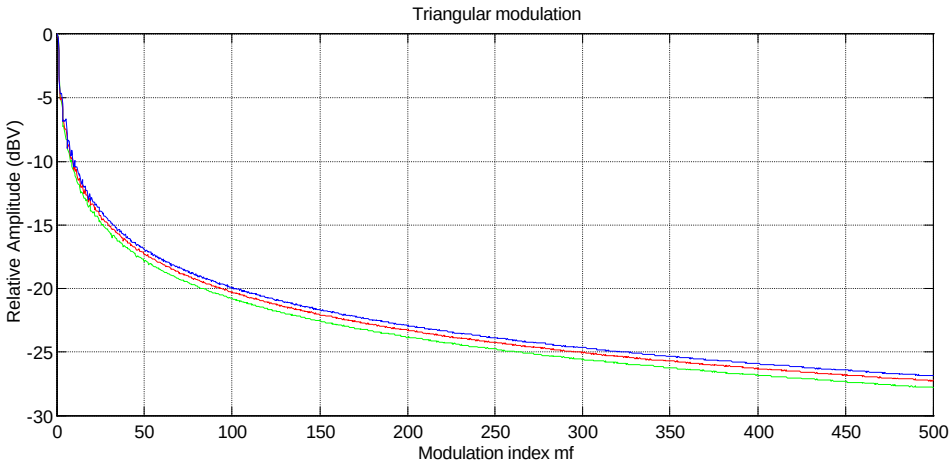

Figure 3-18(d). Maximum relative rms-amplitude ($F_{env,peak}$) of the harmonics envelope for different values of parameter s: s = 0.125 (green line), s = 0.25 (red), s = 0.5 (blue) till m_f = 500

Figures 3-19(a), (b) and (c) plot both F_1 and $F_{env,peak}$ for different values of s (0.5, 0.25 and 0.125). A very clear difference is found respect to the results obtained for sinusoidal modulation [see comparison in Figure 3-19(a) and the related curves in Figures 3-8(a) and (b) in clause 3.1.1]. For triangular modulation, curve of $F_{env,peak}$ stays very near (or even matches) the maximum local values of curve F_1 (see Figures 3-19(b) and (c)); for sinusoidal modulation, $F_{env,peak}$ remained always over F_1. This is just saying that the shape of the side-band harmonic spectra is approximately flat for any triangular modulation, as shown in Figures 3-15 and 3-16. Behaviour of the sinusoidal modulation was completely different; a very large difference between F_1 and $F_{env,peak}$ was observed and the reason was the concave distribution of the side-band harmonics around the carrier frequency.

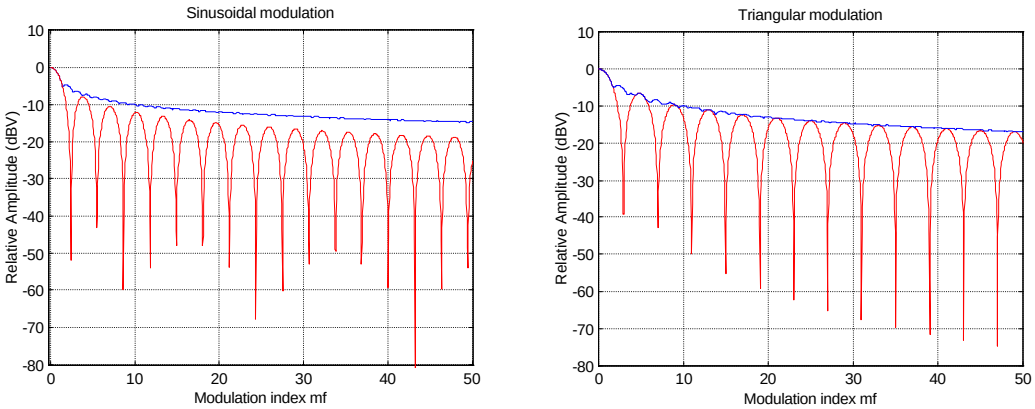

Figure 3-19(a). Comparison of F1 (red line) vs $F_{env,peak}$ (blue line) for sinusoidal and triangular modulation (s = 0.5)

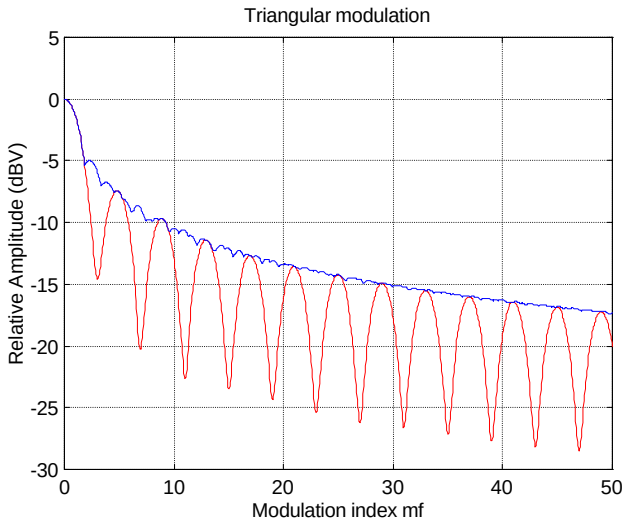

Figure 3-19(b). Comparison of F1 (red line) vs $F_{env,peak}$ (blue line) for s = 0.25

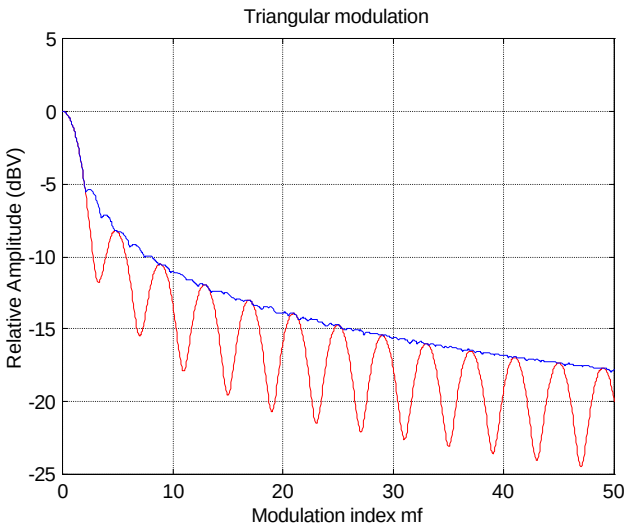

Figure 3-19(c). Comparison of F1 (red line) vs $F_{env,peak}$ (blue line) for s = 0.125

CONSIDERATIONS ABOUT THE LOGARITHMIC BEHAVIOUR OF PARAMETERS $F_{env,peak}$ and F1 FOR s=0.5

In previous figures, it is observed that the evolution of the relatives amplitudes F1 and $F_{env,peak}$ shows a logarithmic trend. In order to quantify this behaviour, both parameters are displayed by using a logarithmic scale for the m_f-axis.

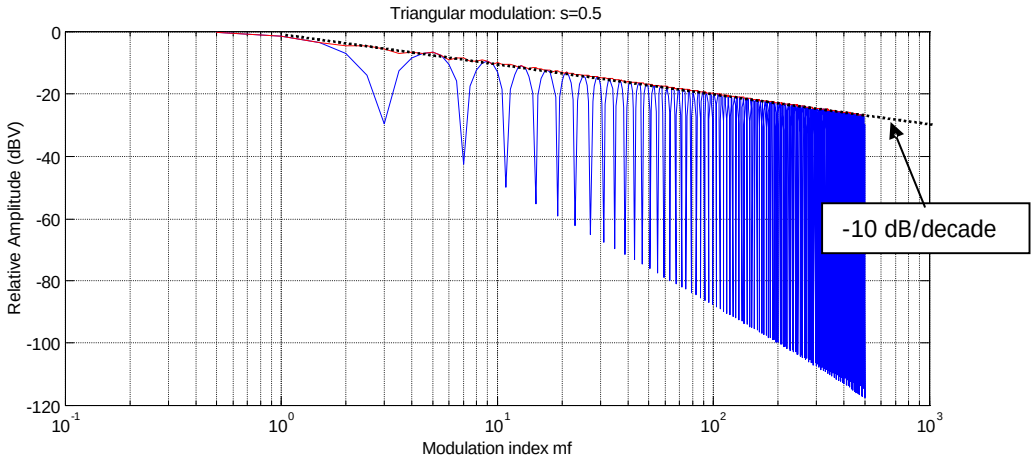

Figure 3-20. $F_{env,peak}$ (red line) and F1 (blue line) for s = 0.5 and m_f-axis in logarithmic scale

Envelopes of both parameters have a clear logarithmic behaviour because of its linear representation when the x-axis is displayed in logarithmic scale (Bode diagrams). In the case of parameter F1, an auxiliary dotted line was drawn, representing the envelope and matching very closely the plot for $F_{env,peak}$. No differences are found respect to the slope: -10 dB/decade for both parameters F1 and $F_{env,peak}$.

3.2.4 Evolution of the peak-to-peak envelope bandwidth Δf_{peak}

Next important parameter to be analysed corresponds to the peak-to-peak bandwidth Δf_{peak} of the side-band harmonics envelope corresponding to the modulated waveform. Figures 3-21(a) to (d) show the behaviour of this parameter versus the modulation index. Each figure has three graphs corresponding to three different values of parameter s, i.e., 0.5 (blue line), 0.25 (red line) and 0.125 (green line), and a certain range of modulation indexes covering a very wide range of modulation indexes.

Observe that the modulating frequency has been specified for every plot because the distance in frequency between two consecutive side-band harmonics is given by f_m.

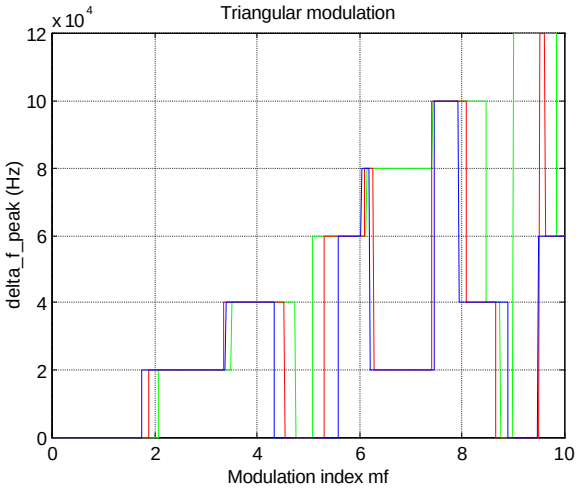

Figure 3-21(a). Peak-to-peak envelope bandwidth (Δf_{peak}) for different values of s: s = 0.125 (green line), s = 0.25 (red), s = 0.5 (blue) and f_m = 10 kHz till m_f = 10

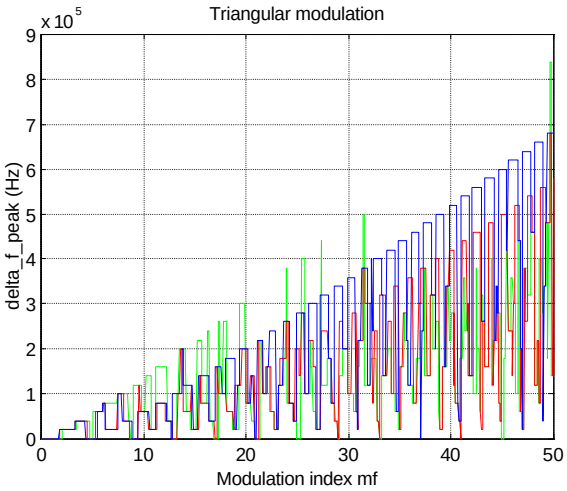

Figure 3-21(b). Peak-to-peak envelope bandwidth (Δf_{peak}) for different values of s: s = 0.125 (green line), s = 0.25 (red), s = 0.5 (blue) and f_m = 10 kHz till m_f = 50

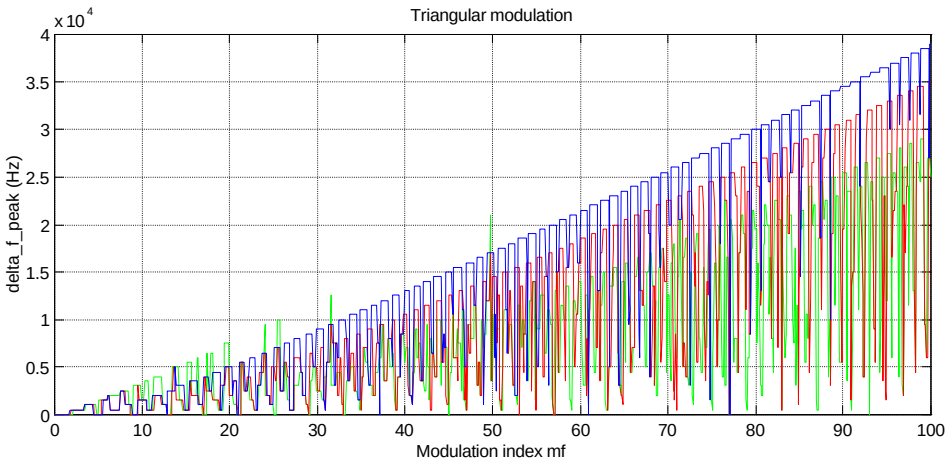

Figure 3-21(c). Peak-to-peak envelope bandwidth (Δf_{peak}) for different values of s: s = 0.125 (green line), s = 0.25 (red), s = 0.5 (blue) and f_m = 250 Hz till m_f = 100

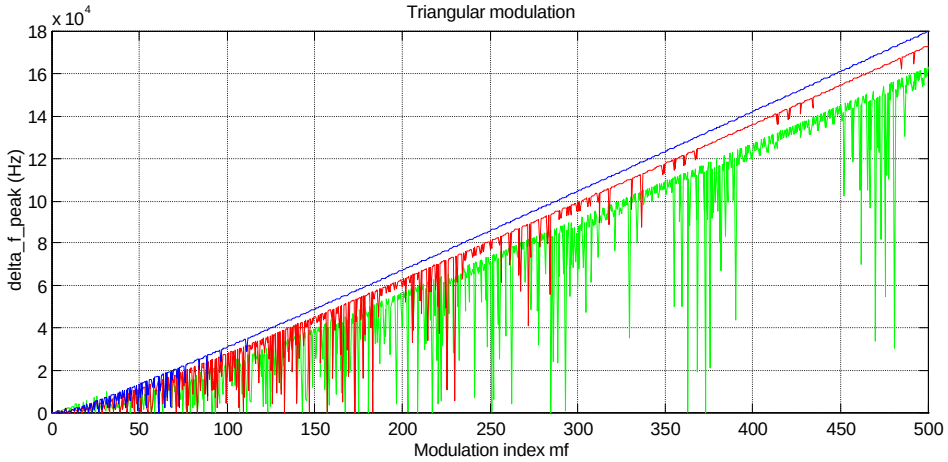

Figure 3-21(d). Peak-to-peak envelope bandwidth (Δf_{peak}) for different values of s: s = 0.125 (green line), s = 0.25 (red), s = 0.5 (blue) and f_m = 200 Hz till m_f = 500

Some conclusions are of interest:

- Maximum values of Δf_{peak} show a linear trend for any value of s along m_f. However, under this theoretical line defined by these maximum values, a chaotic behaviour is shown, which is strongly related to the flat shape of the side-band harmonic spectra distribution. When the whole harmonics tends to match the same value, it becomes very easy to jump from one harmonic to another one, perhaps, very far or perhaps very near to the first one, thus producing this chaotic behaviour. This is more strongly visible for lower values of s (green lines) where it was seen that the side-band harmonic amplitudes is concentrated inside a very narrow oscillation band. A clearer behaviour is observed for s = 0.5 and m_f > 115, showing a similar behaviour compared to the sinusoidal modulation profile, this indicating that s = 0.5 is the value which is to produce a spectra distribution with more concavity, but not loosing the flat outline at any time.
- Higher modulation indexes m_f are to produce wider bandwidths in a linear ratio (only true for maximum values of Δf_{peak}).
- The lower s, the lower Δf_{peak} (only true for maximum values of Δf_{peak}).

3.3 Exponential modulation profile

The third typical modulation profile is that related to an exponential waveform. As presented in 2.3.2.3, parameter p is a very helpful factor because it defines exactly not only the higher or lower curvature of the exponential profile but also its concavity or convexity. It is more useful to declare this parameter as a function of the modulating frequency, that is, $p = k \cdot f_m$, where k was already defined as the concavity factor. Figure 3-22 displays three different exponential profiles where the concavity factor k takes the values 12, 24 and 48.

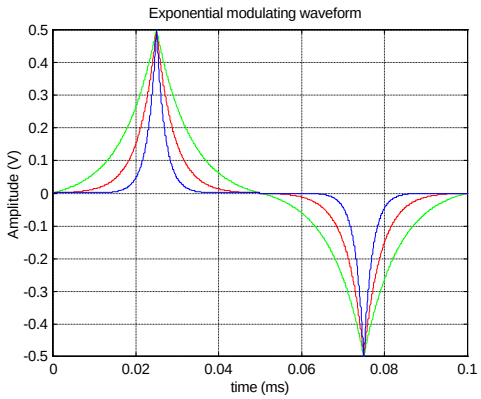

Figure 3-22. Exponential modulation profiles [f_m = 10 kHz]: k = 12 (green), k = 24 (red), k = 48 (blue)

The objective is to study the influence of the parameter p (or the corresponding concavity factor k) on the modulated waveform spectra, that is, how the more or less concavity influences the resulting spectra. It should be taken into account that the three exponential profiles shown above are contained inside a triangular profile; this should be very helpful further to analyse differences between the different types of modulation profiles: sinusoidal, triangular and exponential.

Figure 3-23 contains plots (obtained from the MATLAB algorithm) corresponding to the shape evolution of the side-band harmonics resulting from an exponential modulation (k = 24) of a sinusoidal carrier. A very important difference compared to the previous sinusoidal and triangular modulation is clearly observed: for a triangular modulation, the envelope of the side-band harmonics corresponds to a nearly straight, horizontal line, very opposite to the sinusoidal modulation behaviour, characterised by a concavity between two extreme peaks. However, in the case of an exponential modulation profile, side-band harmonics resulting from the modulation process tend to concentrate

around the carrier frequency, decreasing in amplitude as the harmonic order separates itself from the carrier frequency.

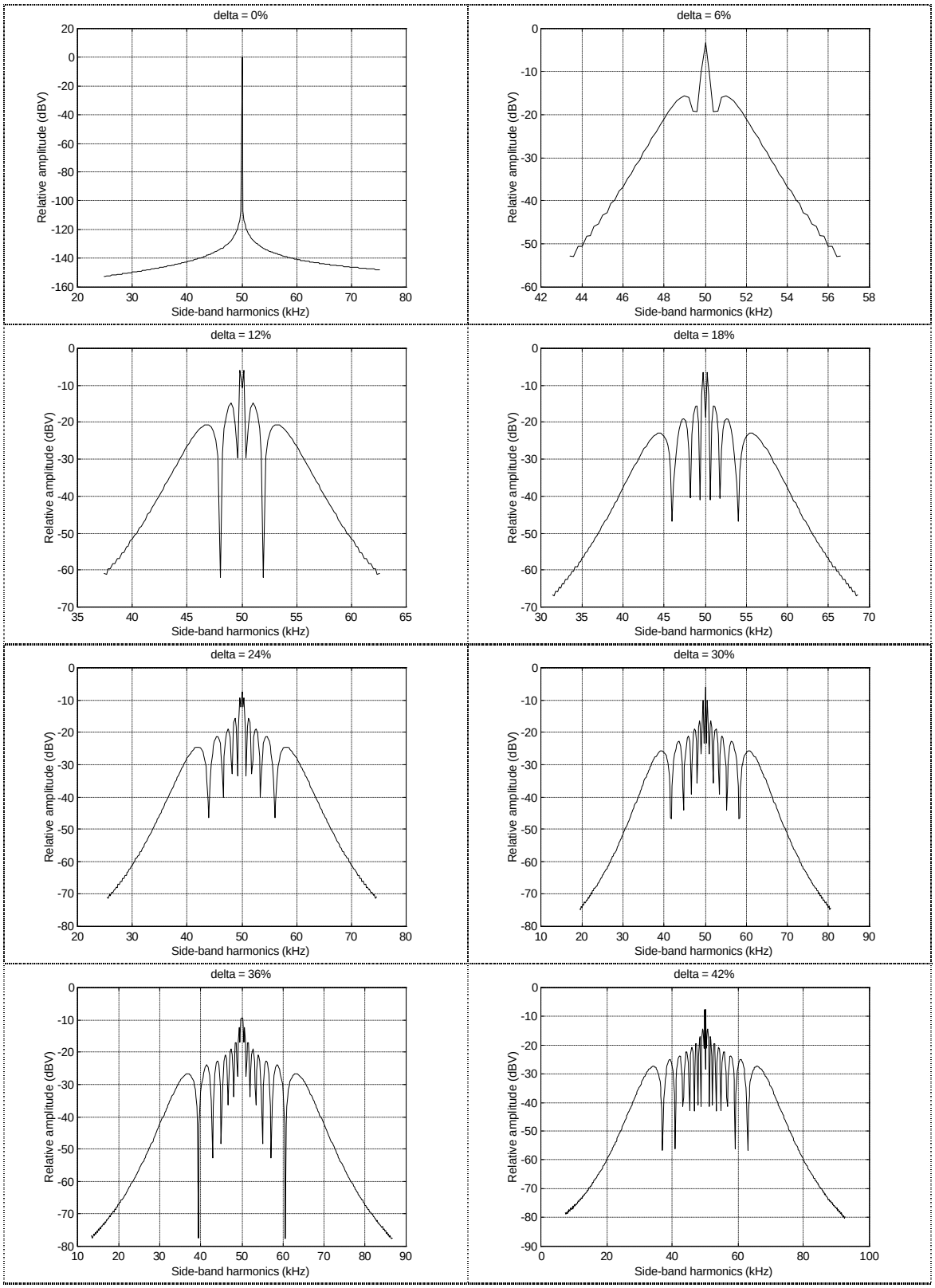

Figure 3-23. Evolution of side-band harmonics envelope: exponential modulation ($k = 24$, $f_c = 50$ kHz, $f_m = 200$ Hz)

Figure 3-24 provides also another interesting point of view. While in Figure 3-23, parameter p (or k) was fixed and the percentage of modulation was varied, in Figure 3-24, a constant δ% = 42 % is fixed while varying the concavity factor k (12, 18, 24 and 48).

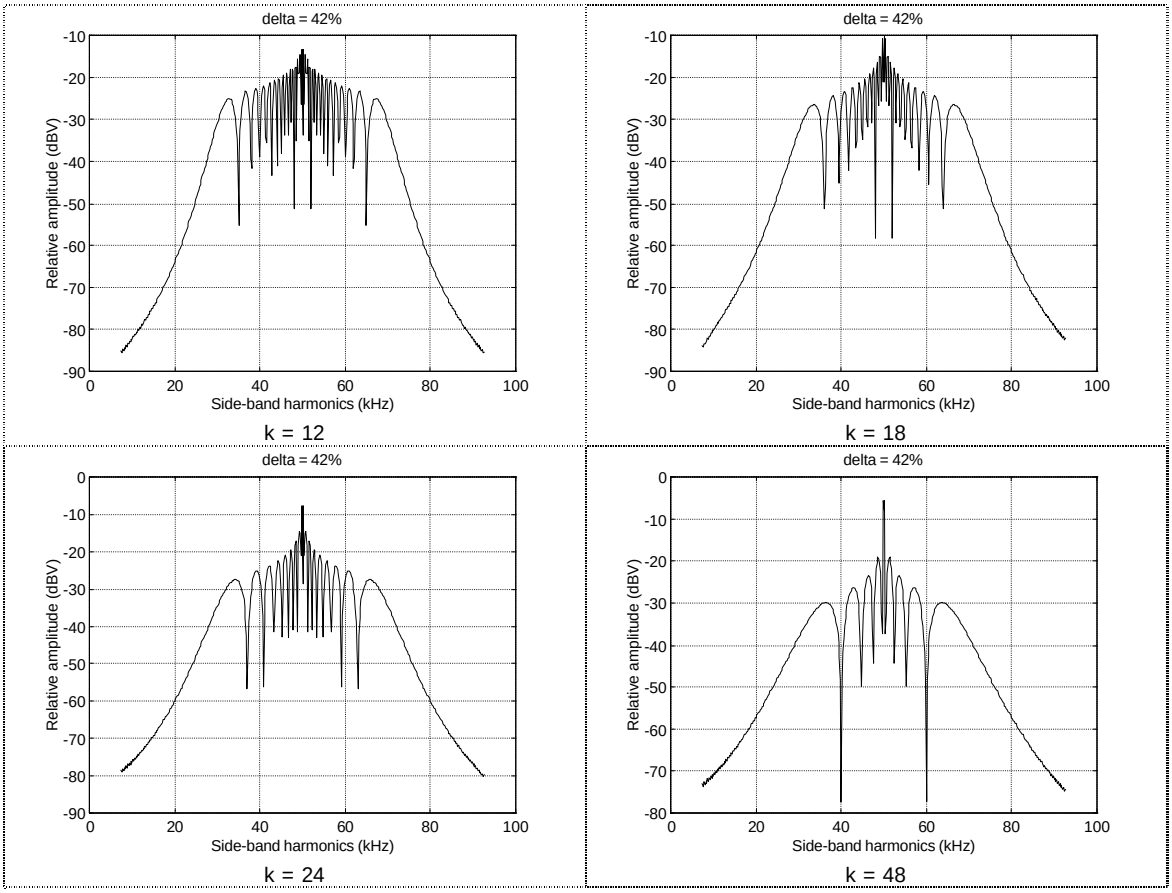

Figure 3-24. Evolution of side-band harmonics envelope: exponential modulation (f_c =50 kHz, f_m = 200Hz)

It seems to be clear that lower concavity factors k are to produce a side-band harmonic distribution whose shape tends to be flat. This is a logical result because lower concavity factors k display an exponential profile very near to a triangular waveform, this last yielding a flat distribution of the side-band harmonics. This way, the higher concavity factor k, the more visible the peak-outline of the side-band harmonic distribution.

3.3.1 Dependence on the modulation index

When the sinusoidal modulation was developed in detail (see clause 3.1), it was demonstrated that the side-band harmonic amplitudes only depended on the modulation index m_f. This aspect facilitates the representation of the different

parameters under study (F_1, $F_{env,peak}$ and Δf_{peak}) along the modulation index m_f, which means a complete generalization of the plots. It was also verified that triangular modulation featured in the same way. Finally, it is time to verify this behaviour in the exponential modulation. To do this, the same calculations as those for triangular profile are to be carried out, that is, different combinations of percentage of modulation δ%, modulating frequency f_m and carrier frequency f_c, but yielding the same modulation index $m_f = \frac{\delta\% \cdot f_c}{100 \cdot f_m}$. If the results match exactly each other, it can be assured that, for exponential modulations, amplitudes of the side-band harmonics only depend on the modulation index too.

m_f	k	δ% (%)	f_c (kHz)	f_m (kHz)	File name
10	12	10	100	1	mf_10
10	12	8	250	2	mf_20
10	12	10	500	5	mf_30
10	12	1	200	0.2	mf_40
10	48	10	100	1	mf_50
10	48	8	250	2	mf_60
10	48	10	500	5	mf_70
10	48	1	200	0.2	mf_80

Table 3-4. Four combinations of δ%, f_c, f_m for the same modulation index m_f and different values of k.

Table 3-4 summarizes the different combinations intended to verify the dependence on the harmonic amplitude of an exponential modulation with the modulation index. This verification was tested for two different values of the parameter k. Results (expressed in V) are shown in Table 3-5, whose values were calculated by using the MATLAB algorithm and grouped by names from mf_10 to mf_80. In this table, figures in bold represent the F1 value of the modulated waveform spectra, just surrounded by the left- and right side-band harmonics.

k = 12				k = 48			
mf_10	mf_20	mf_30	mf_40	mf_50	mf_60	mf_70	mf_80
0.00088143	0.00088041	0.00088143	0.00088052	0.00170967	0.00170566	0.00170967	0.00170718
0.00092598	0.00092583	0.00092598	0.00092580	0.00137958	0.00137898	0.00137958	0.00137921
0.00129471	0.00129374	0.00129471	0.00129430	0.00219611	0.00219222	0.00219611	0.00219323
0.00141990	0.00141975	0.00141990	0.00141988	0.00182118	0.00182059	0.00182118	0.00182069
0.00197571	0.00197475	0.00197571	0.00197480	0.00286346	0.00285969	0.00286346	0.00286119
0.00227906	0.00227892	0.00227906	0.00227888	0.00243529	0.00243473	0.00243529	0.00243497
0.00315360	0.00315269	0.00315360	0.00315330	0.00379448	0.00379081	0.00379448	0.00379171
0.00378264	0.00378251	0.00378264	0.00378266	0.00329975	0.00329921	0.00329975	0.00329928
0.00525250	0.00525160	0.00525250	0.00525157	0.00511916	0.00511562	0.00511916	0.00511714
0.00657582	0.00657569	0.00657582	0.00657564	0.00453012	0.00452961	0.00453012	0.00452986
0.00913666	0.00913581	0.00913666	0.00913652	0.00704739	0.00704394	0.00704739	0.00704469
0.01175527	0.01175515	0.01175527	0.01175536	0.00629543	0.00629493	0.00629543	0.00629497
0.01639837	0.01639752	0.01639837	0.01639741	0.00993753	0.00993420	0.00993753	0.00993579
0.02160706	0.02160694	0.02160706	0.02160692	0.00883103	0.00883055	0.00883103	0.00883085
0.02984947	0.02984868	0.02984947	0.02984964	0.01444524	0.01444198	0.01444524	0.01444253
0.03906972	0.03906962	0.03906972	0.03907000	0.01242287	0.01242240	0.01242287	0.01242239
0.05256135	0.05256055	0.05256135	0.05256029	0.02191411	0.02191099	0.02191411	0.02191284
0.06628392	0.06628380	0.06628392	0.06628382	0.01728005	0.01727961	0.01728005	0.01728001
0.08075703	0.08075629	0.08075703	0.08075774	0.03563332	0.03563024	0.03563332	0.03563038
0.08347758	0.08347748	0.08347758	0.08347777	0.02313474	0.02313431	0.02313474	0.02313413
0.07395679	0.07395598	0.07395679	0.07395409	0.06697261	0.06696970	0.06697261	0.06697278
0.01572186	0.01572172	0.01572186	0.01572019	0.02852642	0.02852603	0.02852642	0.02852686
0.14243881	0.14243951	0.14243881	0.14243841	0.21539708	0.21539414	0.21539708	0.21539329
0.1572387	0.15723878	0.15723868	0.15723875	0.12236177	0.12236138	0.12236177	0.1223615
0.14243996	0.14243928	0.14243996	0.14244038	0.21539372	0.21539658	0.21539372	0.21539746
0.01572221	0.01572216	0.01572221	0.01572374	0.02852623	0.02852583	0.02852623	0.02852523
0.07395633	0.07395708	0.07395633	0.07395898	0.06696836	0.06697103	0.06696836	0.06696802
0.08347750	0.08347740	0.08347750	0.08347717	0.02313476	0.02313441	0.02313476	0.02313481
0.08075580	0.08075644	0.08075580	0.08075502	0.03562973	0.03563241	0.03562973	0.03563238
0.06628390	0.06628382	0.06628390	0.06628386	0.01727992	0.01727956	0.01727992	0.01727939
0.05256052	0.05256118	0.05256052	0.05256148	0.02191013	0.02191269	0.02191013	0.02191101
0.03906962	0.03906952	0.03906962	0.03906920	0.01242281	0.01242247	0.01242281	0.01242271
0.02984835	0.02984897	0.02984835	0.02984805	0.01444154	0.01444407	0.01444154	0.01444373
0.02160705	0.02160697	0.02160705	0.02160704	0.00883088	0.00883054	0.00883088	0.00883048
0.01639749	0.01639812	0.01639749	0.01639829	0.00993357	0.00993601	0.00993357	0.00993467
0.01175519	0.01175511	0.01175519	0.01175495	0.00629532	0.00629500	0.00629532	0.00629520
0.00913559	0.00913618	0.00913559	0.00913555	0.00704360	0.00704600	0.00704360	0.00704555
0.00657580	0.00657573	0.00657580	0.00657583	0.00452993	0.00452963	0.00452993	0.00452961
0.00525159	0.00525218	0.00525159	0.00525229	0.00511518	0.00511749	0.00511518	0.00511633
0.00378257	0.00378249	0.00378257	0.00378240	0.00329958	0.00329929	0.00329958	0.00329946
0.00315254	0.00315310	0.00315254	0.00315260	0.00379060	0.00379287	0.00379060	0.00379238
0.00227902	0.00227895	0.00227902	0.00227905	0.00243507	0.00243478	0.00243507	0.00243478
0.00197477	0.00197533	0.00197477	0.00197539	0.00285941	0.00286161	0.00285941	0.00286056
0.00141982	0.00141975	0.00141982	0.00141969	0.00182096	0.00182069	0.00182096	0.00182084
0.00129365	0.00129418	0.00129365	0.00129374	0.00219213	0.00219429	0.00219213	0.00219377
0.00092593	0.00092587	0.00092593	0.00092596	0.00137931	0.00137904	0.00137931	0.00137906
0.00088045	0.00088098	0.00088045	0.00088101	0.00170554	0.00170762	0.00170554	0.00170666

Table 3-5. MATLAB algorithm results (in volts) for the different combinations in Table 3-4

From the direct analysis of data in Table 3-5, it must be concluded that the amplitude of the harmonics generated during an exponential modulation process only depend on the modulation index for a constant value of k.

This way, and as in the sinusoidal and triangular modulation cases, the following analysis will be carried out by studying the behaviour of the several parameters defined at the beginning of chapter 3 along the modulation index m_f.

As a general extrapolation, it can be thought that the amplitude of the side-band harmonics generated during a frequency modulation process only depends on the modulation index as an argument of a certain function (e.g., Bessel's functions for sinusoidal modulation profile). In this thesis, this has been demonstrated analytically for the sinusoidal modulation profile and verified numerically for triangular and exponential profiles. For any other modulation profiles different of the three mentioned ones, an analytic or numerical verification is mandatory to do before affirming this behaviour. This can be a possible line of investigation in this area.

3.3.2 Evolution of the central harmonic amplitude F_1

In the following Figures 3-25(a) to (e), F_1 (relative amplitude of the harmonic corresponding to the modulated waveform at a frequency f_c) is displayed as a function of the modulation index m_f by means of three graphs corresponding to three different values of parameter k, i.e., 12 (green line), 24 (red line) and 48 (blue line), and a certain range of modulation indexes.

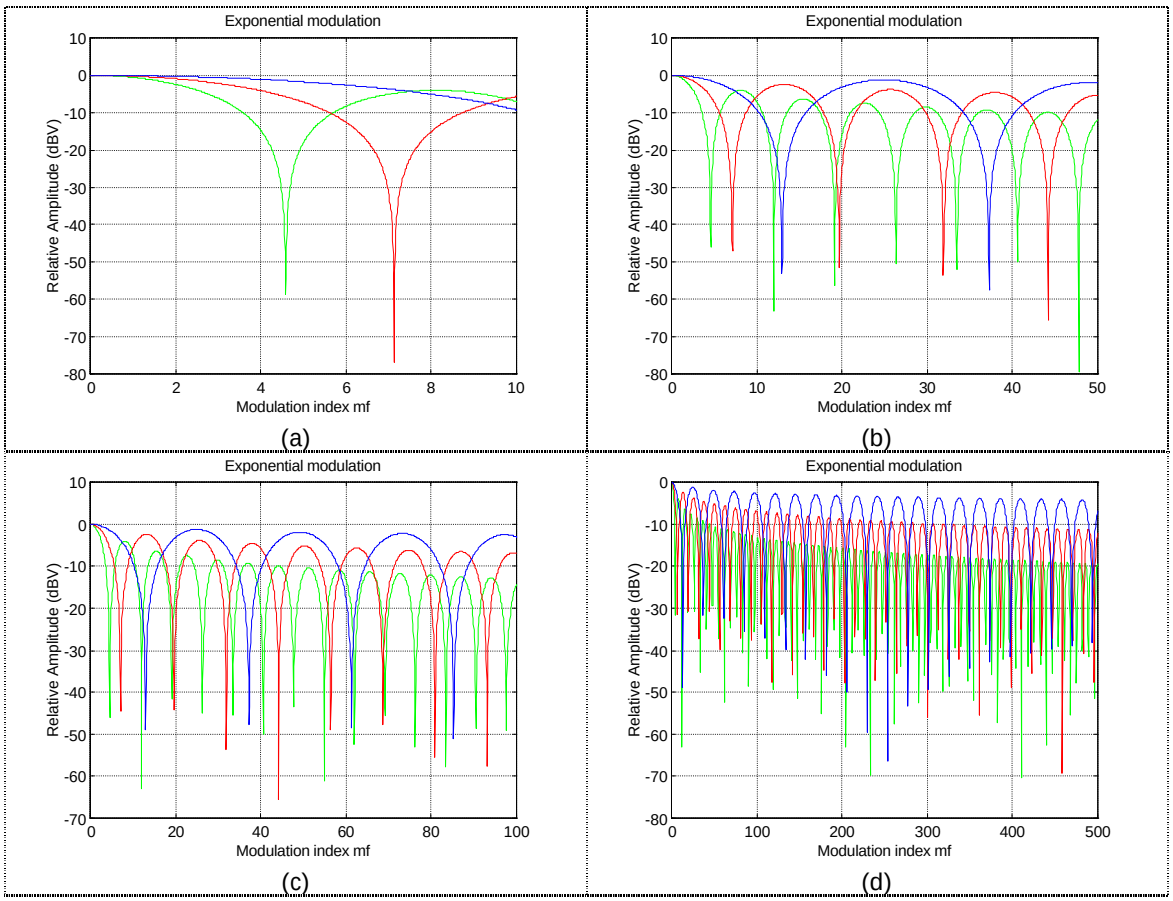

Figure 3-25(a) to (d). Rms-amplitude (F_1) of the carrier harmonic for different values of parameter k: k = 12 (green line), k = 24 (red), k = 48 (blue) and for different zooms of m_f. (Note: relative values respect the non-modulated harmonic).

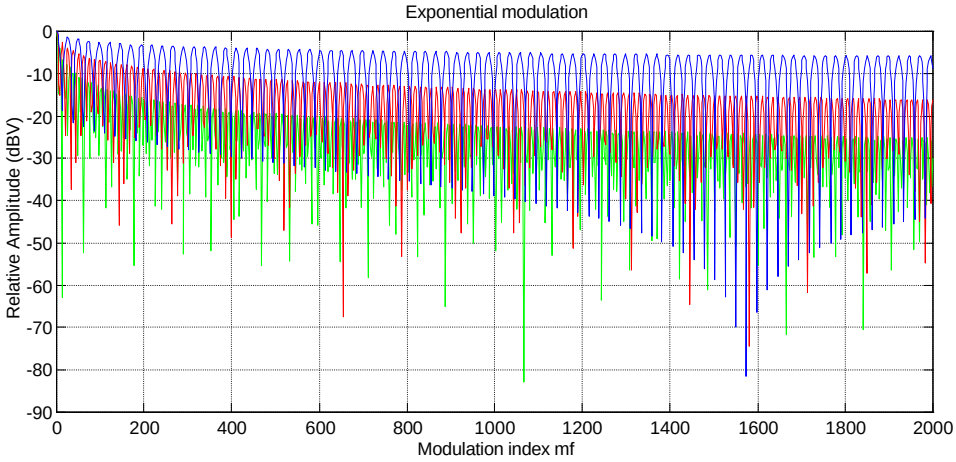

Figure 3-25(e). Rms-amplitude (F_1) of the carrier harmonic for different values of parameter k: k = 12 (green line), k = 24 (red), k = 48 (blue) up to m_f. = 2000 (Note: relative values respect the non-modulated harmonic).

In every case, an oscillation of the amplitude F_1 is present as in the previous modulation profiles; however, an envelope defined by a logarithmic curve joining the local maximum points of every individual oscillation can be drawn. This logarithmic curve gives the maximum attenuation possible with the selected parameters: δ%, f_c and f_m. However, a larger attenuation is also possible, just selecting the proper point where the oscillation reaches a minimum value. For instance, for $m_f > 2.5$ (see Figure 3-25(a)), an attenuation larger than -4 dBV is always to be obtained; however, for $m_f = 4.58$, an attenuation larger than -60 dBV is available. As in other modulation profiles, a special profit of this individual behaviour can be taken just tuning the system to a concrete modulation index in order, for instance, to eliminate the harmonic at the carrier frequency.

Other important conclusions are listed below:

- Higher modulation indexes m_f are to produce higher attenuation for any concavity factor k (regarding the envelope of F_1). However, for a given modulation index m_f, higher concavity factors k are to produce lower attenuation values at the carrier frequency, i.e., F_1. This was expected from Figure 3-24 and it is confirmed here. This way, lower concavity factors k contribute to make the side-band harmonic distribution flatter, approximating the outline to the one obtained for a triangular modulation profile and, therefore, reducing the harmonic amplitude at the carrier frequency and vice versa.

- For m_f > 200, attenuation remains nearly constant; therefore, it is not worthy to work at higher modulation indexes than 200.
- Carrier harmonic cancellation is possible for any concavity factor k just choosing the proper modulation index m_f.
- Oscillation period along m_f depends on the concavity factor k. The higher the concavity factor k, the higher the oscillation period. For instance, for k = 12, the minimum value of F_1 is reached every 7.2 units of m_f; for k = 24, the minimum value of F_1 is reached every 12.2 units of m_f and, finally, for k = 48, the minimum value of F_1 is reached every 24.1 units of m_f.

3.3.3 Evolution of the maximum envelope amplitude $F_{env,peak}$

Following parameter to be analysed corresponds to the maximum rms-amplitude of the side-band harmonic envelope corresponding to the modulated waveform. In the following Figures 3-26(a) to (e), $F_{env,peak}$ is displayed as a function of the modulation index m_f. Each figure consists of three graphs corresponding to three different values of parameter k, i.e., 12 (green line), 24 (red line) and 48 (blue line), and a certain range of modulation indexes covering a wide range of modulation indexes.

From the visual inspections of Figures 3-26 (a) to (e), it can be derived the following conclusions:

- Opposite to the triangular modulation profile, it is here evident the difference of attenuation depending on the concavity factor k affecting the parameter $F_{env,peak}$. From m_f > 20 onwards, lower concavity factors k are to produce larger attenuation values of $F_{env,peak}$.
- The oscillation period (see Figure 3-26.c) corresponding to the parameter $F_{env,peak}$ increases with the concavity factor k, also opposite to the triangular modulation profile where this period remains constant when changing the parameter s.
- A logarithmic behaviour related to the envelope of $F_{env,peak}$ is also present for this exponential modulation profile. For m_f > 200, attenuation starts decreasing in a lower intensity.

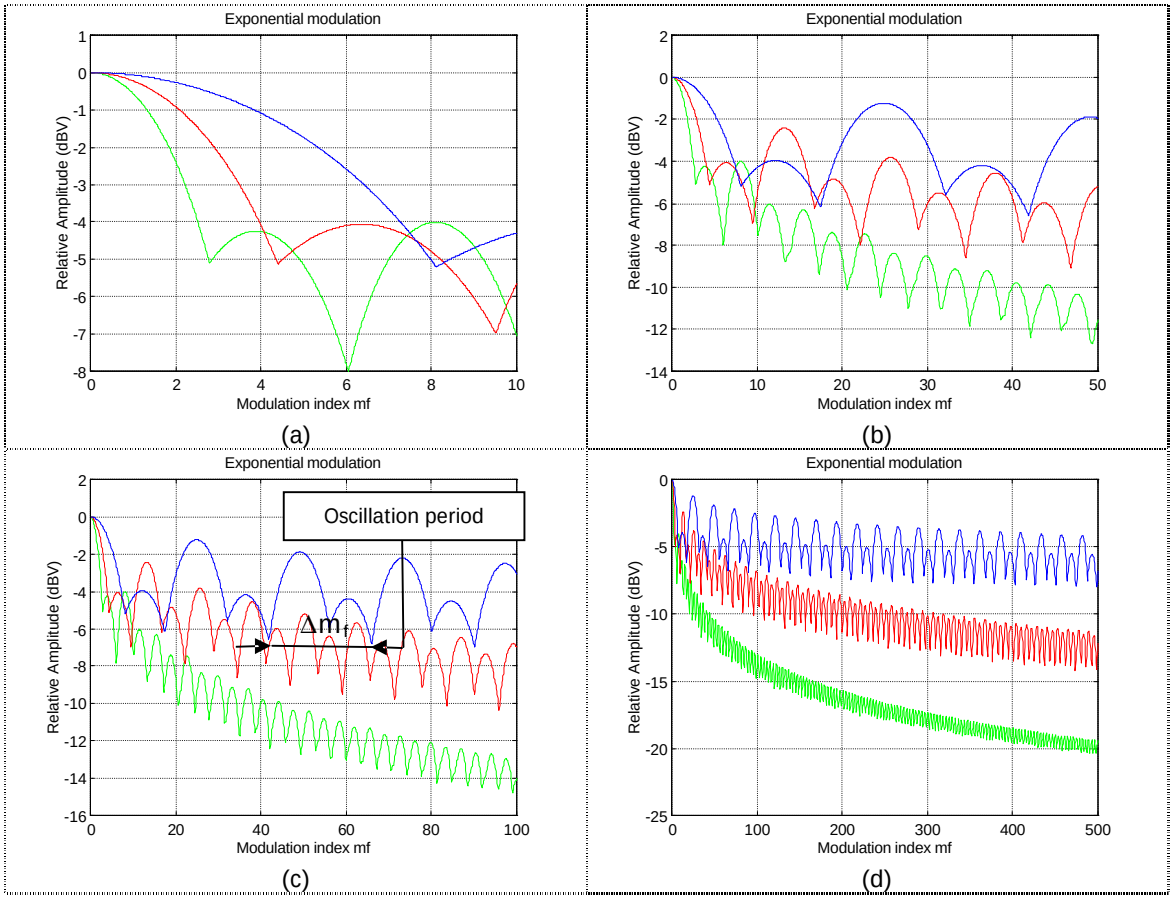

Figure 3-26(a) to (d). Maximum rms-amplitude ($F_{env,peak}$) of the harmonics envelope for different values of parameter k: k = 12 (green line), k = 24 (red), k = 48 (blue) and for different zooms of m_f. (Note: relative values respect the non-modulated harmonic).

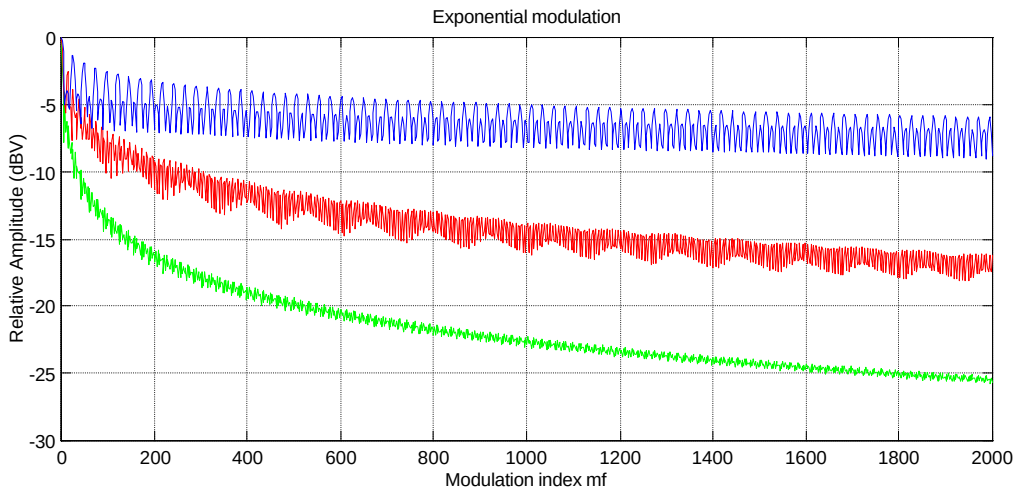

Figure 3-26(e). Maximum rms-amplitude ($F_{env,peak}$) of the harmonics envelope for different values of parameter k: k = 12 (green line), k = 24 (red), k = 48 (blue) and up to m_f. = 2000 (Note: relative values respect the non-modulated harmonic).

Figures 3-27(a), (b) and (c) plot both F_1 and $F_{env,peak}$ for different values of k (48, 24 and 12). A very clear difference is found respect to the results obtained for sinusoidal modulation [see Figures 3-8(a) and (b) in point 3.1.1]. For an exponential modulation, curve of $F_{env,peak}$ stays very near (or even matches) the maximum local values of curve F_1, when, for sinusoidal modulation, $F_{env,peak}$ remained always over F_1. In this case, this indicates that the maximum side-band harmonic amplitude matches the amplitude of the harmonic at the carrier frequency, then, a side-harmonic distribution outline showing a peak at the carrier frequency is expected to find, as shown in Figure 3-23 and 3-24. The behaviour of the sinusoidal modulation was completely different; a very large difference between F_1 and $F_{env,peak}$ was observed and the reason was the concave distribution of the side-band harmonics around the carrier frequency.

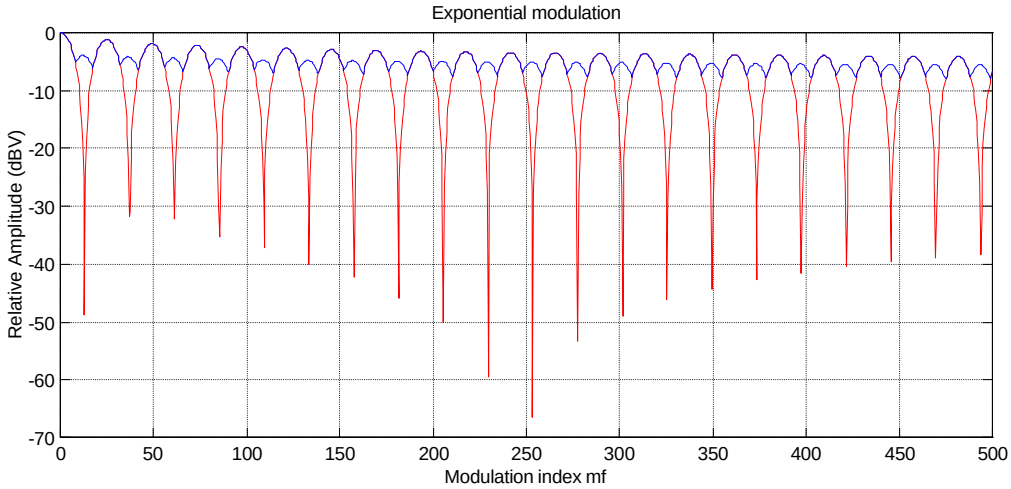

Figure 3-27(a). Comparison of F1 (red line) vs. $F_{env,peak}$ (blue line) for k = 48.

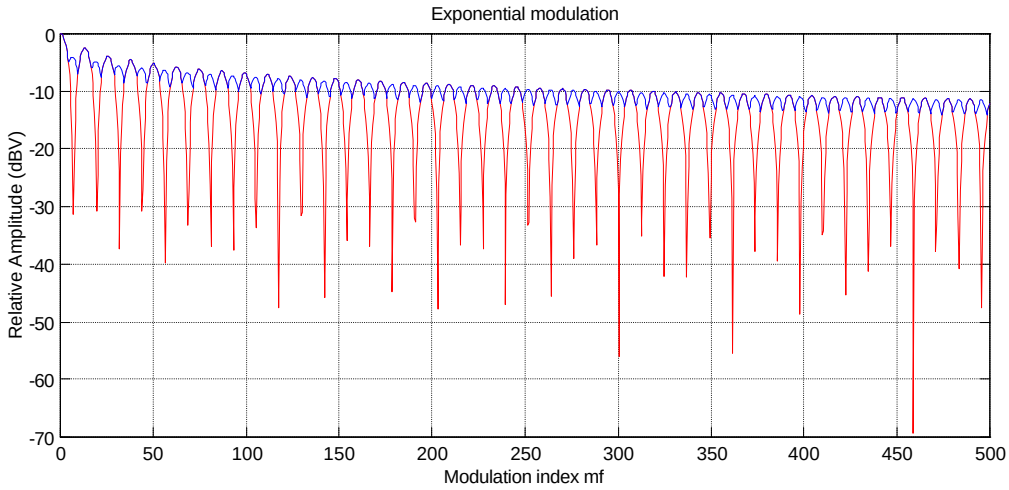

Figure 3-27(b). Comparison of F1 (red line) vs. $F_{env,peak}$ (blue line) for k = 24.

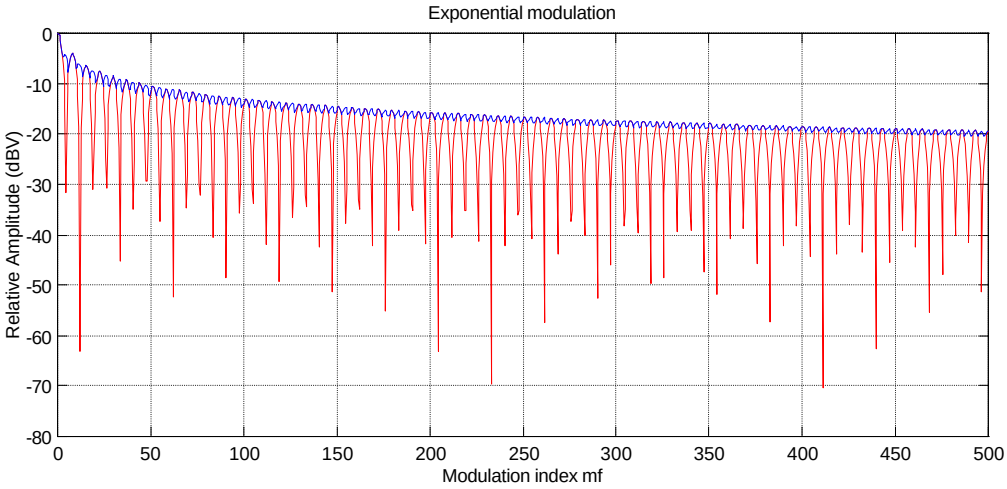

Figure 3-27(c). Comparison of F1 (red line) vs. $F_{env,peak}$ (blue line) for for k = 12.

CONSIDERATIONS ABOUT THE LOGARITHMIC BEHAVIOUR OF PARAMETERS $F_{env,peak}$ and F1 FOR k=24

In previous figures, evolution of the relatives amplitudes F1 and $F_{env,peak}$ shows a logarithmic trend. In order to quantify this behaviour, both parameters should be displayed by using a logarithmic scale for the m_f-axis. In the case of exponential modulation, only the parameter F1 is necessary to represent because it was verified previously the matching of envelopes for both parameters F1 and $F_{env,peak}$.

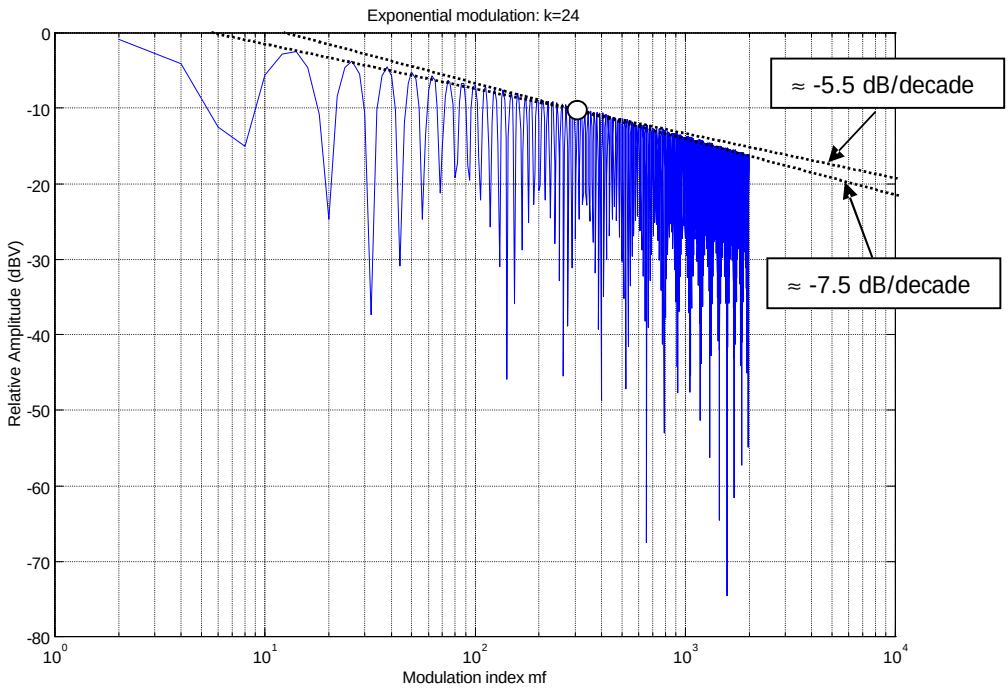

Figure 3-28. F1 for exponential modulation (k = 24) and m_f-axis in logarithmic scale

Envelopes have a logarithmic behaviour because of its linear representation when the x-axis is displayed in logarithmic scale (Bode diagrams) but showing two different slopes before and after the modulation index $m_f \approx 300$: -5,5 dB/decade and -7.5 dB/decade, respectively.

3.3.4 Evolution of the peak-to-peak envelope bandwidth Δf_{peak}

Last parameter to be analysed corresponds to the peak-to-peak bandwidth Δf_{peak} of the side-band harmonics envelope corresponding to the modulated waveform. Figures 3-29(a) to (e) show the behaviour of this parameter versus the modulation index by means of three graphs corresponding to three different values of parameter k, i.e., 12 (green line), 24 (red line) and 48 (blue line), and a certain range of modulation indexes.

Observe that the modulating frequency has been specified for every plot because the distance in frequency between two consecutive side-band harmonics is given by f_m.

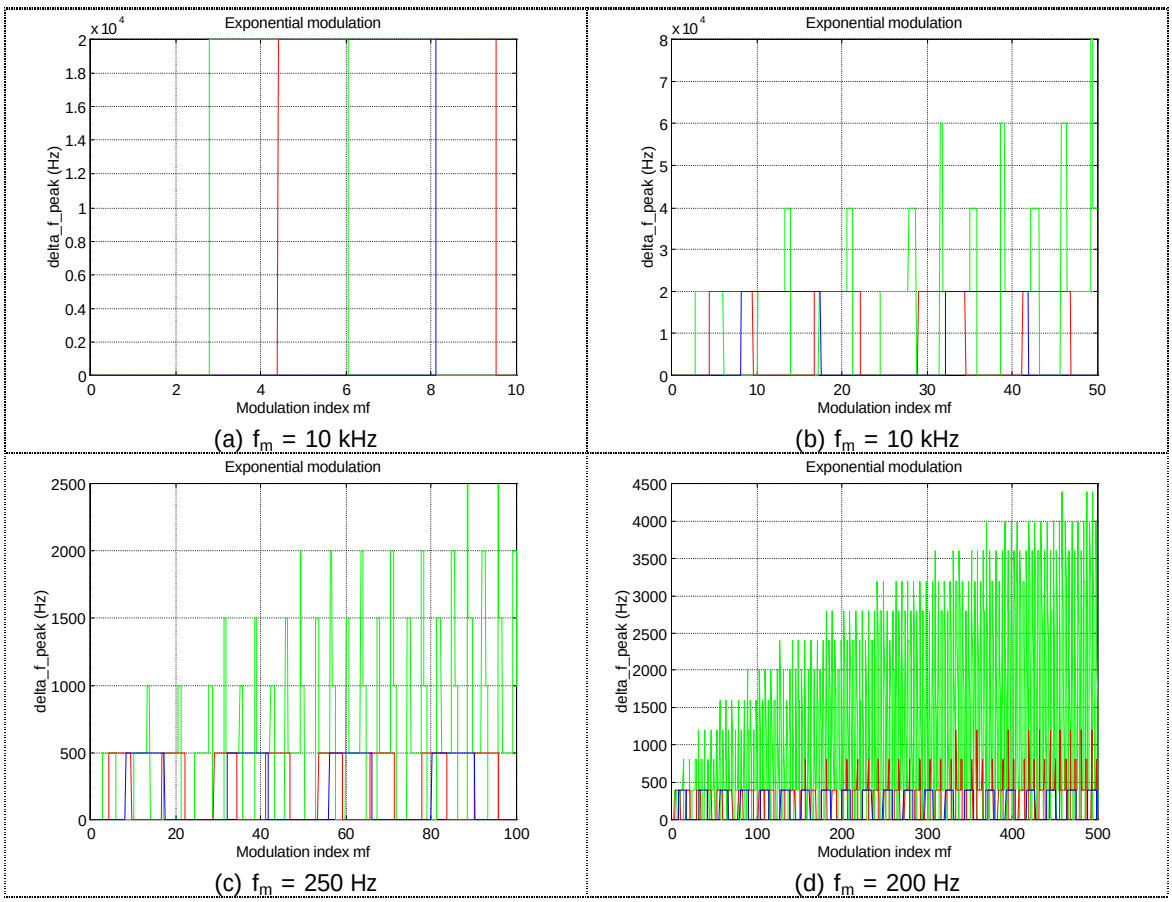

Figure 3-29(a) to (d). Peak-to-peak envelope bandwidth (Δf_{peak}) for different values of k: k = 12 (green line), k = 24 (red), k = 48 (blue) and different values of f_m and m_f.

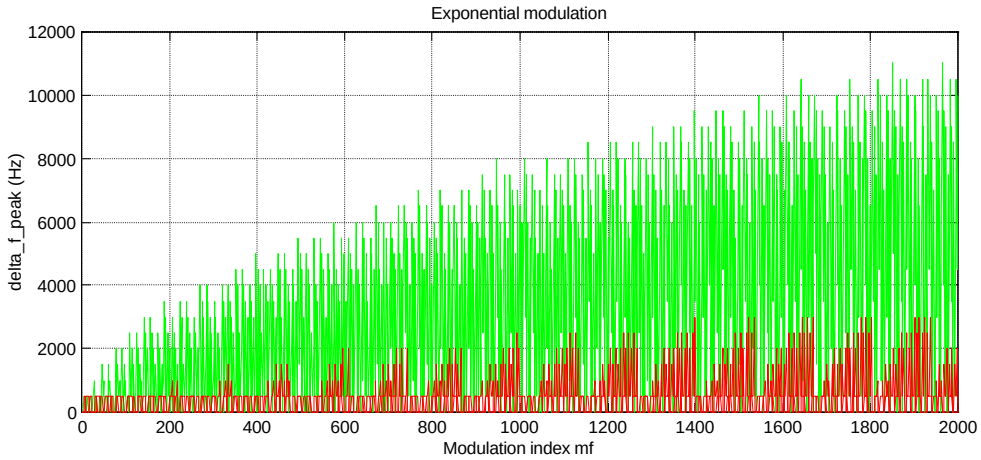

Figure 3-29(e). Peak-to-peak envelope bandwidth (Δf_{peak}) for different values of k: k = 12 (green line), k = 24 (red), k = 48 (blue) and f_m = 250 Hz (up to m_f = 2000)

Apart from the chaotic behaviour of Δf_{peak}, there is one important aspect to remark. From Figure 3-29(e), the maximum Δf_{peak} (found at m_f = 1964) is 11 kHz. Taking into account that this plot was generated with the MATLAB algorithm by using a modulating frequency f_m = 250 Hz and a carrier frequency f_c = 1 MHz, this means that the maximum harmonic order (respect to the carrier frequency) at which a maximum harmonic amplitude is generated is not beyond of $h = \frac{11/2}{0.25} = 22$. The bandwidth of the modulated waveform is $B = 2 \cdot f_m \cdot (1 + m_f) = 2 \cdot 0.25 \cdot (1 + 1964) = 982.5\, kHz$, that is, a total amount of $\frac{982.5}{0.25} = 3930$ harmonics, half at the right side of the carrier frequency and the other half, at the left side.

The fact that the maximum amplitude value is generated at a harmonic order of 22 when the complete spectrum contains 1965 left- or right-band harmonics indicates the concentration of the harmonics around the carrier frequency.

Besides, this concentration of energy around the carrier frequency is bigger as the concavity factor increases. In other words, exponential modulation profiles whose shape approximates an impulse outline will produce side-band harmonic distribution very close around the carrier frequency and, in a limit case, making it not worthy for attenuation purposes.

3.4 Comparison of the different modulation profiles

In order to make a useful comparison of the different modulation profiles here presented, only those profiles whose characteristics seem to be better are to be selected. In the case of a sinusoidal modulation, there is nothing to choose because no shape parameters are to be selected. In the triangular modulation case, the shape parameter s is the one making differences. A value of the parameter s = 0.5 is preferred because it may be used to cancel the harmonic at the carrier frequency (see clause 3.2). Respect to the exponential modulation profile, a low concavity factor k = 12 is selected because it produces a very good attenuation of both F_1 and $F_{env,peak}$.

Anyway, this comparison is related to a first approximation to the most profitable modulation profile to be used in power converters. Some ideas will arise from this analysis, pointing to a concrete specification about requirements for power converters.

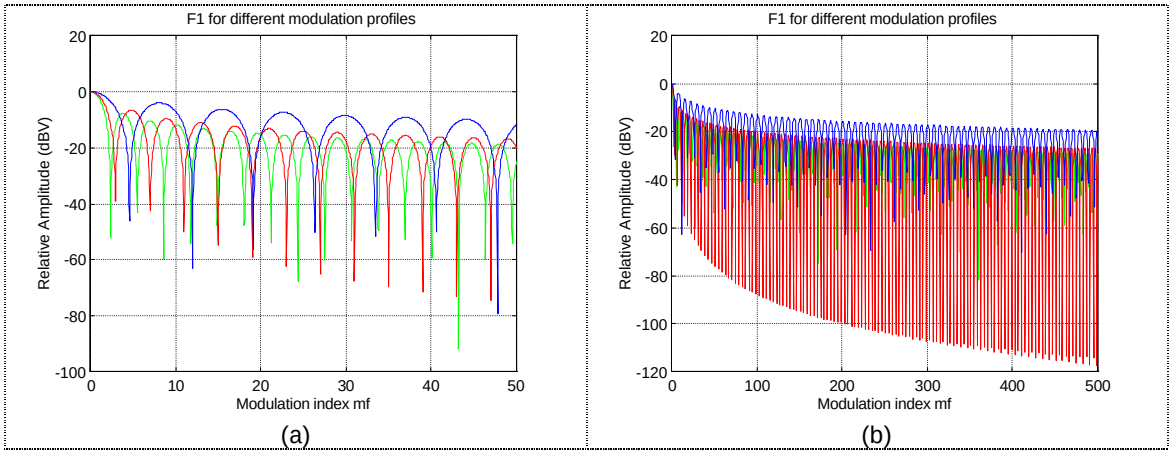

Figure 3-30(a) and (b). Relative rms-amplitude (F_1) of the carrier harmonic for different modulation profiles: sinusoidal (green), triangular [s = 0.5] (red) and exponential [k = 12] (blue) for two zooms of m_f.

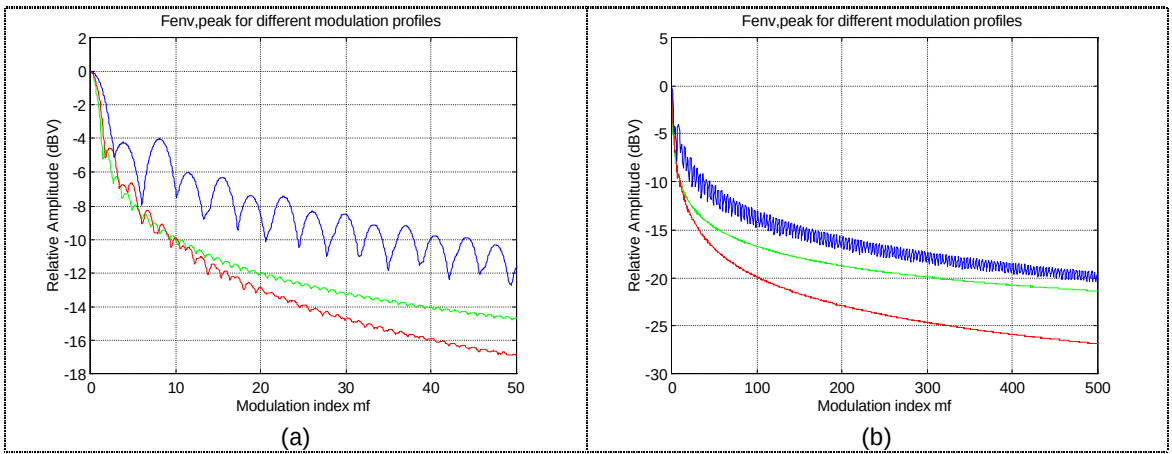

Figure 3-31(a) and (b). Relative rms-amplitude of $F_{env,peak}$ for different modulation profiles: sinusoidal (green), triangular [s = 0.5] (red) and exponential [k = 12] (blue) for two zooms of m_f.

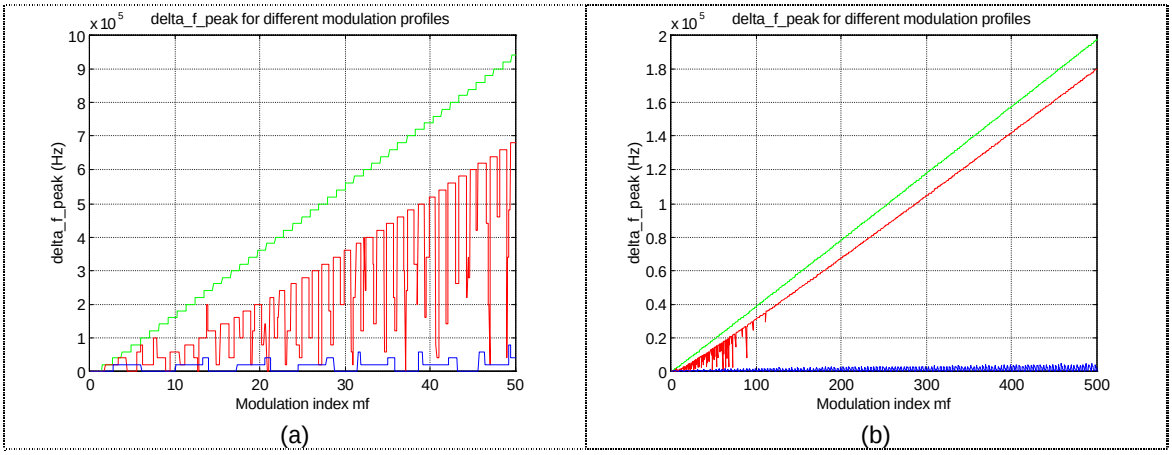

Figure 3-32(a) and (b). Δf_{peak} for different modulation profiles: sinusoidal (green), triangular with s = 0.5 (red) and exponential with k = 12 (blue) for f_m = 10 kHz

Respect to F_1 (see Figure 3-30), a very small difference of 2 dBV appears at high modulation indexes between sinusoidal and triangular modulation; this implies both modulations are equally selectable, at least, regarding F_1. This is not the case of the exponential modulation, whose attenuation of the harmonic at the carrier frequency is very poor compared to the sinusoidal and triangular profiles. Please observe that the three modulation profiles show a different oscillation period along m_f.

But F_1 is just one of the parameters to take into account. When modulating, it is desired to have the whole side-band harmonics amplitude under a certain maximum value, and this information is carried by $F_{env,peak}$ (see Figure 3-31). As expected, exponential profile shows the worst behaviour because of the peak shape of the side-band harmonic distribution, which makes the F_1 value match $F_{env,peak}$ most of the time. If attenuation given by an exponential profile at a certain modulation index m_f is found to be satisfactory, then it can be a good option because the side-band harmonics decrease fast as the side-harmonic order gets farther from the central frequency. But if it is desired to obtain a higher attenuation at the same modulation index, a triangular modulation profile should be selected.

Considering the global behaviour of the modulation, the most important parameter is $F_{env,peak}$. It provides a very useful information because of its global characteristic: the maximum amplitude (respect to the non-modulated carrier frequency) along the whole spectrum distribution as a result of a frequency modulation, that is, all harmonic amplitudes will be under this value $F_{env,peak}$. If the number of new harmonics generated during the modulation process is not of concern but only their amplitudes, this parameter $F_{env,peak}$ should be the target. Then, a flat harmonic distribution is the most

profitable and, therefore, a triangular modulation profile is the most suitable for any application with these characteristics.

Because $F_{env,peak}$ does not oscillate too much, main efforts should be concentrated on obtaining a cancellation of a certain harmonic, normally, the one at the carrier frequency, that is, it is desired a value of F_1 = 0 V or, in a practical case, F_1 < -40 dBV (relative to the non-modulated carrier signal). To do this, a special profit of the oscillation features of the value F_1 (see Figure 3-33) is to be taken. Working points should be selected at those modulation indexes where a harmonic cancellation is available.

3.4.1 Considerations to the complete spectral content of a signal

Another interesting question is related to the whole spectral content of the original non-modulated square waveform controlling the power converter. Till now, a discussion about the first harmonic attenuation by a proper selection of the modulation index was carried out. But it should not be forgotten that the frequency modulation affects the rest of spectral components of the original signal (see clause 2.1.3.2) in a similar way to the first harmonic. For a generic harmonic order h, its modulation index will be $m_f \cdot h$, thus widening its bandwidth and having a different value of attenuation corresponding to $m_f \cdot h$ but always lower than the harmonic amplitude at the carrier frequency (in a logarithmic way). Anyway, the oscillation period (see Figure 3-33) is constant along m_f. This way, selecting a harmonic cancellation point m_f for the first harmonic and a proper oscillation period Δm_f, a number of harmonics at the non-modulated signal frequencies can be cancelled.

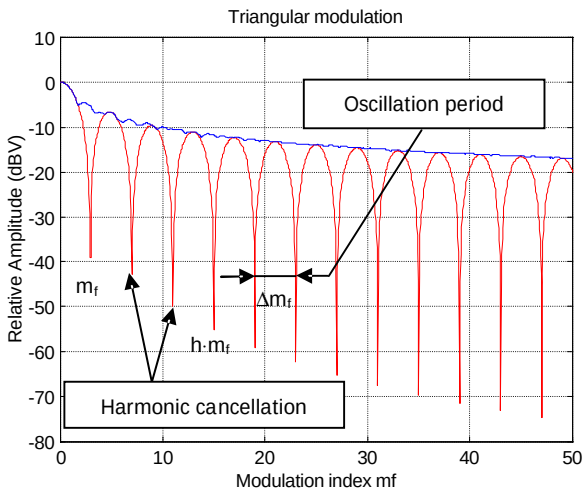

Figure 3-33. Comparison of F1 (red line) vs $F_{env,peak}$ (blue line) for s = 0.5.

This ability of cancelling harmonics is a very worthy property and it is very useful in those systems where both switching (or clock) signal and any other signal in the circuit board have the same frequency and no interference between them is desired.

Oscillation period Δm_f can be expressed as a function of the modulation index m_f:

$$\Delta m_f = n \cdot m_f \tag{3-5}$$

All central harmonics of h-order verifying the following expression (see Figure 3-33)

$$h \cdot m_f = m_f + r \cdot \Delta m_f = m_f + r \cdot n \cdot m_f \qquad \text{r = 1,2,3,...; n = constant} \tag{3-6}$$

are to be cancelled.

Expression (3-6) can be easily expressed as follows:

$$h = 1 + r \cdot n \tag{3-7}$$

The only chance to be able to cancel as many harmonics as possible is to get a proper value of $n = \frac{\Delta m_f}{m_f}$. It is found experimentally that $m_f < \Delta m_f$ and, therefore, n > 1. In fact, parameter n takes the following values depending on the modulation profile:

- Sinusoidal profile: n = 1.3 (according to Figure 3-8.a)
- Triangular profile (mainly, for vertex parameter s = 0.5): n = 1.41 (according to Figure 3-17.a)
- Exponential profile: the value of n depends on the concavity factor k

According to expression (3-7) and considering that r is a natural value, the only way of obtaining the maximum number of central harmonics being cancelled is making the parameter n an integer. Table 3-6 shows harmonic orders to be cancelled for different values of n.

r	n	h (*)	n	h (*)	n	h (*)	n	h (*)
1	1.5	2.5	2	3	2.5	3.5	3	4
2	1.5	4	2	5	2.5	6	3	7
3	1.5	5.5	2	7	2.5	8.5	3	10
4	1.5	7	2	9	2.5	11	3	13
...	...	...	...	...	...	...	...	...
r	1.5	1+1.5·r	2	1+2·r	2.5	1+2.5·r	3	1+3·r

Table 3-6. Different harmonic cancellation as a function of parameters r and n
(*) only natural values of h have a physical meaning

According to Table 3-6, the most profitable option is related to the parameter n to be equal to 2. This value makes possible the cancellation of every odd harmonic amplitude of the non-modulated signal at its central frequency (please remember that a side-band harmonics window is also appearing, but the central frequency corresponding to the odd harmonic order of the non-modulated signal is to be cancelled).

As explained before, exponential profile may be used to tune the oscillation period just selecting a proper concavity factor k and this key point, together with the results of Table 3-6, points to the direct application of SSCG in order to avoid disturbing another significant signal (for instance, a CAN bus telegram inside a car) at the same frequency as the switching power converter. This is developed in more detail further in clause 4.5.

To sum up, another successful key is to select a modulation index m_f and an oscillation period cancelling as many main harmonics as possible. Oscillation period is only tuneable for an exponential modulation profile, through its concavity factor k. For sinusoidal and triangular modulations, no way of tuning is possible. Consequently, the following aspects are to be considered:

- Tuning of the oscillation period is possible for exponential profiles, thus allowing the selection of a certain modulation index and, afterwards, tune the related profile through the concavity factor k.
- If no exponential profile is to be used, no tune of the oscillation period is possible. Another extra consideration to be careful is the one related to the spectrum overlap corresponding to contiguous main harmonics (see clause 2.2.2). And, of course, the problems associated to the use of regulatory RBW's in spectrum analysers (see Annexes 1 and 2).

3.4.2 Considerations to the spectra distribution shape

From the previous analysis and theoretical calculations of the harmonic spectra resulting from a frequency modulation process, some important conclusions can be hereby presented (see Figure 3-34). The first one is related to the triangular modulation profile. These profiles are the unique modulating waveforms which produce a complete flat spectrum distribution shape, independently on the sawtooth parameter s (see related considerations in clause 3.2) as shown in Figures 3-34(c) and (d).

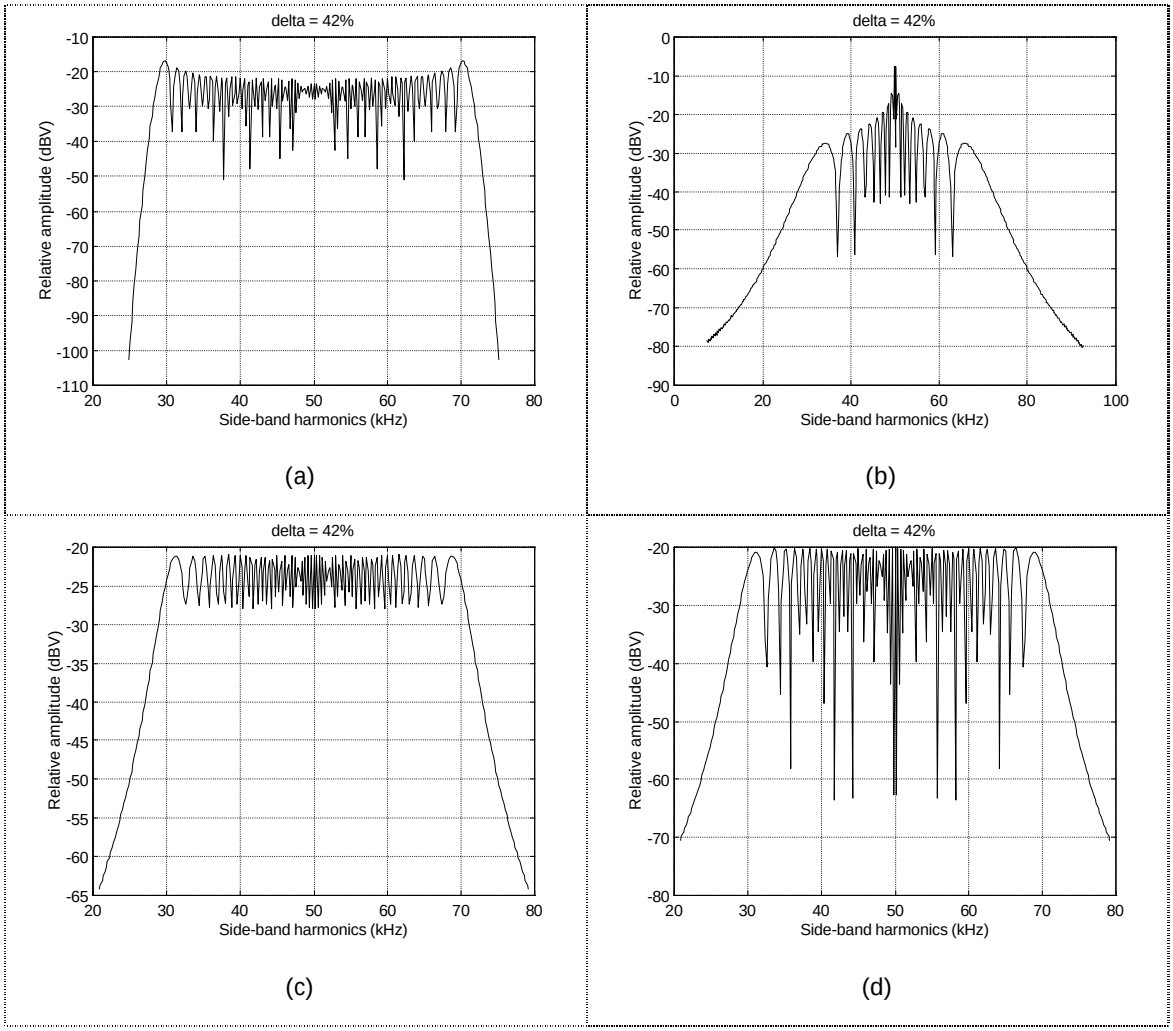

Figure 3-34. Side-band harmonics envelope (f_c=50 kHz, f_m=250 Hz): (a) sinusoidal modulation, (b) exponential modulation (k =12), (c) triangular modulation (s = 0.5), (d) triangular modulation (s = 0.125)

It seems to be that modulation profiles consisting of straight lines, that is, constant slopes during the modulating period are to produce a flat distribution of the side-band harmonics. It is concluded then that modulation profiles, or trams of them, which are inscribed inside the triangular base, as expressed in Figure 3-35, it is to obtain a concentration of the side-band harmonics around the carrier frequency, thus giving a peak aspect to the spectra distribution resulting from the frequency modulation process, as displayed in Figure 3-34(b). In the same way, any modulation profiles, or trams of them, which stay outside the triangular base (see Figure 3-35) are to produce a concentration of the side-band harmonics not at the carrier frequency but in the opposite sides, that is, a concentration around the two frequencies defining the bandwidth resulting from the modulation process, as shown in Figure 3-34(a).

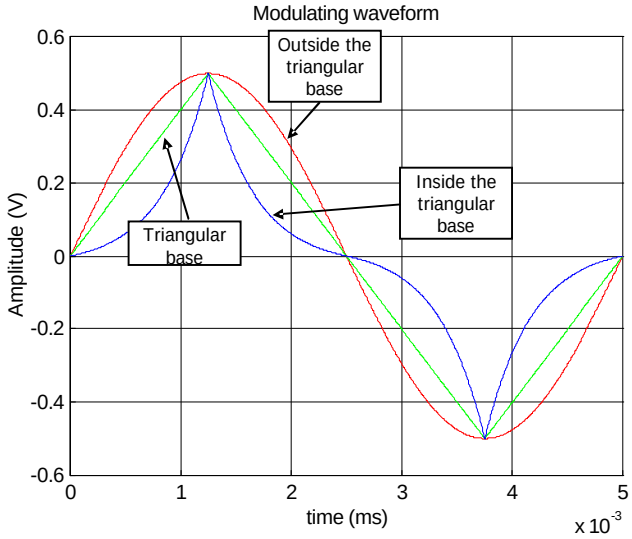

Figure 3-35. Different modulation profiles compared to the triangular base

Such behaviour can be explained approximately by using the frequency modulation concepts presented in clause 2.1.1.1. From expressions (2-3) and (2-4), the instantaneous frequency ω(t) corresponding to the modulated signal can be expressed as follows:

$$\omega(t) = \omega_c + \frac{d\Theta(t)}{dt} \tag{3-9}$$

The relationship between the phase angle and the modulation profile is given by:

$$\frac{d\Theta(t)}{dt} = k_\omega \cdot v_m(t) \tag{3-10}$$

In other words, instantaneous frequency of a modulated waveform is depending only on the modulation profile $v_m(t)$ (as known) with an offset given by the carrier frequency ω_c. But the main interest does not rely on the instantaneous frequency itself but on the variation shape of this instantaneous frequency. This shape can be approximated by the first derivative of ω(t). From expressions (3-9) and (3-10), it is obtained:

$$\frac{d\omega(t)}{dt} = k_\omega \cdot \frac{dv_m(t)}{dt} \tag{3-11}$$

This way, a triangular modulation profile, consisting of only linear trams of constant slope, will have also a constant first derivative. This means that the harmonic energy distribution will be constant along the whole bandwidth of modulation, thus giving a

flat distribution shape. But if a modulation profile tends to be with a very low derivative of $v_m(t)$ during nearly the whole modulation period (for instance, an exponential modulation profile with a very high concavity factor k as explained in clause 2.3.2.3), this means that variation of $\omega(t)$ is very low during nearly the whole modulation period, thus only the carrier frequency will be present and supplying the maximum value to the spectra distribution. This can be the case of the waveforms inside the triangular base in Figure 3-35 and the resulting spectra in Figure 3-34(b). In a similar way, modulation profiles with a tendency to high derivatives of $v_m(t)$ during nearly the whole modulation period will tend to concentrate the energy far away from the central or carrier frequency ω_c. Commonly, a combination of these three cases is to be found but a good division of the profile in several trams will facilitate the application, tram by tram, of the comments above.

Four illustrative plots are presented in Figure 3-36. It consists of two different modulation profiles (Figure 3-36(a) and (b)) and its related spectra distribution (Figure 3-36(c) and (d), respectively).

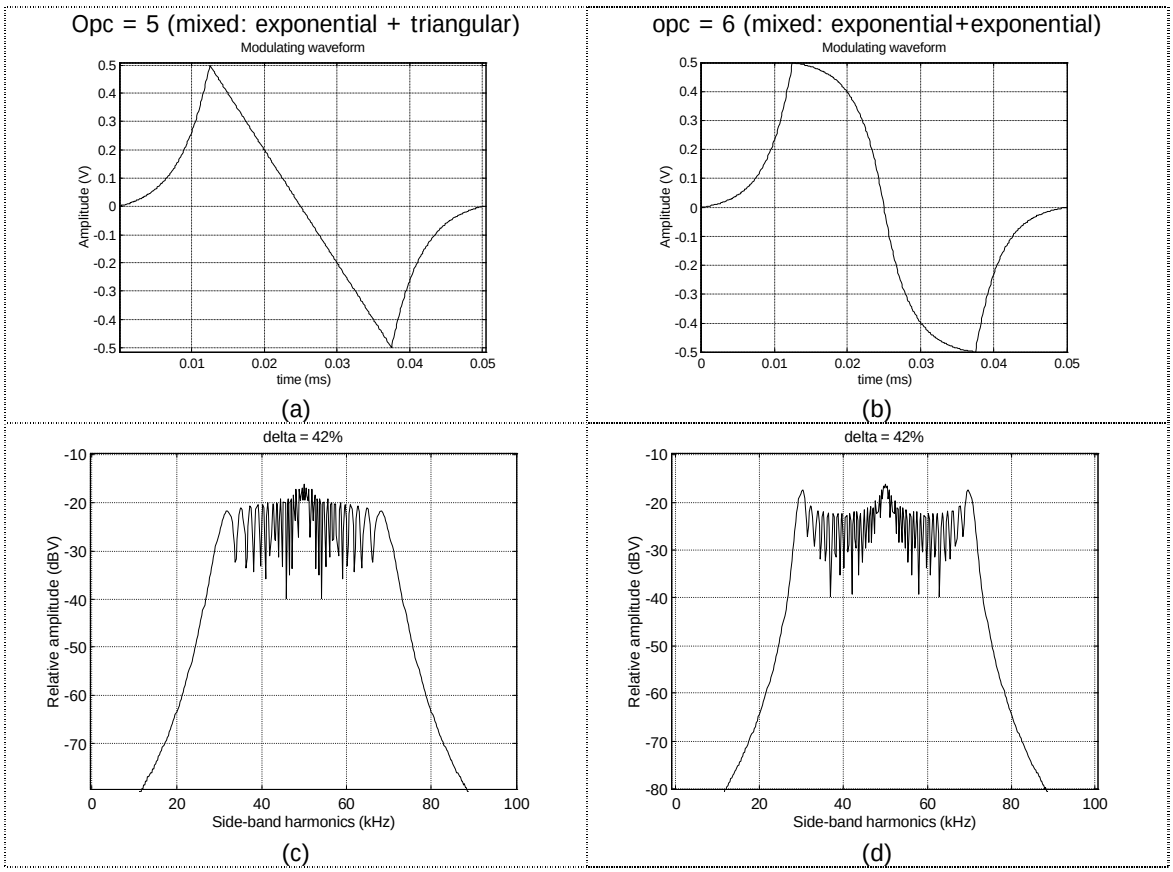

Figure 3-36. Side-band harmonics envelope [f_c=50 kHz; f_m=250 Hz]: (a) exponential + triangular profile and its related spectra (c); (b) exponential + exponential profile and its related spectra (d)

For the case (a)-(c), one half of the modulation period matches exactly a triangular signal while the other half stays inside this theoretical triangular profile. The triangular half tends to get a flat spectra distribution while the exponential half tries concentrating this distribution around the carrier or central frequency. This way, the outline of the resulting spectra distribution is neither flat (as expected for a triangular profile) nor a peak outline (as expected for an exponential profile). The case (b)-(d) is even more significant. Two exponential curves are combined in such a way that the resulting profile is half a period outside the theoretical base waveform and half a period inside this triangular base. The half tram outside the triangular limit will tend to concentrate side-band harmonics around the two frequencies defining the bandwidth generated during the frequency modulation process. In a similar way, the half tram inside the triangular limit tends to concentrate the side-band harmonics around the carrier frequency. Therefore, a final harmonic distribution shape consisting of three peaks (the central and the extreme ones) is to be obtained.

This can be an interesting line of investigation in order to study how different combinations of mathematical profiles should be combined in order to obtain a specific benefit when using SSCG.

3.5 Proposal of control for a real power converter

Pulse-Width Modulation (PWM) is one of the methods to control the output voltage of a power converter. This method employs switching at a constant frequency, adjusting the t_{on} duration of the switch to control the average output voltage.

In the PWM switching at a constant switching frequency, the switch control signal, which controls the state (on and off) of the switch, is generated by comparing a signal level control voltage $v_{control}$ with a repetitive waveform as shown in Figures 3-37(a) and (b). From the general theory of control, the voltage $v_{control}$ is usually obtained by amplifying the error signal, that is, the difference between the actual voltage control and its desired value. The comparison between the repetitive sawtooth waveform (which indeed establishes the switching frequency) and the control voltage $v_{control}$ produces a square waveform whose duty-cycle is determined by the ratio $D = \frac{t_{on}}{T_s} = \frac{v_{control}}{V_{st}}$ because, when the amplified error signal is greater than the sawtooh waveform, the switch control signal becomes high, causing the transistor to turn on

and vice versa. Variation of the output voltage is much slower in time than the switching frequency to allow the system to be accurate when correcting the output voltage deviation.

Just following this classical method of controlling the average output voltage and introducing the concept of SSCG method, a very important conclusion is then obtained: in order to implement a practical SSCG method, it is only necessary to slightly modify the sawtooth generator to generate not a constant frequency sawtooth waveform but a variable frequency signal as shown in Figure 3-38. The SSCG-characteristics of modulation (i.e., modulation profile, modulating frequency f_m and switching frequency peak deviation Δf_c) directly applied to the sawtooth voltage will produce a true SSCG modulation in the complete system. No care must be taken into account related to the duty-cycle because it remains constant during the whole modulating period T_m as shown in Figure 3-38 (see other considerations related to the average value of the modulation profile in clause 2.2.3.1).

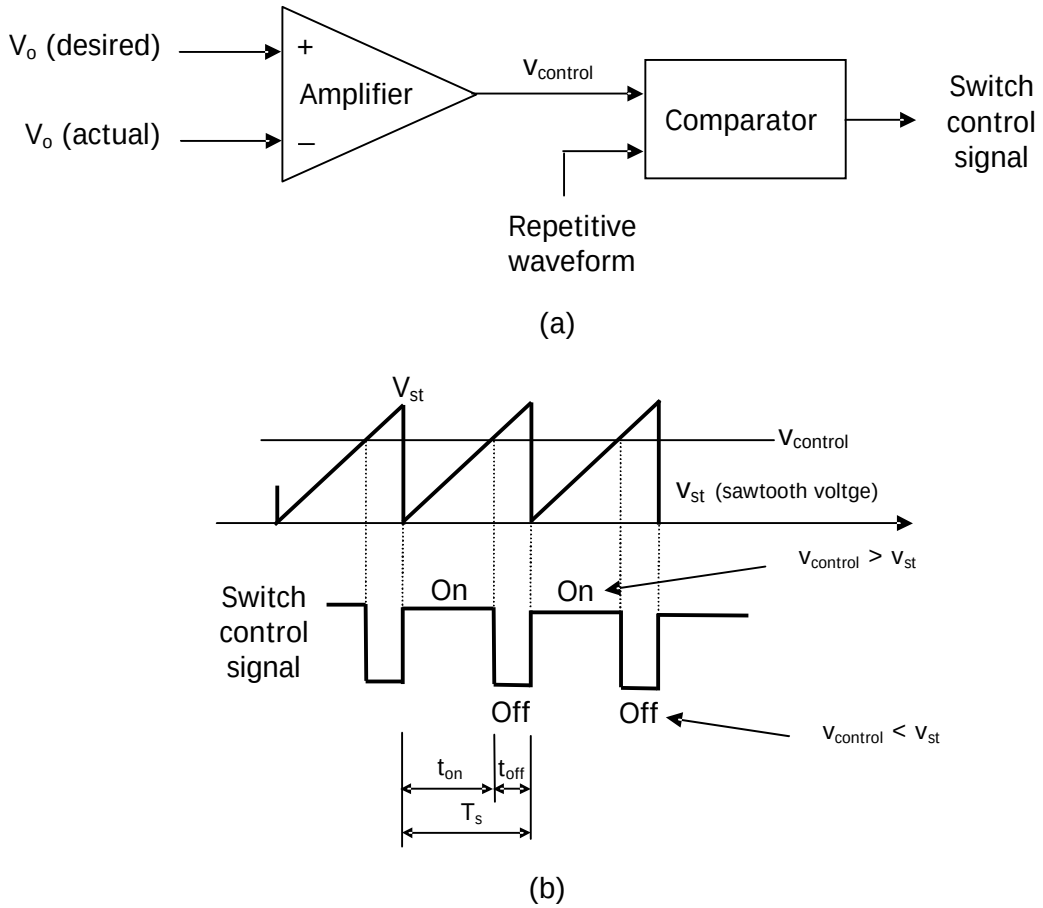

Figure 3-37. Pulse-Width modulator (PWM): (a) block diagram, (b) comparator signals

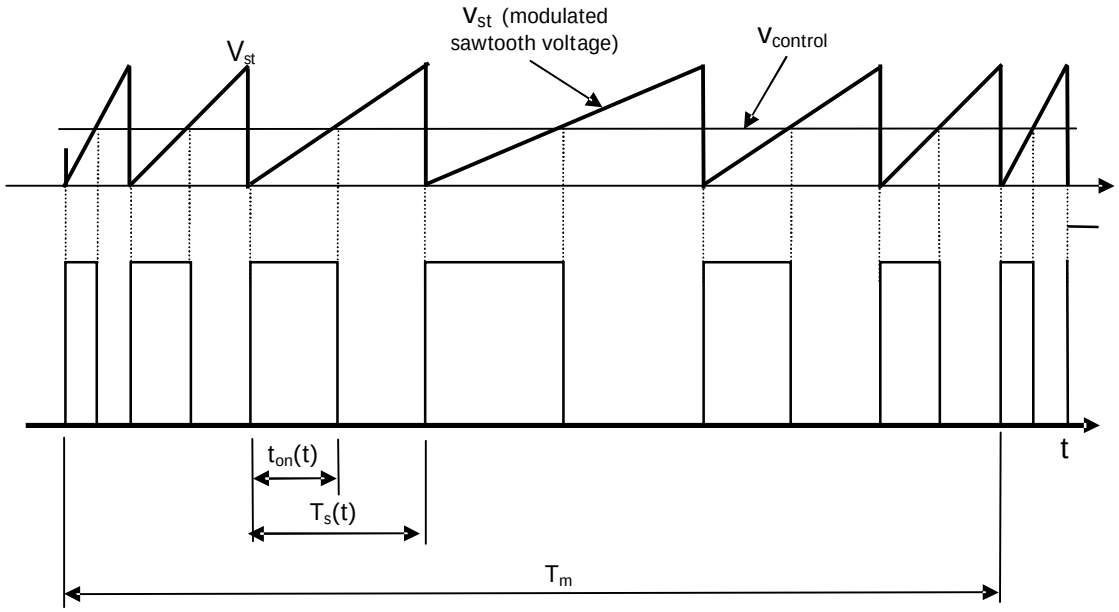

Figure 3-38. Pulse Width modulator with SSCG modulation (FM-PWM): comparator signals

This idea points to the possibility related to the direct replacement of a constant frequency PWM controller by another one whose frequency is modulated following a certain SSCG method. And this is true just taking into account the limitations expressed in the next clause 3.6.

3.6 Considerations to apply a certain SSCG method to switching power converters

One easy conclusion to be derived from the previous analysis is that higher modulation indexes are to produce larger attenuations. Therefore, higher modulation indexes should be selected and, through its definition $m_f = \frac{\delta \cdot f_c}{f_m}$, this can be done by increasing the modulation ratio δ or the carrier frequency f_c or decreasing the modulating frequency f_m.

Switching (carrier) frequency in power converters is not usually too large because the electronics components (diodes and power transistors, mainly) are not able to manage larger power with shorter switching times. Anyway, use of higher switching frequencies is advisable in order to reduce the size and power capability of the passive components (filters, inductances, diodes, transistors and so on) and increase the power efficiency of the converter (> 70 %). Typical commercial switching frequencies for medium powers

are about 200 kHz or less. For instance, National Semiconductor is offering a SIMPLE SWITCHER Power Converter (LM2957) at a fixed switching frequency of 150 kHz managing a maximum output power of 2.5 W (5V, 0.5A) in a step-down topology. The maximum switching frequency of National Semiconductor's switching regulators is limited to 300 kHz (for a maximum output current of 200 mA). Switching frequencies of 1 MHz are also available for low levels of power. Experimental higher frequency power converters are also under study. A 50MHz to 100MHz dc-dc power converter using Gallium Arsenide power switches has been studied. GaAs Schottky rectifiers with high breakdown voltage and very small $R_{on} \cdot C_{on}$ switching quality factor have been fabricated. A 10V to 5V (or 8V) prototype with an output power of 2.6 Watts and a power efficiency of 77% has been reported [Gaye, M. and Ajram, S. and Maynadier, P. and Salmer, G. (2000), "An ultra-high switching frequency step-down DC-DC converter based on Gallium Arsenide devices". Proceedings Gallium Arsenide applications symposium. GAAS 2000, Paris.]

If limitations in switching frequencies are found in order to increase the modulation index, another possibility consists of decreasing the modulating frequency as many as possible. Depending on the switching frequency, lower modulating frequencies f_m can result in a negligible normative benefit due to the regulatory Resolution Bandwidth to be adjusted on the compliant Spectrum Analyzer (see Annexes 1 and 2) as verified experimentally in clause 4.2 in more detail.

Taking into account the limitations related to the switching frequency f_c and the modulating frequency f_m, the only chance to increase the modulation index m_f comes from increasing the modulation ratio δ as much as possible. As explained in clause 2.2.3.4, carrier frequency peak deviation $\Delta f_c = \delta \cdot f_c$ is limited by power converter's filter considerations.

These three parameters and their related limitations are to be studied in more detail in clauses 4.2 and 4.3.

3.7 Summary

In this chapter, a wide analysis regarding the theoretical behaviour of the modulation profiles was carried out, providing simultaneously a quantification of the modulation process according to several significant measure parameters: central harmonic

amplitude F_1, maximum envelope amplitude $F_{env,peak}$ and peak-to-peak envelope bandwidth Δf_{peak}. The same procedure of analysis was applied to the three profiles of interest: sinusoidal, triangular and exponential and the results are summarized in the following points:

1. Results expected from the analytical expressions of sinusoidal modulation are exactly reproduced by the computational algorithms, validating again the MATLAB algorithm.

2. Side-band harmonics resulting from modulation show a different aspect or outline depending on the profile. For a sinusoidal modulation, side-band harmonics tend to concentrate themselves around the two peaks defining the side-band harmonics bandwidth as the modulation index m_f gets higher, which results in a shape of the modulation spectrum envelope showing two peaks at both ends of the bandwidth while the envelope gets a larger concavity between these two peaks. In the case of a triangular modulation profile, envelope of the side-band harmonics corresponds to a nearly flat, straight horizontal line (with harmonic amplitudes concentrated in a narrow range of variation for vertex index $s \neq 0.5$) , very opposite to the sinusoidal modulation behaviour, characterised by a concavity between two extreme peaks and to the case of an exponential modulation profile, where side-band harmonics resulting from the modulation process tend to concentrate around the carrier frequency, decreasing in amplitude as the side-band harmonic order separates itself from the carrier frequency.

3. As just said, a triangular modulation produces a flat side-band harmonics spectrum. Considering a triangular profile as the reference base, profiles plotted outside the triangular profile limits (e.g., sinusoidal) seems to concentrate harmonics around the two peaks defining the bandwidth; in the same way, profiles plotted inside the reference triangular profile (e.g., exponential) concentrate harmonics around the carrier frequency. A combination of these three cases in a generic modulation profile allows the designer to generate whichever shape of the side-band harmonics spectrum.

4. For every modulation profile, amplitude reduction of the side-band harmonics resulting from the modulation process only depends on the modulation index m_f.

5. Regarding the evolution of the central harmonic amplitude F_1, the following considerations for the three profiles under study are of interest:

- Representing the harmonic amplitude F_1 as a function of m_f, it is obtained an attenuation plot whose envelope results in a logarithmical curve. This way, the higher the modulation index, the larger the attenuation; however, this conclusion is only valid considering the envelope. For modulation indexes $m_f <$ 200, attenuation increases very fast due to its logarithmical behaviour. Comparing the three profiles under study, a very small difference of 2 dBV appears at high modulation indexes between sinusoidal and triangular modulation; this is not the case of the exponential modulation, whose attenuation is very poor compared to the two previous profiles.
- Attenuation plots of F_1 show oscillations at a constant period of 1.3 (in units of m_f) for sinusoidal modulation, 1.41 for triangular modulation and a value depending on the concavity factor k for exponential modulation. At every oscillation along m_f -axis, harmonic amplitudes reach a minimum value with attenuation values higher than 40 dB, that is, it can be said that this harmonic is cancelled at this particular m_f. This way, a special profit can be taken just tuning the system to a concrete modulation index in order, for instance, to eliminate the harmonic at the carrier frequency. In the case of exponential modulation profile, it is possible to let the modulation index fix and tune the concavity factor k in order to cancel a particular harmonic. In the case of triangular modulation, no cancellation is possible for vertex index $s \neq 0.5$.

6. Regarding the evolution of the maximum envelope amplitude $F_{env,peak}$, consider the following comments for the three profiles under study:
   - Representing the central maximum envelope amplitude $F_{env,peak}$ as a function of m_f, it is obtained an attenuation plot whose envelope results in a logarithmical curve. Again, the higher the modulation index, the larger the attenuation, only valid considering the envelope of $F_{env,peak}$. For modulation indexes of $m_f <$ 200, attenuation increases very fast due to its logarithmical behaviour. Comparing the three profiles, exponential profile shows the worst behaviour because of the peak shape of the side-band harmonic distribution, which makes the F_1 value matches $F_{env,peak}$ most of the time; however, sinusoidal and, in a much higher quantity, triangular modulations give very good values of attenuation at any side-band harmonic order.

- Attenuation plots of $F_{env,peak}$ show oscillations much smaller than those corresponding to F_1; because of that, main efforts should be concentrated on obtaining a cancellation of a certain harmonic, normally, the one at the carrier frequency.

7. Related to the evolution of the peak-to-peak envelope bandwidth Δf_{peak}, further comments are of interest:

   - For sinusoidal modulation, envelope of Δf_{peak} shows a linear trend respect to m_f, that is, higher modulation indexes m_f are to produce wider bandwidths in a linear ratio. Zooming the plot of Δf_{peak}, it is observed that this parameter increases in steps of a constant value equal to $2 \cdot f_m$.

   - For triangular modulation, maximum values of Δf_{peak} show a linear trend respect to m_f . Under this theoretical straight line, a chaotic behaviour is shown, which is strongly related to the flat shape of the side-band harmonic spectra distribution. However, both sinusoidal and triangular modulations (with vertex index s = 0.5) show approximately the same straight line slope ($\approx 2 \cdot f_m$); for vertex indexes s different of 0.5, this slope is smaller in triangular modulation.

   - For exponential modulation, opposite to the sinusoidal and triangular profiles, no linear trend is detected, just a chaotic behaviour of Δf_{peak}. Moreover, the maximum bandwidth Δf_{peak} is much smaller than for sinusoidal and triangular cases. This indicates the concentration of harmonics around the carrier frequency, which is also bigger as the concavity factor k increases.

8. For every modulation index, it is commonly worthy to work with higher modulation indexes and, through its definition $m_f = \frac{\delta \cdot f_c}{f_m}$, this can be done by increasing the modulation ratio δ or the carrier frequency f_c or decreasing the modulating frequency f_m.

From the comparison of these three different modulation profiles and considering the global behaviour of the modulation, the most important parameter is $F_{env,peak}$. It provides a very useful information because of its global characteristic: the maximum amplitude (respect to the non-modulated carrier frequency) along the whole spectrum distribution as a result of a frequency modulation, that is, all harmonic amplitudes will

be under this value $F_{env,peak}$. If the number of new harmonics generated during the modulation process is not of concern but only their amplitudes, this parameter $F_{env,peak}$ should be the target. Then, a flat harmonic distribution is the most profitable and, therefore, a triangular modulation profile is the most suitable for any application with these characteristics. Exponential profile shows the worst behaviour because of the peak shape of the side-band harmonic distribution. If attenuation given by an exponential profile at a certain modulation index m_f is found to be satisfactory, then it can be a good option because the side-band harmonics decrease fast as the side-harmonic order gets farther from the central frequency

Because $F_{env,peak}$ does not oscillate too much, main efforts should be concentrated on obtaining a cancellation of a certain harmonic, normally, the one at the carrier frequency, that is, it is desired a value of $F_1 = 0$ V or, in a practical case, $F_1 < -40$ dBV (relative to the non-modulated carrier signal). To do this, a special profit of the oscillation features of the value F_1 is to be taken. Working points should be selected at those modulation indexes where harmonic cancellation is available.

Anyway, modulation profile to be selected is depending on the systems necessities or exigencies and no generic formula can be given.

Finally, a proposal of control applied to a real power converter was presented, consisting of simply changing the constant frequency control signal (sawtooth waveform) for a "modulated" sawtooth control signal. In order to be successful, some considerations must be taken into account: limitations of switching frequency f_c (electronic components are not able to manage easily larger power with shorter switching times), limitations of modulating frequency f_m (due to wider regulatory RBWs to be used in the compliant Spectrum Analyzers, in the case of being interested in regulatory measurements, of course) and limitations of modulation ratio δ (due to the cut-off frequency of the low-pass filter in the power converter).

CHAPTER 4

APPLICATION OF SSCG TO EMI EMISSIONS REDUCTION IN SWITCHING POWER CONVERTERS

4. APPLICATION OF SSCG TO EMI EMISSIONS REDUCTION IN SWITCHING POWER CONVERTERS

Although most of the power converters are currently designed to operate by using a constant switching frequency and a variable duty-cycle, some attempts were made in order to verify the effect of modulating the switching frequency [RA-1] and how this modulation affected the power converters EMI emissions. As known, Spread Spectrum Clock Generation (SSCG) modulates the originally constant switching frequency by following a certain modulation profile in order to spread the single harmonic energy into an amount of side-band harmonics having the same energy but smaller amplitudes. This reduction technique has been used and implemented for high frequencies (as those related to clock frequencies in communications and microprocessors systems). This chapter is dedicated to SSCG applied to the reduction of EMI emissions in Switching Power Converters, focusing on the effectiveness of frequency modulation in EMI reduction as a function of different switching frequency ranges and modulation profiles. As exposed previously (chapter 2), theoretical results are obtained just modulating a sine pure wave following several modulation profiles, this one representing each one of the harmonics composing the real square PWM-signal controlling the power converter. A practical test plant was designed in order to generate a modulated square wave from the modulated sinusoidal signal computed by the algorithm; a complete description of this test plan is also included.

Experimental results from a real power converter (making part of the test plant) will be measured. A compliant signal generator will be loaded with the corresponding modulated waveform and its output directly connected to the modulation controller system and, then, through a compliant LISN, the spectral components coming from the power converter finally measured with the spectrum analyzer. Now, some divergences can arise between theoretical results in chapter 3 and the ones here obtained due to influences of the real converter. When necessary and in order to evaluate the influence of the real converter on the expected results, it can be advisable to analyze the modulated signal introducing it directly into the Spectrum Analyzer, that is, the signal generator will be loaded with the corresponding modulated waveform and its output directly connected to the spectrum analyzer (according to Figure 4-1). This way, a very close (nearly exact) relationship must be found between theoretical results and the ones here obtained, without the influence of the real converter.

Influence of the regulatory Resolution BandWidth (RBW) of the spectrum analyzer on the final measured levels will be also investigated. It is important to distinguish between a phenomenon itself and the way it is going to be measured. Although theoretical results show a good performance of frequency modulation regarding to EMI emissions reduction in every case, measurements procedures (normally related to practical limitations of measure equipment or normative aspects) can fade such a real good behaviour even making it negligible. In other words, a good theoretical SSCG system is not a guarantee of good experimental results when measuring.

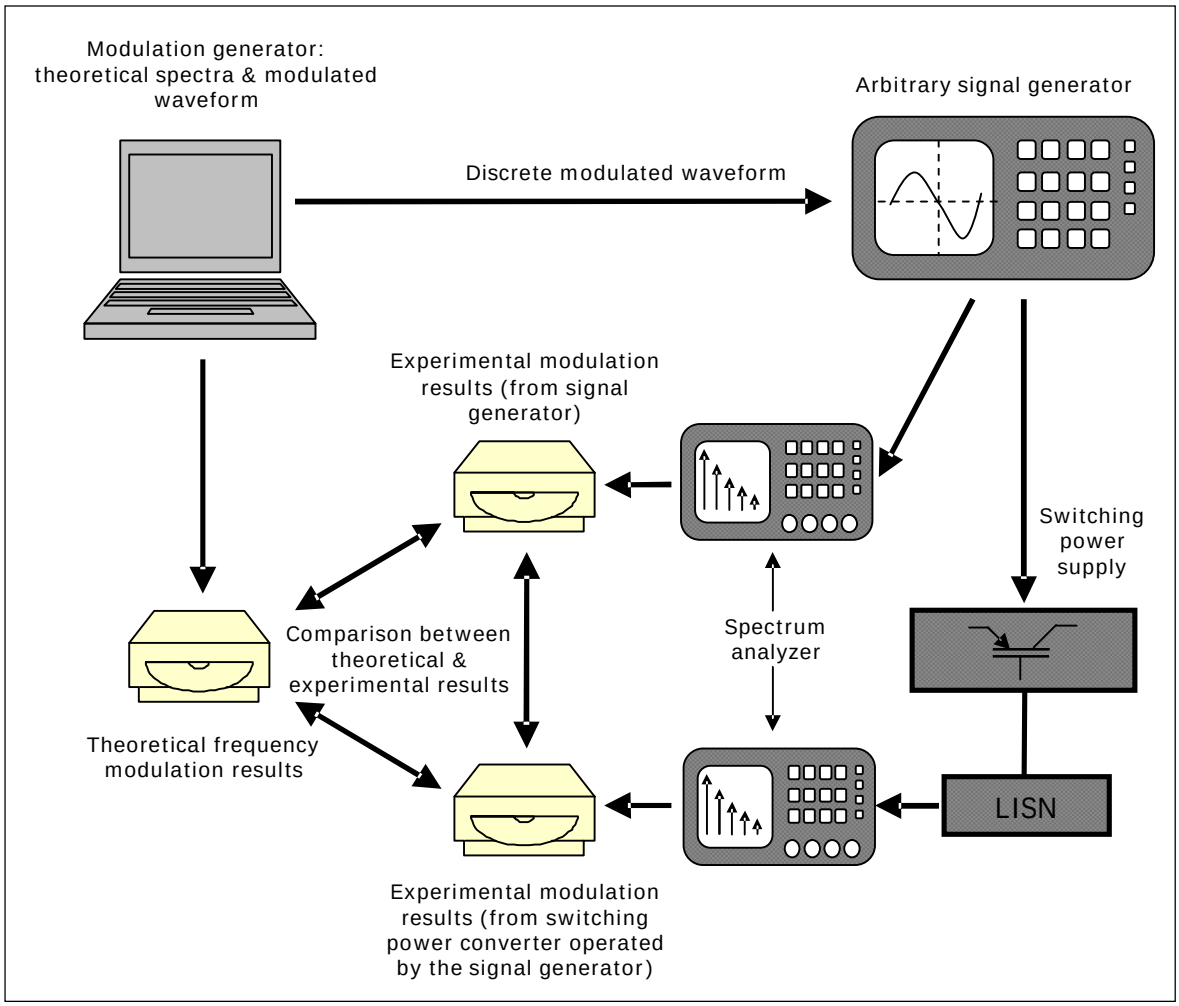

Figure 4-1. Diagram representing the basic operative guidelines of the thesis's development.

Some practical applications of SSCG methods are presented at the end of this chapter:

- It will be exposed a proposal of a practical method to select a valuable SSCG technique applied to Switching Power Converters in order to reduce EMI emissions.

- A valuable comparative measurement of conducted EMI within the range of conducted emissions will be carried out for the three modulation profiles of interest at different switching frequencies, showing the advantages of using SSCG methods as a way or EMI reduction.
- Use of SSCG as a method to avoid interferences to a significant signal.

Figure 4-1 summarizes graphically the operation mode for obtaining experimental results.

GENERIC CONSIDERATIONS (unless otherwise specified):

– Peak amplitude of the sinusoidal carrier signal is 0.5 V.

– Theoretical and experimental results are to be presented as a relative value dBV_{rel} respect to the non-modulated harmonic amplitude, that is:

$$V_{rel} = \frac{V_{rms,harmonic}}{V_{rms,carrier}} \text{ è} \qquad (4\text{ -}1)$$

$$20 \cdot \log_{10}(V_{rel}) = 20 \cdot \log_{10}(V_{rms,harmonic}) - 20 \cdot \log_{10}(V_{rms,carrier}) \qquad (4\text{-}2)$$

$$dBV_{rel} = dBV_{harmonic} - (-9.0309\ dBV) \qquad (4\text{-}3)$$

– Modulation profiles are even waveforms with null-offset. Related considerations were studied in point 2.6.2.4.

– Harmonic components measurements are to be carried out with a compliant spectrum analyzer (Tektronix 2712) in PEAK mode.

– A Tektronix AWG2021 was selected as the signal generator to be used (refer to point 4.1.2 for further information).

For the practical considerations about the physical implementation of the test plant used to measure, please refer to next clause 4.1.3.

4.1 Description of the test plant

Main part of the test plant consists of a switching power conversion system which has to meet several conditions to be useful:

a) It must be able to work with both a constant and variable frequency PWM. This way, measurements without modulation are easy to obtain and ready for comparison with those resulting from a further modulation process. Please note that the main interest is related to the relative amplitude of spectral contents before and after the modulation process.

b) A second (and more complicated to meet) condition is related to the ability of this power conversion system for admitting a modulation of the PWM controlling signal with no loss of linearity or non-negligible side-effects as explained in clause 4.1.2.

c) No optimization of the power conversion system is necessary to be reached. It is not an objective of this thesis to develop the best switching power converter in the world but a conversion system to demonstrate, through an easy verification, the benefits obtained by the fact of using a SSCG method, i.e., a frequency modulation following a certain modulation profile. First, a constant frequency PWM signal is to be applied and the values obtained this way will be measured; second, a frequency modulation of this controlling PWM will be applied and the new spectra will be measured. A further comparison between both measurements will reveal whether a frequency modulation is worthy or not. This is an important aspect which should be kept in mind during the development of this chapter. In order to test several switching frequencies, the power conversion system should be able to manage a relative wide range of frequencies, at least, from 100 kHz to 1 MHz. Of course, the behaviour of the system will differ from the lowest frequency to the highest one but this is not of special concern because the main interest is only related to relative differences under the same environment. Again, power capabilities of this converter are not of interest; this way, simple power converters are of interest because they simplify the design of the switching power converter and allow the use of common electronic components.

d) Finally, in order to meet the criteria imposed by regulatory normative (mainly CISPR 22 and FCC), measurements will be carried out through a compliant LISN.

A first approach to the test plant is presented in Figure 4-2 in several black-boxes which will be filled out later on, especially, the two ones labelled as "UNIT 1" and "UNIT 2".

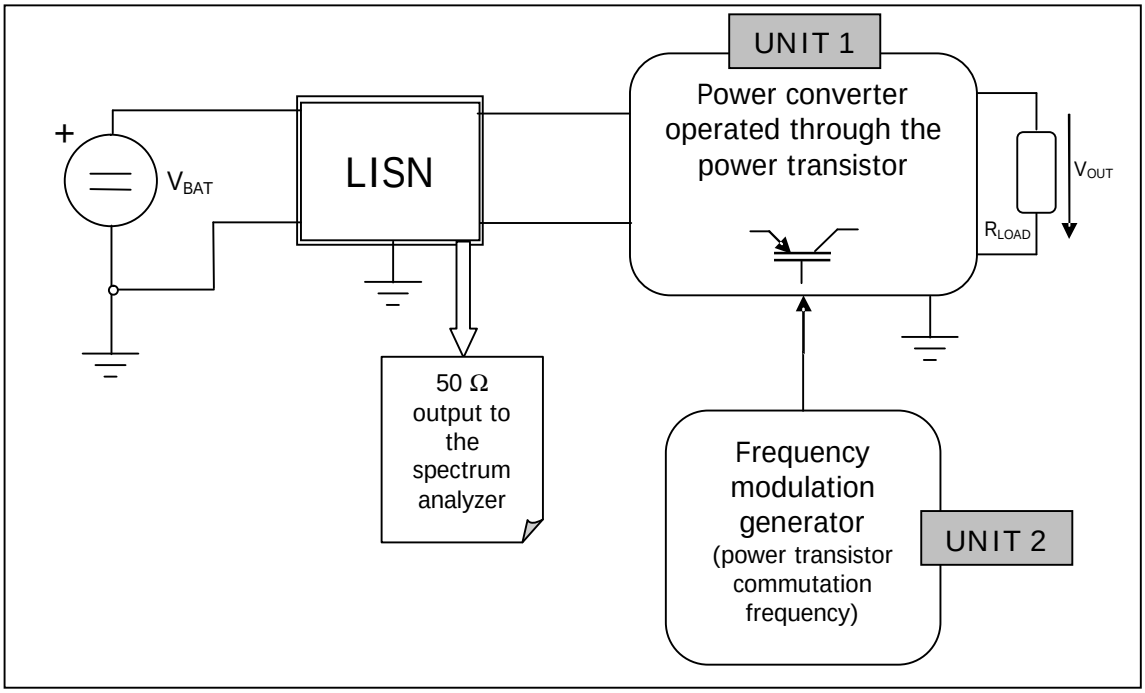

Figure 4-2. Description of the test plant (black boxes)

Onwards, range of the power conversion system parameters is to be listed:

- Switching frequencies (f_c) è 100 kHz to 1 MHz
- Modulating frequencies (f_m) è 0 Hz to 20 kHz
- Percentage of modulation (δ%) è 0 % to 40 %
- Input voltage (V_{BAT}) è 10 V
- PWM duty-cycle (D) è ≈ 50 %
- Output voltage (V_{OUT}) è 5 V (corresponding to a 50% duty-cycle)
- R_{LOAD} è 20 Ω (≈ 1.25 W power output)

Selected values above are based on the following criteria:

a) Switching frequencies (f_c) è 100 kHz to 1 MHz: As exposed later on, better results can be found with switching frequencies beyond 100 kHz. From the normative point of view, another important reason is that CISPR 22 specifies a border frequency of 150 kHz between bands A & B (see clause A2.3 in Annex 2). For the

band A, a 220Hz-resolution bandwidth must be selected on the spectrum analyzer to measure. For the band B, this resolution bandwidth increases until 9 kHz. The resulting compliant measured spectra will be completely different for a power converter being controlled by a frequency of 145 kHz than the same one but controlled by a frequency of 155 kHz, at least, for the first harmonic. In the first case and in a generic situation, harmonics resulting from the modulation process will be displayed on the spectrum analyzer as individual lines corresponding to true individual components while, in the second case, each spectral line on the display can correspond to several true harmonic components, falling inside the wider 9kHz-resolution bandwidth. In other words, attenuation benefits at 145 kHz or 155 kHz are true and very similar in practice; however they are different from the normative point of view, but this is only a conventionalism. This situation will be studied and the results presented in clause 4.2.

b) Modulating frequencies (f_m) è 0 Hz to 20 kHz: Frequency spacing between harmonics resulting from the modulation process is given directly by f_m. Due to the range of switching frequencies (<1MHz), resolution bandwidths to be configured on spectrum analyzers are 220 Hz or 9 kHz. The selected range allows to verify the influence of resolution bandwidths wider and narrower than the modulating frequency. Besides, the limit of 20 kHz will allow the system to vary the modulation index m_f more widely.

c) Percentage of modulation (δ%) è 0 % to 40 %, depending on the carrier frequency: For clock systems, the maximum percentage of modulation is commonly 2.5%. For the lower frequency system under study in this thesis, a wider range of percentages has been assumed in order to investigate the influence of relative high percentages of modulation in the final harmonic spectra. However, the higher carrier frequency, the lower percentage of modulation is to be considered; this way, a maximum percentage of 10% is intended for the highest carrier frequency of 1 MHz due to limitations of the switching components. A maximum frequency of 1.2 MHz was successfully reached using the test plant, corresponding to δ% = 20% (see Figure 4-10).

d) PWM duty-cycle (D) è ≈ 0.5 (or 50 %): There are two important reasons to select this value of duty-cycle. The first one, the system hereby developed can generate a 50% duty-cycle square waveform very easily and quite accurately; the second one,

only odd harmonics are to be generated because the even ones are zero. Obviously, the practical system will not have an exact 50% duty-cycle (see Figure 4-10), then also obtaining even harmonics; however, amplitude of these even harmonics will be much smaller (perhaps negligible) than the odd harmonics.

4.1.1 Power conversion stage (UNIT 1)

This power conversion stage corresponds properly to the switching power converter itself. As known, a numerous variety of power converter topologies is available and well-known. The election of a topology is normally related to several factors such as power conversion ratio, necessity of an output voltage higher/lower than the input voltage, resonance frequencies, etc.

In this thesis, a step-down (BUCK) topology was selected in order to verify the benefits of frequency modulation applied to the PWM controlling signal when measuring EMI emissions (see Figure 4-3).

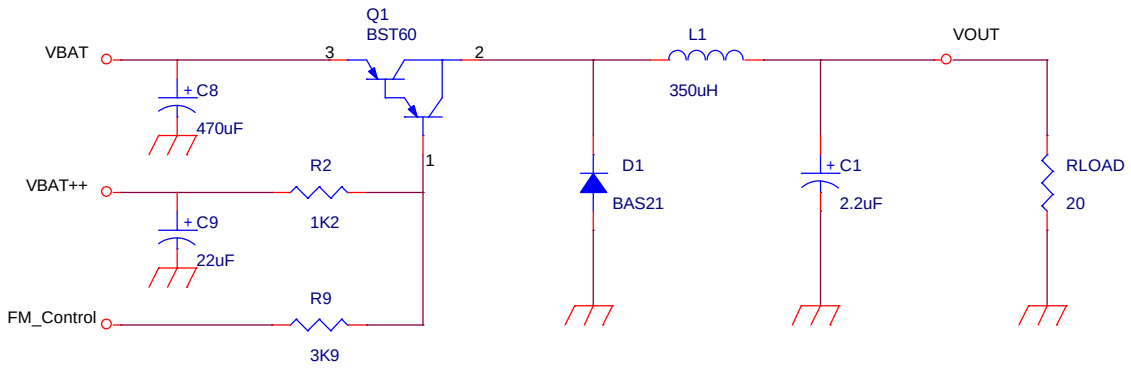

Figure 4-3. Step-down topology selected for measurements

Several reasons were taken into account to select this topology:

a) Benefits after frequency modulation are to be obtained independently on the selected topology (in a higher or lower degree). Major contribution to EMI emissions is very close related to the power transistor switching. Usually, a constant frequency PWM signal (i.e., a square signal) is controlling the power transistor base. This transistor switches ON when a low level (nominally, 0 V) is placed on its base terminal and switches OFF when the base terminal is set to high level (nominally, V_{BAT}). Repercussion of this behaviour on the EMI emissions is direct and clear: current flowing from the V_{BAT} terminal to ground is zero during the transistor OFF-time and a finite value during the ON-time, i.e., a quasi-square

current waveform is flowing through the input terminal V_{BAT}, which generates the corresponding EMI emissions. Shape of the spectral content should be very similar to that of a square waveform (see clause 2.1.3.1); the absolute magnitude of the harmonics, however, will depend on several factors like filter capacitors, test plant layout, parasitic capacitances, length of wires, input and output voltages, load impedance, PWM- constant switching frequency and duty-ratio, etc. This behaviour is common to nearly all power converter topologies, thus allowing the selection of whichever topology if the main purpose is just measuring EMI emissions. Moreover, instead of having a constant PWM switching frequency, it can be modulated by using a frequency modulation method. Now, the ON-OFF behaviour of the transistor will follow the modulated switching frequency and so the currents flowing through the input terminal V_{BAT}. Then, a different shape of the spectral content related to the current flowing through the input terminal is to be found and should be very similar to the spectral content of the modulating signal (i.e., the modulated PWM switching waveform); again, absolute harmonic magnitude will depend on the same factor as exposed previously.

b) After the previous consideration a), there is no objection to select a very simple topology like a step-down converter. This way, main efforts are not concentrated on the power converter design itself but on the further measurements to be carried out. As said before, no optimization of the power conversion system is necessary to be reached because the main interest is related to the relative amplitude of spectral contents before and after the modulation process.

c) This step-down topology allows an easy design of a system valid for the range of values expressed before at the beginning of this chapter. As the switching frequency increases inside the defined variation range, the LC filter (consisting of L1 and C1) becomes more effective, generating a lower ripple at the output voltage.

After all these considerations, an exhaustive description of the circuit calculation is mandatory to be presented. A prestigious reference for the calculation and selection of all components is [RD-2] and it will be the guideline.

1) Calculation of the LC output filter

This low-pass filter consists of one inductance L1 and one capacitor C1. For notation reason, these two components will be referred as L and C, respectively,

along this clause 1). Assuming the step-down power converter is always working in the continuous mode, Figure 4-4 is a fair representation of the current through the inductor i_L.

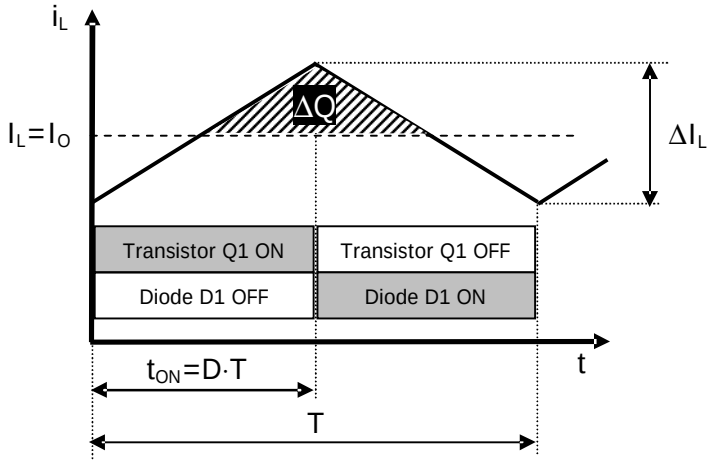

Figure 4-4. Current through the inductor (continuous mode)

- I_L corresponds to the average current through the inductor. Assuming that the average current through the capacitor C is zero (as corresponds to a theoretical capacitor, no leakage is considered or it is negligible), then this average inductor current will flow outside the power converter, thus making true the equality $I_L = I_O$.

- ΔI_L is the ripple of the inductor current. It is an important point to be taken into account because, in continuous mode, the actual maximum current flowing through the transistor Q1 or the diode D1 is not the average I_L but the sum of I_L and $\frac{\Delta I_L}{2}$ (approx.). Then, the larger ΔI_L, the stronger the exigencies for transistor Q1 and diode D1. ΔI_L should be kept as low as possible in order to be able to work with as simple as possible components.

- As shown in Figure 4-4, inductor current positive slope corresponds to the transistor ON-time and the diode OFF-time, while the negative slope corresponds to the transistor OFF-time and the diode ON-time. Of course, during the transitions OFF è ON and, mainly, ON è OFF, dynamic effects are to appear because the whole electric charge inside these devices has to be discharged during a recovering time, especially, when switching ON è OFF. In a

first approach, these effects are not taken into account for these preliminary calculations.

After all these considerations, the calculation of this filter becomes easier now. The ripple ΔI_L is theoretically only depending on the inductor value L, the output voltage V_O, the duty-cycle D and the switching frequency f, as expressed below (4-4):

$$\Delta I_L = \frac{V_O}{L} \cdot (1-D) \cdot \frac{1}{f} \tag{4-4}$$

The main consideration to be assumed in order to formulate the expression (4-4) is that the forward voltage drop through the diode (when switched ON) is zero.

Before being able to apply expression (4-4), an estimation of inductor value L would be of interest. To do this, relationship between the output voltage V_O and its ripple ΔV_O is very useful. This ripple is produced by the charging-discharging process of the real capacitor C and can be derived by the following steps:

$$i_c = C \cdot \frac{dV_O}{dt}$$

Assuming that the ripple component in i_L flows through the capacitor and its average component flows through the load resistor, the shaded area in Figure 4-4 represents an additional charge ΔQ. Therefore, the peak-to-peak voltage ripple ΔV_0 can be written as follows:

$$\Delta V_O = \frac{\Delta Q}{C} = \frac{1}{C} \cdot \frac{1}{2} \cdot \frac{\Delta I_L}{2} \cdot \frac{T}{2} \tag{4-5}$$

From (4-4) and (4-5) (where $f = 1/T$):

$$\frac{\Delta V_O}{V_O} = \frac{1}{8} \cdot \frac{(1-D)}{LC} \cdot \frac{1}{f^2} \tag{4-6}$$

Directly from expression (4-6), the minimum value of inductance L_{min} to obtain a desired maximum ripple at the output takes this aspect:

$$L_{\min} = \frac{V_O}{8} \cdot \frac{(1-D)}{\Delta V_O \cdot C} \cdot \frac{1}{f^2} \tag{4-7}$$

A frequency variation range for the switching frequency f from 100 kHz to 1 MHz was defined. From expression (4-6), the larger switching frequency f, the lower the output

voltage ripple ΔV_O. This confirms that calculation of L_{min} must be done for the minimum switching frequency, i.e, for 100 kHz just to limit a maximum output voltage ripple over the whole range.

Consider the following data in the prototype circuit:

- $\frac{\Delta V_O}{V_O} = 0.01 \quad (1\%)$
- C = 2.2 µF è This capacitance value is available in tantalum capacitors which means, compared to the rest of electrolytic capacitors, a lower ESR and a better dynamic behaviour. Typical polypropylene capacitor of 100 pF in parallel with C was not provided in the circuit in order to magnify the EMI results.
- V_O = 5 V, f = 100 kHz and D = 0.5 (nominal values)

Substitution of values above into equation (4-7) yields the following result:

$$L_{\min} = 284.1 \mu H$$

However, the minimum value of inductance only guarantees a minimum ripple of the output voltage (ΔV_O). Then, if a limitation of the maximum ripple related to the inductor current is desired, expression (4-4) becomes now of interest:

$$\Delta I_L = \frac{V_O}{L} \cdot (1 - D) \cdot \frac{1}{f} \qquad (4\text{-}8)$$

Substituting values above and the recent value of L_{min}, the inductor current ripple to be obtained is:

$$\Delta I_L = 88 mA$$

It is a reasonable value, taking into account that the average inductor current is:

$$I_L = I_O = \frac{V_O}{R_{LOAD}} = \frac{5V}{20\,\Omega} = 250\,mA$$

However, a larger value of inductance ($L > L_{min}$) is to be selected in order to reduce the inductor current ripple. A final value of L=L1=350 µH is selected, which yields an inductor current ripple of:

$$\Delta I_L = 71.43 mA$$

Keep in mind that the higher the switching frequency f, the lower the inductor current ripple; therefore, this value of inductance is good enough for the thesis's purposes. This new selection of inductance will vary the output voltage ripple previously calculated but keeping it always lower than the original one.

In order to summarize the previous discussion, it can be concluded that the larger the:

– Inductance value L1 or

– Output capacitor C1 or

– Switching frequency f,

the lower the inductor current ripple (ΔI_L) and the output voltage ripple (ΔV_O). The maximum current flowing through the transistor will be $I_L + \frac{\Delta I_L}{2} = 285.715\,mA$. On fact, a parallel combination of two tantalum capacitor each of 22 μF was implemented in the final circuit.

SIZE ESTIMATION OF THE TOROID

A toroidal configuration was selected to implement physically the inductor L, because of the well-known behaviour of such devices. A diagram of the currents and voltages across the inductor in a switching power converter is shown in Figure 4-5.

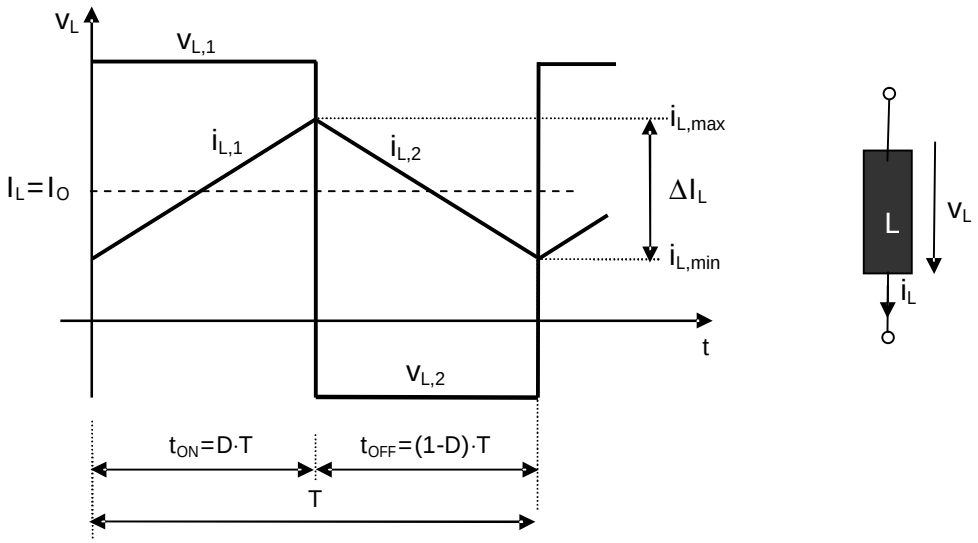

Figure 4-5. Currents and voltages across the inductor (continuous mode)

Equation describing the behaviour of a generic inductor is given by:

$$v_L = L \cdot \frac{di_L}{dt} \tag{4-9}$$

Directly from expression (4-9), maximum inductor current excursion ΔI_L is calculated as follows:

$$\Delta I_L = i_{L,\max} - i_{L,\min} = \frac{1}{L} \cdot v_{L,1} \cdot D \cdot T \tag{4-10}$$

or

$$\Delta I_L = i_{L,\max} - i_{L,\min} = -\frac{1}{L} \cdot v_{L,2} \cdot (1-D) \cdot T \tag{4-11}$$

Calculation of the average inductor current as a function of the peak current excursions is developed below:

$$I_L = \frac{1}{T} \cdot \int_0^T i_L(t) \cdot dt = \frac{1}{T} \cdot \int_0^{t_{on}} i_{L,1}(t) \cdot dt + \frac{1}{T} \cdot \int_{t_{on}}^T i_{L,2}(t) \cdot dt =$$

$$= \frac{1}{T} \cdot \left(\frac{\left(i_{L,\max} - i_{L,\min}\right)}{2} \cdot t_{on} + i_{L,\min} \cdot t_{on} \right) + \frac{1}{T} \cdot \left(\frac{\left(i_{L,\max} - i_{L,\min}\right)}{2} \cdot t_{off} + i_{L,\min} \cdot t_{off} \right) =$$

$$= \left(\frac{D}{2} \cdot \left(i_{L,\max} - i_{L,\min}\right) + D \cdot i_{L,\min} \right) + \left(\frac{1-D}{2} \cdot \left(i_{L,\max} - i_{L,\min}\right) + (1-D) \cdot i_{L,\min} \right) =$$

$$= i_{L,\max} \cdot \left(\frac{D}{2} + \frac{1-D}{2} \right) + i_{L,\min} \cdot \left(-\frac{D}{2} + D - \frac{1-D}{2} + 1 - D \right) =$$

$$I_L = \frac{1}{2} \cdot \left(i_{L,\max} + i_{L,\min}\right) \tag{4-12}$$

Once the currents across the inductor are known, it can be started the selection of the toroid. Figure 4-6 shows a toroid and the main characteristics associated to it, like average radius r and cross-section radius R.

The fist Maxwell's law (or Ampere's law) can be expressed as follows

$$\oint_C \vec{H} \cdot d\vec{l} = \sum_l i_{L,l} \tag{4-13}$$

that is, integral of the scalar product of magnetic field $\vec{H}$ and $d\vec{l}$ along a closed boundary is equal to the sum of currents flowing inside the surface defined by the closed boundary.

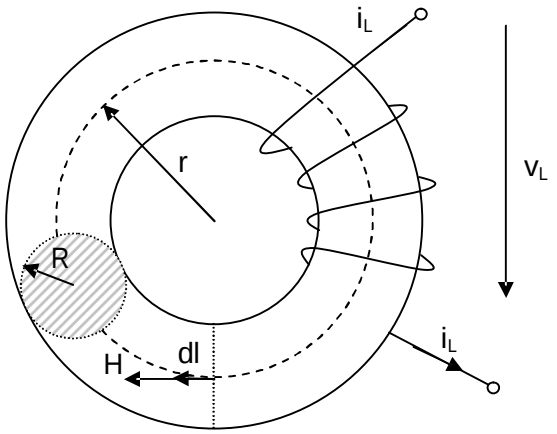

Figure 4-6. Toroid and its related parameters

Assuming that the magnetic field $\vec{H}$ is constant across the whole toroid section and perpendicular to it, the middle line of radius r is selected as close boundary. Expression (4-13) becomes the following one, yielding the module of the magnetic field H:

$$H \cdot 2 \cdot \pi \cdot r = N \cdot i_L$$

$$H = \frac{N \cdot i_L}{2 \cdot \pi \cdot r} \tag{4-14}$$

where N is the number of wire turns around the toroid.

A non-linear relationship between the magnetic flux density B and the magnetic field H is characteristic of a ferromagnetic material of which the toroid is made, relationship expressed normally as the curve in Figure 4-7:

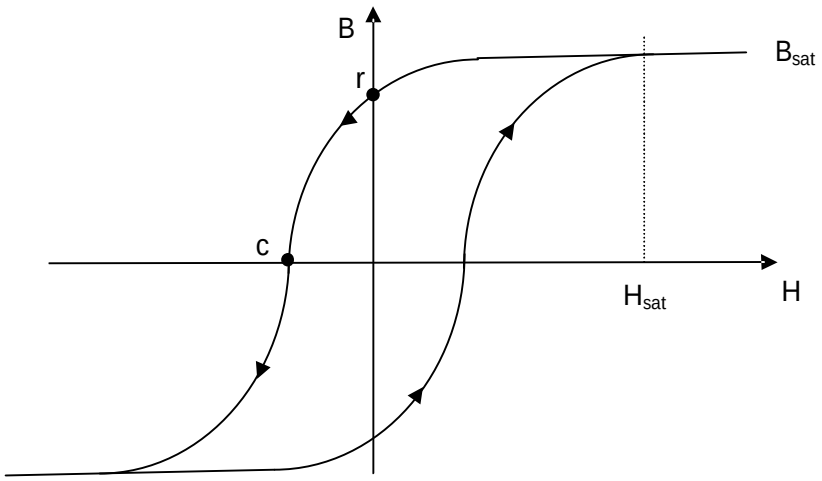

Figure 4-7. Typical histheresis curve of a ferromagnetic material

It has to be guaranteed that the toroid is never reaching saturation. If so, despite the growing current across the inductor (therefore, H too), magnetic flux density keeps a constant value and a null-voltage across the inductor will appear, then transmitting the supply voltage V_{BAT} directly to the load resistor, causing its destruction. This is because the inducted voltage ε along the inductor is given by the variation of magnetic flux ϕ, as expressed onwards:

$$\varepsilon = N \cdot \frac{d\phi}{dt} \text{ and } \phi = \oint \vec{B} \cdot d\vec{s} \qquad (4\text{-}15)$$

Ferrite is the selected material for toroid. Ferrite is an ideal core material for inductors in the frequency range 20 kHz to 3 MHz, due to the combination of low core cost and low core losses. Different ferrites types are available: F, P, R, K, J and W. First four types offer the lowest core losses and highest saturation flux density and are most suitable for high power/high temperature operation. A P-material core was finally selected for the prototype. Saturation values for P-material are (approximate values):

- B_{sat} > 0.5 Tesla at 25 ºC and B_{sat} > 0.39 Tesla at 100 ºC
- H_{sat} > 300 A/m.

Selected toroid for the prototype has the following dimensions: r = 12 mm, R = 4 mm (see Figure 4-6). As derived previously, a maximum inductor current of 300 mA is to be flown around the N = 9 turns of wire, then peak-value to be obtained is calculated directly from expression (4-14):

$$H_{peak} = \frac{9\,turns \cdot 300\,mA}{2 \cdot \pi \cdot 12\,mm} = 35.81\,A/m$$

this peak-value being much lower than the saturation condition H_{sat}.

To determine the maximum flux density (B_{max}) in a core when a symmetrical square wave excitation is applied, equation (4-16) is applied [RD-6]. If a bias current is present, the second summand of equation (4-16) must also be taken into account. The following factors are to be considered:

- applied rms voltage in volts è E ≈ 5 V (voltage across the inductor varies between +5 V and -5V)
- cross sectional area of the magnetic path in cm^2 è $A_e \approx \pi \cdot (0.4\ cm)^2 = 0.503\ cm^2$

- number of turns è N = 9
- minimum operating frequency in MHz è f = 0.1 MHz
- bias current expressed in A è $I_{dc} \approx 0.25$ A (average inductor current)
- core inductance index A_L in nH è it can be estimated for lower frequencies as

$$A_L = \frac{L}{N^2} = \frac{350\ \mu H}{9^2} = 4.321\ \mu H = 4.321 \cdot 10^3\ nH$$

These terms are used in the following combined (ac + dc) formula for flux level:

$$B_{\max} = \frac{E \cdot 10^2}{4 \cdot f \cdot N \cdot A_e} + \frac{N \cdot I_{dc} \cdot A_L}{10 \cdot A_e}(Gauss) \qquad (4\text{-}16)$$

$$B_{\max} = 2.2 \cdot 10^3\ Gauss \approx 0.22 Tesla$$

B_{max} is lower than the saturation magnetic flux density (B_{sat} > 0.39 Tesla) even in the worst case, that is, highest temperature, lowest operation frequency and a theoretical average inductor current higher than the real current found in the final prototype. Then, no problems should be found due to the actual toroid in use.

No other design considerations as heating of both ferrite and iron powder cores were taking into account due to the prototype consideration of the current design.

2) Selection of the diode D1

From Figure 4-4, it must be concluded that direct current through diode D1 reaches the maximum current through the inductor L1, i.e., ≈300 mA.

Selected diode is a BAS21 of Philips Semiconductors. Reasons for this selection are listed below:

a) From the datasheet, a maximum continuous forward current of 200 mA is available. Taking into account that this diode will work under a duty-cycle of 50%, a maximum current of 400 mA is then allowed. Actual necessities will be lower than 300 mA at a duty-cycle of 50%.

b) Dynamically, a diode capacitance lower than 5 pF (at 1 MHz) and a maximum recovery time of 50 ns (from I_F = 30 mA to I_R = 30 mA) suit perfectly actual necessities (see Table 4-1 in the next point)

c) A maximum forward voltage of $V_{f,D1}$ = 1.5 V is expected for a forward current of ≈300 mA. This is also interesting because nearly cancels the emitter-collector

saturation voltage of ≈1.3 V, thus expecting a quasi-square waveform of amplitude near to 10 V.

d) A maximum continuous reverse voltage of 200 V guarantees the blocking capability of the diode.

e) From the logistic point of view, a stock of this diode was available.

3) Calculation of the resistors R2 & R9 attached to the power transistor base (Q1)

A typical configuration of signal transistors being whether in saturation of in cut-off modes does include just one base resistor, for instance, R9. But power transistor must remove more quantity of charge during the switching off. This is the reason for the manufacturer to recommend another resistor (R2) connected to a higher power supply voltage than V_{BAT}, i.e., make the transistor's turning off easier and faster to reach. This is a very important fact because the relative high frequencies being used in this test plant: up to 1 MHz.

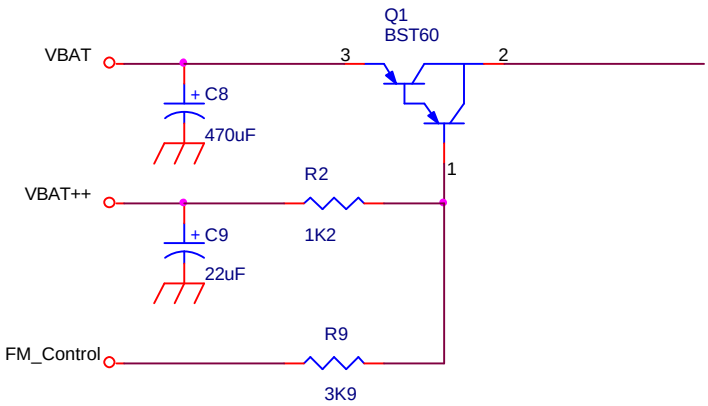

Figure 4-8. Power transistor and the related resistors.

BTS60 is a Darlington transistor of Philips Semiconductors very appropriate to actual necessities. A summary of the main characteristics is listed below:

– Maximum collector current = 500 mA

– Transition frequency f_T = 200 MHz (typical)

– Switching times (from 10% to 90%, and using the topology shown in the previous figure):

  § Turn-on time = 0.5 µs (typical) (I_{Con} = -500 mA & I_{Bon} = -0.5 mA)

  § Turn-off time = 0.7 µs (typical) (I_{Boff} = 0.5 mA)

Faster values than these ones are very difficult to find in quasi-conventional components and this is one of the reasons for this component to be selected.

- Collector-emitter saturation voltage V_{CEsat} < -1.3 V (I_C = -500 mA & I_B = -0.5 mA)
- Base-emitter saturation voltage V_{BEsat} < -1.9 V (I_C = -500 mA & I_B = -0.5 mA)

A critical aspect of this design is to get a transistor switching behaviour as near as possible to the square signal (D ≈ 50 %) represented in the Figure 4-9.

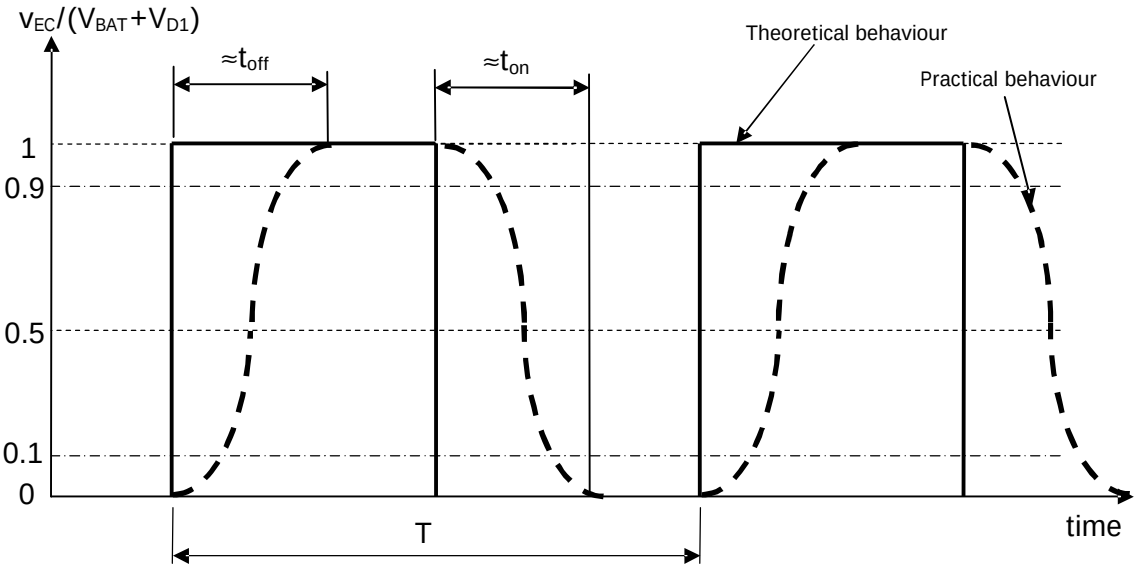

Figure 4-9. Influence of the turn-on and turn-off times in the switching frequency of the power transistor

Of course, lower switching frequencies (i.e., larger periods T) are to have a better behaviour in the sense that turn-on and turn-off times are much smaller (perhaps negligible) than the half-period of the switching waveform. A summary of the time conditions of the signal to be studied further is presented in Table 4-1:

Frequency (kHz)	Period (µs)	Half-period (µs)	Turn-on time (µs) (typical)	Turn-off time (µs) (typical)
100	10	5	0.5	0.7
120	8.334	4.167		
200	5	2.5		
1000	1	0.5		
1100	0.909	0.4545		

Table 4-1. Time considerations related to the operation of the power transistor

As expected, turn-off time is a little higher than turn-on time due, mainly, to the higher recovery time when turning the transistor off. As it can be derived of Figure 4-9, minimum switching period (i.e., maximum switching frequency) is limited by the turn-on and turn-off times (mainly, by the turn-off time), because the only possibility for the signal to go from saturation voltage V_{ECsat} to $V_{BAT}+V_{D1}$ is the turn-off time to be lower or equal (in the worst case) to the half-period of the switching waveform (considering a 50%-duty cycle) and, in a similar way, the possibility for the signal to go from saturation voltage $V_{BAT}+V_{D1}$ to V_{ECsat} is the turn-on time to be lower or equal (in the worst case) to the half-period of the switching waveform (considering, again, a 50%-duty cycle).

From Table 4-1, problems are only expected at the highest frequency of 1 MHz, because the typical turn-off time of the power transistor is higher than the related half period. However, these values are "typical", which means that, after a careful selection of transistors, a component matching better time behaviour will be found. The way used to identify a "proper" transistor at 1 MHz consisted of making it switch at this frequency and measuring the waveform at the collector terminal: if a "good" quasi-square wave is found at this terminal, having a frequency of 1 MHz (actually, the same frequency as in the base terminal) and going from V_{ECsat} to $V_{BAT}+V_{D1}$ and vice versa, it can be said that a proper transistor was found. Pictures in Figure 4-10 (taken with an oscilloscope Tektronix TDS 510A) are intended to show this success in the search: the designed power converter is able to manage frequencies up to ≈1.3 MHz. From the experience, nearly all tested devices presented lower turn-on and turn-off times than the typical ones, what made this selection task very easy.

But things can get worse when considering that the original constant frequency of 1 MHz becomes higher due to the frequency modulation. In this sense, the maximum frequency to be found in this system is given by:

$$f_{\max} = f_{c\max} \cdot (1+\delta_{\max}) = 1\,MHz \cdot (1+0.1) = 1.1\,MHz$$

that is, the last case on Table 4-1.

The same considerations above must be taken into account for this maximum frequency.

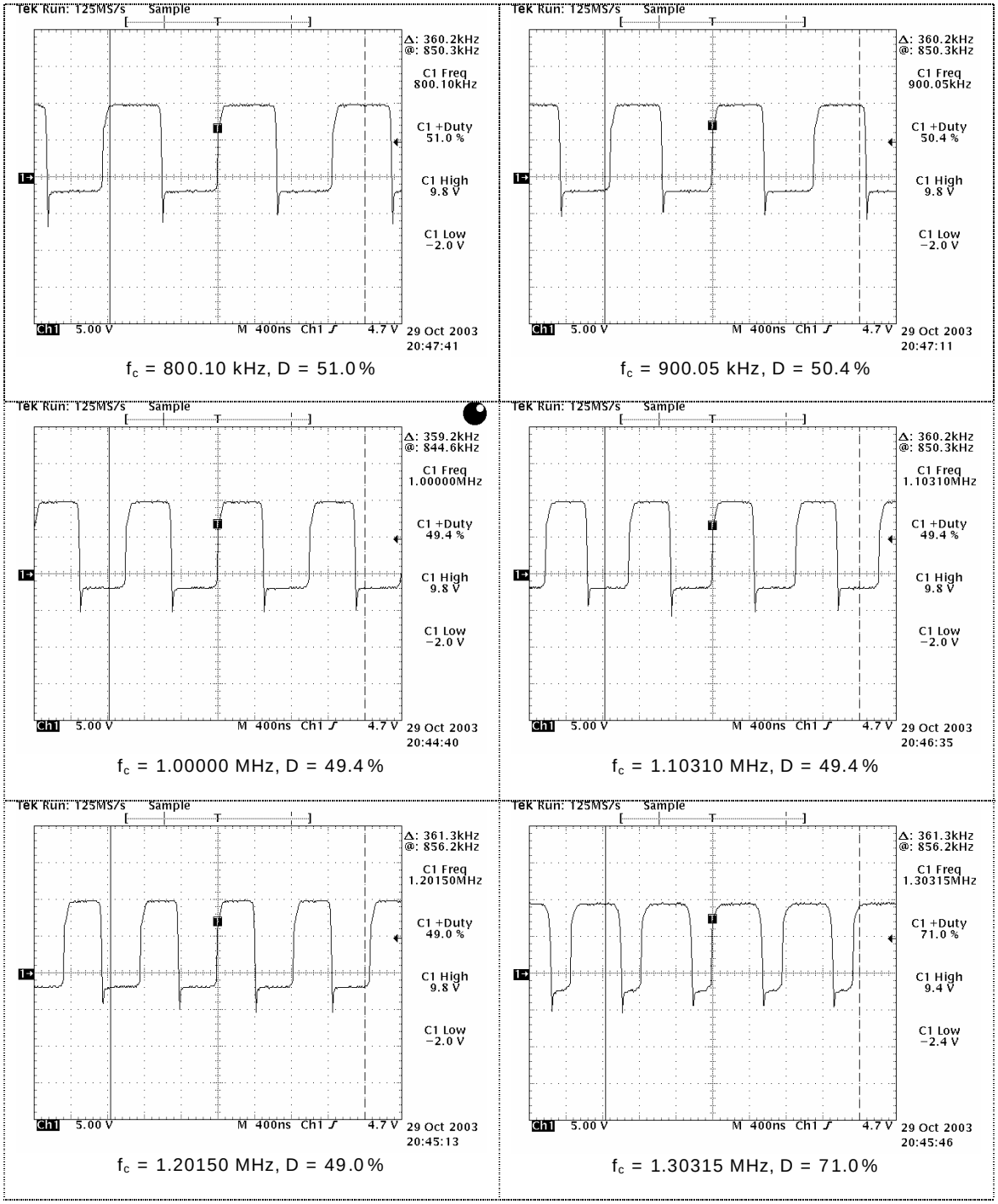

Figure 4-10. Measured waveforms at the collector of power transistor Q1 (pin 2) around the switching frequency of 1 MHz

Anyway, turn-on time is given for a collector current of ≈500 mA. In this prototype, a maximum collector current lower than 300 mA is expected, which means a shorter turn-on time. In the same way, as lower quantity of current should be removed during the recovering time, turn-off time shorts too, helping this process

by increasing the breaking base current over the 0.5 mA (testing current in datasheet to estimate turn-off time).

After all these considerations, calculation of these two base resistors is easier to carry out. Two processes are to be distinguished:

a) Process 1: Power transistor Q1 turns off

Terminal FM_Control is connected to a collector of a signal transistor which controls the power transistor (Q1) turning-on and -off. When Q1 is turned off, terminal FM_Control remains unconnected, then actuating just the resistor R2 while, in early moments, Q1 remains saturated. Under these conditions, the following data are to be considered:

- V_{BAT} = 10 V
- V_{BAT++} = V_{BAT} + 2 V = 12 V
- I_{BQ1off} = 3 mA è Current to turn-off the transistor faster.
- V_{EB1sat} = 1.6 V è Emitter-base saturation voltage a few lower than the one specified in datasheet, due to a lower collector current in the prototype.

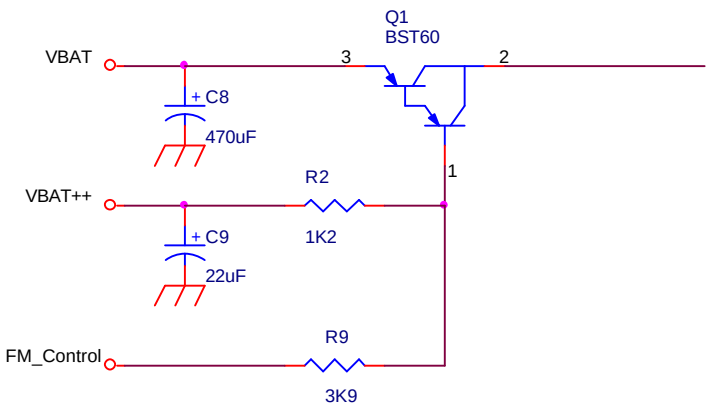

Figure 4-11. Schema to analyze the turning-off of the power transistor Q1

Calculation of R2 follows this way:

$$R_2 = \frac{V_{BAT++} - V_{BAT} + V_{EB1sat}}{I_{BQ1off}} = 1.2\ k\Omega \qquad (4\text{-}17)$$

Thus, a final value of R2 = 1.2 kΩ is selected.

b) Process 2: Power transistor Q1 turns on

As explained previously, terminal FM_Control is connected to a collector of a signal transistor Q2 which controls the power transistor (Q1) turning-on and -off. To turn transistor Q1 on, a low level must be activated at terminal FM_Control, which implies saturation of control transistor Q2.

Transistor Q2 takes part of a comparator; really, the output of this device consists of an open-collector transistor. As seen later on, the selected dual comparator was a LM393 of National Semiconductors. Characteristics of this comparator to be taken into account at this point are those ones related to the open-collector transistor and, more, those related to the saturation mode. The following data, obtained from the LM393 and BST60 datasheets, considered together with the ones shown at Process 1, are of interest:

- V_{CE2sat} = 0.25 V è Typical collector-emitter saturation voltage for collector currents lower than 4 mA.
- Comparator is dual-supplied: V_{ss393+} = +5V & V_{ss393-} = -5V. This is an important point to take into account because the emitter of the open-collector is connected to V_{SS393-}, that is, to -5V.
- I_{BQ1} = 0.3 mA è Q1 base current considering a DC current gain of ≈1000 when in saturation mode, necessary to supply a collector current of ≈300 mA.

Now, it is time to analyse the circuit already shown before:

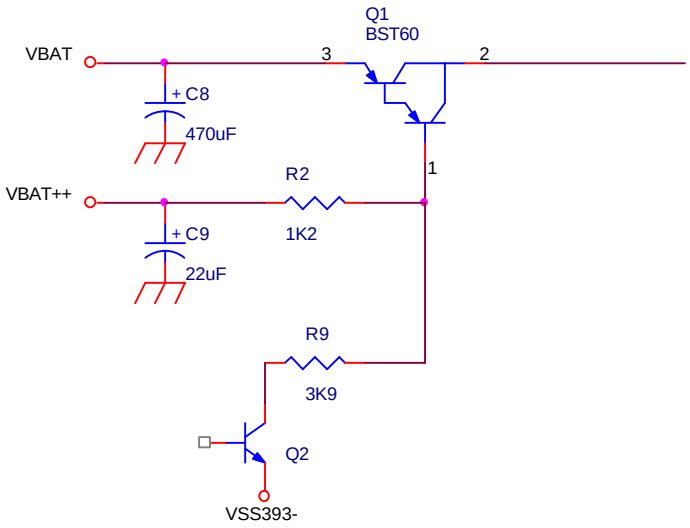

Figure 4-12. Schema to analyze the turning-on of the transistor Q2

Applying Kirchhoff's laws to the base terminal of the transistor Q1, the following expression is derived:

$$I_{BQ1} = \frac{V_{BAT} - V_{EB1sat} - V_{CE2sat} - V_{SS393-}}{R9} - \frac{V_{BAT++} + V_{EB1sat} - V_{VBAT}}{R2} \quad (4\text{-}18)$$

and, directly from expression (4-18), it is obtained the expression to calculate R9:

$$R9 = R2 \cdot \frac{V_{BAT} - V_{EB1sat} - V_{CE2sat} - V_{SS393-}}{R2 \cdot I_{BQ1} + V_{BAT++} + V_{EB1sat} - V_{BAT}} \quad (4\text{-}19)$$

Substitution of values into the expression (4-19) yields the following result:

$$R9 = 1.2 \cdot \frac{10 - 1.6 - 0.25 - (-5)}{1.2 \cdot 0.3 + 12 + 1.6 - 10} = 3.985\ k\Omega \quad (4\text{-}20)$$

Thus, a final value of R9 = 3.9 kΩ is selected.

4) Common considerations to the previous calculated values

Nominal value V_O = 5 V used for calculations in 1) is clearly modified from its nominal value to the practical one given by the saturation voltage of power transistor Q2 (V_{EC1sat}) and the forward voltage of diode D1 ($V_{f,D1}$).

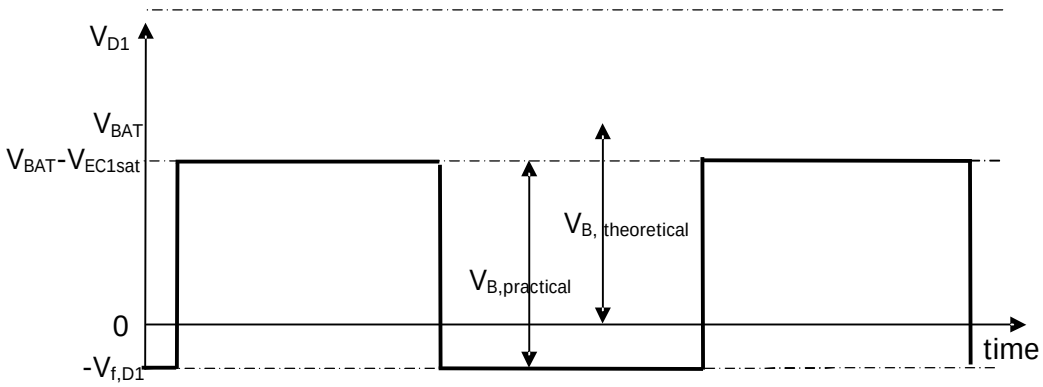

Figure 4-13. Influence of the real components in the practical output voltage

From Figure 4-13, the following expression is derived:

$$V_{B,practical} = V_{BAT} - V_{EC1sat} + V_{f,D1} \approx 10 - 1.3 + 1.5 = 10.2\ V \quad (4\text{-}21)$$

$$V_{B,theoretical} = V_{BAT} = 10\ V \quad (4\text{-}22)$$

Anyway, the final output voltage $V_{O,practical} = D \cdot (V_{B,practical} - V_{f,D1})$ is fixed by both the practical input voltage ($V_{B,practical}$–$V_{f,D1}$) and the duty-cycle, this last one

depending, mainly, on the turn-on and off times of the power transistor Q1. An estimated value of $V_{O,practical} = 0.5 \cdot (10.2 - 1.5) = 4.35\,V$ is expected at the output of the power converter. Obviously, apart of these harmonics generated by the fact of not having a perfect square signal, a duty-cycle not equal to 50% is to produce even harmonics. This is not important due to the relative comparison between harmonic amplitudes under the same environment.

The divergence between theoretical and practical output voltages does not affect the previous calculation where this value was taken into account: it results negligible respect to this calculations because of the approximate calculations of the affected components (inductor L, capacitor C_O) and the estimations of the currents through the diode D1 and power transistor Q1.

Another point of interest is the presence of a filter capacitor at the input of supply terminal such as V_{BAT} and V_{BAT++} (see Figure 4-3). 470 μF and 22 μF, respectively, were found experimentally.

Finally, as it was exposed at the end of 1) Calculation of the LC filter, a parallel combination of two tantalum capacitor each of 22 μF was implemented in the final circuit.

4.1.2 Frequency modulation generator (UNIT 2)

This frequency modulation stage corresponds properly to the generation of the modulating waveform to finally control the commutation of the power transistor Q1 at UNIT 1.

Some attempts have been made along the time to generate easily a frequency modulation of the PWM signal which controls the commutation of a power transistor. In reference [RA-1], an integrated circuit UC383 of UNITRODE CORPORATION (belonging to Texas Instruments) was used. This is a High Speed PWM Controller valid for switching frequencies up to 1 MHz. It was thought as a fixed switching frequency controller, whose frequency is set by a resistor connected to pin 5 and a capacitor to pins 6, 7 (when in conventional or voltage mode). Authors of reference [RA-1] modified this circuitry slightly in order to obtain a frequency modulated switching frequency and so, carry out further measurements of EMI emissions. They fixed the value of capacitor at pins 6,7 but conceived a topology at pin 5 consisting of a parallel

structure of a conventional resistor (really, an adjustable resistor to fix the central frequency) and a transistor (2N2369) as shown in Figure 4-14.

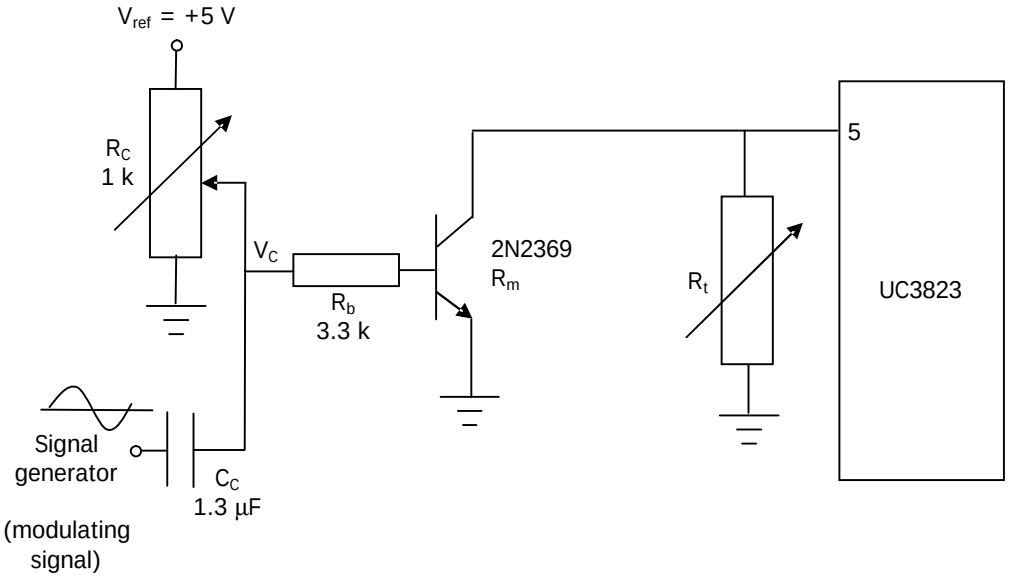

Figure 4-14. Variable switching frequency control at reference [RA-1]

Total resistance seen from pin 5 is the parallel of the variable R_m (the collector-emitter resistance of the transistor) and the fixed R_t. As R_m varies (around its dc working point given by R_C) following a sinusoidal profile (injected through C_C from a signal generator), the parallel value of R_m an R_t should do it in the same way and then, the resulting switching frequency too.

But there is a problem related to this scheme, which was one of the main reasons for not being applied in this thesis. Control voltage amplitude V_C versus switching frequency is not a linear relationship. Due to the nonlinearity of the variable switching frequency circuit in Figure 4-14, the side-band is not symmetrical with respect to the fundamental frequency (90 kHz) thus concentrating harmonics mainly in one side of the harmonic window resulting from the modulation process. Therefore, this was not an accurate way of generating a frequency modulation in order to carry out further EMI measurements and to derive some conclusions.

Requirements for the variable switching frequency circuit to be implemented are listed below:

– Nonlinearities are not allowed: the modulated waveform must follow exactly the selected modulation profile and this is independent on the type of modulation profile, i.e., sinusoidal, triangular, exponential and whichever one.

- Only duty-cycles of ≈50 % are to be generated. Main interest is not related to control the output voltage because, first, there is nothing to control due to the fixed load resistor; second, a 50% duty-cycle prevents the system from generating even harmonics (although small variations around this 50% make even harmonics appear, this is not of concern); and third, only ratios between non-modulated harmonic amplitude and side-band harmonics (resulting from the modulation process) are of interest and this feature does not depend on the duty-cycle.
- The switching frequency system must work with any modulation profile.
- Input signal for this switching frequency system comes from a signal generator because, this way, it is possible to test as many modulation profiles as needed and very easily. Special care must be taken when selecting a signal generator, guaranteeing this device matches actual requirements.

To meet all criteria expressed above, it was thought to be very worthy that the signal generator itself was able to output not only the modulating signal (like in circuitry of Figure 4-14) but also the complete, modulated waveform. This way, a "perfect" frequency modulated sinusoidal waveform would be available at the signal generator's output, avoiding the nonlinearity problems in [RA-1]. This idea is easily implemented now because of the MATLAB algorithm presented in 2.3. A sampled waveform corresponding to a sinusoidal carrier being modulated by following several modulation profiles is generated directly by this algorithm. As discussed previously in 2.3.1, all necessary and sufficient conditions were taken into account in order to generate a sampled signal like the Nyquits's theorem and so on; then, sampled signal from the MATLAB algorithm can be directly entered into the signal generator. At its output, the modulated waveform is available.

One consideration is very important to keep in mind: carrier signal is a sinusoidal waveform and not the square one necessary to switch the power transistor on and off. Then, a further treatment of this signal at the signal generator's output has to be done. In summary, this output signal will be extracted from the signal generator by a circuitry with power adaptation, further amplified and finally squared by a zero-crossing detector with an open-collector output which will control the power transistor. Figure 4-15 shows all these steps together in a typical flow chart.

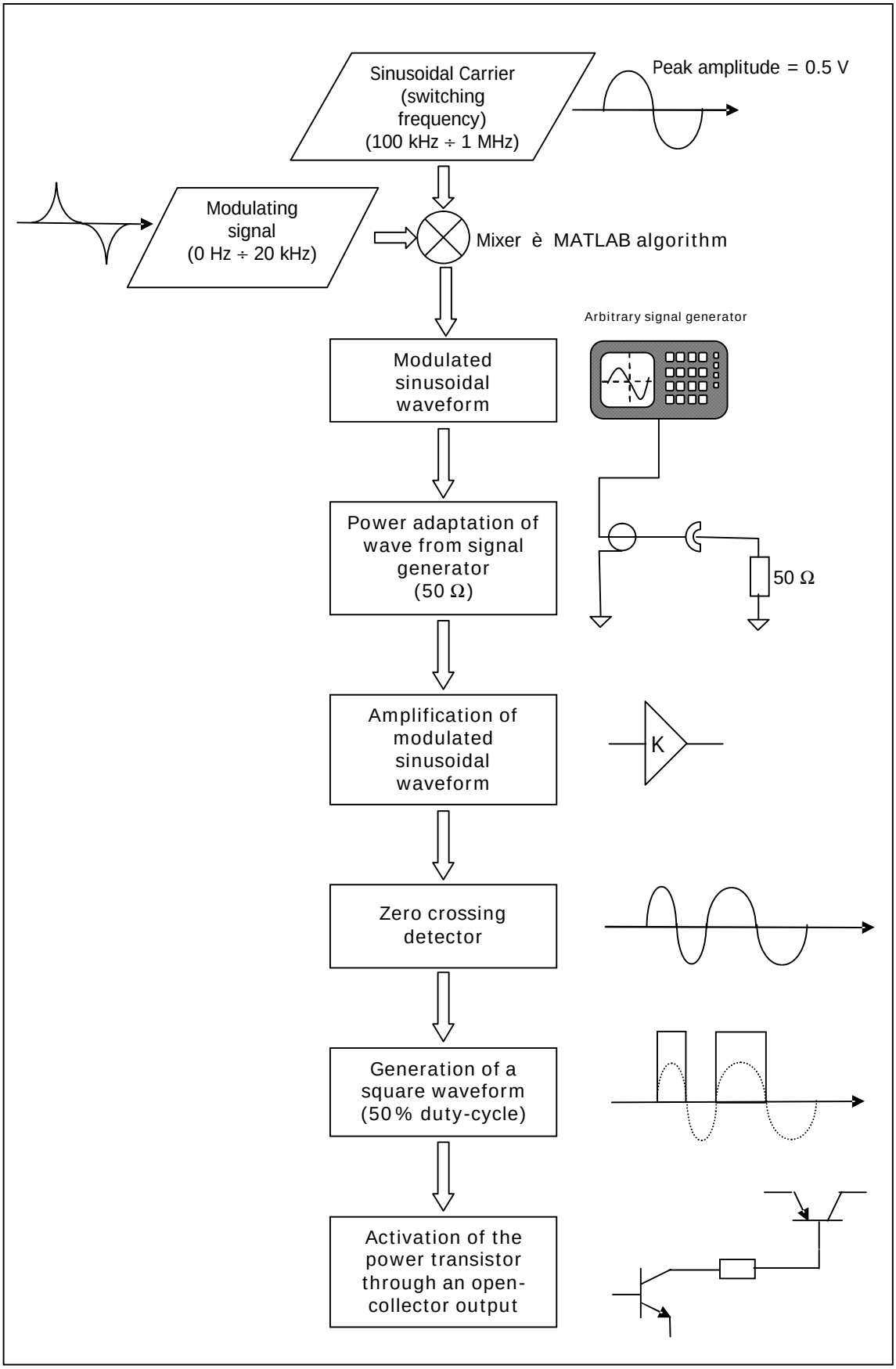

Figure 4-15. Flow chart of the frequency modulation generation stage

Practical implementation of the flow chart in Figure 4-15 is shown below (Figure 4-16):

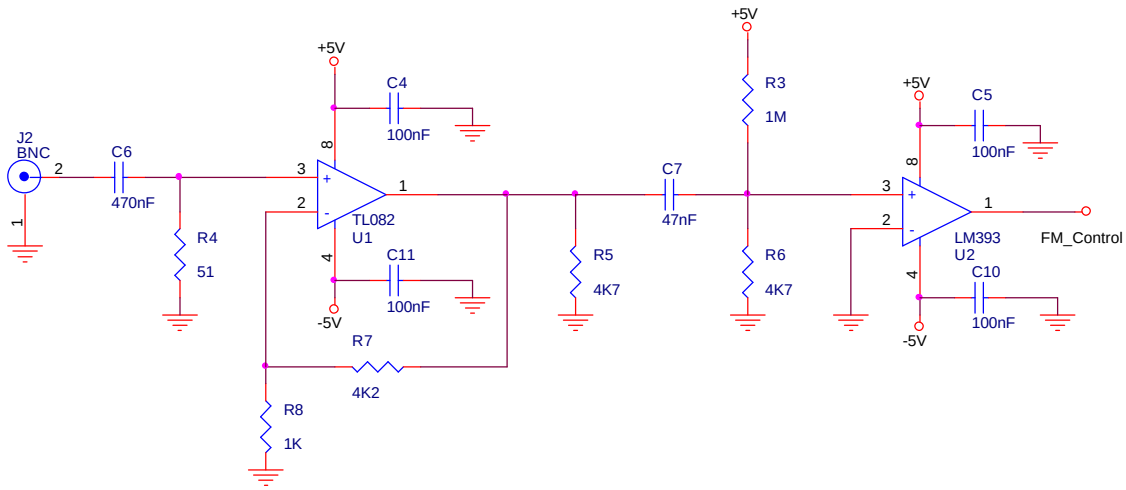

Figure 4-16. Circuitry for the generation of frequency modulated square waveforms.

Onwards, a detailed description of each part is to be carried out. A discussion about the reasons to select such components is also inserted.

1) Selection guide for the signal generator

A Tektronix AWG2021 was selected as a signal generator. The maximum frequency to be generated is lower than 2 MHz and this is currently a value reachable by nearly all signal generators. The AWG2021 offers 250 MS/s and 256 k deep memory. The standard configuration provides one 5 V_{p-p} output (into 50 Ω dc) with 12-bit vertical resolution. The AWG2021 easily simulates signals where moderate point definition and long records are required for simulating very complex waveform conditions. Memory clock frequency ranges from 10 Hz to 250 MHz, when a maximum of 42 MHz is expected to be used here. Data points of waveform size range from 64 to 256 K in multiples of 8 (a maximum of 16 K are expected according to the algorithm).

2) Power adaptation at the output of the signal generator

In order to maximize the power supplied by the signal generator, a power adaptation is advisable. In few words, output impedance of the signal generator must match the one connected to the generator, i.e., the impedance that the signal generator is seeing to be connected to it. Generator output impedance is commonly 50 Ω but this is a configurable parameter in some equipment; then, a special care must be taken when using a specific signal generator.

The adaptation stage here proposed is shown in Figure 4-17.

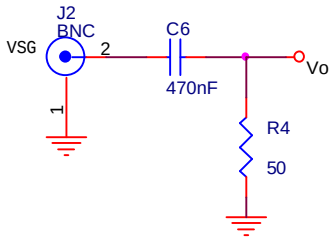

Figure 4-17. Power adaptation stage of the generator's output

Along the whole circuitry, no dc component is expected to be present on the signal. To guarantee this aspect, several configurations have been assumed along the circuit. At this adaptation stage, a capacitor is provided in order to block the possible dc component coming from the signal generator. Any offset due to an undesirable dc component must be blocked by this capacitor but it must allow the FM signal to flow through it with nearly no attenuation.

In order to get an impedance of 50 Ω, capacitor C6 should have a short-circuit behaviour at the frequencies of interest, that is, from 100 kHz onwards. As concluded from the observation of Figure 4-16, the next stage following this adaptation module is an operational amplifier, showing an input impedance (over 10^{12} Ω) much more higher than 50 Ω. This next stage can be assumed as an open-circuit what makes the calculations easier because of the non-influence between stages in cascade.

Waveform coming from the signal generator has peak amplitude of 0.5 V, that is, a peak-to-peak amplitude of 1 V. Voltage across R4 (V_o=V_{R4}) is given by the following expression:

$$V_o = V_{SG} \cdot \frac{2 \cdot \pi \cdot f \cdot R4 \cdot C6}{\sqrt{1+(2 \cdot \pi \cdot f \cdot R4 \cdot C6)^2}} \tag{4-23}$$

where V_{SG} represents the amplitude of the signal generator output.

Although the minimum central frequency under test is 100 kHz, calculation of capacitor C6 is to be done for a much lower frequency (e.g., 50 kHz) in order to absorb all possible frequency deviations due to the modulation process. Please consider the following data:

– f = 50 kHz

– ratio $\frac{V_o}{V_{SG}}$ must be over ≈99% è no signal attenuation is present due to C6.

– R4 = 50 Ω

Proper operation over expression (4-23) together with the values above yields a value of C6 = 470 nF. This is the minimum value acceptable for this capacitor C6.

3) Amplification of the waveform after the power adaptation stage

At this stage, a signal without dc component should be present, with peak amplitude of ≈0.25 V (due to the voltage divisor of the previous adaptation stage). It must also be said that this stage is not mandatory to be implemented if the signal generator is able to give out an approximate V_{pp} > 2 V at its output, because the response delay time of the next stage (comparator) is depending on the signal excursion at its input. Then, in order to have the chance to connect any signal generator system, an amplification stage was included in this prototype.

A maximum frequency of 1.1 MHz is expected at the input of the operational amplifier. This corresponds to a 1MHz-carrier frequency modulated by a modulation signal with a percentage of modulation equal to 10%.

The main part of this stage consists of an operational amplifier in a typical non-inverting configuration.

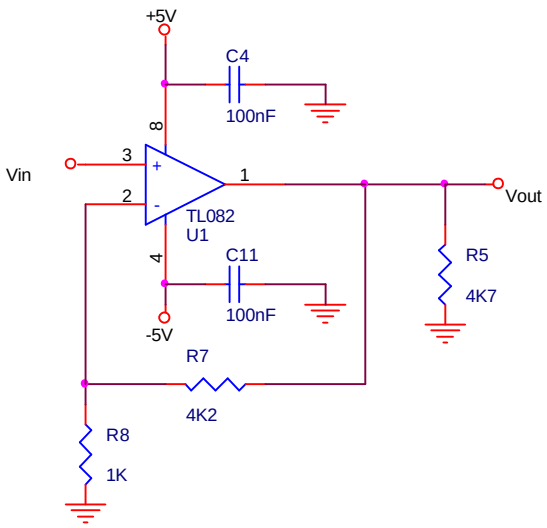

Figure 4-18. Non-inverting amplification configuration after power adaptation stage

As seen in Figure 4-18, a TL082 of National Semiconductor was selected. The next considerations made this decision reasonable:

- The TL082 offers a typical gain-bandwidth product of 4 MHz, enough for this application. Considering that a gain of ≈5 is configured and the maximum frequency present in the system is lower than 1.1 MHz, the practical gain-bandwidth product is 5×1.1MHZ = 5.5 MHz. This is, of course, higher than the typical 4 MHz, which means an attenuation of the output amplitude (i.e., an actual gain lower than the theoretical value of 5). This does not represent any problems because, despite this undesirable attenuation at limit values, the amplifier output amplitude will be large enough to activate the comparator input at the next stage.
- A dual supply voltage is mandatory.
- The maximum slew-rate for a sinusoidal waveform is expressed by $SR = A \cdot 2 \cdot \pi \cdot f$ (SR = Slew-rate in V/μs, A = peak amplitude in V and f = frequency in MHz). In this prototype, the maximum slew-rate takes place under the following limit circumstances: A = 0.25 V and f = 1.1 MHz, yielding a slew-rate of 1.728 V/μs. However, TL082 offers a typical 13 V/μs, large enough for the actual purposes.
- A total harmonic distortion lower than 0.02%, a typical Common-Mode Rejection Ratio (CMRR) of 100 dB and a typical Power Supply Rejection Ratio (PSRR) of 100 dB are available at TL082, meeting completely all necessities.
- Finally, from the logistic point of view, this is a typical component, easy to find. Design philosophy is to build a practical system but using the commonest, cheapest and simplest components.

Voltage gain of the configuration in Figure 4-18 is calculated as follows:

$$\frac{V_{out}}{V_{in}} = \frac{V_{R5}}{V_{pin3}} = 1 + \frac{R7}{R8} \tag{4-24}$$

For the selected values (R7 = 4.2 kΩ, R8 = 1 kΩ), a theoretical gain of 5.2 is expected. Taking into account that the expected peak-value at the amplifier input (pin 3) is 0.25 V, a peak-value of 1.3 V is to be found at the amplifier output, across the resistor R5, a load resistor intended for amplifier stabilization subjects. Amplitude values at the amplifier output are strongly related to the behaviour of the voltage comparator at the next stage. The larger voltage excursion at the comparator input, the faster response time.

Two de-coupling capacitors (100 nF) are also inserted in order to filter and stabilize the power supply pins of this operational amplifier.

Along the whole circuitry, no dc component is expected to be present on the signal.

4) Square waveform generation

The configuration to generate a square waveform from a sinusoidal one is shown in Figure 4-19. It consists of a typical zero-crossing detection stage, when a dual-supply comparator is to use.

A LM393 of National Semiconductor was selected for this stage due to the following reasons:

- High precision comparators.
- Allow sensing near ground (very useful when detection of zero-crossing).
- Offer an integrated open-collector output.
- When a large signal excursion (>>100 mV) is present at the input of the comparator, a typical response time of 300 ns is available, enough for the actual timing considerations. As calculated in the previous stage, a peak-to-peak excursion of 2.6 V is to be expected at the amplifier output and, therefore, after crossing the coupling capacitor C7, at the comparator input.
- Finally, as expressed previously, this is a typical component, easy to find, so keeping the design philosophy of building a practical system but using the commonest, cheapest and simplest components.

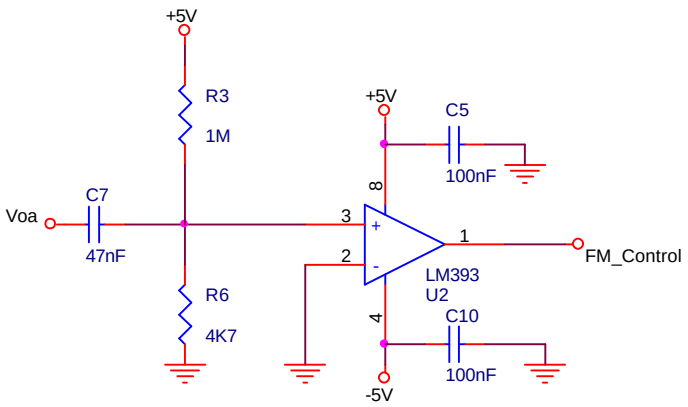

Figure 4-19. Square-wave generation configuration after the amplification stage

The couple of resistors R3 and R6 is intended for generating a very low offset at the input + of the comparator. When no signal is present along the system, it must be guaranteed a voltage at pin 3 slightly higher than voltage at pin 2, i.e., voltage at pin 3 must be slightly over Ground. This way, it is assured that the open-collector output (FM_Control) is cut-off and activation of the power transistor Q1 is not possible. If FM_Control were always activated (low level), power transistor Q1 would also be turned on, then supplying the input V_{BAT} voltage directly to the load resistor, causing probably the destruction of both transistor and load resistor. Voltage at pin 3 (V_{pin3}) for the selected values in Figure 4-19 yields the following value:

$$V_{pin3} = +5V \cdot \frac{R6}{R3 + R6} \qquad (4\text{-}25)$$

$$V_{pin3} = +5V \cdot \frac{4.7}{1000 + 4.7} = 23.4\ mV$$

that is, large enough to produce an offset but negligible for the peak-to-peak expected signal voltage of 2.6 V at pin 3.

At the input of this stage, a coupling capacitor is provided in order to block the possible dc component coming from the previous amplification stage. Any offset due to an undesirable dc component must be blocked by this capacitor but it must allow the FM signal to flow through it with nearly no attenuation.

Although the minimum central frequency under test is 100 kHz, calculation of capacitor C7 is to be done for a much lower frequency (e.g., 50 kHz) in order to absorb all possible frequency deviations due to the modulation process. Consider the following data in Figure 4-19:

- f = 50 kHz
- ratio $\frac{V_{pin3}}{V_{oa}}$ must be kept over ≈99%, where V_{pin3} is the input voltage at pin 3 of the comparator and V_{oa}, the voltage from the operational amplifier output è no signal attenuation is present due to the capacitor.
- R_{par} = R3//R6 = 1MΩ//4.7kΩ = 4.678 kΩ. The input impedance of pin 3 is much higher than this value of R_{par}; therefore, considering only the value of R_{par} for the filter calculation is enough.

Voltage at pin 3 can be therefore calculated as follows:

$$V_{pin3} = V_{oa} \cdot \frac{2 \cdot \pi \cdot f \cdot R_{par} \cdot C7}{\sqrt{1 + \left(2 \cdot \pi \cdot f \cdot R_{par} \cdot C7\right)^2}} \qquad (4\text{-}26)$$

Proper operation over expression (4-26) together with the values listed above yields a value of C7 = 47 nF. This represents an estimation of the minimum value acceptable for this capacitor.

Finally, two de-coupling capacitors (100 nF) are also inserted in order to filter and stabilize the power supply pins of this voltage comparator.

4.1.3 Physical implementation

After the whole considerations and development carried out in the previous points, Figure 4-2 can be redrawn in order to show a more detailed description of the complete system (Figure 4-20):

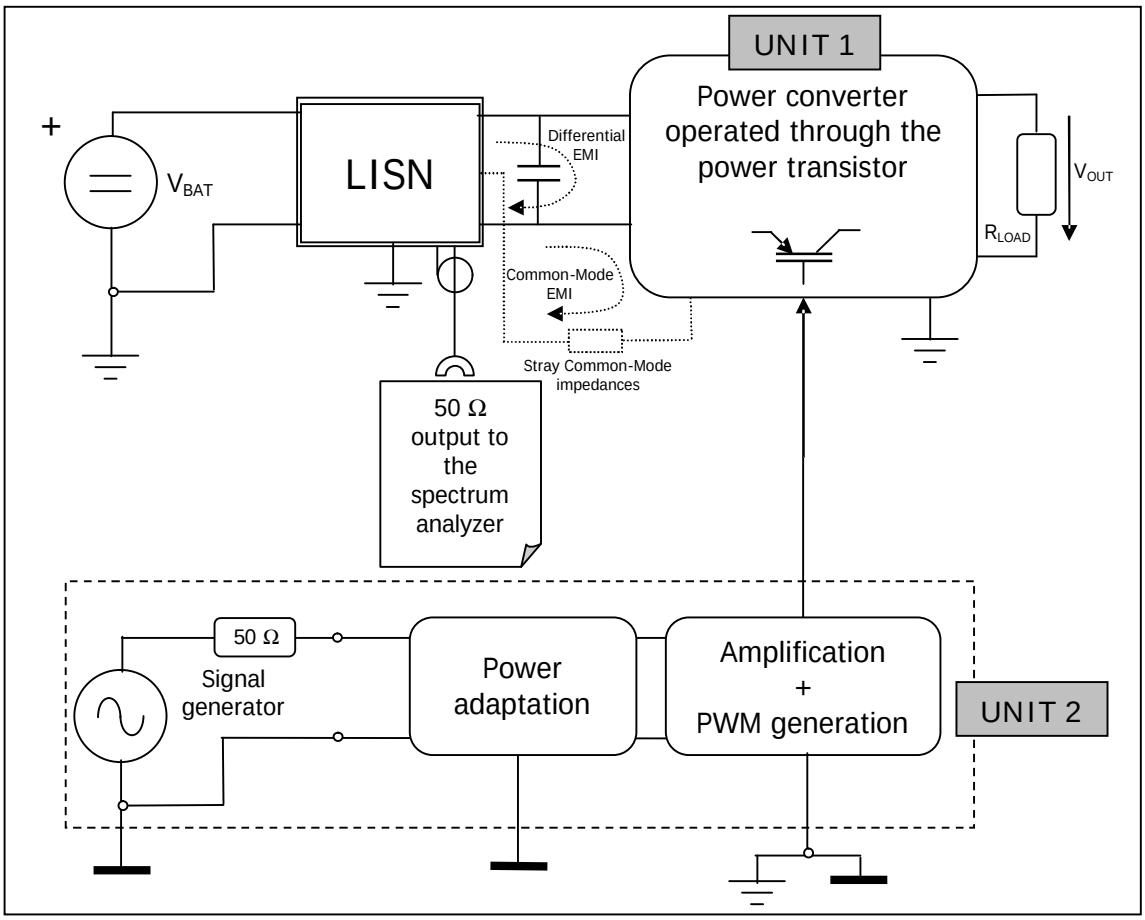

Figure 4-20. A more detailed description of the test plant (black boxes)

Before the physical implementation of the prototype, a PSPICE simulation of the test plant was considered to be helpful. From the simulation results in Annex 4, it can be concluded that no special problems should be found in the practical test plant. Of course, good simulation results are not a guarantee of proper working of the real prototype but they indicate that it will work, in the worst case, with some modifications over the original design. From the results after making the prototype, it can be said that no modification had to be carried out.

Finally, the physical implementation of UNITS 1 and 2 in Figure 4-20 leads to the development of the power converter prototype (Figures 4-21 and 4-22), this one working on an environment as shown in Figure 4-23, resulting in the final test plant.

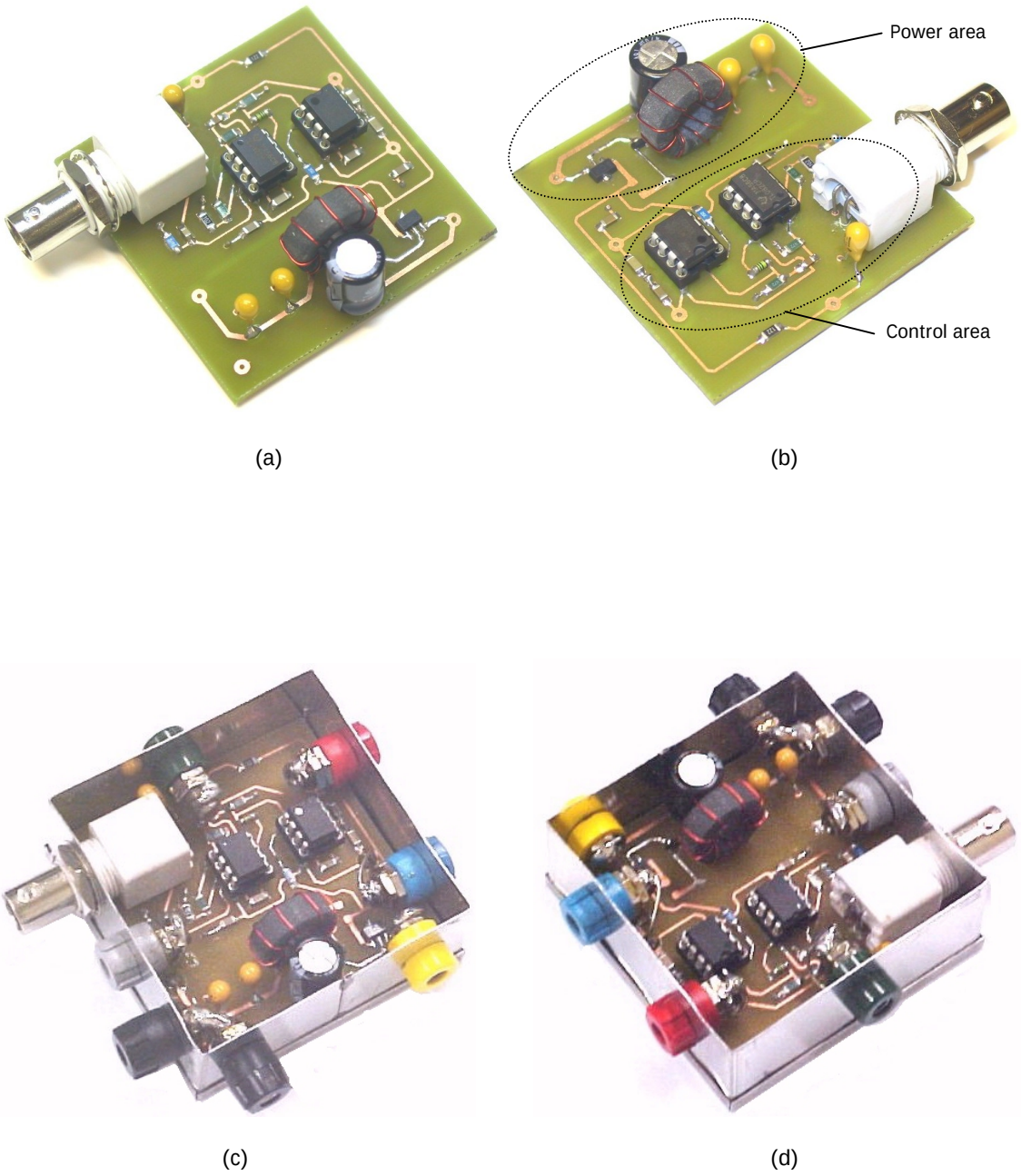

Figure 4-21. Photographs of the step-down converter (UNITS 1 and 2 in Figure 4-20): (a) & (b) Two different perspectives of the component area (Top layer); (c) & (d) The same perspectives in the final prototype consisting of a metallic box and input/output terminals.

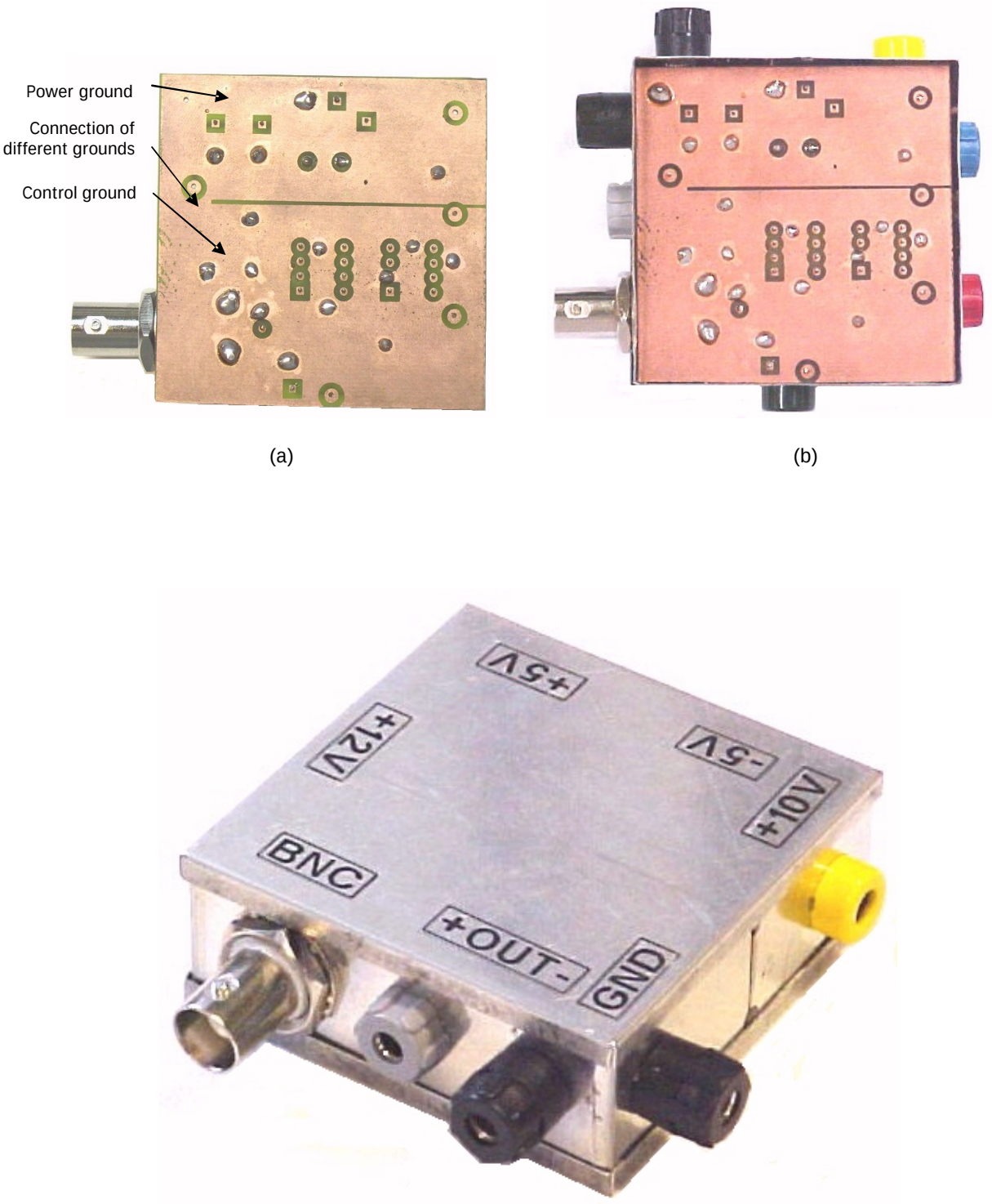

(a) (b)

(c)

Figure 4-22. Photographs of the step-down converter (UNITS 1 and 2 in Figure 4-20): (a) Ground plane (Bottom layer); (b) Ground plane in the final prototype (metallic box and input/output terminals); (c) Final prototype.

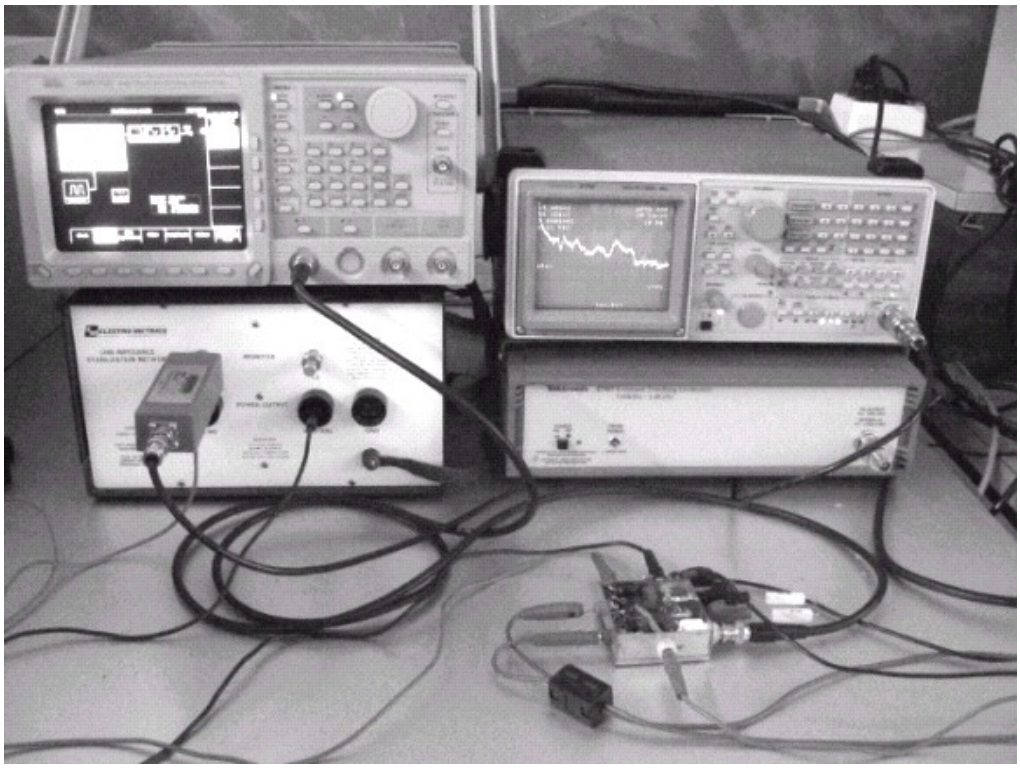

Figure 4-23. Photograph of the experimental test plant

Some notes of interest must be explained referred to the power converter design (please refer to Annex 6):

- The prototype is separated into two areas (Figure 4-21(b)): a control area corresponding to the UNIT 2 in Figure 4-20 and a power area implementing the UNIT 1. Special attention was paid to the PCB layout and components arrangement in order to achieve these high values of switching frequencies (up to 1.3 MHz).
- This separation of functionalities in different areas allows the converter to have two different ground planes connected in a very small area (see Figure 4-22(a)), thus separating the different ground behaviour of a power system or the control part and isolating mainly the control area of the pernicious effects of the switching in the power area.
- The whole prototype was enclosed in a metallic box in order to achieve a good electromagnetic isolation of the prototype (Figure 4-22(c)).

All instruments were placed on the top of a conductive plane which was earthed. Figure 4-23 shows a photograph of the experimental test plant. In all the cases under test, the converter was driven with a fixed duty cycle of D=0.5. Output voltage is V_{OUT}

≈ 4V (instead of the expected 5 V, due to the diode forward voltage drop) and the power supplied by this converter is ≈1.25W.

4.2 Influence of the Spectrum Analyzer's RBW

In order to show the influence of regulatory RBWs when measuring EMI emissions, some of the previous modulations were used in the power converter presented in clause 4.1 based on a step-down topology. A previously modulated sinusoidal wave, generated numerically [RB-1], is stored in a compliant Arbitrary Function Generator (Tektronix AWG2021). To generate a proper PWM signal controlling the power switch (transistor), a previous stage of signal adaptation, amplification and zero-crossing detection is implemented to square the previous sinusoidal wave but preserving the current modulation. This way, a modulated square signal (≈50%-duty cycle) is also obtained at the input of the step-down converter (V_{BAT} = 10 V and R_{LOAD} = 20 Ω).

Conducted emissions are measured by a compliant spectrum analyzer (Tektronix 2712) by means of a monophase-LISN, whose schema is shown in Figure 4-24:

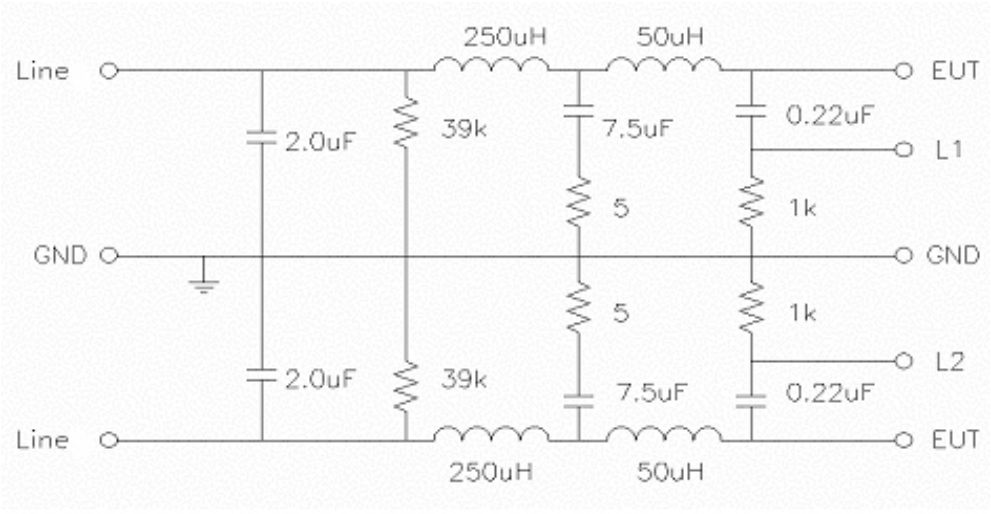

Figure 4-24. Schema of the compliant monophase-LISN used for measurements in the thesis (NOTE: EUT=Equipment Under Test)

The boundary between Band A and B in CISPR22 & 16-1 is set to 150 kHz, also fixing the RBW to be adjusted. For a 120kHz-switching frequency, a 200Hz-RBW is to be used; however, a few kHz upwards (at 200 kHz) this RBW is fixed to 9 kHz

Figure 4-25 shows the measured spectra for an exponential modulation with concavity factor k = 12 (f_c=120 kHz, f_m=1 kHz and δ%=10%, that is, m_f = 12) considering both the regulatory 200Hz-RBW and the optional 9 kHz-RBW.

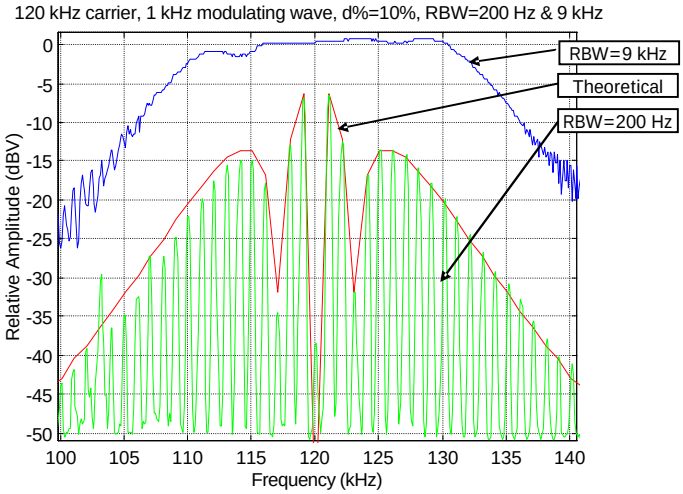

Figure 4-25. f_c =120 kHz, f_m =1 kHz, δ% = 10%, exponential modulation, RBW=200 Hz vs. 9 kHz Theoretical (red), experimental at RBW=200 Hz (green) and at RBW=9 kHz (blue and cyan lines) results (SPAN = 5 kHz, VBW = 300 Hz (green), 10 kHz (blue))

Just preserving the same data above except for the nominal switching frequency (f_c =200 kHz & 1 MHz), measured results for an exponential modulation are shown in Figures 4-26 & 4-27. In this case, a regulatory 9kHz-RBW must be used although a 200Hz-RBW is also included for comparison purposes.

As derived from the theoretical analysis, measurements show that higher modulation indexes produce higher attenuations.

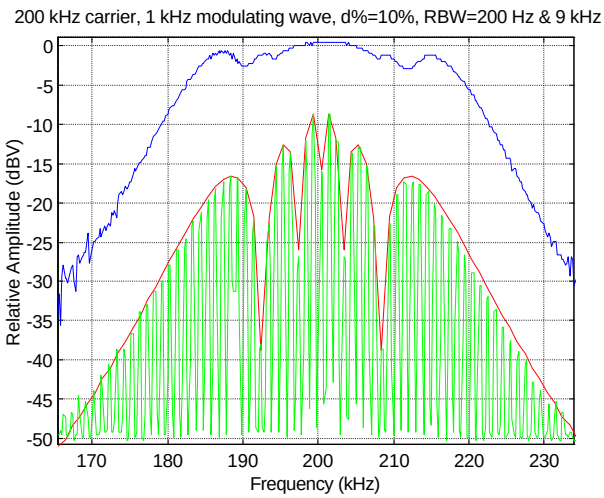

Figure 4-26. f_c =200 kHz, f_m =1 kHz, δ% = 10%, exponential modulation, RBW=200 Hz vs. 9 kHz Theoretical (red), experimental at RBW=200 Hz (green) and at RBW=9 kHz (blue and cyan lines) results (SPAN = 10 kHz, VBW = 300 Hz (green), 10 kHz (blue))

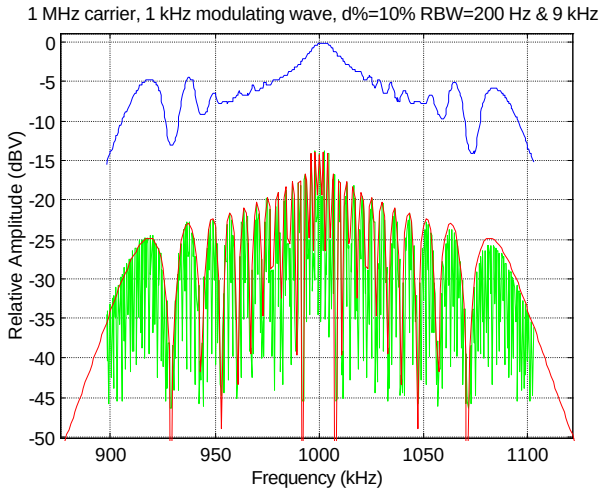

Figure 4-27. f_c =1 MHz, f_m =1 kHz, δ% = 10%, exponential modulation, RBW=200 Hz vs. 9 kHz Theoretical (red), experimental at RBW=200 Hz (green) and at RBW=9 kHz (blue and cyan lines) results (SPAN = 20 kHz, VBW = 300 Hz (green), 10 kHz (blue))

As the side-band harmonic bandwidth [$B = 2 \cdot f_m \cdot (1 + m_f) = 2 \cdot (\Delta f_c + f_m)$] increases, the influence of the selected RBW is less significant. To get it, both f_m and δ% (for a defined f_c) can be increased. As a larger modulation index seems to produce a better behaviour, both aspects lead to a selection of larger δ% (or its equivalent peak deviation Δf_c).

A more interesting study is presented in Figure 4-28. It was demonstrated that side-band harmonics amplitudes (and, therefore, the final outline or shape of the harmonics window) only depend on the modulation index m_f. Plots in Figure 4-28 have been obtained for a sinusoidal modulation of a 200kHz-carrier and a modulation index of 8. As expected, side-band harmonic spectra share exactly the same shape and amplitudes but separated by its corresponding modulating frequency f_m. Theoretical results are displayed in red, measurements at 200Hz-RBW in green (with video filter deactivated, i.e., video bandwidth VBW = 300 Hz) and measurements at 9kHz-RBW in blue (with video filter also deactivated, i.e., VBW = 10 kHz). Plots (a) and (b) in Figures 4-28, 4-31 and 4-32 also includes a trace in cyan representing the envelope at RBW = 9 kHz after passing through the video filter with VBW = 100 Hz in order to average or smooth the trace. The rest of plots in these Figures (i.e., plots (c), (d), (e) and (f)) are not displaying this cyan trace because there is no difference between measurements with video filter activated (VBW = 100 Hz) or deactivated (VBW = 10 kHz).

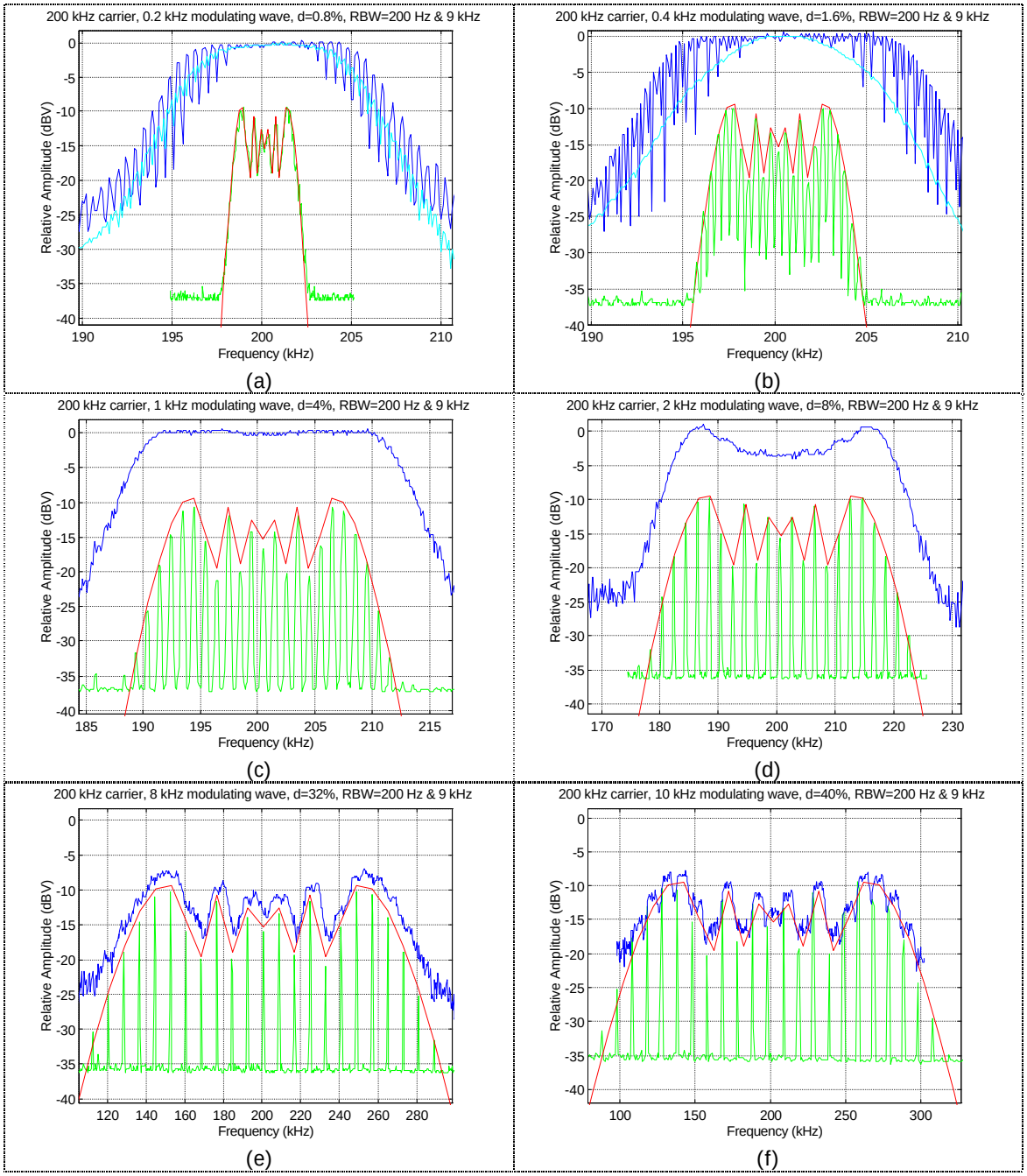

Figure 4-28. Sinusoidal profile with constant $m_f = 8$: theoretical (red line), experimental for RBW=200 Hz (green line and VBW = 300 Hz) and for RBW= 9 kHz (blue and cyan line) results (with VBW = 10 kHz for blue line and VBW = 100 Hz for cyan line).

As explained in Annex 1, the Resolution Bandwidth (RBW) of any spectrum analyzer determines the final shape of the spectrum. Ideally, only single harmonic components should be displayed on the spectrum analyzer, each one corresponding to the side-band harmonics generated during, for instance, the modulation process. But this ideal behaviour is only present when RBW<f_m.

Figure 4-29 shows the harmonic spectra corresponding to the modulation of a sinusoidal waveform (shadow area) at a frequency f_c (i.e., the one representing each main harmonic of the non-modulated signal). On one hand, BW represents the bandwidth of the modulated signal, whose value is obtained by applying the Carson's rule; on the other hand, a theoretically square filter of width RBW moves onto the right inside the SPAN value defined in the spectrum analyzer.

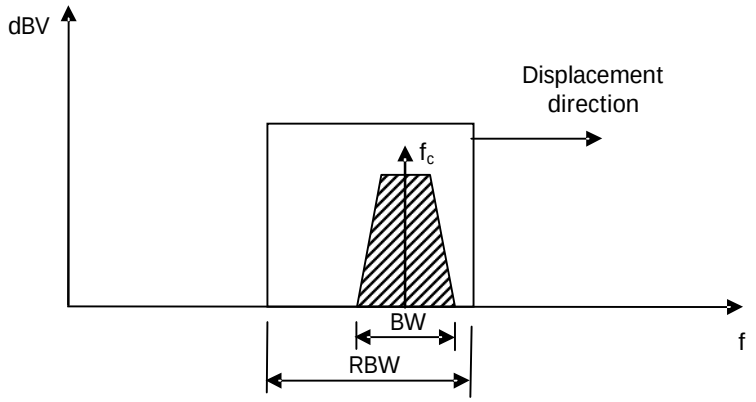

Figure 4-29. Displacement of the IF-filter (and its related RBW) in a spectrum analyzer

The whole harmonics falling inside this RBW are to be added arithmetically, as explained in clause A1.4 of Annex 1. This way, movement of this filter from left to right produces a final shape of the spectra differing quite enough from the actual one (shadow area) as shown in Figure 4-30.

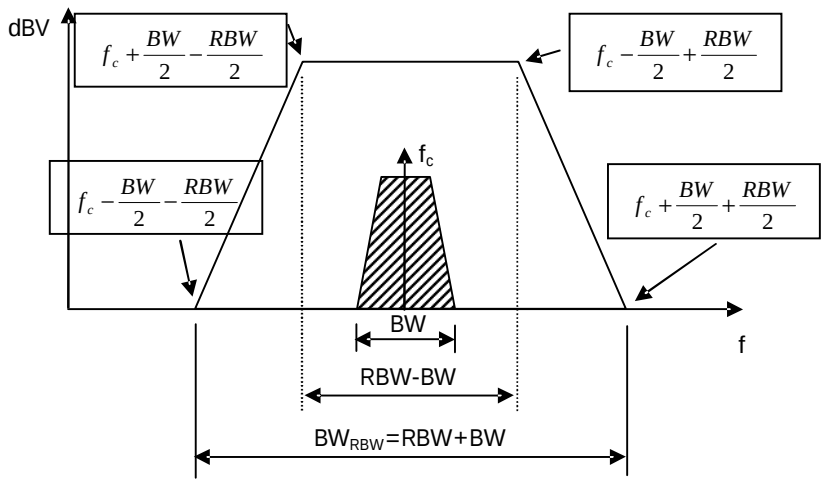

Figure 4-30. Effect of the RBW when measuring the side-band harmonics

If RBW is larger than the modulation bandwidth BW (RBW>BW), a measured spectra showing a trapezoidal outline independent on the original modulation distribution (shadow area) is to be obtained and, what it is worse, displaying on the spectrum analyzer the same amplitude as the non-modulated harmonic along a wider bandwidth than the original one. Things can not get worse any more; because of that, this situation must be always avoided. Figures 4-28(a) and (b) are practical examples of this problem.

As the modulation bandwidth BW gets wider respect to the selected RBW, benefits are slowly coming. This way, an appreciated harmonic attenuation is only to be measured if the condition BW >> RBW is accomplished. A practical approximation for this inequality can be estimated through the plots in Figure 4-28. Then, Figure 4-28(d) starts showing a measured attenuation; a very good one is also displayed in Figure 4-28(e) and, of course, in Figure 4-28(f) where the condition RBW<f_m is met. But it is not necessary to reach the condition RBW < f_m to get a useful measured attenuation. From values in Figure 4-28(d), $BW = 2 \cdot f_m \cdot (1 + m_f) = 2 \cdot 2 \cdot (1+8)$ =36 kHz and RBW = 9 kHz. Then, the following relationships can be assumed from the experimental results to establish the limit where measured attenuation starts being worthy (valid for m_f>>1):

$$BW \geq 4 \cdot RBW \tag{4-27}$$

$$f_m \geq 2 \cdot \frac{RBW}{1+m_f} \tag{4-28}$$

This is also corroborated by the triangular and exponential profiles, as shown in Figures 4-31 and 4-32.

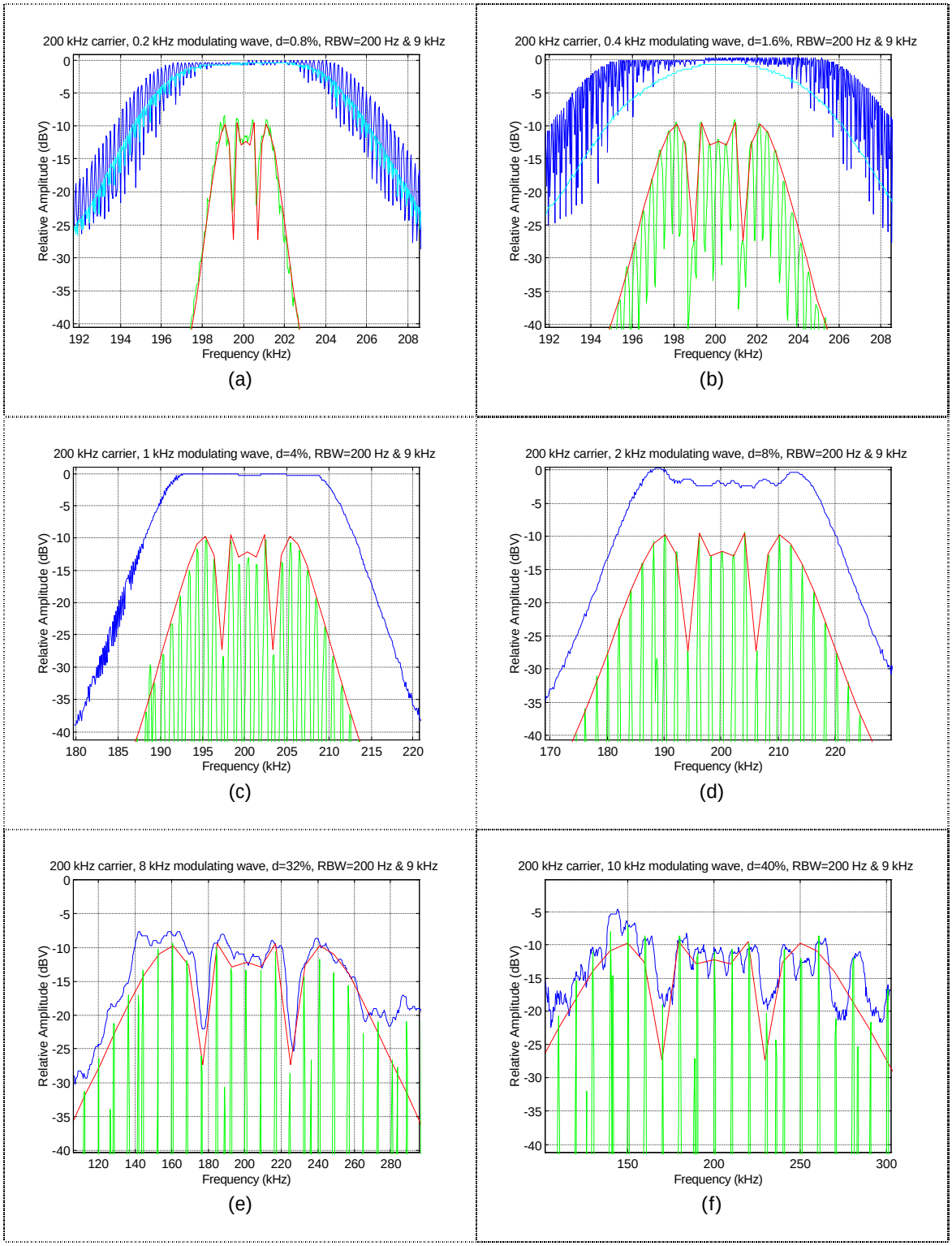

Figure 4-31. Triangular profile with constant m_f = 8 and s = 0.5: theoretical (red line), experimental for RBW=200 Hz (green line and VBW = 300 Hz) and for RBW= 9 kHz (blue and cyan line) results (with VBW = 10 kHz for blue line and VBW = 100 Hz for cyan line).

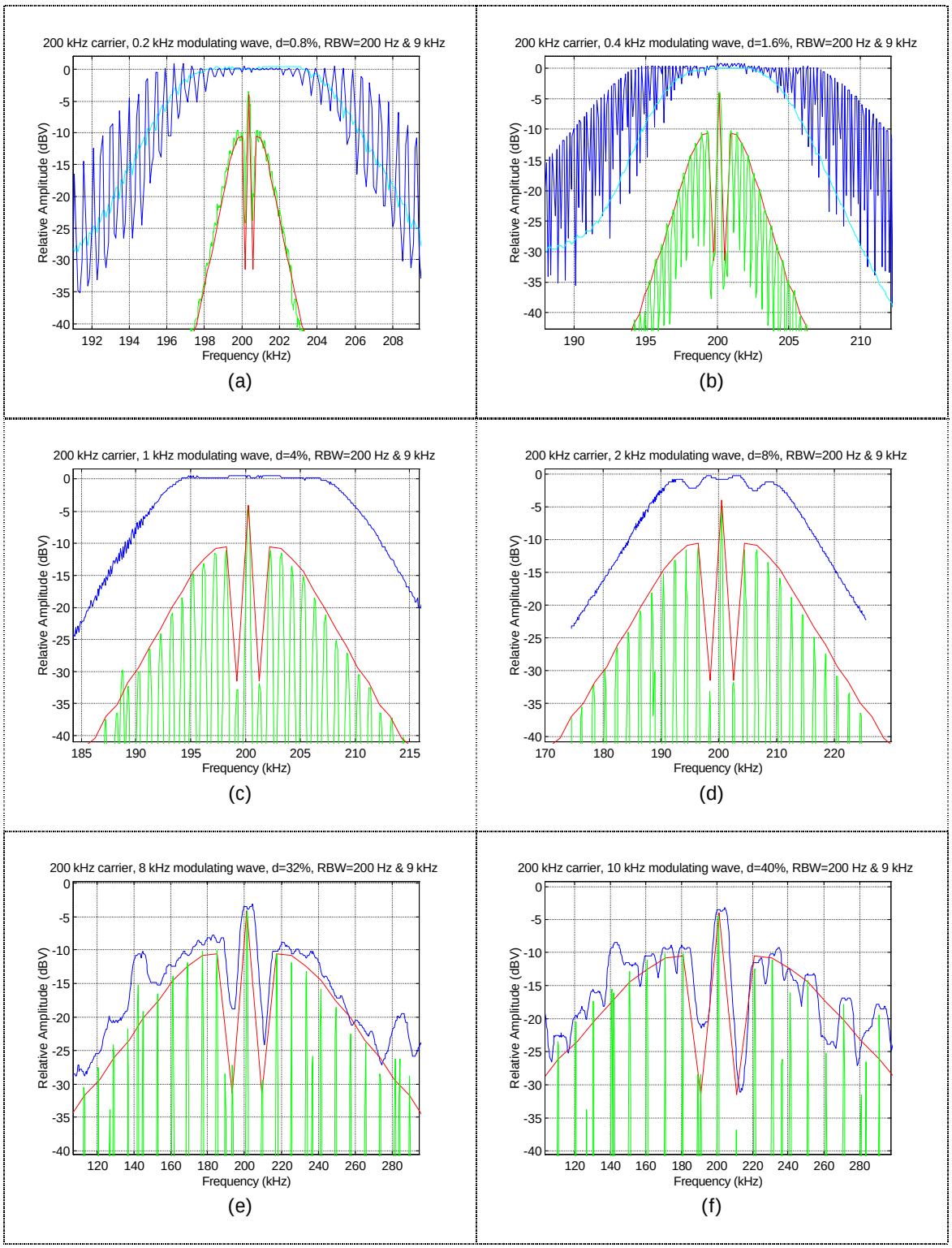

Figure 4-32. Exponential profile with constant m_f = 8 and k = 12: theoretical (red line), experimental for RBW=200 Hz (green line and VBW = 300 Hz) and for RBW= 9 kHz (blue and cyan line) results (with VBW = 10 kHz for blue line and VBW = 100 Hz for cyan line).

4.3 Proposal of a practical method to select a valuable SSCG technique applied to Switching Power Converters

All theoretical developments and practical considerations presented along this thesis allow now to present this point: how to select a worthy SSCG method for a switching power supply, i.e., the modulation profile, the switching frequency and its peak deviation through the percentage of modulation and the modulating frequency in order to obtain normative benefits. It is important to distinguish between a phenomenon itself and the way it is going to be measured. Although theoretical results show a good performance of frequency modulation regarding to EMI emissions reduction in every case, measurements procedures (normally related to practical limitations of measure equipment or normative aspects) can fade such a good behaviour even making it negligible. In other words, a good theoretical SSCG system is not a guarantee of a good experimental result when measuring according to normative regulations: this aspect is desired to solve with this selection proposal.

It consists of several steps as shown in Figure 4-34, steps which are to be developed onwards.

STEP 1: Selection of the modulation profile

(Please refer to previous comments and results already presented in clause 3.4).

Considering the global behaviour of the modulation, the most important parameter is $F_{env,peak}$. It provides a very useful information because of its global characteristic: the maximum amplitude (respect to the non-modulated carrier frequency) along the whole spectrum distribution as a result of a frequency modulation, that is, all harmonic amplitudes will be under this value $F_{env,peak}$. If the number of new harmonics generated during the modulation process is not of concern but only their amplitudes, this parameter $F_{env,peak}$ should be the target. Then, a flat harmonic distribution is the most profitable and, therefore, a triangular modulation profile is the most suitable for any application with these characteristics. Exponential profile shows the worst behaviour because of the peak shape of the side-band harmonic distribution. If attenuation given by an exponential profile at a certain modulation index m_f is found to be satisfactory, then it can be a good option because the side-band harmonics decrease fast as the side-harmonic order gets farther from the central frequency.

Because $F_{env,peak}$ does not oscillate too much, main efforts should be concentrated on obtaining a cancellation of a certain harmonic, normally, the one at the carrier frequency, that is, it is desired a value of F_1 = 0 V or, in a practical case, F_1 < -40 dBV (relative to the non-modulated carrier signal). To do this, a special profit of the oscillation features of the value F_1 is to be taken. Working points should be selected at those modulation indexes where harmonic cancellation is available.

Anyway, modulation profile to be selected is depending on the systems necessities or exigencies and no generic formula can be given.

STEP 2: Selection of the modulation index m_f

Theoretical analysis carried out in the previous sections for several modulation profiles makes now an easy task to choose the modulation index necessary to achieve a certain attenuation. Please refer to all comments and results presented along the chapter 3.

STEP 3: Selection of the switching (carrier) frequency f_c

For designs already in use, where it is of interest substituting the current constant switching frequency for a new frequency modulated by a SSCG method, this is an imposed parameter; for new designs, this is one of the most important parameters to be selected. Switching (carrier) frequency in power converters is not usually too large because the electronics components (diodes and power transistors, mainly) are not able to manage larger power with shorter switching times. Please review related considerations already presented in clause 3.6.

STEPS 4 & 5: Selection of the normative RBW and the modulating frequency f_m

Although higher switching frequencies are always of interest (due to their benefits of lower converter size and higher efficiencies), a special care must be taken respect to the Spectrum Analyzer's RBW. The associated normative (both FCC and CISPR-22) was already presented in detail in clause A2.3 (Annex2), where it is clearly defined the RBW to be used at every frequency range or band. Because power converters switching frequencies are normally below 30 MHz (the boundary between bands B and C [RE-1]), there are only two possible RBWs of interest in switching power converters: 200 Hz (band A) and 9 kHz (band B). The boundary between these two bands is set to 150 kHz.

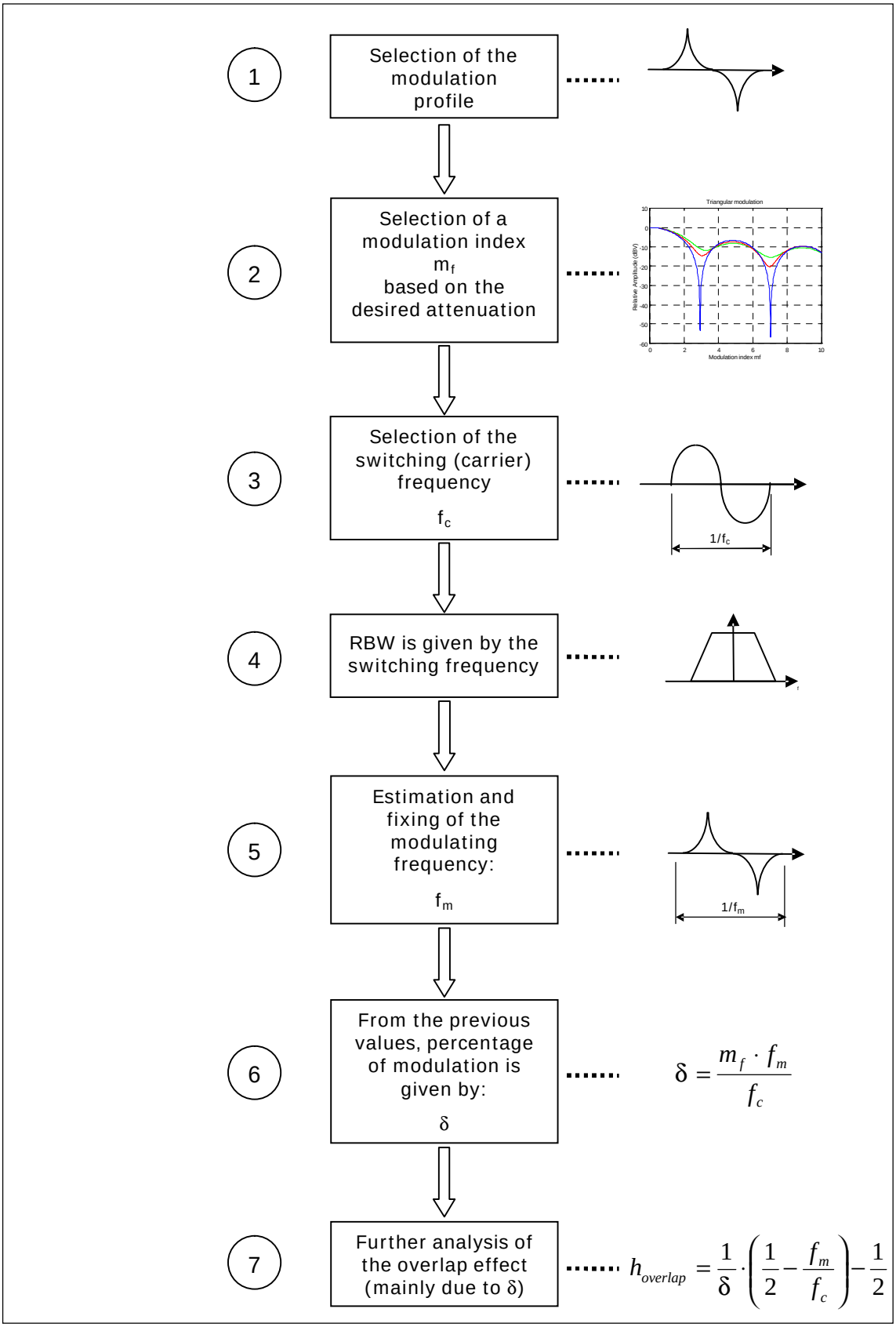

Figure 4-34. SSCG method selection proposal

Usually, the first harmonics of the non-modulated switching signal stay inside the band A (depending on the carrier frequency) thus allowing a 200Hz-RBW setup in the spectrum analyzer; beyond an usually low harmonic order, signal spectra is staying inside the band B, this meaning a wider normative RBW of 9 kHz. For instance, a switching frequency of 120 kHz has its first harmonic inside the band A and the rest ones (up to 30 MHz) inside the band B, then a change of the RBW beyond 150 kHz is to be done.

As exposed in clause 4.2, Spectrum Analyzer's RBW affects seriously the practical measurements and, depending on the case, making the SSCG method produce negligible or even worse results as theoretically expected. This way, a SSCG method can be worthy to be implemented for RBW = 200 Hz but less (or even not) worthy for RBW = 9 kHz (please note that all side-harmonics falling inside the RBW are to be added arithmetically, thus giving a larger value than expected). In other words, for a given carrier frequency, it is possible to have a valuable SSCG method for the first harmonics (because the use of a 200Hz-RBW) but not worthy for the rest of harmonics because a 9KHz-RBW must be used in the Spectrum Analyzer. All these comments are referred to situations where a normative measurement is of interest.

Considering the equation 4-28 and the two RBWs under study, in order to obtain valuable attenuation benefits for harmonic orders inside the band B (150 kHz – 30 MHz) with a 9kHz-RBW, the following expression must be accomplished:

$$f_m \geq 2 \cdot \frac{RBW_{9kHz}}{1 + h \cdot m_f} \tag{4-29}$$

Equally, only attenuation benefits for harmonics inside the band A (9 kHz-150 kHz) are to be obtained if the following expression is met (where only the first harmonic is considered) when using a 200Hz-RBW:

$$f_m \geq 2 \cdot \frac{RBW_{200Hz}}{1 + m_f} \tag{4-30}$$

In order to use the same modulating frequency f_m for both bands A & B when using two different RBWs, the following expression can be applied:

$$\frac{RBW_{200Hz}}{1 + m_f} = \frac{RBW_{9kHz}}{1 + h \cdot m_f} \tag{4-31}$$

The first harmonic order h making true the expression (4-31) is:

$$h = \frac{\left(1 + m_f\right) \cdot RBW_{9kHz}}{m_f \cdot RBW_{200\,Hz}} - \frac{1}{m_f} \tag{4-32}$$

$$h \approx 45 \cdot \left(1 + \frac{1}{m_f}\right) \tag{4-33}$$

For modulation indexes $m_f >> 1$, equation (4-33) can be approximated to $h \approx 45$. That is, when using different RBWs along the frequency axis, it is started obtaining attenuation benefits beyond the 45th.

Due to this high value of harmonic order, it should be always used RBW_{9kHz} in expression (4-28) in order to calculate the proper modulating frequency f_m and, this way, obtaining valuable attenuation benefits from the first harmonic onwards. Of course, user does not loose the possibility of using the 200Hz-RBW when measuring inside the band A, what it will be surely done.

STEP 6: Determination of the modulation ratio δ

Once values of f_c, f_m, m_f have been selected, calculation of the modulation ratio results from the direct application of the expression (4-34):

$$\delta = \frac{m_f \cdot f_m}{f_c} \tag{4-34}$$

STEP 7: Further analysis of the overlap effect

As exposed in clause 2.2.2, contiguous side-band harmonics windows can influence themselves beyond a certain main harmonic order. Expression (4-35) was derived, giving the harmonic number at which overlap effect starts occurring:

$$h_{overlap} = \frac{1}{\delta} \cdot \left(\frac{1}{2} - \frac{f_m}{f_c}\right) - \frac{1}{2} \tag{4-35}$$

and its approximation (see considerations in clause 2.2.2):

$$h_{overlap} \approx \frac{1}{2 \cdot \delta} \tag{4-36}$$

This harmonic order $h_{overlap}$ should be as high as possible in order to avoid this undesirable effect of adding harmonics of different windows resulting from the

modulation of every main harmonic and this is something strongly related to the modulation ratioδ.

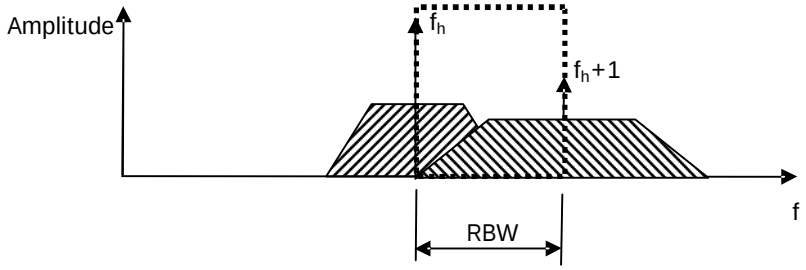

Figure 4-35. Overlap effect: worst case

If the condition f_c < RBW is met, negligible attenuation benefits are to be obtained because the first two main harmonics $f_c=f_1$ and f_2 are falling inside the RBW, producing a larger amplitude as expected. Beyond $h_{overlap}$, there must be a harmonic order at which overlap is to occur between the right-half window corresponding to the main harmonic f_h and the left-half window of the main harmonic f_{h+1}, thus the spectrum analyzer giving an amplitude value very near (although always lower) to the non-modulated harmonic amplitude. For values f_c >> RBW (common situation), overlap is expected at higher main harmonics orders.

4.4 Comparative measurements of conducted EMI within the range of conducted emissions (0 Hz ÷ 30 MHz) [RB-3]

Experimental results obtained using sinusoidal, triangular (s = 0.5) and exponential (k = 12) modulation profiles are shown for the whole range of conducted emissions (0 Hz ÷ 30 MHz). The values of the different parameters for the three modulations profiles are shown in the following Table 4-2:

Central frequency f_c	Modulating frequency f_m	Percentage of modulation δ%	Modulation index m_f
200 kHz	10 kHz	30 %	6
1 MHz	10 kHz	6 %	6

Table 4-2. Different modulation parameters yielding the same modulation index

Experimental and theoretical results are shown in Figures 4-36 and 4-37. A very important reduction (usually larger than 10 dB) is obtained for any modulation profile along the complete range of conducted emissions (up to 30 MHz) with a RBW = 9 kHz.

Best results are obtained by using a triangular modulation profile because of its flat distribution of the harmonics resulting from the modulation process. Good results are also available for lower switching frequencies as shown for f_c = 200 kHz and even lower, just adjusting properly the modulation parameters.

It is expected theoretically for a generic harmonic order h to show the same reduction ratio when the same modulation profile and index are applied. That is, harmonic order h=2 of the 200kHz-wave (at 400 kHz) must be attenuated in the same ratio as harmonic order h=2 of the 1MHz-wave (at 2 MHz) and so on. In order to compare both signals, only the first 30 harmonics of the 200kHz-wave are of interest because the 1MHz-signal only has 30 harmonics in the range of conducted emissions (<30 MHz), that is, up to a frequency of 6 MHz in Figure 4-36 and up to 30 MHz in Figure 4-37. Surprisingly, larger attenuation is experimentally found for the 1MHz-wave inside this range. This is directly related to overlap of contiguous spectra as anticipated in clause 2.2.2. According to equation (2-37), overlap is expected at the following harmonic orders:

- 200kHz-wave è $h_{overlap} = \frac{1}{\delta} \cdot \left(\frac{1}{2} - \frac{f_m}{f_c} \right) - \frac{1}{2} = \frac{1}{0.3} \left(\frac{1}{2} - \frac{10}{200} \right) - \frac{1}{2} = 1$

- 1MHz-wave è $h_{overlap} = \frac{1}{\delta} \cdot \left(\frac{1}{2} - \frac{f_m}{f_c} \right) - \frac{1}{2} = \frac{1}{0.06} \left(\frac{1}{2} - \frac{10}{1000} \right) - \frac{1}{2} \approx 8$

Due to the large percentage of modulation corresponding to the 200kHz-wave, overlap starts occurring practically beyond the first harmonic (Figure 4-36). However, overlap appears beyond the 8^{th} harmonic for the 1MHz-wave in Figure 4-37. That is, side-band harmonics of, at least, two contiguous spectra are adding their amplitudes thus giving a larger amplitude than the expected for a single harmonic spectrum. Besides, theoretical shape of the side-band spectrum is faded by this overlap effect, resulting in a measured spectrum displayed as a regular plot line, as shown in Figure 4-37(b).

From theoretical calculations (see Figure 3-10 for sinusoidal modulation, Figure 3-18 for triangular modulation with s = 0.5 and Figure 3-26 for exponential modulation with k = 12), an attenuation from -8 dB to -10 dB is expected for the three first harmonics (independently of the modulation profile, in practice) and these are also obtained experimentally, according to Figures 4-36 and 4-37.

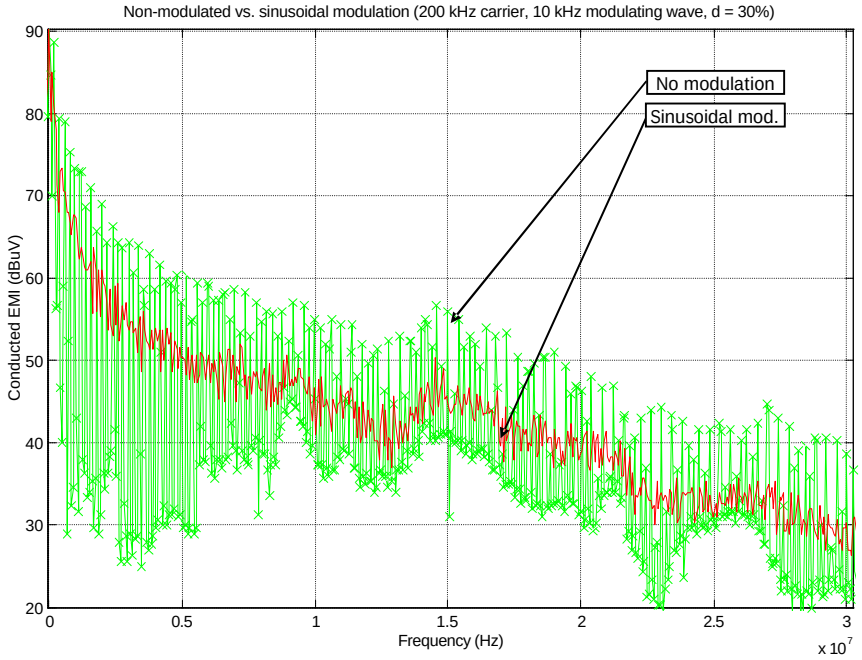

(a)

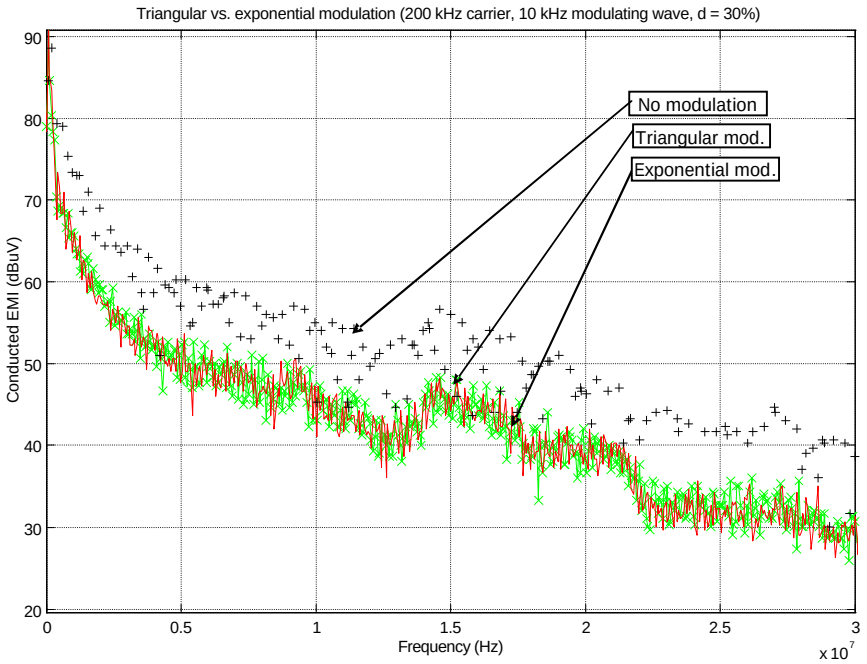

(b)

Figure 4-36. Normative measurements in Bands A & B for a switching frequency of 200 kHz: (a) comparison of results when no modulation is present (green line) and with sinusoidal modulation (red line è f_m = 10 kHz, δ% = 30%); (b) comparison between triangular (s=0.5, green line) and exponential (k=12, red line) modulation profiles. (RBW = 9 kHz)

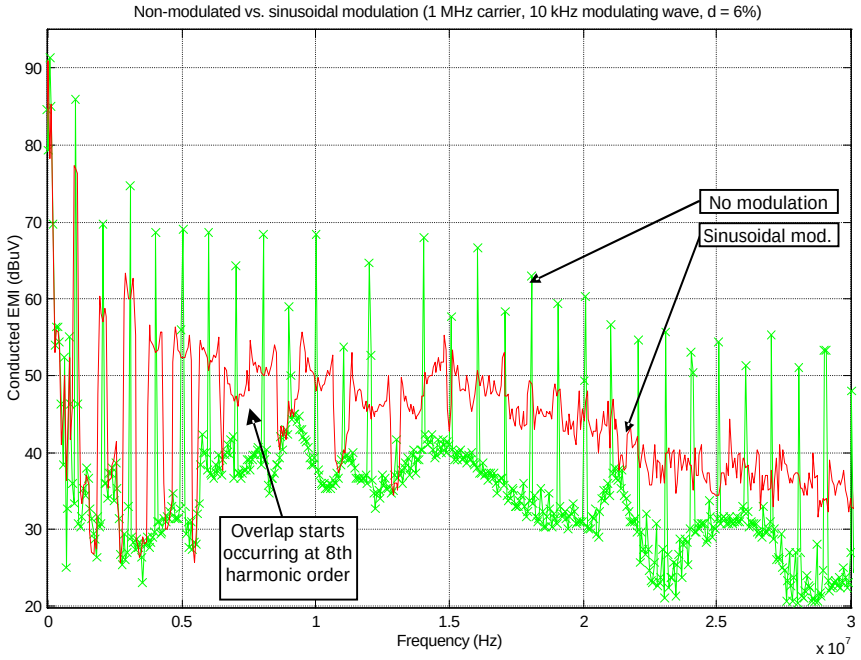

(a)

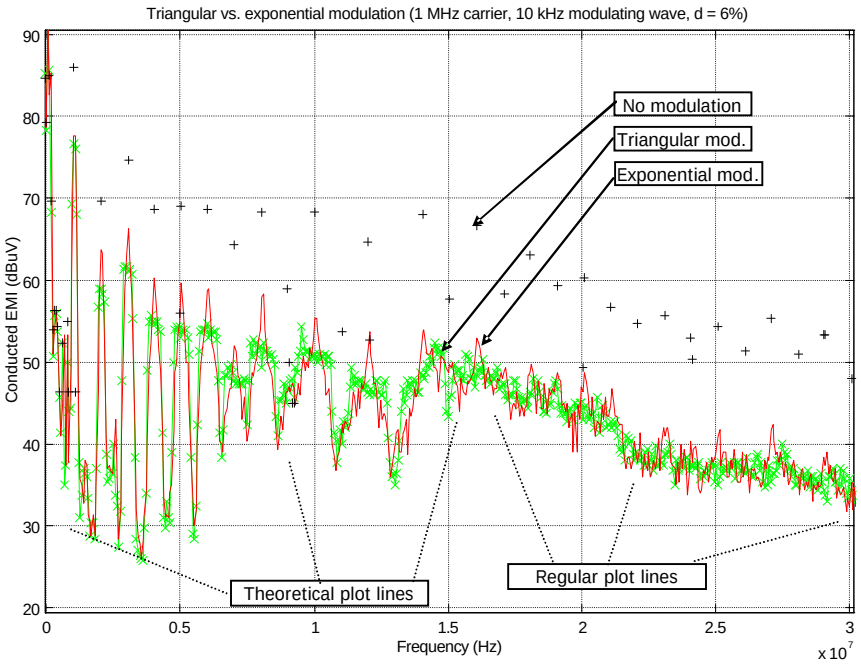

(b)

Figure 4-37. Normative measurements in Bands A & B for a switching frequency of 1 MHz: (a) comparison of results when no modulation is present (green line) and with sinusoidal modulation (red line è f_m = 10 kHz, δ% = 6%); (b) comparison between triangular (s=0.5, green line) and exponential (k=12, red line) modulation profiles. (RBW = 9 kHz)

A last illustrative example is shown in Figure 4-38. This is really a zoom of Figures 4-37(a) and 3-8 around the 10 MHz-frequency or the related $m_f = 6 \cdot 10 = 60$. At this frequency (h = 10), attenuation of the central harmonic is about $F_{1,exper}$ = -20 dB while the two peaks denoting a sinusoidal modulation are about $F_{env,exper}$ = -15 dB down. But this was theoretically expected as shown in Figure 4-38(b) according to values $F_{env,theor}$ = -20.77 dB and $F_{env,theor}$ = -15.22 dB.

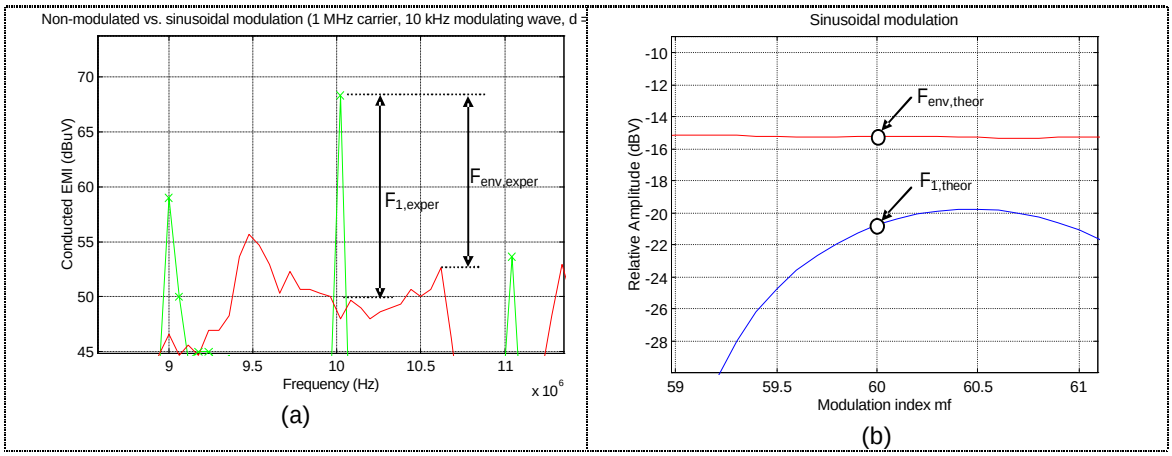

Figure 4-38. (a) Zoom of Figure 4-37(a) and (b) Zoom of Figure 3-8

As a final conclusion, SSCG is a competent method of reducing EMI emissions along the whole range of conducted emissions. Experimental attenuation is predictable by the theoretical calculations in the thesis for all those harmonics not verifying the overlap effect. Anyway, this overlap effect influences the attenuation in a very small ratio although it must always be taken into account in order to reach the expected results.

4.5 SSCG as a method to avoid interfering a certain signal

As initially presented in clause 3.4, exponential profile may be used to tune the oscillation period just selecting a proper concavity factor k and this key point, together with the results of Table 4-3, points to the direct application of SSCG in order to avoid disturbing another significant signal. The application here proposed deals with not interfering a CAN bus telegram inside an automobile, telegram transmitted at the same clock frequency as the switching power converter. In a first step, this sounds contradictory and the designer can think about using another different switching frequency in order to avoid this interference. And this is really a good and well-known solution. But SSCG permits obtaining more benefits.

SSCG provides the harmonic cancellation at the frequencies of interest, which are the harmonic orders decided and totally controlled by the designer. As a result of the modulation process, some side-band harmonics are to appear but always showing smaller amplitudes than the original harmonics without modulation. That is, besides avoiding interferences with the target signal, SSCG can provide attenuation of the harmonics respect to the 'no-modulation' case.

As presented in clause 3.4.1:

$$h = 1 + r \cdot n \tag{4-37}$$

The only chance to be able to cancel as many harmonics as possible is to get a proper value of $n = \frac{\Delta m_f}{m_f}$. It is found experimentally that $m_f < \Delta m_f$ and, therefore, n > 1.

According to expression (4-37) and considering that r is a natural value, the only way of obtaining the maximum number of central harmonics being cancelled is making the parameter n an integer. Table 4-3 shows harmonic orders to be cancelled for different values of n.

r	n	h (*)	n	h (*)	n	h (*)	n	h (*)
1	1.5	2.5	2	3	2.5	3.5	3	4
2	1.5	4	2	5	2.5	6	3	7
3	1.5	5.5	2	7	2.5	8.5	3	10
4	1.5	7	2	9	2.5	11	3	13
...	...	...	...	...	...	...	...	...
r	1.5	1+1.5·r	2	1+2·r	2.5	1+2.5·r	3	1+3·r

Table 4-3. Different harmonic cancellation as a function of parameters r and n
(*) only natural values of h have a physical meaning

According to Table 4-3, the most profitable option is related to the parameter n to be equal to 2. This value makes possible the cancellation of every odd harmonic amplitude at its central frequency (please remember that a side-band harmonics window is also appearing, but the central frequency corresponding to the odd harmonic order is to be cancelled). Figure 4-39 shows the exponential modulating waveform which makes n equal to 2, as desired (k = 150, f_m = 1 kHz). This is, of course, one possibility to generate a value of n = 2. According to its definition $n = \frac{\Delta m_f}{m_f}$, values $\Delta m_f = 114 - 38$ and $m_f = 38$ will result in $n = \frac{114 - 38}{38} = 2$.

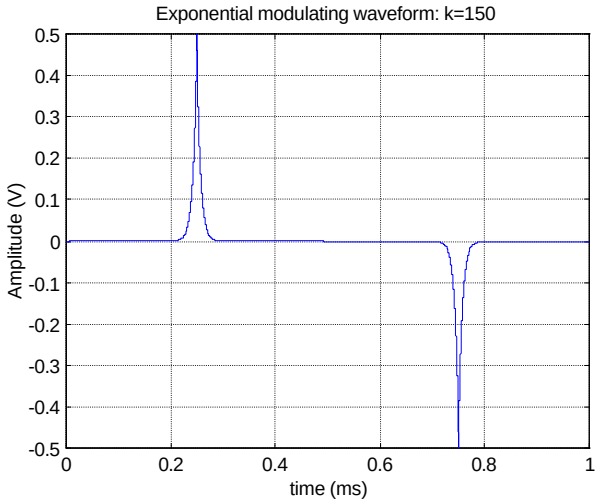

Figure 4-39. Exponential modulating waveform: k = 150, f_m = 1 kHz, corresponding to a value of n = 2

It is already known that higher concavity factors k are to produce lower attenuations. In Figure 4-40 (corresponding to the modulating waveform in Figure 4-39), the expected minimum attenuation corresponding to the odd harmonics is 4 dB (blue line) for the whole side-band harmonics generated during the modulation process. This way, both cancellation of central harmonic frequencies and attenuation of the rest are achieved, as expected in SSCG systems.

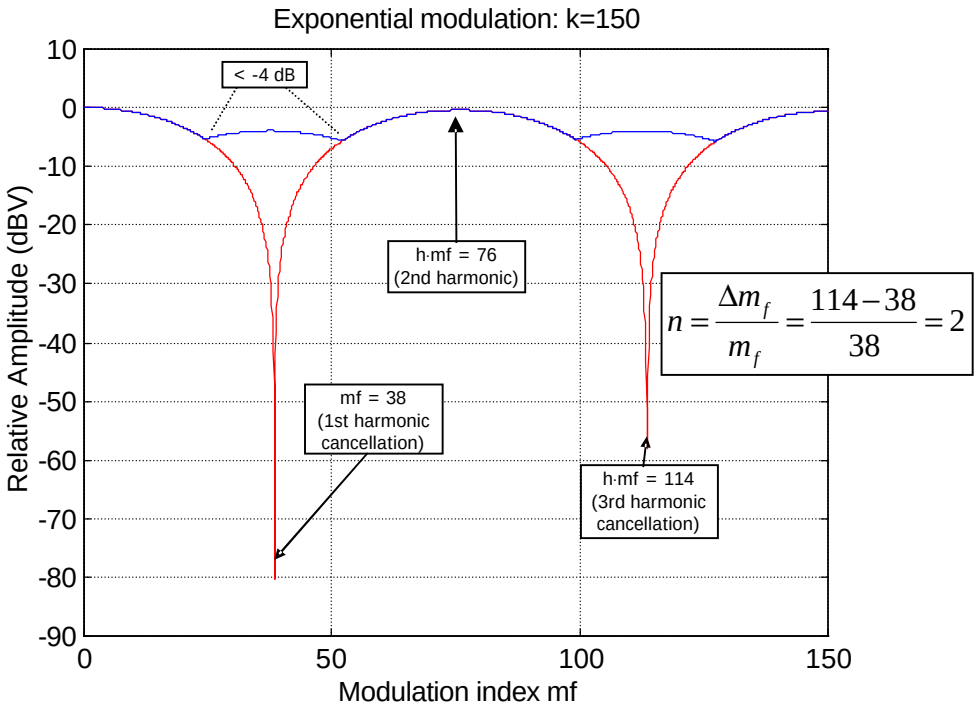

Figure 4-40. Exponential modulation (k = 150): Rms-amplitude (F_1) of the carrier harmonic (red line) and the maximum rms-amplitude ($F_{env,peak}$) of the harmonic envelope (blue line)

The target signal to be preserved completely is, for instance, a CAN message at high speed (500 kHz) [RD-7]. This is a trapezoidal signal of nominal duty-cycle D = 50%. Because of that, only odd harmonics are expected; this way, preventing the CAN-system from external interferences at these odd harmonic frequencies, no distortion or undesired coupling is to happen. This is the intention of the following experiment. Assuming a power converter working at the same frequency as the CAN-system (f_c = 500 kHz), a proper modulation process will allow the power converter to cancel its harmonic amplitudes at the frequencies being equal to the harmonics of the CAN signal.

Next plots in Figures 4-41 and 4-43 show the experimental measurements when the power converter switching frequency of the test plant was modulated by an exponential profile with the following parameters:

- Modulation index m_f = 38 (according to the results in Figure 4-40)
- Concavity factor k = 150
- Modulating frequency f_m = 1 kHz
- Switching frequency f_c = 500 kHz
- Percentage of modulation $\delta = \frac{f_m \cdot m_f}{f_c} \cdot 100 = 7.6\ \%$

The first six odd-harmonics at multiples of the switching frequency (500 kHz) are displayed in Figure 4-41. A strong attenuation is observed at these odd-harmonic orders by means of the exponential modulation under test. Besides, the largest side-band harmonics resulting from the modulation process are ≈4 dB smaller (in average) than the original harmonics, that is, when no modulation is present, as expected theoretically (see previous comments).

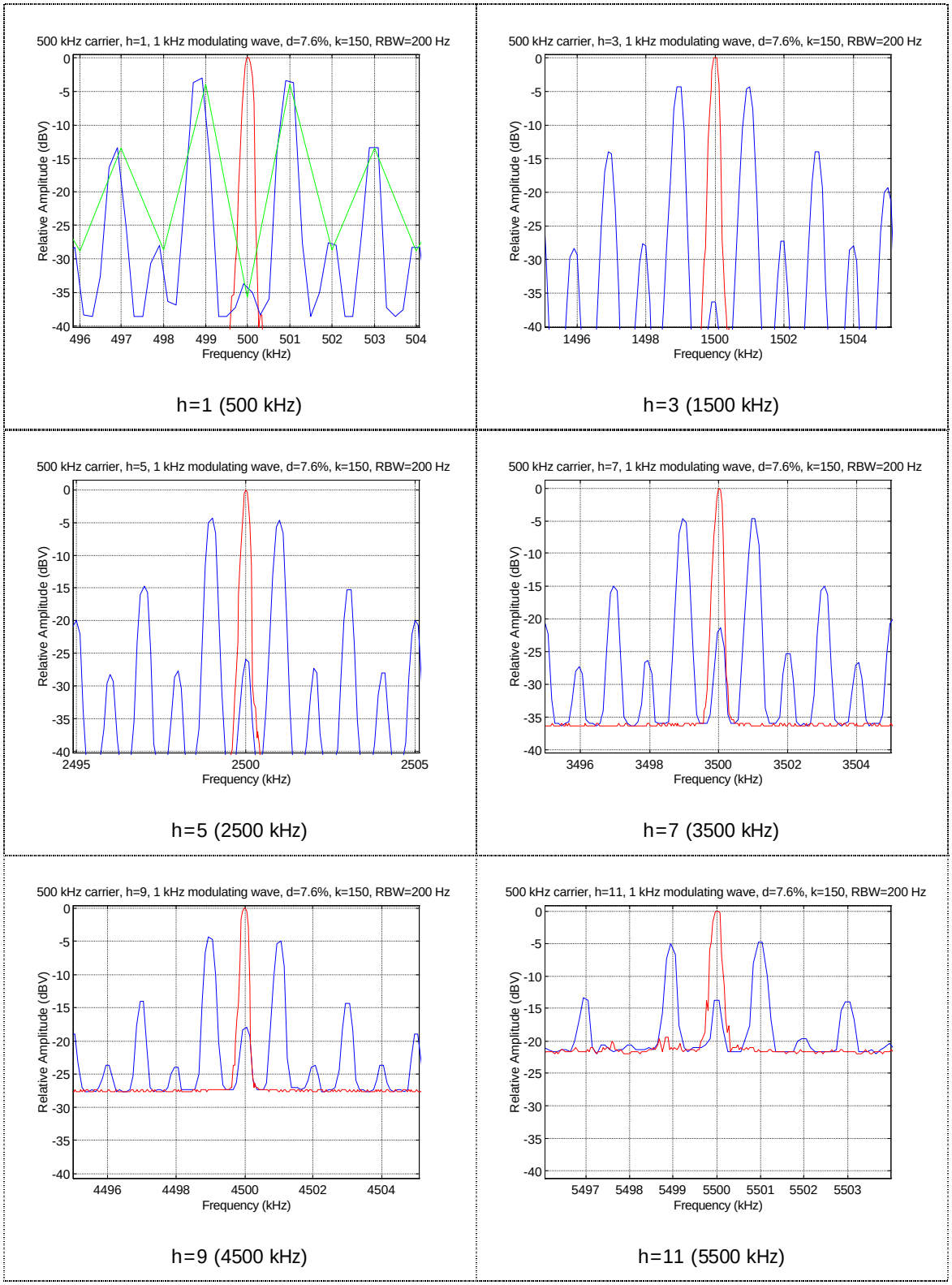

Figure 4-41. Attenuation of odd-harmonics at multiples of 500 kHz: theoretical value (green line), harmonics before modulation (red line) and side-band harmonics after exponential modulation (blue line)

In order to show this attenuation more clearly, only odd-harmonics at multiples of 500 kHz are shown in Figure 4-42. Values of attenuation range from -14 dBV to -36 dBV, as shown in Figure 4-42(b). The attenuation results are then very valuable but, of course, larger theoretical attenuations were expected. Differences between theoretical and experimental results are easy to explain. According to Figure 4-40, an offset around a certain cancellation point m_f (for instance, 38 or 114) will produce theoretically smaller attenuations due to the inverted cone shape around the cancellation point. Matching exactly all the cancellations points, that is, respecting the oscillation period in Figure 4-40, is a guarantee of complete harmonic cancellation but this is not so easy to achieve in practice because of the variability of the different equipment integrating the modulation system. This way, a very good matching of the cancellation points is preferred at those harmonic orders with significant amplitudes, usually the first ones.

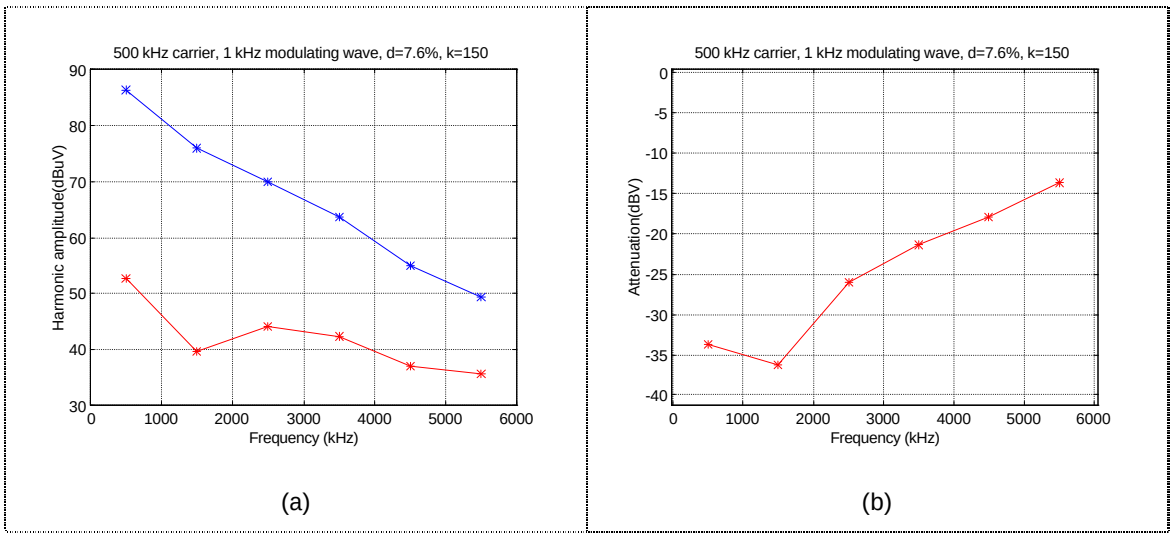

Figure 4-42. (a) Measured amplitude of odd-harmonics before modulation (blue line) and after modulation (red line); (b) Attenuation of odd-harmonics (multiples of 500 kHz)

However, a power converter is nearly never working at a constant duty cycle of 50%. This way, not only odd harmonics are to be generated but also even harmonics. Of course, these even harmonics are also modulated. However, the attenuation of these even harmonics is very poor, as shown in Figure 4-40, where the second harmonic is displayed at m_f=76. A theoretical attenuation of -0.4 dB is expected for the second harmonic, corresponding to m_f=76. The first five even-harmonics generated for the power converter are displayed in Figure 4-43.

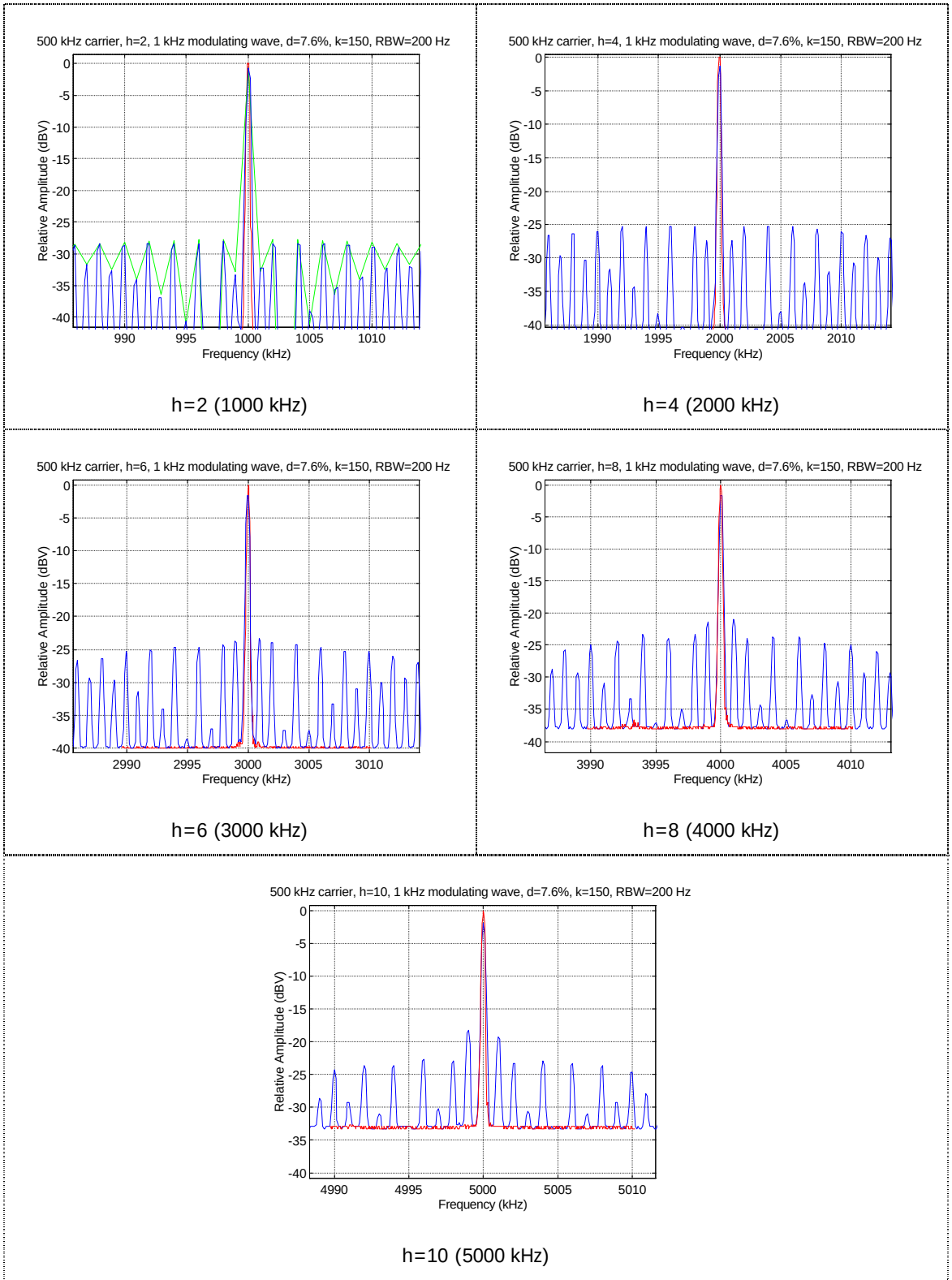

Figure 4-43. Attenuation of even-harmonics at multiples of 1000 kHz: theoretical value (green line), harmonics before modulation (red line) and side-band harmonics after exponential modulation (blue line)

Theoretical behaviour is fairly reproduced in the experimental results shown in Figure 4-43. Only even-harmonics at multiples of 1000 kHz are shown in next Figure 4-44.

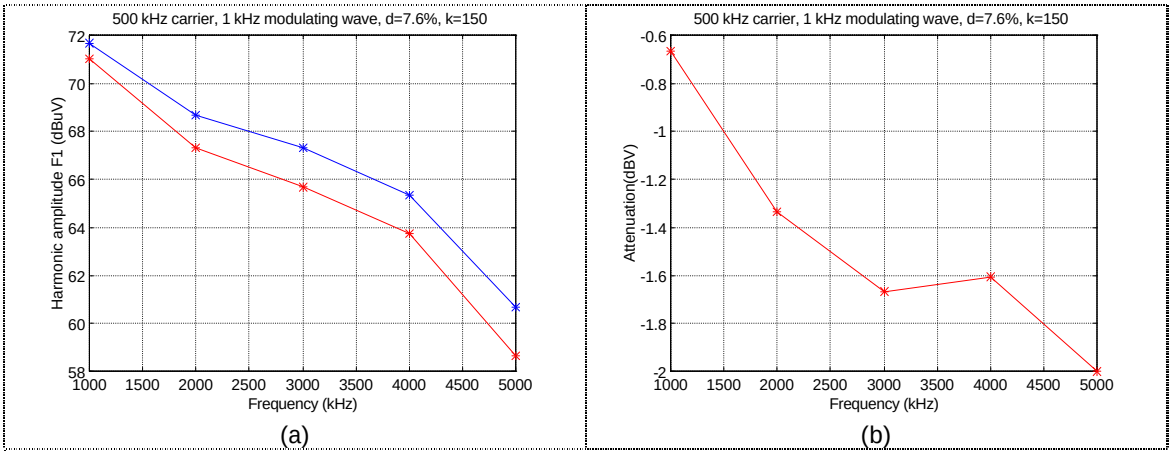

Figure 4-44. (a) Measured amplitude of even-harmonics before modulation (blue line) and after modulation (red line); (b) Attenuation of even-harmonics (multiples of 1000 kHz)

Attenuation values range from -0.6 dBV to -2 dBV, as shown in Figure 4-44(b). This way, a very poor attenuation is obtained for even harmonic orders. This fact should not be of special concern because the experiment's target-signal only consists of odd-harmonics, but it must be taken into account when even-harmonics are also part of the generic signal.

4.6 Summary

In this chapter, a real power converter able to operate at frequencies from 100 kHz to 1.2 MHz was designed. A test plant was also provided, including the previous power converter controlled by a PWM-frequency modulated signal generated in a modulation stage. This controlling signal, originally a sinusoidal waveform coming from a signal generator, is power-adapted, amplified and squared by a zero-crossing detector and finally, applied to the base of the power transistor. A measuring layout consisting of a ground plane, a LISN and a compliant spectrum was used to carry out all measurements, these ones presented as relative values respect to the non-modulated signal.

Some aspects related to SSCG systems, already presented theoretically in chapters 2 and 3, were here tested and verified. A practical focus was always kept in mind in order to show the benefits of using a SSCG method:

– Influence of the compliant Spectrum Analyzer's RBW.

– Proposal of a method to select a valuable SSCG when normative measurements are of interest.

– Conducted EMI (0÷30 MHz) with and without SSGC modulations.

– SSCG as a method to avoid interferences with a certain signal.

As explained along the thesis, real EMI attenuation benefits are always obtained. This true reduction capability can be faded by normative considerations, mainly related to the regulatory RBW to be set on the compliant Spectrum Analyzer. Only when normative measurements are of interest, a special care must be taken to select a proper SSCG method in order to maintain these EMI attenuation benefits when measuring.

Experimental results in clause 4.2 show that modulating frequencies verifying the condition $f_m > 2\frac{RBW}{1+m_f}$ (where RBW is the Resolution Bandwidth and m_f, the modulation index) start producing worthy measurements, not being necessary to reach the condition RBW < f_m to achieve a useful measured attenuation. With this new condition and the previous experimental results, a guideline to select a valuable SSCG method is offered in clause 4.3, consisting of 7 steps. Each step deals with a different parameter of a SSCG method, being a summary of all previous results obtained along the thesis.

In order to assess the validity of using a SSCG method along the range of conducted emissions (0÷30 MHz), a practical example of SSCG modulation is presented in clause 4.4. Attenuation results are shown for the three modulation profiles under study (sinusoidal, triangular and exponential) and for two different sets of modulation parameters. It is observed some undesired effects like side-band spectra overlap and, therefore, lower attenuation than expected at higher frequencies but it is clearly evidenced an attenuation higher than 10 dB for every modulation profile along the whole range of conducted emissions, what allows to assure that SSCG is a worthy method to reduce EMI emissions coming from switching power converters.

Finally, a special application of SSCG techniques is presented in clause 4.5 related to the ability of frequency modulation to cancel harmonics at certain frequencies. Practical application deals with the possibility of having two systems sharing the same frequency. The systems here presented are a CAN-system at high speed (500 kHz) and a power converter operated at 500 kHz. In order to avoid any interferences from the power converter to the CAN-system, a SSCG modulation is implemented in the

switching power converter in such a way that harmonics at multiples of 500 kHz coming from the power converter are cancelled in practice; this way, no interference is expected in the CAN-system even when both systems are working nominally at the same frequency.

CHAPTER 5

CONCLUSIONS

5. CONCLUSIONS

EMI attenuation benefits of SSCG are well-known, mainly applied to systems with higher frequency signals such as clock lines and clock-related waveforms (port lines, serial communications and so on). Presence of SSCG-techniques in digital systems is not strange in some commercial applications (mainly, in personal computers and microcontrollers) but it is nearly unknown in the world of switching power converters, characterised by lower frequency signals. A first question was related to the worthy possibility of implementing such techniques in switching power converters in order to reduce EMI emissions produced by the PWM signal controlling these converters or, even more, avoid undesired interferences with other systems working at the same nominal frequency. Anyway, before facing this task, it is useful (when not mandatory) to describe and systematize theoretically the behaviour of these special kind of frequency modulation called SSCG. Although theoretical development only considers the modulation of a sinusoidal waveform (for convenience), it is demonstrated the validity of all results when a generic signal is present, just paying attention to the right use of the harmonic order h in every expression derived for the modulation of a sinusoidal waveform. Square waves, common in power converters, can be split up in a series of sinusoidal waves (fundamental + harmonics è Fourier series). The benefits of SSCG on a sinus wave are observed in each harmonic, so it is worthy to make the theoretical study on a sinusoidal carrier. Some conclusions are extracted from this theoretical analysis:

– After modulation, a single harmonic changes into an amount of side-band harmonics with amplitudes smaller than the non-modulated harmonic and separated by a frequency f_m (modulating frequency). Amplitudes of side-band harmonics resulting from modulation show a different aspect or outline depending on the modulation profile. For a sinusoidal modulation profile, side-band harmonics tend to concentrate themselves around the two peaks defining the side-band harmonics bandwidth as the modulation index m_f gets higher. This results in a shape of the modulation spectrum envelope showing two peaks at both ends of the bandwidth while the envelope gets a larger concavity between these two peaks. In the case of a triangular modulation profile, envelope of the side-band harmonics corresponds to a nearly flat, straight horizontal line (with harmonic amplitudes

concentrated in a narrow range of variation for vertex index $s \neq 0.5$) , very opposite to the sinusoidal modulation behaviour, characterised by a concavity between two extreme peaks and to the case of an exponential modulation profile, where side-band harmonics resulting from the modulation process tend to concentrate around the carrier frequency, decreasing in amplitude as the side-band harmonic order separates itself from the carrier frequency.

- As just said, a triangular modulation produces a flat side-band harmonics spectrum. Considering a triangular profile as the reference base, profiles plotted outside the triangular profile limits (e.g., sinusoidal) seems to concentrate harmonics around the two peaks defining the bandwidth; in the same way, profiles plotted inside the reference triangular profile (e.g., exponential) concentrate harmonics around the carrier frequency. A combination of these three cases in a generic modulation profile allows the designer to generate whichever shape of the side-band harmonics spectrum.

- For every modulation profile, amplitude reduction of the side-band harmonics resulting from the modulation process only depends on the modulation index m_f. This way, a graphical representation of attenuation versus modulation index is presented as theoretical results. Values of attenuation are referred as relative amplitudes before and after modulation.

- Some parameters were defined in order to quantify the attenuation characteristics: F_1 is the RMS-amplitude of the harmonic corresponding to the modulated waveform at the carrier (switching) frequency f_c; $F_{env,peak}$ is the maximum RMS-amplitude of the side-band harmonic envelope corresponding to the modulated waveform: it provides a very useful information because all side-band harmonics amplitudes will be under this value $F_{env,peak}$; Δf_{peak} is the distance in frequency between the two envelope peaks of value $F_{env,peak}$.

- Regarding the evolution of amplitude F_1, the following considerations for the three profiles under study are of interest:

  § Representing the harmonic amplitude F_1 as a function of m_f, it is obtained an attenuation plot whose envelope results in a logarithmical curve. This way, the higher the modulation index, the larger the attenuation; however, this conclusion is only valid considering the envelope. For modulation indexes $m_f <$ 200, attenuation increases very fast due to its logarithmical behaviour.

Comparing the three profiles under study, a very small difference of 2 dBV appears at high modulation indexes between sinusoidal and triangular modulation; this is not the case of the exponential modulation, whose attenuation is very poor compared to the two previous profiles.

§ Attenuation plots of F_1 show oscillations at a constant period of 1.3 (in units of m_f) for sinusoidal modulation, 1.41 for triangular modulation and a value depending on the concavity factor k for exponential modulation. At every oscillation along m_f -axis, harmonic amplitudes reach a minimum value with attenuation values higher than 40 dB, that is, it can be said that this harmonic is cancelled at this particular m_f. This way, a special profit can be taken just tuning the system to a concrete modulation index in order, for instance, to eliminate the harmonic at the carrier frequency. In the case of exponential modulation profile, it is possible to let the modulation index fix and tune the concavity factor k in order to cancel a particular harmonic. In the case of triangular modulation, no cancellation is possible for vertex index $s \neq 0.5$.

– Regarding the evolution of the maximum envelope amplitude $F_{env,peak}$, consider the following comments for the three profiles under study:

§ Representing the maximum envelope amplitude $F_{env,peak}$ as a function of m_f, it is obtained an attenuation plot whose envelope results in a logarithmical curve. Again, the higher the modulation index, the larger the attenuation, only valid considering the envelope of $F_{env,peak}$. For modulation indexes of $m_f < 200$, attenuation increases very fast due to its logarithmical behaviour. Comparing the three profiles, exponential profile shows the worst behaviour because of the peak shape of the side-band harmonic distribution, which makes the F_1 value matches $F_{env,peak}$ most of the time; however, sinusoidal and, in a much higher quantity, triangular modulations give very good values of attenuation at any side-band harmonic order.

§ Attenuation plots of $F_{env,peak}$ show oscillations much smaller than those corresponding to F_1; because of that, main efforts should be concentrated on obtaining a cancellation of a certain harmonic, normally, the one at the carrier frequency.

– Related to the evolution of the peak-to-peak envelope bandwidth Δf_{peak}, further comments are of interest:

§ For sinusoidal modulation, envelope of Δf_{peak} shows a linear trend respect to m_f, that is, higher modulation indexes m_f are to produce wider bandwidths in a linear ratio. Zooming the plot of Δf_{peak}, it is observed that this parameter increases in steps of a constant value equal to $2 \cdot f_m$.

§ For triangular modulation, maximum values of Δf_{peak} show a linear trend respect to m_f . Under this theoretical straight line, a chaotic behaviour is shown, which is strongly related to the flat shape of the side-band harmonic spectra distribution. However, both sinusoidal and triangular modulations (with vertex index s = 0.5) show approximately the same straight line slope ($\approx 2 \cdot f_m$); for vertex indexes s different of 0.5, this slope is smaller in triangular modulation.

§ For exponential modulation, opposite to the sinusoidal and triangular profiles, no linear trend is detected, just a chaotic behaviour of Δf_{peak}. Moreover, the maximum bandwidth Δf_{peak} is much smaller than for sinusoidal and triangular cases. This indicates the concentration of harmonics around the carrier frequency, which is also bigger as the concavity factor k increases.

– From the comparison of the three different modulation profiles under study and considering the global behaviour of the modulation, the most important parameter is $F_{env,peak}$ because all harmonic amplitudes (resulting from the modulation process) will be under this value $F_{env,peak}$. If the number of new harmonics generated during the modulation process is not of concern but only their amplitudes, this parameter $F_{env,peak}$ should be the target. Then, a flat harmonic distribution is the most profitable and, therefore, a triangular modulation profile is the most suitable for any application with these characteristics. Exponential profile shows the worst behaviour because of the peak shape of the side-band harmonic distribution. If attenuation given by an exponential profile at a certain modulation index m_f is found to be satisfactory, then it can be a good option because the side-band harmonics decrease fast as the side-harmonic order gets farther from the central frequency.

Previous comments constitute the answer to one of the thesis's objectives: to have SSCG-techniques analytically expressed and systematized; this way, this objective is covered successfully.

Once a detailed theoretical description of the SSCG modulation is available, the second question (as expressed above) is related to the worthy possibility of implementing such techniques in switching power converters in order to reduce EMI emissions produced by the PWM signal controlling these converters or, even more, avoid undesired interferences with other systems working at the same nominal frequency. This is the main objective of the thesis and it can be assure that SSCG techniques can be worthy and successfully implemented in switching power converters in order to cover both attenuation exigencies.

The key point is to find a proper modulation index m_f covering the attenuation necessities. Previous theoretical aspects facilitate the selection of the proper modulation index. Because of its definition $m_f = \frac{\delta \cdot f_c}{f_m}$, this is done by selecting properly the modulation ratio δ, the carrier frequency f_c and the modulating frequency f_m. In order to be successful in the selection of these values, some considerations must be taken into account:

- Carrier (or switching) frequency f_c, and modulating frequency f_m (defines the distance in frequency between two consecutive side-band harmonics) are of interest when measuring with spectrum analyzers: their RBW (Resolution Bandwidth) and measure mode (peak, quasy-peak and average) are responsible for giving different measured values of the same physical fact of modulation; as a general asseveration, the larger the selected RBW, the higher the obtained measure because more side-band harmonics can fall inside this RBW, adding their amplitudes. Switching (carrier) frequency in power converters is not usually too large because the electronics components (diodes and power transistors, mainly) are not able to manage larger power with shorter switching times. Anyway, use of higher switching frequencies is advisable in order to reduce the size and power capability of the passive components (filters, inductances, diodes, transistors and so on) and increase the power efficiency of the converter (> 70 %).

  As the attenuation increases with larger modulation indexes, higher switching frequencies f_c are preferred.

- Modulation index m_f (together with f_m, defines the bandwidth of the FM waveform), carrier frequency peak deviation Δf_c (defines the peak frequency excursion around f_c) and modulation ratio δ are responsible for the spectrum

overlap at higher harmonic orders because of the growing side-band harmonics bandwidth resulting from the modulation process. Parameters f_m and Δf_c define the side-band harmonics bandwidth around the carrier (or switching) frequency, thus giving the lowest working frequency present in the system ($\approx f_c - \Delta f_c$) which must be higher than the cut-off frequency of the low-pass filter integrated in the power converter in order to avoid frequencies under cut-off to be present on the output voltage. As explained along the thesis, real EMI attenuation benefits are always obtained. This true reduction capability can be faded by normative considerations, mainly related to the regulatory RBW to be set on the compliant Spectrum Analyzer. Only when normative measurements are of interest, a special care must be taken to select a proper SSCG method in order to maintain these EMI attenuation benefits when measuring. Experimental results show that modulating frequencies verifying the condition $f_m > 2\frac{RBW}{1+m_f}$ (where RBW is the Resolution Bandwidth and m_f, the modulation index) start producing worthy measurements, not being necessary to reach the condition RBW < f_m to achieve a useful measured attenuation.

It is commonly worthy to work with higher modulation indexes and, through its definition $m_f = \frac{\delta \cdot f_c}{f_m}$, this can be done by increasing the modulation ratio δ or the carrier frequency f_c or decreasing the modulating frequency f_m.

– Related to the previous point, overlap starts at main harmonic order given by the following expression $h_{overlap} = \frac{1}{\delta} \cdot \left(\frac{1}{2} - \frac{f_m}{f_c} \right) - \frac{1}{2}$. This overlap is the main reason for not obtaining the expected attenuation at higher harmonic orders. In order to assess the validity of using a SSCG techniques along the range of conducted emissions (0÷30 MHz), a practical example of SSCG modulation was carried out. Attenuation results were shown for the three modulation profiles under study (sinusoidal, triangular and exponential) and for two different sets of modulation parameters. It was observed some undesired effects like side-band spectra overlap and, therefore, lower attenuation than expected at higher frequencies but it was clearly evidenced an attenuation higher than 10 dB for every modulation profile along the whole range of conducted emissions, what allows to assure that SSCG is

a worthy method to reduce EMI emissions coming from switching power converters.

- Regarding modulation profiles (define the shape of the resulting modulated waveform spectrum and the possibility of up- and down-spreading SSCG techniques), it was also demonstrated there was no influence of the modulation profile on the output voltage of a power converter; a voltage offset in the modulation profile does not modify the final modulation spectrum but only the central frequency of the side-band harmonics window, thus being an easy way to implement up- and down-spreading modulation techniques; in a similar way, resulting modulated wave spectrum is independent on a possible phase-shift in the modulation profile. Anyway, modulation profile to be selected is depending on the systems necessities or exigencies and no generic formula can be given

Finally, SSCG-techniques offer the capability of moving the modulation spectrum as desired (of course, with certain limitations); this fact can be profitable in order to avoid undesired interferences with other systems. A special application of SSCG techniques was presented in order to show the ability of frequency modulation to cancel harmonics at certain frequencies. Practical application dealt with the possibility of having two systems at the same nominal frequency. Systems here presented were a CAN-system at high speed (500 kHz) and a power converter operated at 500 kHz. In order to avoid any interferences from the power converter to the CAN-system, a SSCG modulation was implemented in the switching power converter in such a way that harmonics at multiples of 500 kHz coming from the power converter were cancelled in practice; this way, no interference is expected in the CAN-system even when both systems are working nominally at the same frequency. This way, SSCG provides the harmonic cancellation at the frequencies of interest, which are the harmonic orders decided and totally controlled by the designer.

In summary, the three objectives proposed at the beginning of the thesis were successfully covered, being a proper starting point for further lines of investigation as exposed below.

5.1 Further lines of investigations

Investigation tasks keep a strong similarity with the pioneer who opens the way to a new world but who is neither able to realise the importance of his discovers nor finish the mission. These are the tasks for people coming behind, who take the actual status as a starting point and give their own contribution. Following points are open themes to be dealt with:

- Parallel converters connected to the same DC bus.

  If several converters are connected to the same DC bus, it is expected an interaction of all EMI emission products coming from these converters. How this mutual influence is and which benefits are expected is another point of study.

- Practical implementation of SSCG in a PWM-Controller.

  Although a SSCG-control scheme for a real power converter was proposed in the thesis, it is of interest to develop a proper practical implementation of it, in order to make this modulation attractive, not only technically but also economically.

- Mixed modulation profiles.

  Three modulation profiles (sinusoidal, triangular and exponential) were considered in detail. Some basic points were also developed in order to show the behaviour of mixing profiles (e.g., triangular + exponential). This is an open point with great possibilities of producing satisfactory results.

- SSCG applied to nondeterministic or random signals (data lines).

  Signal of interest in the thesis respond to periodic, deterministic waveforms like those present in power converters or in digital systems (clock signal). Study of SSCG-modulation applied to random signals (characterising data lines) is of great interest due to the wide presence of these signals in almost every actual electronic device. How conclusions in the thesis can be extended to nondeterministic signals is another point of study.

- Power converters based on multi-switches.

  Only one switch or interrupter was considered in the power converter used in this thesis. How several interrupters working together in the same power converter affect the results here expressed is to study.

- Selective cancellation of disturbing frequencies.

  SSCG-techniques offer the capability of moving the modulation spectrum in a controlled way; this fact can be profitable in order to avoid undesired interferences with other systems. A particular case was already presented in the thesis (see clause 4.5), but much more can be obtained.

- SSCG applied to Resonant Converters.

  Switching frequencies in the megahertz range, even tens of megahertz, are being contemplated in resonant converters in order to reduce the size and the weight of transformers and filter components and, hence, to reduce the cost as well as the size and the weight of power electronic converters. Realistically, the switching frequencies can be increased to such high values only if the problems of switch stresses, switching losses and the EMI associated with the switch-mode converters can be overcome and here is where SSCG can play a very important role.

C H A P T E R

6

REFERENCES

6. REFERENCES

[6-A] PREVIOUS PAPERS AND PUBLICATIONS:

[RA-1] F. Lin and D.Y. Chen, "Reduction of Power Supply EMI Emission by Switching Frequency Modulation", Virginia Power Electronics Center, Virginia Polytechnic Institute and State University. The VPEC Tenth Annual Power Electronics Seminar, September 20-22, 1992. Blacksburg, Virginia 24061.

[RA-2] Keith B. Hardin, John T. Fessler and Donald R. Bush, "Spread Spectrum Clock Generation for the Reduction of Radiated Emissions", IEEE Symposium on Electromagnetic Compatibility, 1994 (Chicago).

[RA-3] Keith B. Hardin, John T. Fessler and Donald R. Bush, "Digital Circuit Radiated Emission Suppression with Spread Spectrum Techniques", Interference Technology Engineers Master (ITEM) 1994.

[RA-4] Keith B. Hardin, John T. Fessler and Donald R. Bush, "A Study of the Interference Potential of Spread Spectrum Clock Generation Techniques", IEEE International Symposium on Electromagnetic Compatibility, 1995.

[RA-5] Keith B. Hardin, John T. Fessler, Nicole L. Webb, John B. Berry, Andrew L. Cable and Mike J. Pulley, "Design Considerations of Phase-Locked Loop Systems for Spread Spectrum Clock Generation Compatibility", IEEE Symposium August 1997 (Austin, Texas).

[RA-6] Yongsam Moon, Deog Kyoon Jeong, Gyudong Kim, "Clock Dithering for Electromagnetic Compliance using Spread Spectrum Phase Modulation", IEEE International Solid-State Circuits Conference, 1999.

[RA-7] K.K Tse, Henry Shu-Hung Chung, S.Y.(Ron) Hui, H.C. So, “Analysis and Spectral Characteristics of a Spread-Spectrum Technique for conducted EMI Suppression” ; IEEE Transactions on Power Electronics, Vol. 15 Nº 2, March 2000.

[RA-8] R. Giral, A. El Aroudi, L. Martínez-Salamero, R. Leyva, J. Maixe, "Current Control Technique for Improving EMC in Power Converters", IEE Electronics Letters, 1st March 2001, Vol.37, No.5.

[RA-9] H.G. Skinner, K.P. Slattery, "Why Spread Spectrum Clocking of Computing Devices is not Cheating", Proc. 2001 IEEE Int. Symp. Electromagnetic Compatibility, vol. 1, pp. 537-540, Aug. 2001.

[RA-10] Hiroshi Sadamura, Takayuki Daimon, Takayuki Shindo, Haruo Kobayashi, Takao Myono, Tatsuya Suzuki, Shuhei Kawai and Takashi IIJima, "Spread-Spectrum Clocking in Switching Regulators to Reduce EMI", Third IEEE Asia-Pacific Conference on ASICs (AP-ASIC), Taipei, Taiwan, August 6-8, 2002.

[RA-11] Keith B. Hardin, Robert A. Oglesbee and Fred Fisher, "Investigation Into the Interference Potential of Spread-Spectrum Clock Generation to Broadband Digital Communications", IEEE Transactions on Electromagnetic Compatibility, Vol. 45, No. 1, February 2003.

[6-B] AUTHOR'S PAPERS AND PUBLICATIONS:

[RB-1] A. Santolaria, J. Balcells, D. González, "Theoretical & Experimental Results of Power Converter Frequency Modulation", Proceedings of the 28th Annual Conference of the IEEE Industrial Electronics Society, 2002 (Sevilla, Spain).

[RB-2] A. Santolaria, J. Balcells, D. González, J. Gago, "Evaluation of Frequency Modulation in EMI Emissions Reduction applied to Switching Power Converters", Proceedings of the 29th Annual Conference of the IEEE Industrial Electronics Society, 2003 (Virginia, USA).

[RB-3] A. Santolaria, J. Balcells, D. González, J. Gago, "EMI Reduction in Switching Power Converters by means of Spread Spectrum Modulation Techniques", (Paper accepted in February, 2004 for PESC'04).

[6-C] PATENTS, APPLICATION NOTES AND OTHER RELATED PUBLICATIONS:

[RC-1] T.G. Habetler, D.M. Divan, "Acoustic Noise Reduction in Sinusoidal PWM Drives Using a Randomly Modulated Carrier", IEEE Transactions on Power Electronics, July 1991.

[RC-2] K. Hardin et al., "Spread Spectrum Clock Generator and Associated Method", U.S. Patent 5 488 627, Jan., 30 1996.

[RC-3] K. Hardin et al., "Spread Spectrum Clock Generator and Associated Method", U.S. Patent 5 867 524, Jan., 30 1996.

[RC-4] K. Hardin, "Spread Spectrum Clock Generator", U.S. Patent 5 631 920, May, 20 1997.

[RC-5] Cornelis D. Hoekstra, "Frequency Modulation of Systems Clocks for EMI reduction", Hewlett-Packard Journal, August 1997.

[RC-6] E. McCune and V. Goedjen, "Reducing EMI with Spread Spectrum Clocking", Insight, Volume 2, Issue 4, 1997.

[RC-7] J. Siago, "New IC Features Reduce EMI from Switching Regulator Circuits", Linear Technology Magazine, February 1997.

[RC-8] Intel, "Notes on SSC and Its Timing Impacts", Michael T. Zhang, Intel Corp. Rev. 1.0, February 1998.

[RC-9] Intel, "CK97 Clock Synthesizer Design Guidelines", June 1998.

[RC-10] S. Bolger and S. O. Darwish, "Use Spread Spectrum Techniques to Reduce EMI", EDN, May 21st, 1998.

[RC-11] Howard Johnson, "Intentional Clock Modulation", EDN, August 3rd, 1998.

[RC-12] Booth et al., "Spread Spectrum Clock Generator and Associated Method", U.S. Patent 5 872 807, Feb., 2 1999.

[RC-13] Intel, "Design for EMI", Application Note AP-589, February 1999.

[RC-14] Analog Devices Inc., "Implementing Random Space Vector Modulation with the ADMCF32X", Application Note ANF32X-54, December 2000.

[RC-15] K. Hardin, "Variable Spread Spectrum Clock", U.S. Patent 6 167 103, Dec., 26 2000.

[RC-16] K. Hardin et al., "Method and Apparatus for Compensating a Spread Spectrum Clock Generator", U.S. Patent 6 292 507, Sept., 18 2001.

[RC-17] Integrated Circuit Systems (ICS), "Application Note: Using Spread Spectrum in ICS products".

[RC-18] Agilent Technologies, "AN 150: Spectrum Analysis Basics", Application Note.

[RC-19] Agilent Technologies, "AN 1383-1: Spectral Analysis Using a Deep-Memory Oscilloscope Fast Fourier Transform (FFT)", Application Note.

[RC-20] Agilent Technologies, "AN 1303: Spectrum Analyzer Measurements and Noise", Application Note.

[6-D] RELATED LITERATURE:

[RD-1] Herbert L. Krauss, Charles W. Bostian, Frederick H. Raab, "Estado Sólido en Ingeniería de Radiocomunicación", Ed. Limusa, 1984.

[RD-2] Ned Mohan, Tore M. Undeland, William P. Robbins, "POWER ELECTRONICS: Converters, Applications and Design", John Wiley & Sons, Inc. 1989.

[RD-3] Clayton R. Paul, "Introduction to Electromagnetic Compatibility", John Wiley & Sons, Inc. 1992.

[RD-4] Howard Johnson, "High Speed Digital Design: A Handbook of Black Magic", Prentice Hall, 1993.

[RD-5] Rodger E. Ziemer, William H. Tranter, "Principles of Communications: Systems, Modulation, & Noise, 4E", ISBN 0-471-12496-6, John Wiley & Sons, December, 1994.

[RD-6] J. Luis Muñoz Sáez, S. Hernández González, "Sistemas de Alimentación Conmutados", ISBN 84-283-2347-X, Paraninfo, 1996.

[RD-7] Wolfhard Lawrenz, "CAN System Engineering: from theory to practical applications", ISBN 0-387-94939-9, Springer-Verlag New York, Inc. 1997.

[RD-8] Alan V. Oppenheim, Ronald W. Schafer, John R. Buck, "Discrete-Time Signal Processing", ISBN 0-137-54920-2, Prentice Hall, February 15th, 1999.

[RD-9] Irving Gottlieb, Delmar Publishing, "Basic Modulation Principles", ISBN 0-790-61198-8, Delmar Learning, September 1st, 1999.

[RD-10] Ronald N. Bracewell, "The Fourier transform and its applications", ISBN 0-07-116043-4, 1999.

[RD-11] Peter Bloomfield, "Fourier analysis of time series: an introduction", ISBN 0-471-88948-2, 2000.

[RD-12] Samuel D. Stearns, "Digital Signal Processing with Examples in MATLAB", ISBN 0-849-31091-1, CRC Press, August 28th, 2002.

[6-E] EMC / EMI REGULATORY NORMATIVE:

[RE-1] International Electrotechnical Commission, "Specification for Radio Disturbance and Immunity Measuring Apparatus and Methods – Part 1: Radio Disturbance and Immunity Measuring Apparatus", CISPR, Geneva, Switzerland, CISPR 16-1, Second Edition, 1999-10.

[RE-2] International Electrotechnical Commission, "Information Technology Equipment – Radio Disturbance Characteristics – Limits and methods of measurement", CISPR, Geneva, Switzerland, CISPR 22, Third Edition, 1997-11.

[RE-3] International Electrotechnical Commission, "Information Technology Equipment – Radio Disturbance Characteristics – Limits and methods of measurement", CISPR, Geneva, Switzerland, CISPR 22 Amendment - 1, 2000-08.

[RE-4] Federal Communications Commission (FCC), "Title 47 - Telecommunication, Chapter I - Federal Communications Commission, Part 15 - Radio Frequency Devices", March 13th, 2003

[RE-5] Federal Communications Commission (FCC), "MP-4 FCC Methods of Measurement of Radio Noise Emission from Computing Devices", July, 1987.

GLOSSARY

OF

TERMS

GLOSSARY OF TERMS

Terms	Symbol / Expression	Definition / Explanation
Carrier frequency peak deviation[(1)]	Δf_c	Peak excursion of the carrier (switching) frequency f_c.
Carrier frequency	f_c	Frequency of the generic carrier signal to be modulated during a modulation process.
Central frequency	Central frequency	For modulation of a sinusoidal waveform, it is equivalent to Carrier frequency; for modulation of a generic signal, it is the frequency of each central harmonic corresponding to the modulation of each main harmonic.
Central harmonic	Central harmonic	Side-band harmonic at the frequency corresponding to the central point of the spectral window resulting from the modulation process. For a symmetrical modulation around a frequency f, side-band harmonic at frequency f is called central harmonic.
Concavity factor	k	It defines exactly the concavity or convexity of an exponential waveform.
EMI	EMI	Electromagnetic Interference. Because of rapid changes in voltages and currents within a switching power converter, power electronic equipment is a source of electromagnetic interference with other equipment as well as with its own proper operation. EMI is transmitted in two ways: conducted and radiated. There are various standards that specify the maximum limit on the EMI: CISPR, IEC, VDE, FCC and the Military Standards.
Frequency Modulation	FM	A form of angle modulation in which the instantaneous frequency of a carrier is caused to depart from the carrier frequency by an amount proportional to the instantaneous value of the modulating wave.

[(1)] See Figure G-1

Terms	Symbol / Expression	Definition / Explanation
IF filter	IF	Intermediate-frequency filter. Passband filter intended to accept only the mixing products of interest coming from the mixer. See Annex 1.
Instantaneous frequency	$f(t) \leftrightarrow \omega(t)$	Instantaneous frequency of the modulated waveform resulting from a modulation process.
Instantaneous frequency deviation	$\delta f(t) \leftrightarrow \delta\omega(t)$	In frequency modulation, deviation of instantaneous frequency $\omega(t)$ respect to the constant carrier frequency $\omega_c = 2 \cdot \pi \cdot f_c$ è $\delta\omega(t) = \omega(t) - \omega_c$
Line Impedance Stabilization Network	LISN	Device whose first purpose is to prevent EMI from disturbing the measurements; the second purpose is to ensure that measurements made at one test site will be comparable with measurements at another test site.
Local oscillator	LO	Local oscillator. It makes possible the tuning process across the selected span in order to obtain a display with a range of frequencies represented on the horizontal axis. See Annex 1.
Main harmonic		Each one of the harmonics making part of a periodic waveform (Fourier series). See also side-band harmonics and Figure 2-7.
Modulating frequency[(1)]	f_m	Frequency of the waveform responsible of the modulation process.
Modulation index	m_f	A very common ratio in frequency modulation responding to the expression $m_f = \frac{\Delta\omega_c}{\omega_m} = \frac{\Delta f_c}{f_m}$
Modulation profile[(1)]	$v_m(t)$	Shape of the modulating wave, it is the main responsible for the spectrum outline resulting from a modulation process.

(1) See Figure G-1

Terms	Symbol / Expression	Definition / Explanation
Modulation ratio	δ	Peak excursion of the switching or carrier frequency referred to itself è $\delta = \frac{\Delta f_c}{f_c}$
Modulating wave[(1)]	$v_m(t)$ V_m	Waveform used to modulate the original constant carrier frequency. V_m is the peak amplitude of the modulating wave.
Parameter F_1	F_1	F_1 is the RMS-amplitude of the harmonic corresponding to the modulated waveform at the carrier (switching) frequency f_c (referred normally to the RMS-amplitude of the harmonic corresponding to the non-modulated carrier waveform at a frequency f_c). See Figures 3-1 and 3-2.
Parameter $F_{env,peak}$	$F_{env,peak}$	$F_{env,peak}$ is the maximum RMS-amplitude of the side-band harmonics envelope corresponding to the modulated waveform: it provides a very useful information because all side-band harmonics amplitudes will be under this value $F_{env,peak}$ (referred normally to the RMS-amplitude of the harmonic corresponding to the non-modulated carrier waveform at a frequency f_c). See Figures 3-1 and 3-2.
Parameter Δf_{peak}	Δf_{peak}	Δf_{peak} is the distance in frequency between the two envelope peaks of value $F_{env,peak}$. See Figures 3-1 and 3-2.
Percentage of modulation	$\delta\%$	Modulation ratio δ expressed as a percentage.
Pulse-Width Modulation	PWM	Pulse-Width Modulation (PWM) is one of the methods to control the output voltage of a power converter. This method employs switching at a constant frequency, adjusting the t_{on} duration of the switch (respect to the switching period T) to control the average output voltage.
Resolution Bandwidth	RBW	Resolution bandwidth of the spectrum analyzer's filter. This is the filter whose selectivity determines the analyzer's ability to resolve (indicate separately) closely frequency-spaced signals.

(1) See Figure G-1

Terms	Symbol / Expression	Definition / Explanation
Sensitivity factor[(1)]	k_ω	Factor of proportionality of the instantaneous frequency deviation respect to the modulating signal voltage $v_m(t)$ expressed in rad/sec/V or Hz/V è $\delta\omega(t) = k_\omega \cdot v_m(t)$
Side-band harmonic	Side-band harmonic	After modulation, an individual (main) harmonic is spread into an amount of sub-harmonics having the same energy but smaller amplitudes than the original harmonic. These sub-harmonics are called Side-band harmonics. See also Main harmonic and Figure 2-7.
Side-band harmonics window	Side-band harmonics window	After modulation, an individual harmonic is spread into an amount of sub-harmonics normally enclosed into a finite bandwidth called side-band harmonics window. See Figure 2-7.
Span	Span	The frequency range represented by the horizontal axis of the display. Generally, frequency span is given as the total span across the full display.
Spread Spectrum Clock Generation	SSCG	Technique to reduce the conducted and radiated emissions produced by constant frequency signals. Instead of maintaining a constant frequency, SSCG systems modulate the clock frequency following certain modulation profiles, thereby spreading the harmonic energy into an amount of side-band harmonics having the same energy but smaller amplitudes, which normally corresponds to spreading conducted and radiated energy over a wider frequency range.
Sweep time	ST	The time to tune the local oscillator across the selected span. Sweep time does not include the dead time between the completion of one sweep and the start of the next. In non-zero spans, the horizontal axis is calibrated in both frequency and time, and sweep time is usually a function of frequency span, resolution bandwidth and video bandwidth.

(1) See Figure G-1

Terms	Symbol / Expression	Definition / Explanation
Switching frequency	f_c	Frequency of the PWM-signal controlling the power converter commutation.
Vertex index	s	It controls the vertex position of the triangular waveform from 0 to $T_m/2$, thus making the implementation of profiles such a sawtooth waveform very easy. Vertex index s can range from 0 to 1, and, for a classical triangular profile, s = 0.5.
Video bandwidth	VBW	The cutoff frequency (3-dB point) of an adjustable low-pass filter in the video circuit. When the video bandwidth is equal to or less than the resolution bandwidth, the video circuit cannot fully respond to the more rapid fluctuations of the output of the envelope detector. The result is a smoothing of the trace. The degree of averaging or smoothing is a function of the ratio of the video bandwidth to the resolution bandwidth.
Video filter	VF	A post-detection, low-pass filter that determines the bandwidth of the video amplifier. Used to average or smooth a trace. See Video Bandwidth.

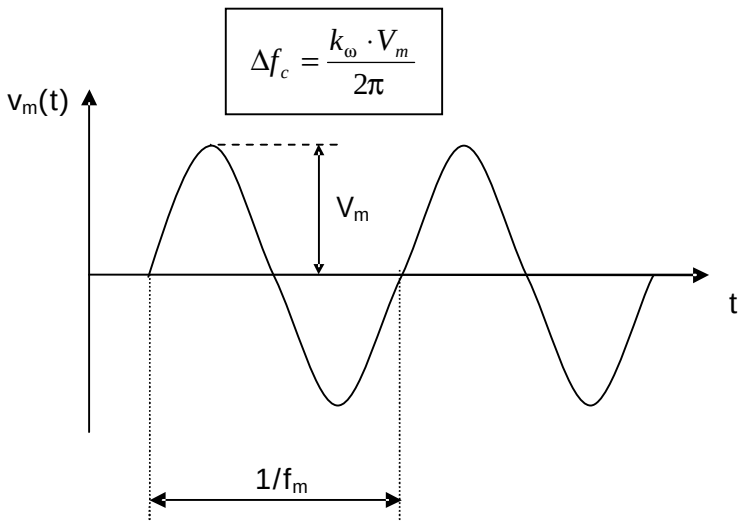

Figure G-1. Modulation waveform profile and related parameters.

ANNEXES

ANNEX 1

ANNEX 2

ANNEX 3

ANNEX 4

ANNEX 5

ANNEX 6

ANNEX 7

ANNEX 1

SPECTRUM ANALYZERS: PRACTICAL CONSIDERATIONS

ANNEX 1:

SPECTRUM ANALYZERS: PRACTICAL CONSIDERATIONS

The use of a spectrum analyzer to measure the signal spectral content is onwards discussed, since the ability to use this important instrument correctly is critical to the correct evaluation of the product's compliance (or non-compliance) with regulatory requirements.

This discussion is mainly intended for explaining important aspects of superheterodyne spectrum analyzers. Such analyzers can also be described as frequency-selective, peak-responding voltmeters calibrated to display the RMS value of a sine wave. It is important to understand that the spectrum analyzer is not a power meter, although it is normally used to display power directly. Obviously it is possible to calibrate this special voltmeter to indicate power just knowing the resistance across which this value is measured.

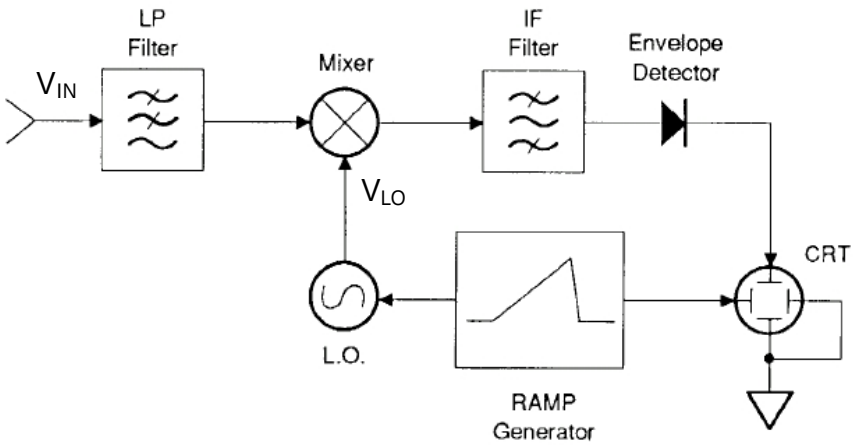

Figure A1-1. Superheterodyne spectrum analyzer

Figure A1-1 shows a block diagram of a superheterodyne spectrum analyzer (heterodyne ó to mix, to translate frequencies, super ó super-audio or above the audio frequencies). As shown in Figure A1-1, an incoming signal (V_{IN}) passes through a low-pass filter (LP filter) to a mixer, where it mixes with a signal coming from the local oscillator (V_{LO}). Because the mixer is a non-linear device, its output contains spectral components at [RD-1]:

- the two original signal frequencies (f_{IN} and f_{LO})
- their harmonics ($h_{IN} \cdot f_{IN}$ and $h_{LO} \cdot f_{LO}$)
- the sums and differences of the original frequencies ($f_{LO} \pm f_{IN}$ and $f_{IN} \pm f_{LO}$) and their harmonics ($h_{LO} \cdot f_{LO} \pm h_{IN} \cdot f_{IN}$ and $h_{IN} \cdot f_{IN} \pm h_{LO} \cdot f_{LO}$)

Any mixed signals falling inside the passband of the intermediate-frequency (f_{IF}) filter are further processed, essentially rectified by the envelope detector, digitized (in most current analyzers) and finally displayed on a screen.

Of all the products emerging from the mixer, the two with the largest amplitudes, and therefore the most desirable, are those created from the sum of the local oscillator (V_{LO}) and the input signal (V_{IN}) and from the difference of the local oscillator (V_{LO}) and the input signal (V_{IN}), that is, the products at frequencies $f_{LO} \pm h_{IN} \cdot f_{IN}$ (onwards $f_{sig} = h_{IN} \cdot f_{IN}$). In this kind of spectrum analyzer, it is desired that one of these products to fall within the passband of the IF filter in order to get the signal harmonic of interest. For this to happen, the signal harmonic of interest must be above or below the f_{LO} frequency an amount of f_{IF}.

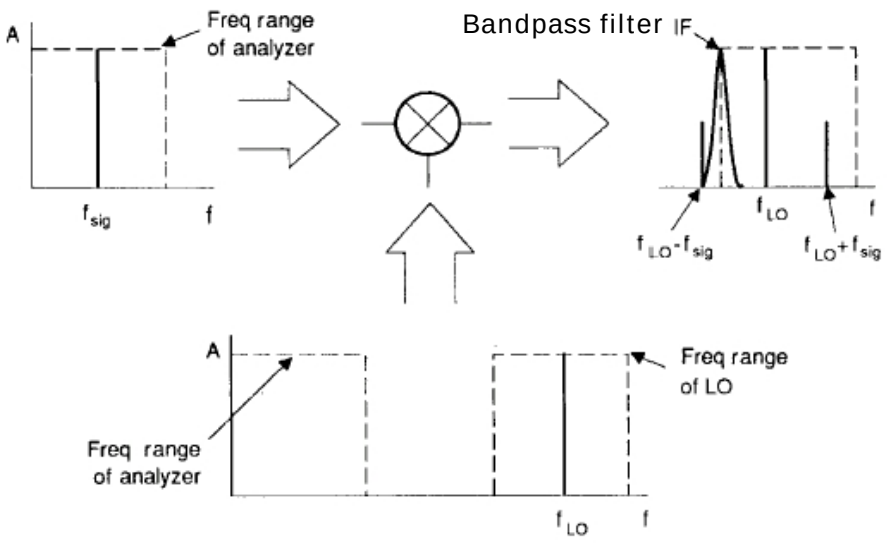

Figure A1-2. f_{LO} must be tuned to $f_{IF}+f_{sig}$ to produce a response on the display

A1.1 Tuning considerations

Obviously f_{LO} and f_{IF} must be adjustable in order to cover the desired frequency range. Normally f_{IF} is fixed and f_{LO} is swept. Criteria to choose these two values can be summarized as follows (see Figure A1-2):

- f_{IF} must be higher than the frequency range of the spectrum analyzer (see Figure A1-3). If f_{IF} stays within the frequency range of the analyzer, there is no way to distinguish between this frequency (also present at the output of the mixer) and another one of the same frequency but coming from the input signal.

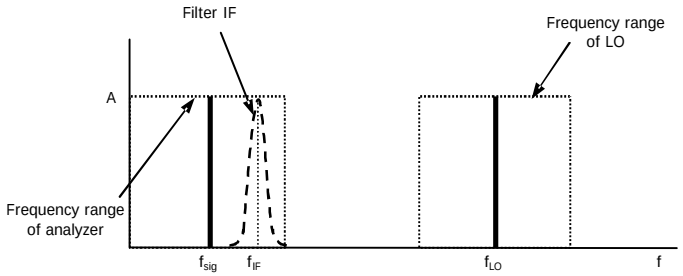

Figure A1-3. f_{IF} inside the frequency range of the spectrum analyzer

- As established before, largest mixing products are $f_{LO} \pm f_{sig}$. To cover the entire frequency range, f_{LO} must range from f_{IF} to $f_{IF} + f_{sig,max}$, as shown in Figure A1-4.

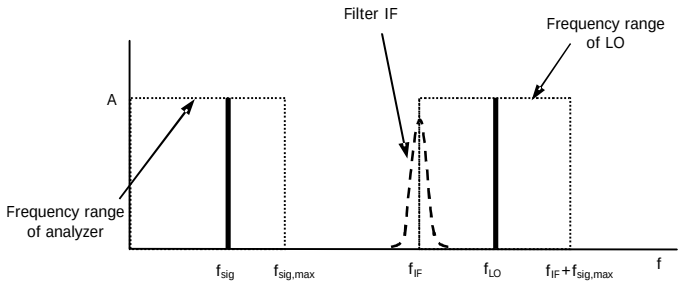

Figure A1-4. Frequency range width of spectrum analyzer and LO

- If a frequency of the input signal f_{sig} is larger than f_{IF} (see Figure A1-5) and, during the tuning process, the expression $f_{IF}+f_{LO} = f_{sig}$ is verified, then a mixing product equal to $f_{sig} – f_{LO} = f_{IF}$ is immediately and constantly displayed. That is, the architecture of Figure A1-2 could also result in a tuning range from $f_{IF}+f_{LO,min}$ to $f_{IF}+f_{LO,max}$. This is not desirable and it is now easy to understand the reason for the low-pass filter in Figure A1-1 to be present at the input, just to avoid these frequencies higher than $f_{IF}+f_{LO,min}$ and signals at the intermediate frequency f_{IF} itself to reach the mixer.

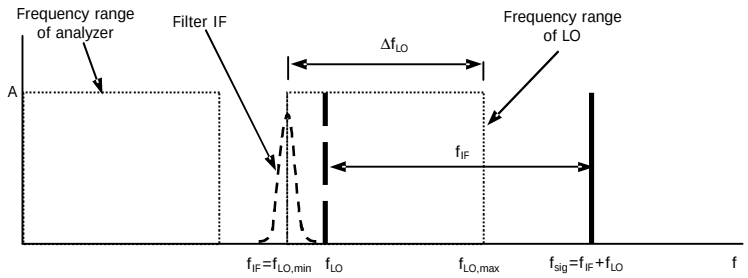

Figure A1-5. Input frequencies around f_{IF} or larger than $f_{IF}+f_{LO,min}$ are filtered out

A1.2 Resolution considerations

ANALOG IF FILTERS:

a) Definite width responses

Frequency resolution is the ability of a spectrum analyzer to distinguish different input sinusoids into distinct responses. Normally the problem comes when these sinusoids are very close in frequency.

Theoretically two signals should show two separate frequency lines on the display, no matter how close in frequency are. This is directly derived from Fourier principles. However a closer look at a superheterodyne receiver shows that signal harmonics are displayed as definite width responses instead of a single line. This is related to the intrinsic functioning of the superheterodyne spectrum analyzer as it is explained onwards. The output of a mixer contains the sum and difference products plus the two original signals (input and LO). The intermediate frequency is determined by a bandpass filter and it is this filter which selects the desired mixing products and rejects all others. Because the input signal is fixed and the local oscillator is swept, the products from the mixer are also swept.

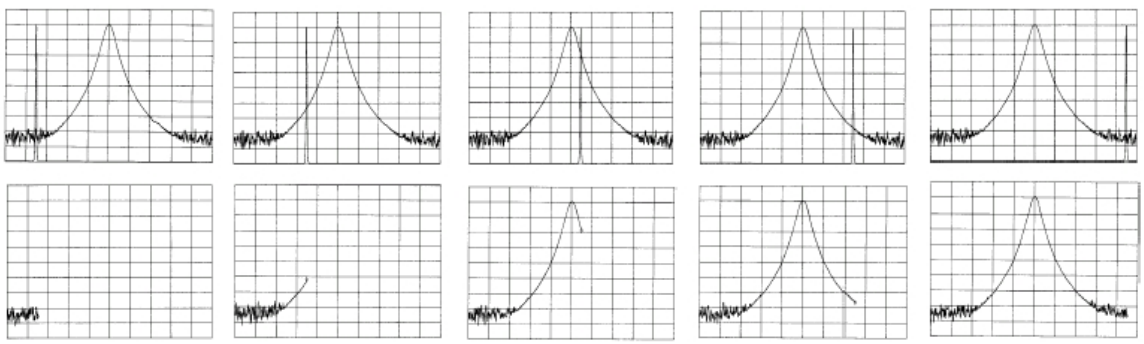

Figure A1-6. As a mixing product sweeps past the IF filter, its shape is traced on the display

During this sweep, a mixing product moving upwards through the IF bandpass filter will trace on the display the characteristics of this filter (see Figure A1-6). So unless two signals are far enough apart, the traces they make fall on top of each other (a kind of fading) and look like only one response showing an amplitude larger than each original signal.

b) Bandwidth selectivity

If two different mixing products or signals (in general) drop into the IF filter bandwidth, the sweep process of LO (which traces the characteristics of the IF filter as explained above) generates two different skirts for each signal as in Figure A1-7.

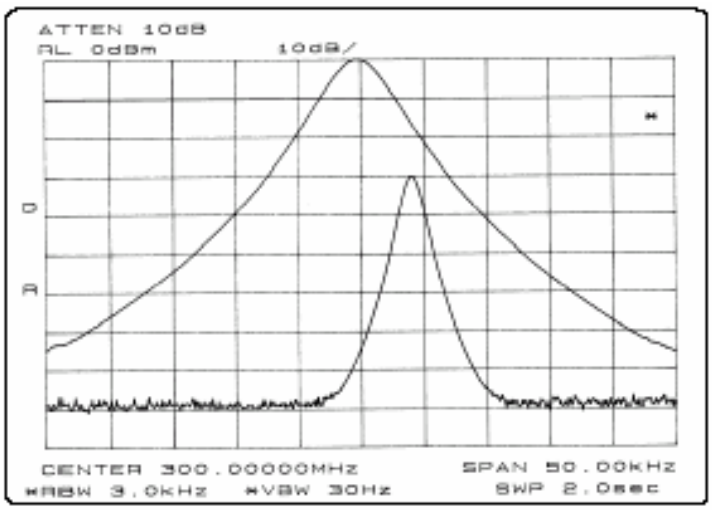

Figure A1-7. A low-level signal can be lost under skirt of the response to a larger signal

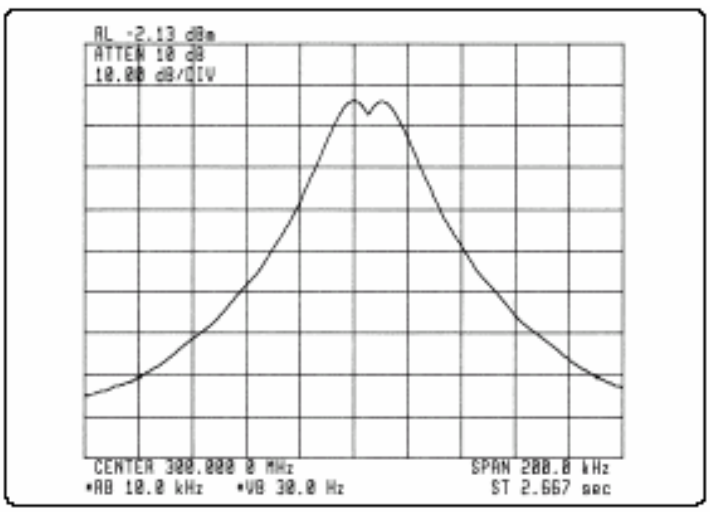

Figure A1-8. Two equal-amplitude sinusoids separated by the 3 dB BW of the selected IF filter can be resolved

If these two signals have different amplitudes (more usual than not), the smaller signal can be lost under the skirt of the response traced out by the larger, as seen in Figure A1-7. In the case of two sinusoidal waveforms of equal amplitude, the resolution of the 3 dB BW of the IF filter can resolve this two signals as shown in Figure A1-8.

Another specification must be defined to take this feature into account: bandwidth selectivity. Normally this parameter is specified as the ratio of the 60 dB to the 3 dB bandwidths, as shown in Figure A1-9 (every manufacturer specifies its own bandwidth selectivity, like 60:6 dB, 25:1 dB, etc)

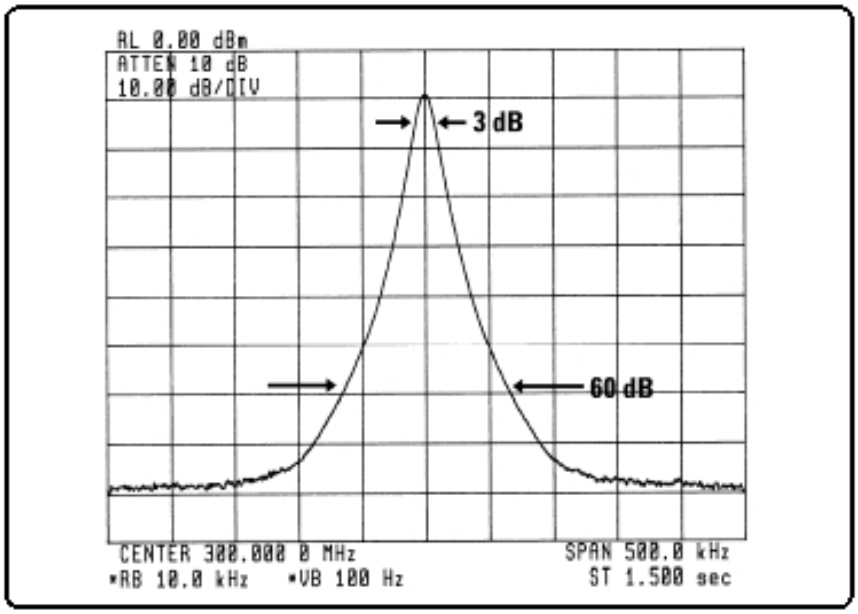

Figure A1-9. Bandwidth selectivity, ratio of 60 dB to 3 dB bandwidths

Taking two signals separate Δf_{sig} in frequency and differing ΔdB_{sig} in amplitude and assuming a logarithmic amplitude and a linear frequency scale for the spectrum analyzer, it can be assumed that the filter skirt is straight between the two points defining bandwidth selectivity, i.e., between BW_H and BW_L, when a ratio H:L dB is selected (for instance, 60:3 dB implies ΔdB_H = 60 dB and ΔdB_L = 3 dB).

From Figure A1-10, the following expression (A1-1) can be derived:

$$\Delta dB_{sig} = \Delta f_{sig} \cdot \frac{\Delta dB_H - \Delta dB_L}{\frac{BW_H}{2} - \frac{BW_L}{2}} \qquad \text{(A1-1)}$$

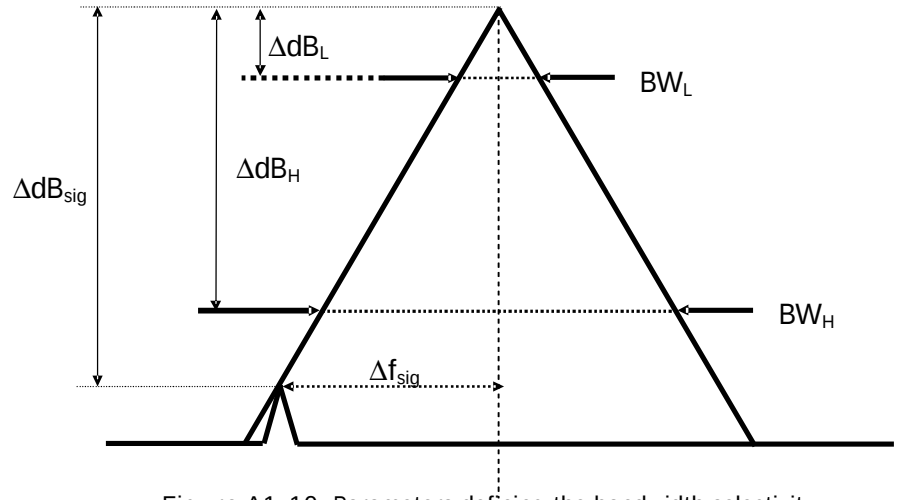

Figure A1-10. Parameters defining the bandwidth selectivity.

To resolve signals differing Δf_{sig} in frequency and ΔdB_{sig} in amplitude, expression (A1-1) must be accomplished in the worst case. The expression above represents the limit to trace out the two signals separately.

DIGITAL IF FILTERS:

Some spectrum analyzers use digital techniques to implement their narrower resolution-bandwidth filters. Normally the linear analog signal coming from the mixer is mixed down again to a lower frequency (for instance, 4.8 Hz) and passed through a bandpass filter only, for instance, 600 Hz wide. This IF signal is then amplified, sampled at a 6.4 kHz rate and digitized. Once in digital form, the signal is analyzed by using a Fast Fourier Transform algorithm. To do this, the analyzer must be fixed-tuned (not sweeping) because the transform must be done on a time-domain signal.

An advantage of digital processing is a bandwidth selectivity of 5:1, also available on the narrowest filters, the ones commonly selected to separate the most closely spaced signals.

A1.3 Sweep time considerations

ANALOG RESOLUTION FILTERS:

Sweep time is the time the analyzer takes to tune the LO across the selected span. Sweep time is usually a function of frequency span, resolution bandwidth and video bandwidth and affects directly the time taken to complete a measurement.

Resolution bandwidth comes into play because the IF filters are band-limited circuits requiring finite times to charge and discharge. If the mixing products are swept

through them too fast, there will be a loss of displayed amplitude as shown in Figure A1-11 (see also envelope detector considerations below).

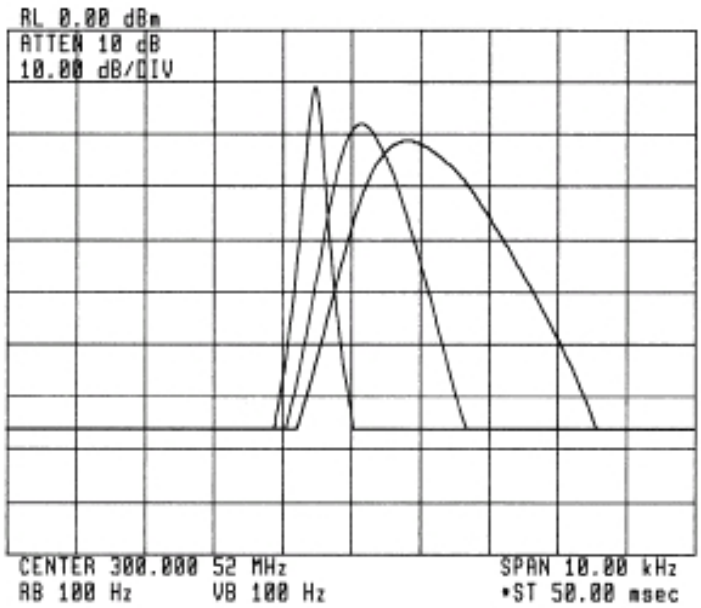

Figure A1-11. Sweeping too fast causes a drop in the displayed amplitude and a shift in the indicated frequency

The time a mixing product stays within the passband of the IF filter is expressed as follows:

$$\text{Time in passband} = ST \cdot \frac{RBW}{Span} \qquad \text{(A1 -2)}$$

where:

- RBW is the resolution bandwidth
- ST is the sweep time
- Span is the frequency range represented by the horizontal axis of the display, commonly distributed across the full ten divisions in a spectrum analyzer.

On the other hand, the rise time of a filter is inversely proportional to its bandwidth this way:

$$\text{Rise time} = \frac{k}{RBW} \qquad \text{(A1 -3)}$$

where k is a constant of proportionality between 2 and 15.

Making the times in (A1-2) and (A1-3) equal and solving for sweep time, it is obtained:

$$ST = k \cdot \frac{Span}{RBW^2} \qquad \text{(A1 -4)}$$

An important message is obtained from the expression above: a change in the resolution bandwidth (RBW) has a dramatic effect on the sweep time in order to maintain a calibrated display. If a sweep time longer than the maximum available in the analyzer is called for, a message of uncalibrated display appears.

DIGITAL RESOLUTION FILTERS:

Effects of digital resolution filters are normally different from those related to analog filters. The signal being analyzed is processed in, for instance, 600 Hz blocks. When selecting the 10 Hz resolution bandwidth, the analyzer is in effect simultaneously processing the data in each 600 Hz block through 60 contiguous 10 Hz filters. If the digital processing were instantaneous, a factor-of-60 reduction in sweep time could be expected; in practice it is lower but significant nonetheless.

A1.4 Envelope detector considerations

Spectrum analyzers convert the IF signal to video with an envelope detector. Figure A1-12 shows the simplest implementation of such a detector.

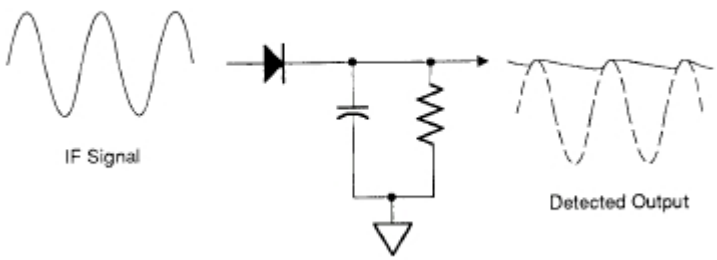

Figure A1-12. Envelope detector

Detector time constants are such that the voltage across the capacitor equals the peak value of the IF signal at all times, that is, the detector can follow the fastest possible changes in the envelope of the IF signal but not the instantaneous value of the IF signal itself.

This IF signal comes from a bandpass filter whose resolution bandwidth is selectable. Normally, this bandwidth is adjusted in order to distinguish each spectral component of

the input signal. However, when two or more spectral components are present within the bandwidth (see Figure A1-13), which measured value is expected?

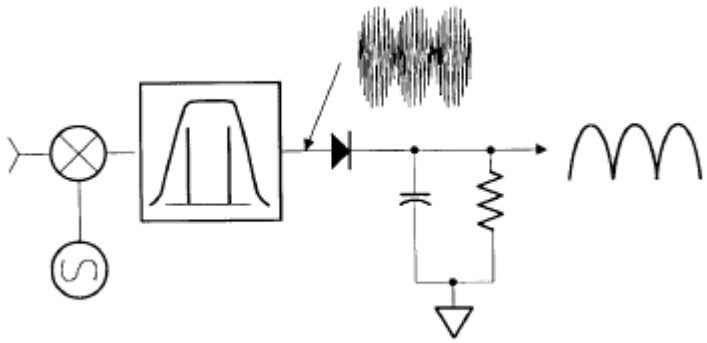

Figure A1-13. Output of the envelope detector

Assuming only two spectral components within the passband, these two sine waves interact to create a beat note. The envelope of the IF signal varies as shown above in Figure A1-13.

The envelope detector is what makes the spectrum analyzer a voltmeter and not a power meter. Assuming two equal-amplitude signals are within the bandpass filter at the same time, a power meter would indicate a power level 3 dB above either signal, that is, the total power of the two signals. Assuming these two signals are close enough, the analyzer display will vary between a value twice the voltage of either (6 dB greater) and zero (-∞ on the log scale). The explanation is very simple: two sine waves at different frequencies are continuously changing in phase with respect to each other, thus adding their amplitudes when in phase and going to zero when out of phase.

So the envelope detector follows the changing amplitude values of the peaks of the signal from the IF chain but not the instantaneous values, giving the analyzer spectrum its voltmeter characteristics.

A1.5 Measurement mode

Three modes of measurement are available on a spectrum analyzer: peak, quasi-peak and average. Each mode can give different results when measuring depending on the kind of signal at the input because the intention of each measurement mode is different and purpose-specific.

a) Peak mode

When using this mode, the spectrum analyzer is displaying on the screen the maximum (actually rms) value of the sinusoidal harmonic. A simple peak detector is shown in Figure A1-14, where the input represents a harmonic whose peak level is V_o. Of course, commercial spectrum analyzer uses a more complicated peak detector than this, but it is enough for explanation purposes.

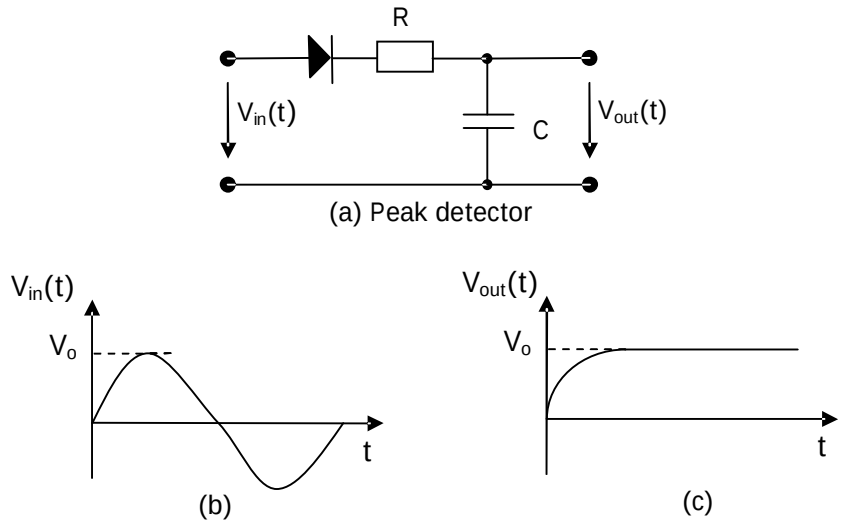

Figure A1-14. Simple peak detector

b) Quasi-peak mode

A simple quasi-peak detector is illustrated in Figure A1-15. (Again, typical quasi-peak detectors are more sophisticated than this, but this circuit will illustrate the essential points and concepts). If the input signal consists of "spikes" that are widely separated in time regarding to the time constant R2·C of the quasi-peak detector, the capacitor will begin to charge until the first spike turns off. It will then discharge through R2. If the next spike occurs after a length of time that allows the capacitor to completely discharge, the waveform shown in Figure A1-15(c) is to appear at the output of the spectrum analyzer. However, if the spikes occur more closely than the constant R2·C, the capacitor will not have fully discharged before the next spike occurs (Figure A1-15(e)). Thus the output signal will continue to increase to some limit. Although this is a simplistic illustration of the function of a quasi-peak detector, it nevertheless illustrates the important point that infrequently occurring signals will result in a measured quasi-peak level that is considerably smaller than a peak detector would give. Thus infrequent events (in relation to the

time constant) may be of sufficient magnitude to give distressingly large received levels on a spectrum analyzer that is set to the peak detector function, yet their quasi-peak levels may not exceed the regulatory limit and are therefore of no consequence. In other words, if the quasi-peak levels exceed the regulatory limits, peak levels will surely exceed the limits (supposing limits are equal for quasi-peak and peak modes).

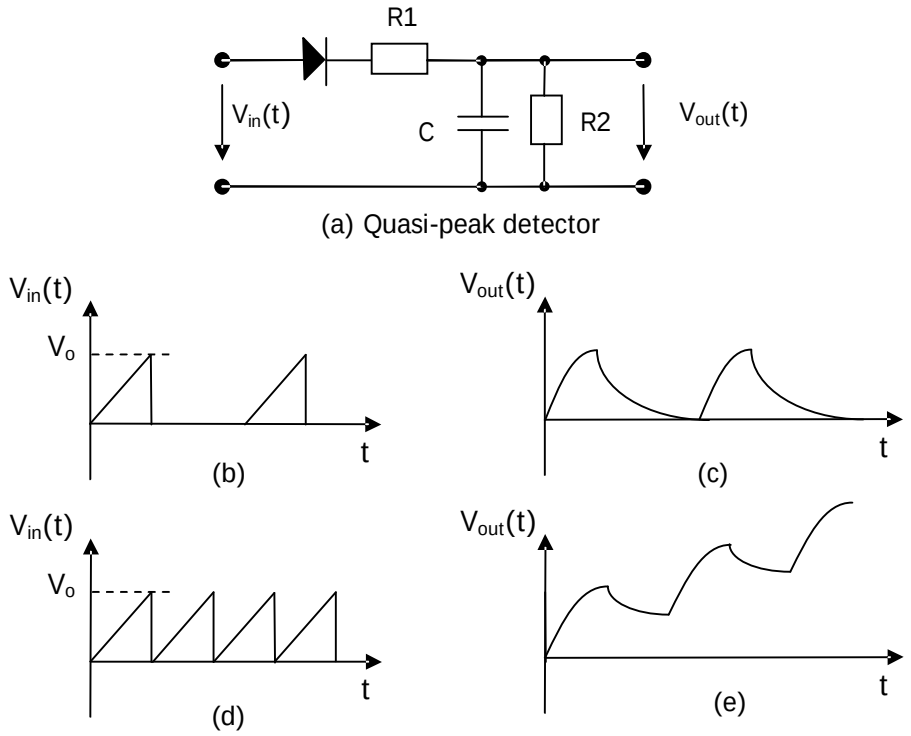

Figure A1-15. Simple quasi-peak detector

The reason to use a quasi-peak detector function is related to the intent of the regulatory limits to prevent interference in radio and wire communication receivers. Infrequent spikes and other events do not substantially prevent the listener from obtaining the desired information. However, a continuous signal modulation results in a continuous detected signal in the radio, and would therefore substantially interfere with the listeners' ability to obtain the desired transmitted information.

c) Average mode

The average levels are obtained with an average detector, which is basically a narrow filter (video filter), placed after the usual envelope detector, that passes only the dc component of the time-varying envelope of the detected waveform. This is useful in uncovering CW (single-frequency or continuous wave) signals that

are buried in a broadband spectrum, as frequently occurs in switching power supply waveforms.

A1.6 Video filtering and display smoothing

Spectrum analyzers display signals plus their own internal noise, as shown in Figure A1-16.

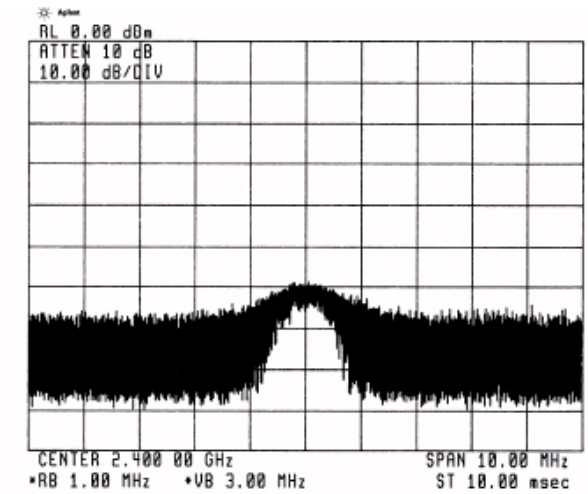

Figure A1-16. Spectrum analyzers display signal plus noise

To reduce the effect of noise on the displayed signal amplitude, it is common to smooth or average the display, as shown in Figure A1-17.

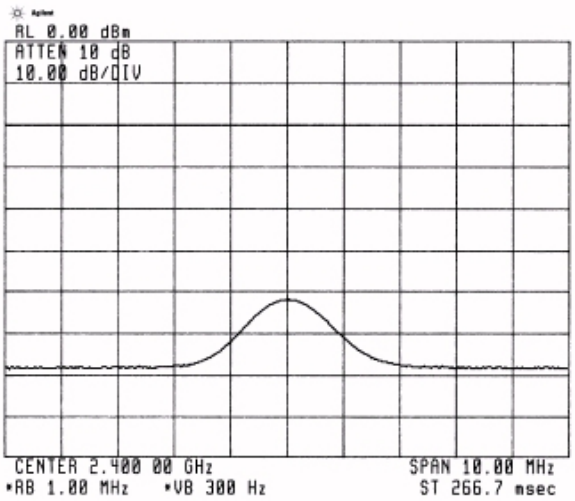

Figure A1-17. Display of Figure A1-16 after full smoothing

Most superheterodyne analyzers include a variable video filter for this purpose. The video filter is a low-pass filter that follows the detector and determines the bandwidth

of the video circuits that drive the vertical deflection system of the display. As the cutoff frequency of the video filter is reduced to the point at which it becomes equal or less than the bandwidth of the selected resolution (IF) filter, the video system can no longer follow the more rapid variations of the envelope of the signals passing through the IF chain. The result is an averaging or smoothing of the displayed signal when noisy signals are present while, at the same time, having no effect on constant signals.

Because the video filter has its own response time, the sweep time gets longer: $ST = k \cdot \frac{Span}{RBW \cdot VBW}$

where:

- RBW is the resolution bandwidth
- VBW is the video bandwidth (the cutoff frequency of the adjustable low-pass filter in the video circuit)
- ST is the sweep time
- Span is the frequency range represented by the horizontal axis of the display, commonly distributed across the full ten divisions in a spectrum analyzer.
- k is a constant of proportionality between 2 and 15.

Most analyzers that sweep time automatically account for video bandwidth as well as span and resolution bandwidth.

ANNEX 2

NORMATIVE REQUIREMENTS TO MEASURE EMI

ANNEX 2:

NORMATIVE REQUIREMENTS TO MEASURE EMI

It is important to clearly specify how product emissions must be measured when attempting to verify compliance with the limits and the limits themselves. Different interpretations of the same normative can give different results of the measured data at different measurement sites. Every standard that sets out limits on radiated and conducted emissions (FCC, CISPR 22 and MIL-STD-461) has a related standard that clearly defines how the data are to be measured. This includes test procedure, test equipment, bandwidth, test antennas, etc. The specification of the method for gathering the data is critically important so that the governing agency can be sure that data gathered on a product at one company's test site can be validly compared to the limits and to data gathered at another test site. Otherwise the governing agency as well as the product manufacturer cannot be assured that the product's emissions comply with the limits. Onwards, a summary of the measurement procedures that apply to the FCC ([RE-4], [RE-5]) and CISPR 22 ([RE-1], [RE-2], [RE-3]) requirements are presented.

A2.1 Radiated emissions

Although radiated emissions are not of complete interest for this thesis, it is worthy to expose some considerations which are useful for an understanding of measuring EMI. When measuring conducted perturbations with a spectrum analyzer, it is normally found a closer relationship between theoretical and measured results, while in the case of radiated emissions, several antenna and transmission factors affect the measured results in such a way that some differences may arise between theoretical and measured values

FCC specifies that the measurements of radiated and conducted emissions must be performed on the complete system. All interconnect cables to peripheral equipment must be connected and the system must be in a typical configuration. Cables and system must also be configured in a representative way such that the emissions are maximized.

The FCC radiated emissions are to be measured at a distance of 10 m for Class A products and 3 m for Class B products. In the same way, CISPR 22 radiated emissions are to be measured at a distance of 30 m for Class A products and 3÷10 m for Class B products. These measurements are to be made over a ground plane using a tuned dipole antenna at an open-field test site. Furthermore, measurements are to be made with the measurement antenna in the vertical position (perpendicular to the ground plane) and in the horizontal position (parallel to the ground plane). In order to cover the range of frequencies, a broadband antenna is usually selected in order not to readjust the antenna in length at each frequency.

The requirement of conducting the test at an open-field test site presents measurement difficulties because of the great pollution of emissions presents around the product under test. To solve this, preliminary screening tests are usually conducted in a semianechoic chamber as illustrated in Figure A2-1. This chamber consists of two parts: (1) a shielded room and (2) radio-frequency absorbing cones lining the walls and the ceiling. The shielded room is intended to prevent external signals from contaminating the test. The absorbing cones are intended to prevent reflections of the emissions from the walls and the ceiling. Reflections can and do occur at the ground plane (floor) of the chamber. The absorbing cones are intended to simulate an open-field site. FCC and CISPR 22 specify that the measurement antenna must also be scanned from a height of 1 m to 4 m above the ground plane and the maximum signal obtained in that scan be recorded for that frequency.

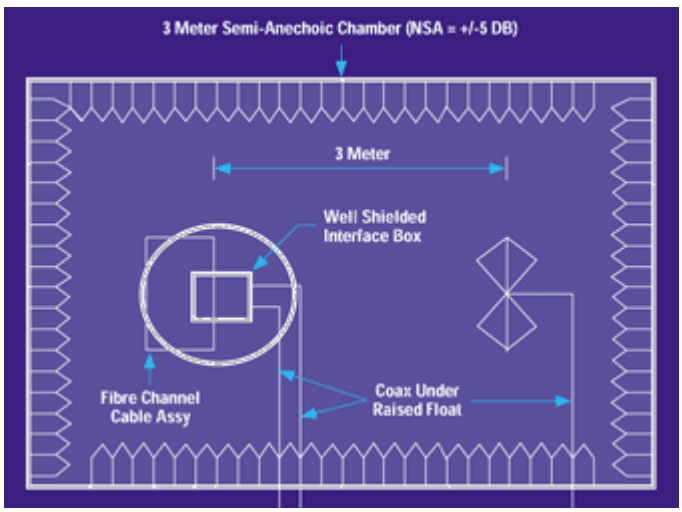

Figure A2-1. Illustration of the use of a semianechoic chamber for the measurement of radiated emissions

One final test requirement needs to be addressed. The FCC and CISPR 22 test procedures specify that the bandwidth (6 dB) of the spectrum analyzer or receiver that is used to measure the radiated emissions must be at least 100 kHz. If the emission at a particular frequency is very narrow, such as a clock harmonic, the bandwidth of the receiver is not of much concern. However, if the emission is due to fairly broadband source, the bandwidth of the receiver directly determines the signal level that is measured: the wider the bandwidth, the larger the measured level.

A related issue is the detector used in the output stage of the receiver. Typical spectrum analyzers use peak detectors that record the maximum signal level at the desired frequency.

A2.2 Conducted emissions

The intent of the conducted emission limits is to restrict the noise current passing out through the product's ac power cord. The reason for this is that these noise currents will be placed on the common power net of the installation. The common power net of an installation is an array of interconnected wires in the installation walls, and as such, represents a large antenna. Noise currents that are placed on this power net will therefore radiate quite efficiently, which can produce interference.

Therefore the conducted emission that should be measured is the noise current conducted out through the ac power cord of the product. Yet the FCC and CISPR conducted emissions limits are given in units of volts. This is because the tests are to be conducted by inserting a line impedance stabilization network (LISN) in series with the ac power cord of the product. In order to understand the performance of this device, a summarized overview of the standard ac power distribution system. In Europe, ac voltage used in residential and business environments has a frequency of 50 Hz and a rms voltage of 220 V (currently, this voltage has been adjusted to 240 V). This power is transmitted to these sites at various other, higher voltages, by a tri-phase system, composed of three wires (called phase wires) and a ground wire connected to earth (neutral wire). The voltage between each two phase wires is 380 V. At the service entrance panel in the home, the 220 V is obtained between one phase wire and the neutral one. A forth or safety wire is carried throughout the residence along with these four wires. Those currents exiting the product via the phase and the

neutral wires are to be measured. Thus, like the radiated emission measurements, two measurements are needed for conducted emissions, phase and neutral.

The LISN and its use are illustrated in Figure A2-2. Two purposes are defining the LISN:

- The first purpose is to prevent EMI from disturbing the measurements. The inductor L_1 blocks noise over the conducted emission frequency range from the product to the ac power cord and vice versa.
- The second purpose is to ensure that measurements made at one test site will be comparable with measurements at another test site. The possibility of this inconsistency between test sites is in the variability of the ac impedance seen looking into the ac power net from site to site. Measurements of the ac impedance seen looking into the ac power net at different locations show variability from site to site in addition to the variability with the frequency. The second purpose of the LISN is, then, to present a constant impedance in frequency and from site to site to the product between phase and ground and between neutral and ground.

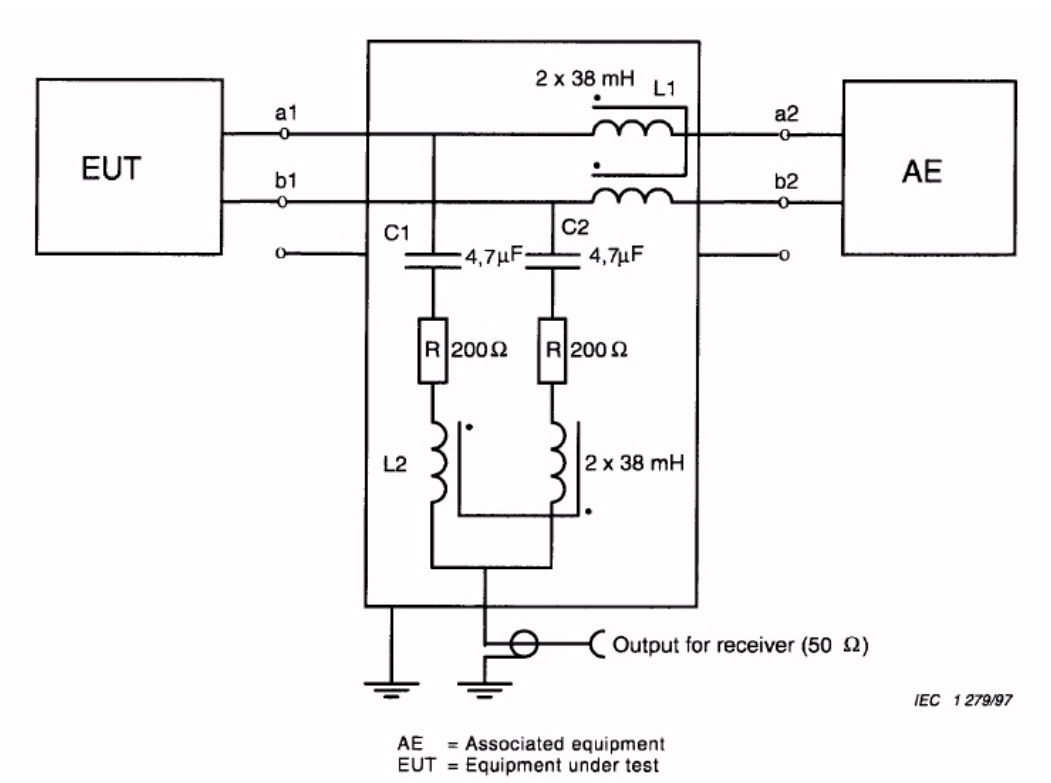

Figure A2-2. LISN for use with unscreened single balanced pairs (CISPR 22, Annex D, Figure D.1)

An output for a receiver (50 Ω) such a spectrum analyzer is available in order to measure the noise spectra flowing out from the product under test. Each voltage (or

the corresponding currents) must be measured over the frequency range fixed by the regulatory normative and the emissions must not exceed the limits established in this normative.

A point of critics to these norms: no difference is established between common- and differential measurement modes. However, solutions to be implemented are very dependant on the problem source, that is, dependant on a common- or differential mode interference.

A2.3 Measurement detector: bandwidth and measure mode

A key ingredient in determining the level that is displayed by the spectrum analyzer at a given frequency is the bandwidth selected on this equipment. The smaller the bandwidth, the higher the possibility to find the lowest possible values on the spectrum analyzer. The regulatory agencies realize this so they set a minimum bandwidth to be used for the measurement.

a) CISPR 22 & 16-1:

CISPR 22 establishes that measurement must be carried out using quasi-peak and average detector receivers. Anyway, to reduce testing time, a peak detector receiver may be used instead of these two last ones. In case of dispute, measurements with a quasi-peak detector receiver will take precedence when measuring to the quasi-peak limits and the same for average measurements. Table A2-1 summarizes the requirements of CISPR 22 (and its corresponding CISPR 16-1) for both bandwidths (6 dB) and measure mode at the different ranges of frequencies when measuring with spectrum analyzers or scanning receivers:

CISPR 22 CISPR 16-1	Band A 9 kHz÷150 kHz	Band B 150 kHz÷30 MHz	Band C 30 MHz÷300 MHz	Band D 300 MHz÷1 GHz
Quasi-peak detector receiver	220 Hz	9 kHz	120 kHz	120 kHz
Peak detector receiver	100 Hz÷300 Hz (preferred 200 Hz)	8 kHz÷10 kHz (preferred 9 Hz)	100 kHz÷500 kHz (preferred 120 kHz)	100 kHz÷500 kHz (preferred 120 kHz)
Average detector receiver	100 Hz÷300 Hz (preferred 200 Hz)	8 kHz÷10 kHz (preferred 9 Hz)	100 kHz÷500 kHz (preferred 120 kHz)	100 kHz÷500 kHz (preferred 120 kHz)

Table A2-1. CISPR 22: bandwidths (6 dB) and measure modes

From the values listed above, a common bandwidth can be established for the three measure modes: quasi-peak, peak and average. As it is easy to derive from Table A2-1, quasi-peak detector values can be taken as the common ones.

b) FEDERAL COMMUNICATIONS COMMISSION (FCC):

As specified at Title 47, Chapter I, Part 15, Subpart A and Section 15.35, on any frequency or frequencies below or equal to 1000 MHz, the limits are based on measuring equipment employing a CISPR 16-1 quasi-peak detector function and related measurement bandwidths, unless otherwise specified. As an alternative to CISPR quasi-peak measurements, the responsible party, at its option, may demonstrate compliance with the emission limits using measuring equipment employing a peak detector function, properly adjusted for such factors as pulse desensitization, as long as the same bandwidths as indicated for CISPR quasi-peak measurements are employed. Thus, Table A2-1 above is also valid for FCC measuring purposes.

ANNEX 3

CONCEPTS OF FOURIER TRANSFORM

ANNEX 3:

CONCEPTS OF FOURIER TRANSFORM

Although this chapter is not intended to be a reference of the Fourier transform, some concepts and expression must be presented in order to make the understanding of the thesis easier. Theoretical part of the thesis is completely based on the fundaments of the Fourier Transform and, moreover, in its computational implementation through the Fast Fourier Transform (FFT). Literature and references for a wider explanation of Fourier Transform is numerous and the reader is referred to them ([RD-10], [RD-11]).

The essence of the Fourier transform of a waveform is to decompose or separate the waveform into a sum of sinusoids of different frequencies. If these sinusoids sum to the original waveform then the Fourier transform of the waveform has been determined. The pictorial representation of the Fourier transform is a diagram which displays the amplitude and frequency of each of the determined sinusoids.

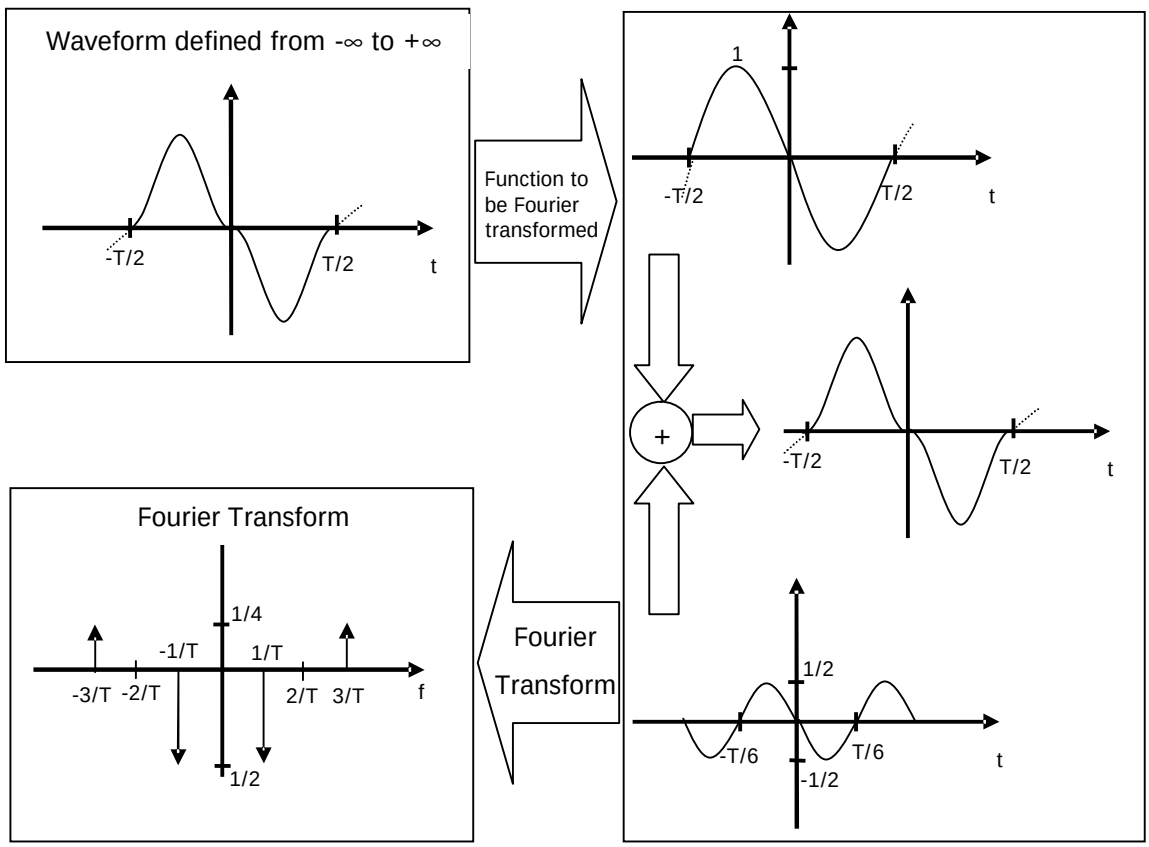

Figure A3-1. Interpretation of the Fourier transform

A usual convention is displaying both positive and negative frequency sinusoids for each frequency and halving the amplitude accordingly, as shown in Figure A3-1.

The Fourier transform identifies or distinguishes the different frequency sinusoids (and their respective amplitudes) which combine to form an arbitrary waveform. Mathematically, this relationship is stated as

$$H(f) = \int_{-\infty}^{\infty} h(t) \cdot e^{-j2\pi \cdot f \cdot t} dt \qquad \text{(A3 -1)}$$

where h(t) is the waveform to be decomposed into a sum of sinusoids and H(f) is the Fourier transform of h(t). Note that the Fourier transform is not of easy interpretation (as expressed above) because it is defined from -∞ to +∞.

It is normally associated the analysis of periodic functions such a square wave with Fourier series rather than Fourier transforms but it is easy to demonstrate that Fourier series is a special case of the Fourier transform.

If the waveform h(t) is not periodic then the Fourier transform will be a continuous function of frequency; that is, h(t) is represented by the summation of sinusoids of all frequencies. In order to illustrate this aspect, consider the pulse waveform and its Fourier transform shown in Figure A3-2. In this example, the Fourier transform indicates that one sinusoid frequency becomes indistinguishable from the next and, as a result, all frequencies must be considered.

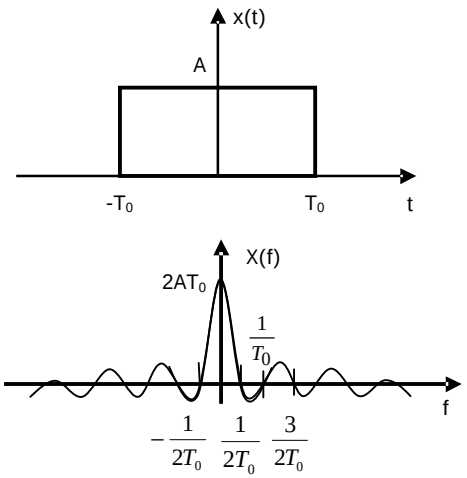

Figure A3-2. Fourier Transform of a pulse waveform

The Fourier transform is then a frequency domain representation of a continuous function. Of course, both h(t) and H(f) contain the same information differing only in

the manner of presenting this information. Fourier analysis allows one to examine a function from another point of view, the transform domain.

In general, the Fourier transform is a complex quantity:

$$H(f) = R(f) + jI(f) = |H(f)| \cdot e^{j\theta(f)} \qquad \text{(A3-2)}$$

where:

- R(f) is the real part of the Fourier Transform
- I(f) is the imaginary part of the Fourier transform
- |H(f)| is the amplitude of Fourier spectra of h(t) and is given by $\sqrt{R^2(f) + I^2(f)}$
- θ(f) is the phase angle of the Fourier transform and is given by $\tan^{-1}\left(\frac{I(f)}{R(f)}\right)$

A3.1 Fourier series

In the technical literature, Fourier series is normally developed independently on the Fourier integral in expression (A3-1). However, with the introduction of distribution theory, Fourier series can be theoretically derived as a special case of the Fourier integral.

Fourier series is a common way of expressing any periodic signal as a sum of its harmonic components [RD-1]:

$$F(t) = F_0 + \sum_{h=1}^{\infty} F_h(t) \qquad \text{(A3-3)}$$

where F_0 represents the average (dc) component of the original signal and F_h, each one of the infinity of harmonics.

Periodic signals can be represented as linear combinations or more basic signals that are referred to as basis functions and denoted as $\phi_n(t)$:

$$x(t) = \sum_{n=0}^{\infty} c_n \cdot \phi_n(t) \qquad \text{(A3-4)}$$

The trigonometric Fourier series uses the sinusoidal basis functions (orthogonal functions as required):

$$\phi_n = \begin{cases} 1 & for\ n = 0 \\ \cos\left(2\pi n \frac{t}{T}\right) & \\ \sin\left(2\pi n \frac{t}{T}\right) & for\ n = 1,2,3... \end{cases} \qquad \text{(A3-5)}$$

The series expansion of x(t) in expression (A3-4) with period T becomes:

$$x(t) = a_0 + \sum_{n=1}^{\infty} a_n \cdot \cos\left(2 \cdot \pi \cdot n \cdot \frac{t}{T}\right) + \sum_{n=1}^{\infty} b_n \cdot \sin\left(2 \cdot \pi \cdot n \cdot \frac{t}{T}\right) \qquad \text{(A3-6)}$$

where the expansion coefficients are:

$$a_0 = \frac{1}{T}\int_0^T x(t) \cdot dt \qquad \text{(A3-7)}$$

$$a_n = \frac{2}{T}\int_0^T x(t) \cdot \cos\left(2 \cdot \pi \cdot n \cdot \frac{t}{T}\right) \cdot dt \qquad \text{(A3-8)}$$

$$b_n = \frac{2}{T}\int_0^T x(t) \cdot \sin\left(2 \cdot \pi \cdot n \cdot \frac{t}{T}\right) \cdot dt \qquad \text{(A3-9)}$$

and a_0 is the average value of the signal. The terms for n=1 are referred to as the fundamental frequency terms, with fundamental radian frequency $\omega_0 = 2\pi/T$ or cyclic frequency $f_0 = 1/T$. The n=2 terms are referred to as the second-harmonic terms with frequency $2 \cdot f_0 = 2/T$, the n=3 terms are referred to as the third-harmonic terms with frequency $3 \cdot f_0 = 3/T$ and so on.

The trigonometric Fourier series can be written in an equivalent but more useful form, referred to as the complex exponential form, as follows. From Euler's identity, the expressions below can be derived:

$$\cos \omega t = \frac{e^{j\omega t} + e^{-j\omega t}}{2} \qquad \text{(A3-10)}$$

$$\sin \omega t = \frac{e^{j\omega t} - e^{-j\omega t}}{2j} \qquad \text{(A3-11)}$$

The complex-exponential form of the Fourier series can be derived by substituting (A3-10) and (A3-11) into (A3-6) and becomes:

$$x(t) = \sum_{n=-\infty}^{n=\infty} c_n \cdot e^{jn\omega_0 t} \qquad \text{(A3 -12)}$$

where the expansion coefficients are given by:

$$c_n = \frac{1}{T}\int_0^T x(t) \cdot e^{-jn\omega_0 t}\, dt \qquad \text{(A3 -13)}$$

Note that the complex form of the Fourier series contains, in addition to positive-valued harmonic frequencies ω_0, $2\omega_0$, $3\omega_0$,..., negative-valued harmonics $-\omega_0$, $-2\omega_0$, $-3\omega_0$,... In addition, the expansion coefficients c_n may be complex-valued, whereas the expansion coefficients in the trigonometric Fourier series are real-valued. At first glance, it may seem that the physical intuition present in the trigonometric Fourier series has been lost in the complex form, but this is not the case. Note that for each positive value of n there is a corresponding negative value of n. Coefficients c_n and c_{-n} are the conjugates of each other:

$$c_{-n} = \frac{1}{T}\int_0^T x(t) \cdot e^{jn\omega_0 t}\, dt = c_n^* \qquad \text{(A3 -14)}$$

and can also be expressed as follows:

$$c_n = |c_n| \angle c_n = |c_n| \cdot e^{j\angle c_n} \qquad \text{(A3 -15)}$$

$$c_n^* = |c_n| \cdot e^{-j\angle c_n} \qquad \text{(A3 -16)}$$

The complex-exponential form in expression (A3-12) may be written as

$$x(t) = c_0 + \sum_{n=1}^{\infty} c_n \cdot e^{jn\omega_0 t} + \sum_{n=-1}^{-\infty} c_n \cdot e^{jn\omega_0 t} \qquad \text{(A3 -17)}$$

Changing the second summation to positive n gives:

$$x(t) = c_0 + \sum_{n=1}^{\infty} c_n \cdot e^{jn\omega_0 t} + \sum_{n=1}^{\infty} c_n^* \cdot e^{-jn\omega_0 t} \qquad \text{(A3 -18)}$$

Substituting (A3-15) and (A3-16) into (A3-18) gives:

$$x(t) = c_0 + \sum_{n=1}^{\infty} |c_n| \cdot e^{j(n\omega_0 t + \angle c_n)} + \sum_{n=1}^{\infty} |c_n| \cdot e^{-j(n\omega_0 t + \angle c_n)} \qquad \text{(A3 -19)}$$

$$= c_0 + \sum_{n=1}^{\infty} |c_n| \left(e^{j(n\omega_0 t + \angle c_n)} + e^{-j(n\omega_0 t + \angle c_n)} \right) \qquad \text{(A3 -20)}$$

$$x(t) = c_0 + \sum_{n=1}^{\infty} 2 \cdot |c_n| \cdot \cos\left(n\omega_0 t + \angle c_n\right) \qquad \text{(A3 -21)}$$

Therefore, in order to obtain the expansion coefficients for the one-sided spectrum (positive frequencies only), the coefficients c_n for the double-sided spectrum must be doubled while the dc component remains unchanged. Note that expression (A3-21) is formally identical to that exposed in expression (A3-3).

A3.2 Discrete Fourier transform

Because of the wide range of problems which are susceptible to be solved by means of the Fourier transform, particularly the spectral components of a waveform as a result of a modulation process, it is expected the logical extension of Fourier transform to the digital computation. However, discretization implies the answer to the difficult question of knowing how the discrete Fourier Transform relates to the continuous Fourier Transform. In order to answer this question, it is normally found preferable to derive the discrete Fourier Transform as a special case of the continuous Fourier transform theory.

Numerical integration of equation (A3-1) implies the relationship

$$H\left(\frac{n}{NT}\right) = \sum_{k=0}^{N-1} h(kT) \cdot e^{-j \cdot 2 \cdot \pi \cdot n \cdot k / N} \qquad n = 0, 1, \text{L}, N-1 \qquad \text{(A3-22)}$$

Expression (A3-22) is also known as Discrete Fourier Transform where:

- T is the sampling interval.
- N is the number of equidistant samples inside the truncation interval T_0.

The expression (A3-22) relates N samples of time and N samples of frequency by means of the continuous Fourier transform. The discrete Fourier transform is then a special case of the continuous Fourier transform. If it is assumed that the N samples of the original function h(t) are one period of a periodic waveform, the Fourier transform of this periodic function is given by the N samples as computed by (A3-22).

The discrete Fourier is of interest primarily because it approximates the continuous Fourier transform. The validity and accuracy of this approximation is strictly related to

the waveform under analysis. Differences normally arise because of the discrete transform requirements for sampling and truncation. Onwards, a special attention will be focused on the band-limited periodic functions where the truncation interval is equal to the period of the signal, because these are the kind of signals to be found through the development of the thesis.

A3.2.1 Band-Limited Periodic Waveforms: Truncation Interval Equal to Period

Consider the function h(t) and its Fourier transform illustrated in Figure A3-3. The idea is to sample h(t), truncate the sampled function to N samples and, finally, apply the discrete Fourier transform according to expression (A3-22). A graphical development of this process is shown is Figure A3-3. Waveform h(t) is sampled by multiplication with the sampling function illustrated in Figure A3-3(b). Sampled waveform h(kT) and its Fourier transform are illustrated in Figure A3-3(c). Note that for this example there is no aliasing and that, as a result from time domain sampling, the frequency domain has been scaled by the factor 1/T; the Fourier transform impulse now has an area of A/2T rather than the original area of A/2. The sampled waveform is truncated by multiplication with the rectangular function illustrated in Figure A3-3(d); Figure A3-3(e) illustrates the sampled and truncated waveform. As shown, the rectangular function was selected so that the N sample values remaining after truncation equate to one period of the original waveform h(t).

The Fourier transform of the finite length sampled waveform [Figure A3-3(e)] is obtained by convolving the frequency domain impulse functions of Figure A3-3(c) and the sin f/f frequency function of Figure A3-3(d). Figure A3-3(e) illustrates the convolution results: an expanded view of this convolution is shown in Figure A3-4(b). A sin f/f function (dashed line) is centered on each impulse of Figure A3-4(a) and the resultant waveforms are additively combined (solid line) to form the convolution result.

With respect to the original transform H(f), the convolved frequency function [Figure A3-4(b)] is significantly distorted. However, when this function is sampled by the frequency sampling function illustrated in Figure A3-3(f) the distortion is eliminated. This follows because the equidistant impulses of the frequency sampling functions are separated by $1/T_0$; at these frequencies the solid line of Figure A3-4(b) is zero except at the frequency $1/T_0$.

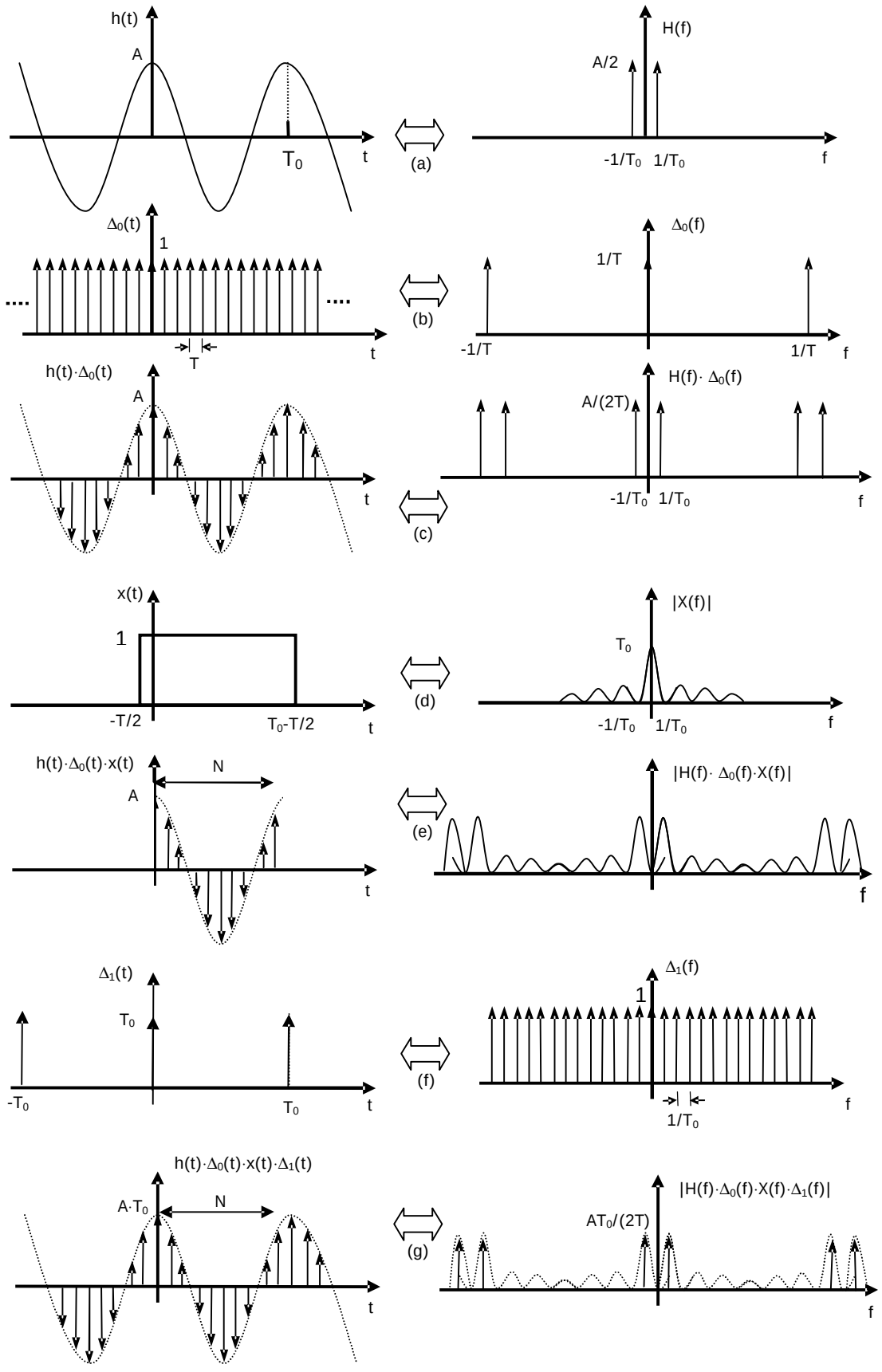

Figure A3-3. Discrete Fourier Transform of a band-limited waveform when T_0=truncation interval

Frequency $1/T_0$ corresponds to the frequency domain impulses of the original frequency function H(f). Because of time domain truncation, these impulses have now an area of $AT_0/2T$ rather than the original area of A/2. Figure A3-4(b) does not take into account that the Fourier transform of the truncation function x(t) illustrated in Figure A3-3(d) is actually a complex frequency function; however, the same results would have been obtained if considering a complex function.

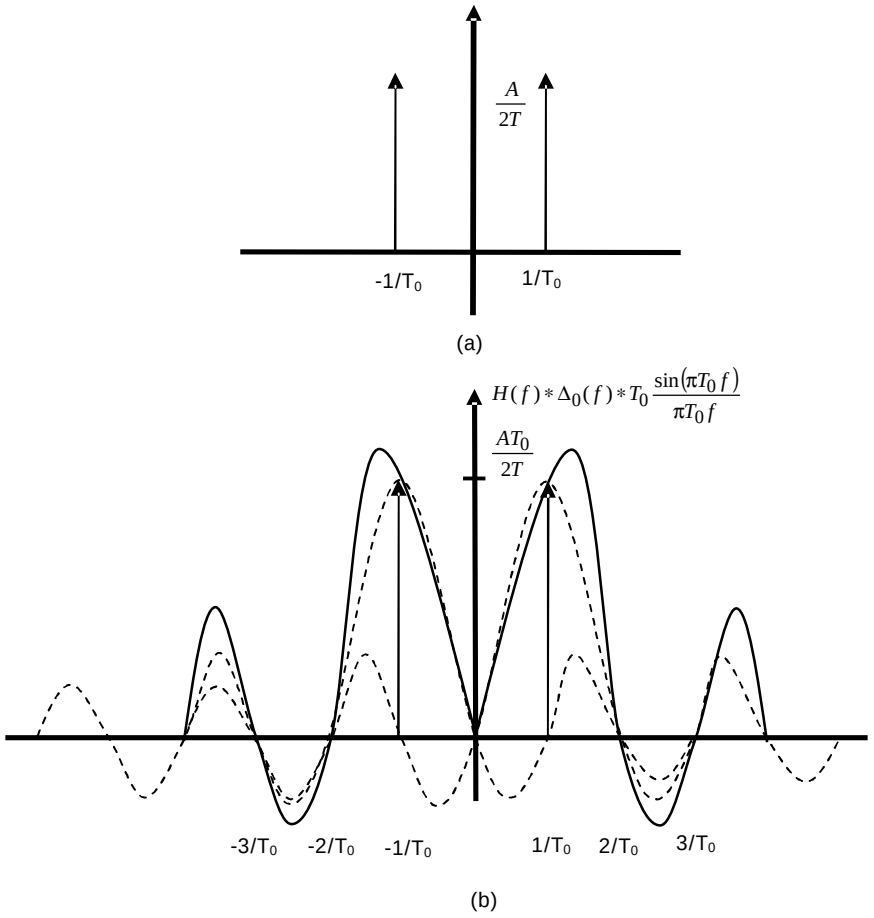

Figure A3-4. Expanded illustration of the convolution of Fig. A3-3(c)

Multiplication of the frequency function of Figure A3-3(e) and the frequency sampling function $\Delta_1(f)$ implies the convolution of the time functions shown in Figures A3-3(e) and (f). Because the sampled truncated waveform [Figure A3-3(e)] is exactly one period of the original waveform h(t) and since the time domain impulse functions of Figure A3-3(f) are separated by T_0, then their convolution yields a periodic function as illustrated in Figure A3-3(f). This is simply the time domain equivalent to the previously discussed frequency sampling which yielded only a single impulse or frequency

component. The time function of Figure A3-3(g) has maximum amplitude of AT_0, compared to the original maximum value of A as a result from the frequency domain sampling.

Examination of Figure A3-3(g) indicates the process corresponds to take the original time function, sample it and then multiply each sample by T_0. The Fourier transform of this function is related to the original frequency function by the factor $AT_0/2T$. Factor T_0 is common and can be eliminated. To compute the continuous Fourier transform by means of the discrete Fourier transform, it is necessary to multiply the discrete time function by the factor T which yields the desired A/2 area for the frequency function. Equation (A3-22) thus becomes

$$H(\frac{n}{NT}) = T \cdot \sum_{k=0}^{N-1} h(kT) \cdot e^{-j \cdot 2 \cdot \pi \cdot n \cdot k / N} \qquad n = 0, 1, \text{L}, N-1 \qquad \text{(A3-23)}$$

This example represents the only class of waveforms for which the discrete and continuous Fourier transforms are exactly the same within a scaling constant. Equivalence of the two transforms requires:

- The time function h(t) must be periodic
- h(t) must be band-limited
- the sampling rate must be at least two times the largest frequency component of h(t) è Nyquist's theorem
- the truncation function x(t) must be non-zero over exactly one period (or integer multiple period) of h(t)

A3.2.2 Truncation windows

In those real situations where the signal spectral content is initially unknown and, for instance, a digital spectrum analyzer is to be used to obtain these spectrum, the truncation window shape determines the side-lobes shape given by the DFT (again, when the truncation window width does not equates the signal period):

a) Rectangular window

The Fourier transform of this window (see Figure A3-6) shows a narrow main lobe and infinite side lobes decreasing gradually. The main problem is that these side lobes are able to hide true spectral lines in the neighbourhood. The distance between zeros of the main lobe is 2·F and the first side lobe is at 13.3 dB under the main lobe. This

window is not recommended to use it together with spectral analyzers but only as a conceptual understanding tool of the DFT (and, therefore, of the FFT).

b) Hanning window

The Fourier transform of a Hanning window results in a main lobe wider than that obtained for the rectangular window but side lobes disappearing quickly. The main lobe width is of 4·F (where F=1/T, and T is the window width, according to Figure A3-5) and the first side lobe appears at 31.5 dB under the main lobe. This window generates considerable measure errors (although lower than 1.5 dB). However, it is recommended to display the resulting spectra because of the better qualitative results.

c) Flattop window

In this case, the main lobe (resulting from the application of the Fourier transform) is wider than those obtained in the two previous windows; however, the side lobes decrease in the frequency domain very quickly. The main lobe width is of 8·F and the first side lobe is at 70.4 dB under the main lobe. This window is recommended to measure harmonics properly, because of the low measure error (lower than 0.1 dB). However, it is not recommended to distinguish close frequencies because of its wide main lobe and the mentioned problem of hiding neighbour frequencies.

These three windows and the related Fourier transforms are shown in the following pictures (Figures A3-5 and A3-6) [RC-18]:

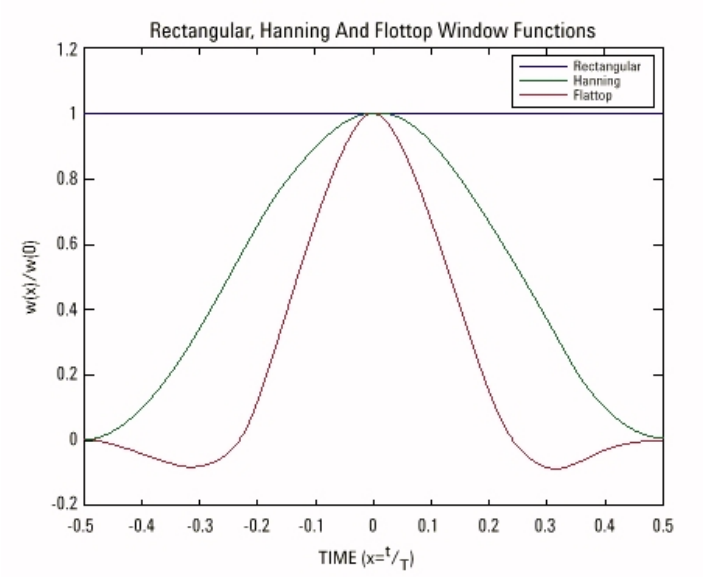

Figure A3-5. Rectangular, Hanning and Flattop Window Functions

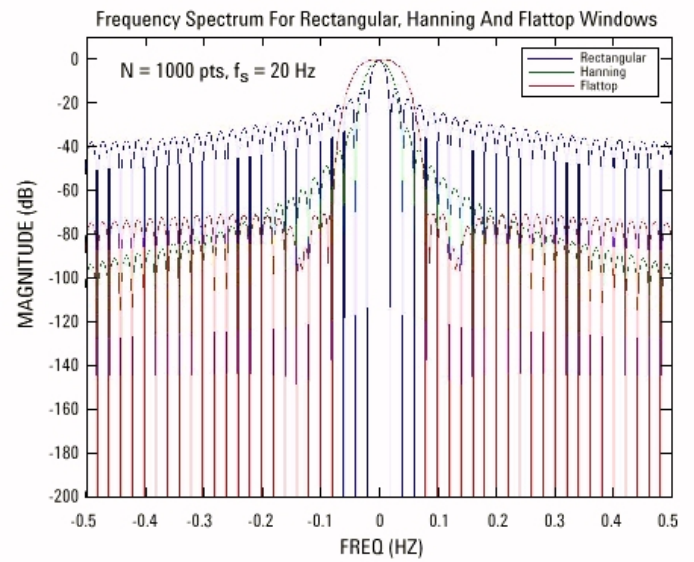

Figure A3-6. Rectangular, Hanning and Flattop Window frequency spectrum

A3.3 Fast Fourier Transform (FFT)

Interpretation of Fast Fourier Transform results does not require a well-grounded education in the algorithm itself but rather a through understanding of the discrete Fourier transform. This follows from the fact that the FFT is simply an algorithm (i.e., a particular method of performing a series of computation) that can compute the discrete Fourier transform much more quickly than other available algorithms.

A careful inspection of equation (A3-22) reveals that if there are N data points of the function h(kT) and it is desired to determine the amplitude of N separate sinusoids, then computation time is proportional to N^2, the number of complex multiplications.

An obvious requirement existed for the development of techniques to reduce the computing time of the discrete Fourier transform. In 1965, Cooley and Tukey published their mathematical algorithm which has become known as the Fast Fourier Transform [Reference "Cooley, J. W., and Tukey, J. W., "An algorithm for the machine calculation of complex Fourier series", Mathematics of Computation (1965), Vol. 19, No. 90, pp. 297-301"].

The Fast Fourier Transform is a computational algorithm (implementing the Discrete Fourier Transform) which reduces the computing time of expression (A3-22) to a time proportional to $N \cdot \log_2 N$.

ANNEX 4

MATLAB ALGORITHM CODE LINES

ANNEX 4:

MATLAB ALGORITHM CODE LINES

```
% File name: SSCG.m
% Creation date: 01.01.2001
% Last update date: 31.10.2003
% Comments: Frequency modulation of a sinusoidal waveform by using a selectable modulation profile.
% Only symmetrical modulation around the carrier signal.
% Note: Due to the selection of a complete period of the modulated signal (equal to 1/fm), no aliasing
effect is present and, theferore, computed values match exactly the theoretical ones.

% Preparing the workspace

clear all;                          % Removes all variables, functions and MEX links from the
                                    % current workspace
clf reset;                          % Deletes everything and also resets all figure properties,
                                    % except position, to their default values
printyn = 1;                        % Control variable to plot modulation profile, its integral and
                                    % the resulting frequency spectra: 1 = yes; 0 = no

% 1.- Definitions and parameters

fc = 1.2e+5;                        % Frequency (Hz) of the sinusoidal signal to be modulated
                                    % (carrier waveform)
fm = 1e+3;                          % Frequency (Hz) of the modulating signal

Tc = 1/fc;                          % Period of the signal to be modulated
Tm = 1/fm;                          % Period of the modulating signal
                                    % WARNING: So that the MATLAB function fft() works
                                    % properly, the ratio fc/fm must be integer
amp_c = 0.5;                        % Peak amplitude of the carrier signal (then,
                                    % pk2pk=2*amp_m) expressed in volts.
amp_m = 0.5;                        % Peak amplitude of the modulating signal (then,
                                    % pk2pk=2*amp_m) expressed in volts. This value does not
                                    % take part directly in the calculation of the spectra; its true
                                    % influence is related to the algorithm through delta_fc (see
                                    % below), because Kw * amp_m = 2* pi * delta_fc (see
                                    % point 2.3.2). It is only intended for graphic representation
                                    % purposes.


pi = 3.1415926;

s = 0.5;                            % Only for triangular modulation profile (see 2.3.2.2)

for delta = 10:10                   % delta è  percentage of modulation expressed in %,
                                    % that is, delta = 10 means 10% (see point 2.1.1.2.1)

% Some initializations

  vm = 0;                           % Initial value of the modulating waveform (see 2.3.2)
  theta = 0;                        % Initial value of the time-dependant angle (see 2.3.2)

% Some necessary calculations

  if rem(fc,fm) > 0                 % Because of the necessity of a ratio fc/fm integer
    fm = fc/(fix(fc/fm)+1)          % we choose the nearest frequency fm towards zero
```

```
  end                                   % which makes fc/fm integer

  ratio=fc/fm                           % Just to check that fc/fm is integer
  Tm = 1 / fm;                          % A recalculation of Tm is mandatory, mainly if fm changed

  delta_fc = delta/100*fc               % Peak deviation of the carrier signal (see point 2.1.1.1)
  mf = delta_fc/fm                      % Modulation index (see 2.1.1.1)

  bandwidth = 2*delta_fc+2*fm;          % Bandwidth of the spectra resulting from the modulation
                                        % (direct application of the Carson's rule) [see point 2.1.2]
                                        % Necessary to estimate the Nyquits's sampling frequency.

% 2.- Process of calculation

% 2.1.- Calculation of the number of points (power of 2) to compute the FFT

 fmax = fc+2.5*bandwidth                % Maximum frequency to be found after modulation
                                        % Because the Carson's bandwidth does not take into
                                        % account the whole spectra (only the 98% of the energy)
                                        % an extra range over this bandwidth is necessary.

fsampling = 2 * fmax                    % Direct expression of the Nyquist's theorem: the sampling
                                        % frequency must be at least twice the maximum frequency
                                        % of the original signal.

p = fix(log2(fsampling/fm))+1           % Requirement of FFT is a number of points being a power
                                        % of 2
N = 16*pow2(p)                          % Total number of samples to compute the FFT
fsampling = fm * N                      % Final sampling frequency (actual)


% 2.2. Selection of the modulating signal

% opc = 1       Sinusoidal
% opc = 2       Triangular
% opc = 3       Exponential
% opc = 4       Sampled modulation profile
% opc = 5       Mixed (triangular + exponential)
% opc = 6       Mixed (exponential + exponential)

opc = 1;                                % Variable to select the modulation signal

% 2.2.1.- Sinusoidal frequency modulation of a sinusoidal carrier (see 2.3.2.1)

  if opc == 1                           % Sinusoidal modulation
    k = 1:N;                            % Although in 2.3.2.4, k = 0..N-1, for convenience a range
                                        % from 1 to N is here selected

    t = k*Tm/N;                         % Discretization in the time domain of the resulting
                                        % waveform period which is always Tm è sample spacing

    vm = amp_m*sin(fm*t*2*pi);          % Expression of the modulating waveform, only for
                                        % representation purposes

    theta = mf * (1- cos(fm*t*2*pi));   % Integral of the modulating waveform

    f = amp_c*cos(fc*t*2*pi + theta);   % Modulated waveform
  end

  if opc == 2                           % Triangular modulation (see 2.3.2.2)

    for k=1:N                           % Although in 2.3.2.4, k = 0..N-1, for convenience a range
```

```
                                        % from 1 to N is here selected

    t= k*Tm/N;                          % Discretization in the time domain of the resulting
                                        % waveform period which is always Tm è sample spacing

    if k <= s*N/2
      vm(k)=2*amp_m*fm/s*t;             % Expression of the modulating waveform
      theta(k)=2*pi*delta_fc*fm*t*t/s;  % Integral of the modulating waveform

    elseif k > s*N/2 & k <= N*(1-s/2)
      vm(k)=amp_m/(1-s)*(1-2*fm*t);
      theta(k)=theta(s*N/2)+2*pi*delta_fc/(1-s)*(-fm*t*t+t+s/(2*fm)*(s/2-1));
                                        % In order to use theta(s*N/2) this way, s must be
                                        % equal to 1/even_number
    elseif k > N*(1-s/2) & k <= N
                vm(k)=2*amp_m/s*(fm*t-1);
                theta(k)=theta(N*(1-s/2))+2*pi*delta_fc*1/s*(fm*t*t-2*t+(1-s*s/4)/fm);
                                        % In order to use theta(N*(1-s/2)) this way, s must be
                                        % equal to 1/even_number

    end

    f(k)=amp_c*cos(fc*t*2*pi + theta(k));          % Modulated waveform
  end
end

if opc == 3                             % Exponential modulation (see 2.3.2.3)

  p=12*fm;                              % Parameter defining the curvature grade of the exponential

  R=1/(exp(p/(4*fm))-1);                % Common factor to improve computing time

  for k=1:N                             % Although in 2.3.2.4, k = 0..N-1, for convenience a range
                                        % from 1 to N is here selected

    t= k*Tm/N;                          % Discretization in the time domain of the resulting
                                        % waveform period which is always Tm è sample spacing

    if k <= N/4
      vm(k) = amp_m*R*(exp(p*t)-1);     % Expression of the modulating waveform
                                        % Integral of the modulating waveform
      theta(k) = 2*pi*delta_fc*R/p*(exp(p*t)-p*t-1);

    elseif k > N/4 & k <= N/2
      vm(k) = amp_m*R*(exp(p/(2*fm))*exp(-p*t)-1);
      theta(k) = theta (N/4)+2*pi*delta_fc*R/p*(-exp(-p*t)*exp(p/(2*fm))+exp(p/(4*fm))-
              p*t+p/(4*fm));
    elseif k > N/2 & k <= 3*N/4
      vm(k) = amp_m*R*(1-exp(-p/(2*fm))*exp(p*t));
      theta(k) = theta(N/2)+2*pi*delta_fc*R/p*(-exp(p*t)*exp(-p/(2*fm))+p*t-p/(2*fm)+1);

    elseif k > 3*N/4 & k <= N
      vm(k) = amp_m*R*(1-exp(p/fm)*exp(-p*t));
      theta(k) = theta(3*N/4)+2*pi*delta_fc*R/p*(exp(-p*t)*exp(p/fm)-exp(p/(4*fm))+p*t-3/4*p/fm);
    end
  vm(N) = 0;
  theta(N) = 0;
  f(k)=amp_c*cos(fc*t*2*pi + theta(k));  % Modulated waveform
  end
end

if opc == 4                             % Sampled modulation profile (see 2.3.2.4)
```

```
                                        % No offset considered
    load filename.txt                   % The file containing the discrete samples has the following
    vm = filename;                      % structure (text file, separators are feedlines):
    NP = filename (1);                  % first line: number of samples or points below (NP)
    i = 1:NP;                           % next lines: value (in volt) of the samples (vm)
    vm(i) = filename (i+1);
    suma_vm = vm(1);
    i = 1;
    theta(1) = 0;                       % Keep in mind that NP*ΔT = N*ΔT_N = T_m and this is a
    for k=1:N                           % condition to produce the sample file
      t=(k-1)/(N*fm);
      if NP*(k-1) >= i*N;               % and the reason for this inequality to work properly
        i = i +1;
        suma_vm = suma_vm + vm(i);
        theta(i) = 2*pi/NP/fm*(delta_fc * suma_vm);
                                        % Expression (2-117) in point 2.3.2.4

      end
      f(k)=amp_c*cos(fc*t*2*pi + theta(i));
    end
  end

  if opc == 5                           % Mixed (triangular + exponential)

    p=12*fm;
    R=1/(exp(p/(4*fm))-1);

    for k=1:N
      t= k*Tm/N;
      if k <= N/4
        vm(k) = amp_m*R*(exp(p*t)-1);
        theta(k) = 2*pi*delta_fc*R/p*(exp(p*t)-p*t-1);
      elseif k <= 3*N/4
        vm(k)=2*amp_m*(1-2*fm*t);
        theta(k)=theta(N/4)+4*pi*delta_fc*(-fm*t*t+t-3/(16*fm));
      elseif k <= N
        vm(k) = amp_m*R*(1-exp(p/fm)*exp(-p*t));
        theta(k) = theta(3*N/4)+2*pi*delta_fc*R/p*(exp(-p*t)*exp(p/fm)-exp(p/(4*fm))+p*t-3/4*p/fm);
      end

      f(k)=amp_c*cos(fc*t*2*pi + theta(k));
    end
  end

  if opc == 6                           % Mixed (exponential + exponential)

    p=15*fm;
    R=1/(exp(p/(4*fm))-1);
    for k=1:N
      t= k*Tm/N;
      if k <= N/4
        vm(k) = amp_m*R*(exp(p*t)-1);
        theta(k) = 2*pi*delta_fc*R/p*(exp(p*t)-p*t-1);
      elseif k > N/4 & k <= N/2
        vm(k) = 1+amp_m*R*(1-exp(-p/(2*fm))*exp(p*t));
        theta(k) = theta(N/4) + 2*pi*delta_fc*((t-Tm/4)*(1+R)-R/p*(exp(-p*Tm/4)*exp(p*t)-1));
      elseif k > N/2 & k <= 3*N/4
        vm(k) = amp_m*R*(exp(p*3/(4*fm))*exp(-p*t)-1)-1;
        theta(k) = theta(N/2) - 2*pi*delta_fc*(R/p*exp(p*Tm/4)*(exp(p*Tm/2)*exp(-p*t)-1)+(t-
                   Tm/2)*(1+R));
      elseif k > 3*N/4 & k <= N
        vm(k) = amp_m*R*(1-exp(p/fm)*exp(-p*t));
```

```
        theta(k) = theta(3*N/4)+2*pi*delta_fc*R/p*(exp(-p*t)*exp(p/fm)-exp(p/(4*fm))+p*t-3/4*p/fm);
      end
    f(k)=amp_c*cos(fc*t*2*pi + theta(k));
    end
  end

% 2.3.- Calculation of the FFT

  Y = fft(f,N);
  Y = Y(1:1+N/2);                    % Only the 1 + N/2 first points  contain the spectra
                                     % information:
                                     % 1 is the dc component and 1+N/2, the Nyquist component
% 2.4.- Graphical representation

  k=(0:N/2)*fm;
  f_ini = fc-1.0*bandwidth           % Window of width (2*bandwidth) centered at fc to
                                     % display the significant spectra resulting from modulation
  f_fin = fc+1.0*bandwidth

  range = round(f_ini/fm:2+f_fin/fm); % Given the actual frequencies, vector points are calculated
                                     % by dividing them per fm.

  if printyn == 1

    kk = (1:N)*Tm/N*1000;            % Index related to the horizontal axis to be displayed
                                     % on the graphics.

% Graphics of the modulating signal

    subplot(3,1,1),plot (kk,vm);
    grid
    zoom
    title ('Modulating waveform')
    xlabel ('time (ms)');
    ylabel ('Amplitude (V)');

    pause

% Graphics of the modulating waveform integral

    subplot(3,1,2),plot (kk,theta);
    grid
    title ('Modulating waveform integral')
    xlabel ('time (ms)');
    ylabel ('Angle (rad)');

    pause

% Graphics of the FFT

    MOD_FFT = 2/N*abs(Y(range))/sqrt(2); % Peak values of every side-band harmonic resulting from
                                     % the modulation are simply calculated by multiplying the
                                     % module of the value given by the function FFT per 2/N
                                     % Afterwards, divide the result per square root of 2 in order
                                     % to obtain the rms value (in volts).


    dBV = 20*log10(MOD_FFT);         % Values in dBV (of a rms amplitude)

    subplot(3,1,3),bar (k(range)/1000,dBV)
    grid
    title ('After modulation')
```

```
      xlabel ('Side-band harmonics (kHz)');
      ylabel ('Amplitude (dBV)');

      pause

   end
end

% Finally, some information must be saved into files.

            % Modulated signal (N samples). This file will be used later to be downloaded (after some
            % previous treatments) into the arbitrary function generator.
fid = fopen ('C:\f_genert.txt', 'w');
fprintf (fid, '%12.8f \n', f);
fclose (fid);

            % Significant spectral components values
fid = fopen ('C:\f_spectr.txt', 'w');
fprintf (fid, '%6.2f %12.8f\n', [fm/1000*(range-1);MOD_FFT]);
fclose (fid);
```

ANNEX 5

CONSIDERATIONS ABOUT EMC UNITS EXPRESSED IN DECIBELS

ANNEX 5:

CONSIDERATIONS ABOUT EMC UNITS EXPRESSED IN DECIBELS

Decibels have the property of compressing data and other useful characteristics, as expressing the gain or loss of a signal as a difference between the output signal and the input signal. Although it is commonly referred as dB, some considerations must be done in order to avoid a wrong usage of it.

Decibels are valid to express any ratio of two physical unit as volts, amperes, watts and whichever combinations of them. EMC units are normally expressed this way:

– dB è it is a power reference

– dBV è With "V" at the end, this is a voltage reference.

– dBA è With "A" at the end, this is a current reference.

– and so on

1. BASIC DEFINITIONS

Commonest units in EMC expressed in decibels are watts and volts. As decibels are the ratio of two quantities, absolute power, voltage or current levels are expressed in dB by giving their value above or referenced to some base quantity. This way, some 'sub-units' are used depending on the reference; for instance, a voltage referenced to 1 mV will be expressed in dBmV, where the 'm' represents the 1mV-reference. More examples are listed below:

POWER (W):

- dB è power referred to 1W è $dB = 10 \cdot \log_{10} \frac{P(W)}{1 \cdot W}$
- dBm è power referred to 1mW è $dBm = 10 \cdot \log_{10} \frac{P(mW)}{1 \cdot mW}$
- dBµ è power referred to 1µW è $dB\mu = 10 \cdot \log_{10} \frac{P(\mu W)}{1 \cdot \mu W}$

RMS-VOLTAGES (V):

- dBV è voltage referred to $1V_{RMS}$ è $dBV = 20 \cdot \log_{10} \frac{V_{RMS}(V)}{1 \cdot V}$

- dBmV è voltage referred to 1mV$_{RMS}$ è $dBmV = 20 \cdot \log_{10} \frac{V_{RMS}(mV)}{1 \cdot mV}$
- dBµV è voltage referred to 1µV$_{RMS}$ è $dB\mu V = 20 \cdot \log_{10} \frac{V_{RMS}(\mu V)}{1 \cdot \mu V}$

2. EQUATIONS OF CONVERTION

If a value referred to power dBx is desired to be referred to rms-voltage dByV, the following equation applies (x, y can be 'm', 'µ' or blank):

$$dByV = 20 \cdot \log_{10} \frac{\sqrt{10^{\frac{dBx}{10}} \cdot x(in\ W) \cdot Z_o(\Omega)}}{y(in\ V)}$$

where Z_o (Ω) is the impedance across which the voltage is applied.

Example: Conversion from dBm to dBµV

$$dBuV = 20 \cdot \log_{10} \frac{\sqrt{10^{\frac{dBm}{10}} \cdot 0.001 \cdot Z_o(\Omega)}}{0.000001}$$

TABLES OF CONVERSION (SYSTEMS OF 50 Ω)

POWER EXPRESSED IN è	dB	dBm	dBµ
dBV	+ 16.99	- 13.01	- 43.01
dBmV	+ 76.99	+ 46.99	+ 16.99
dBµV	+136.99	+ 106.99	+ 76.99

é
RMS-VOLTAGE é
EXPRESSED IN é

Example: dBV = dBm – 13.01

TABLES OF CONVERSION (SYSTEMS OF 75 Ω)

POWER EXPRESSED IN è	dB	dBm	dBµ
dBV	+ 18.75	- 11.25	- 41.25
dBmV	+ 78.75	+ 48.75	+ 18.75
dBµV	+ 138.75	+ 108.75	+ 78.75

é
RMS-VOLTAGE é
EXPRESSED IN é

Example: dBV = dBm – 11.25

3. OTHER IMPORTANT RELATIONSHIPS

POWER TERMS	RMS-VOLTAGE TERMS
$dB = dBm - 30$ $dBm = dB\mu - 30$ $dB = dB\mu - 60$	$dBV = dBmV - 60$ $dBmV = dB\mu V - 60$ $dBV = dB\mu V - 120$

4. MAXIMUM VOLTAGE AT THE MEASURE EQUIPMENT INPUT STAGE

Most measurement instruments admit a maximum value of voltage or current, commonly, at their input stage. If this maximum value is exceeded, a physical damage is likely to occur to this input stage. This maximum value depends on the equipment and can be extracted from the user's manual. Most of the times, this limit is also shown on the equipment, near the physical input (BNC or any other connectors). Next tables show the maximum voltages to be applied at the input of the measure equipment (e.g., a spectrum analyzer) for different input limits (in dBm) and depending on the input impedance configured on this equipment.

Ø Input limit of 20 dBm

	Impedance at the system input	
Maximum signal voltage	50 Ω	75 Ω
V_{rms}	2.24 V	2.74 V
V_{peak}	3.16 V	3.87 V
WITH ATTENUATOR OF 10 dB		
V_{rms}	7.07 V	8.66 V
V_{peak}	10 V	12.25 V

Ø Input limit of 10 dBm

	Impedance at the system input	
Maximum signal voltage	50 Ω	75 Ω
V_{rms}	0.71 V	0.87 V
V_{peak}	1.00 V	1.22 V
WITH ATTENUATOR OF 10 dB		
V_{rms}	2.24 V	2.74 V
V_{peak}	3.16 V	3.87 V

In order to prevent possible electrical overstresses at the input stage of a measurement equipment, mainly when users are not sure about the signal level, an attenuator is commonly used, as shown in the next figure.

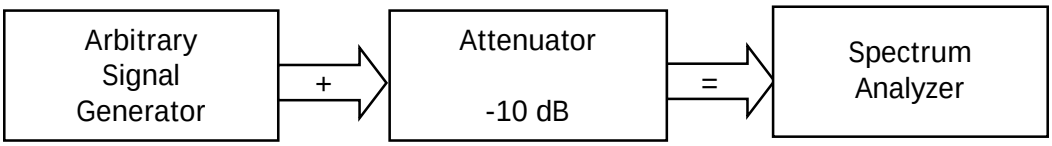

dBm	+	-10 dB	=	dBm
dBV	+	-10 dB	=	dBV (*)

(*) Assuming the spectrum analyzer's input impedance is equal to the impedance of the attenuator.

ANNEX 6

SCHEMATICS AND PCBs CORRESPONDING TO THE TEST PLANT

ANNEX 6:

SCHEMATICS AND PCBs CORRESPONDING TO THE TEST PLANT

Prototype (power converter + control stage) used to measure the practical EMI emissions was designed by using the software package OrCAD. Two specific tools of this software were finally used: OrCAD Capture 9.2.3 and OrCAD Layout 9.2.3.

OrCAD Capture is intended to design the schematics; these schematics become the base point to finally design the printed circuit board.

In the next pages, schematics and PCBs corresponding to the prototype are presented. An OrCAD project named "FM_STDW.OPJ" was created. Two files are of main interest:

- "FM_STDW.DSN": Schematics designed with Orcad Capture 9.2.3
- "FM_STDW.MAX": Printed circuit board designed with Orcad Layout 9.2.3

Pictures in the next pages were obtained from these two files.

SCHEMATICS OF THE TEST PLANT: "FM_STDW.DSN"

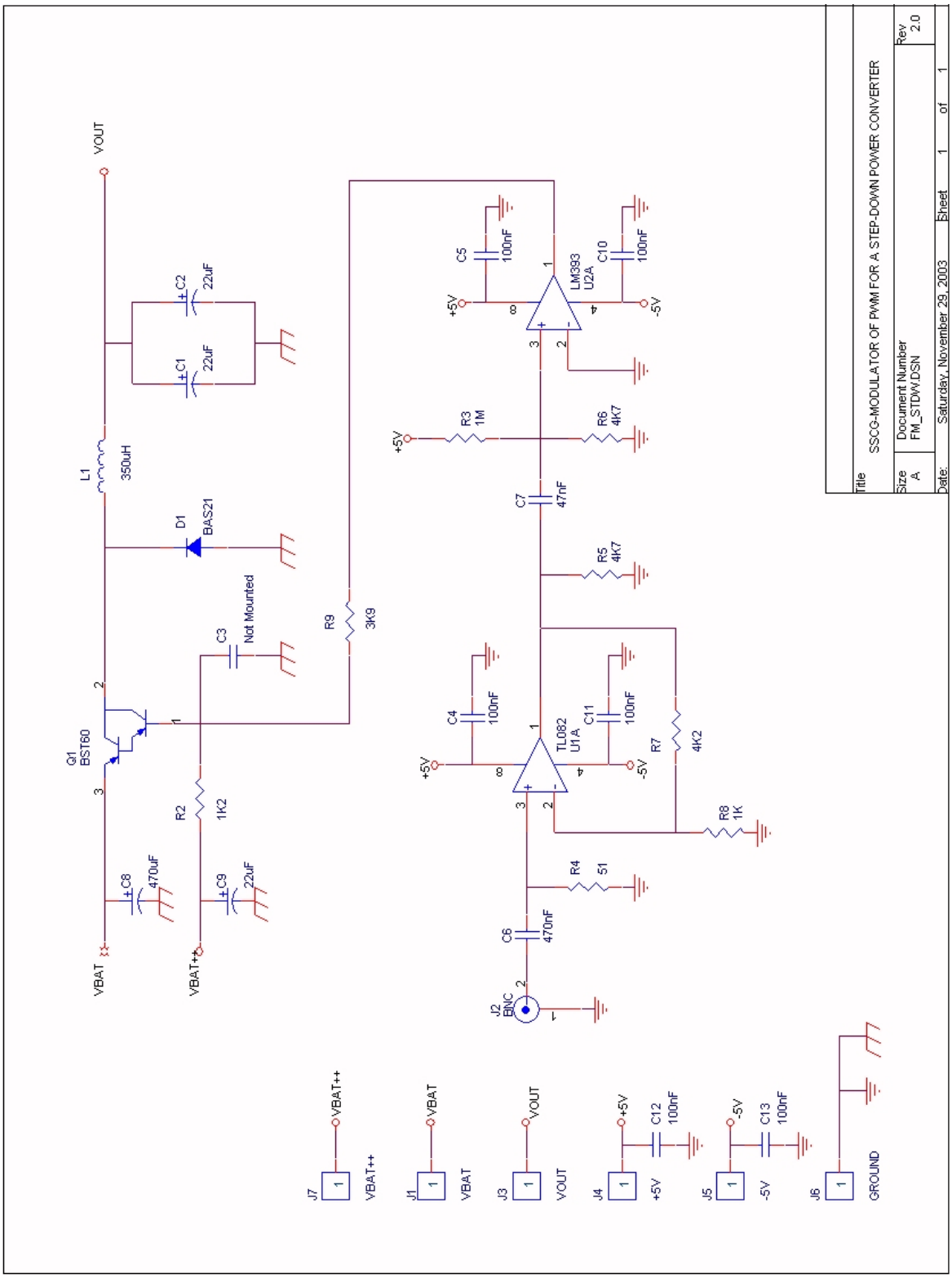

PCB OF THE TEST PLANT: "FM_STDW.MAX"

§ TOP & BOTTOM LAYERS

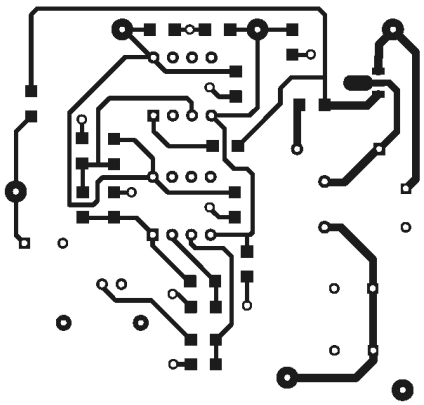

TOP LAYER

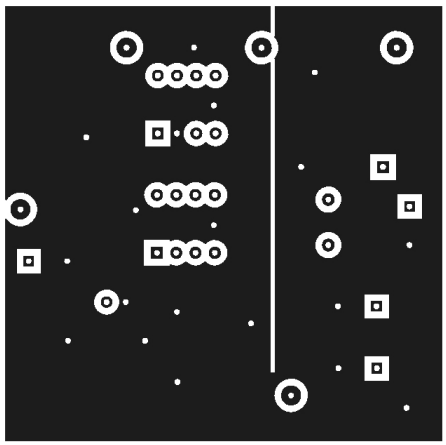

BOTTOM LAYER

§ COMPONENTS LAYOUT

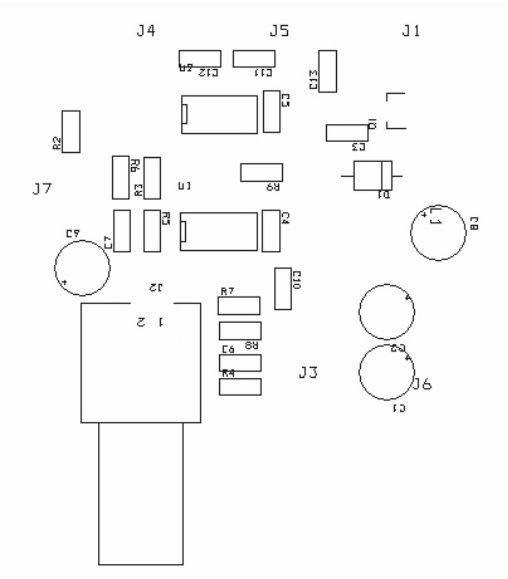

ANNEX 7

PSPICE SIMULATION OF THE TEST PROTOTYPE

ANNEX 7:

PSPICE SIMULATION OF THE TEST PROTOTYPE

Test prototype presented in Annex 6 was previously simulated in order to estimate the ability of this power converter to reach the higher level of frequency, around 1 MHz. The software used to carry out this simulation was PSpice 9.2.3 (now included in the OrCad software package).

In the two following two pages, simulations for both 1 MHz and 100 kHz are shown. Components, their values and characteristics match exactly the ones presented in Annex 6 (FM_STDW.DSN). The "Fm_stdw_schematic1.net" file with all interconnections and component values is inserted at the end of this annex.

Three plots are displayed at each graph:

- V(Q1:c) è plot corresponding to the square waveform expected at the collector of the power transistor Q1. Frequency and duty cycle values are numerically presented.
- V(R5:2) è plot corresponding to the waveform at the output of the power converter. Average value is numerically presented.
- V(L1:2) è plot corresponding to the waveform at the output of the amplification stage, in order to show the equality between the input frequency from the signal generator and the frequency generated by controlling the power transistor.

From the simulation results, it can be now concluded that no special problems should be found in the practical test prototype.

The difference of duty-cycle values for the range 100 kHz to 1 MHz is lower than 14%, thus expecting a ratio of variation for the duty-cycle around 1.55%/100 kHz. As an example, for an input voltage of 10 V and a theoretical duty cycle of 50 %, the variation of the output voltage for a frequency deviation of 100 kHz (δ% = 10 % and f_c = 1 MHz) is expected to be around 1.55%·10 V = 0.155 V (about 3.1 % of the theoretical output voltage of 5 V). Of course, practical results will differ from these values (mainly due to the output capacitor) but they are good enough to continue.

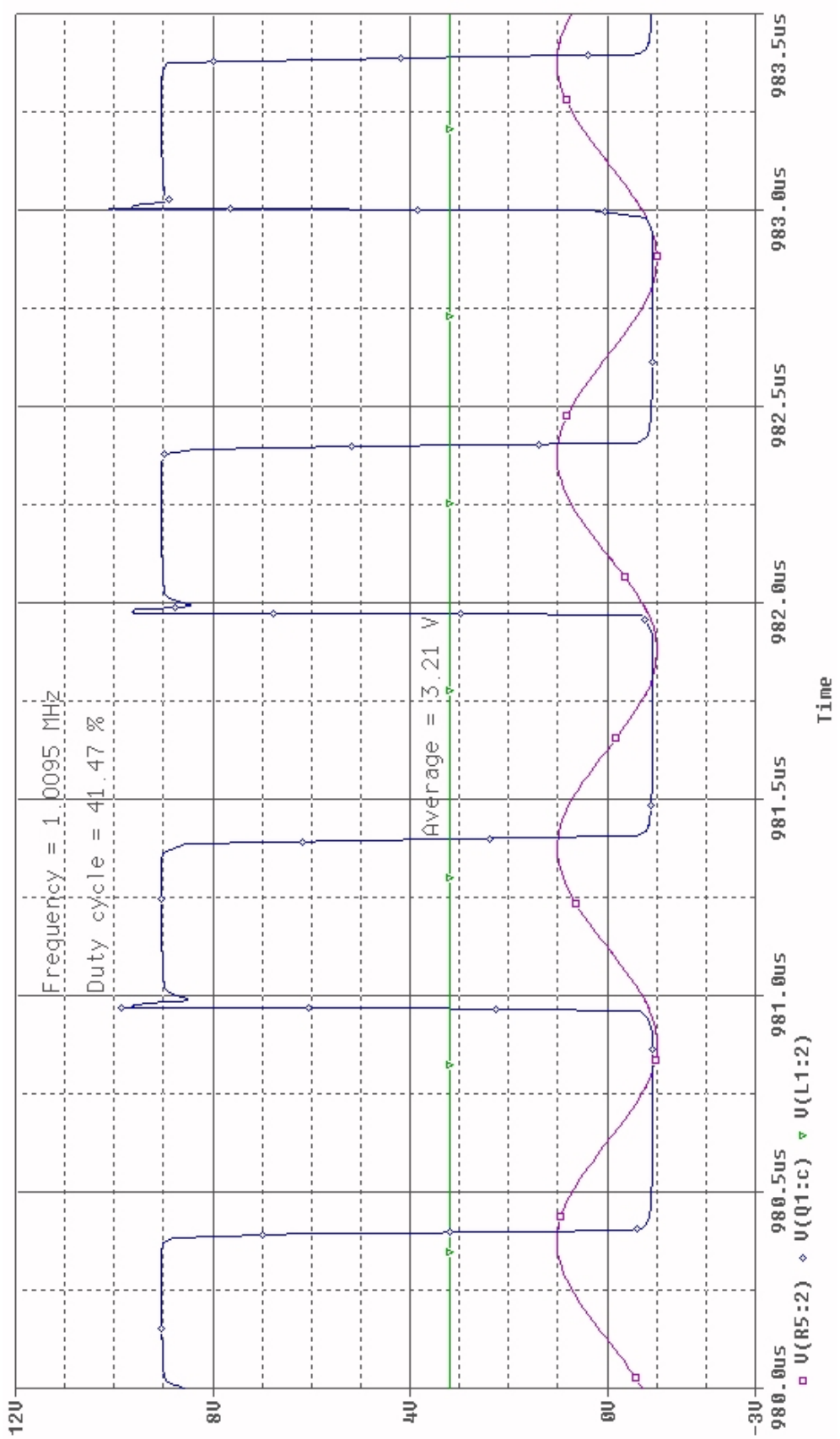

Simulated waveforms for a switching frequency of 1 MHz

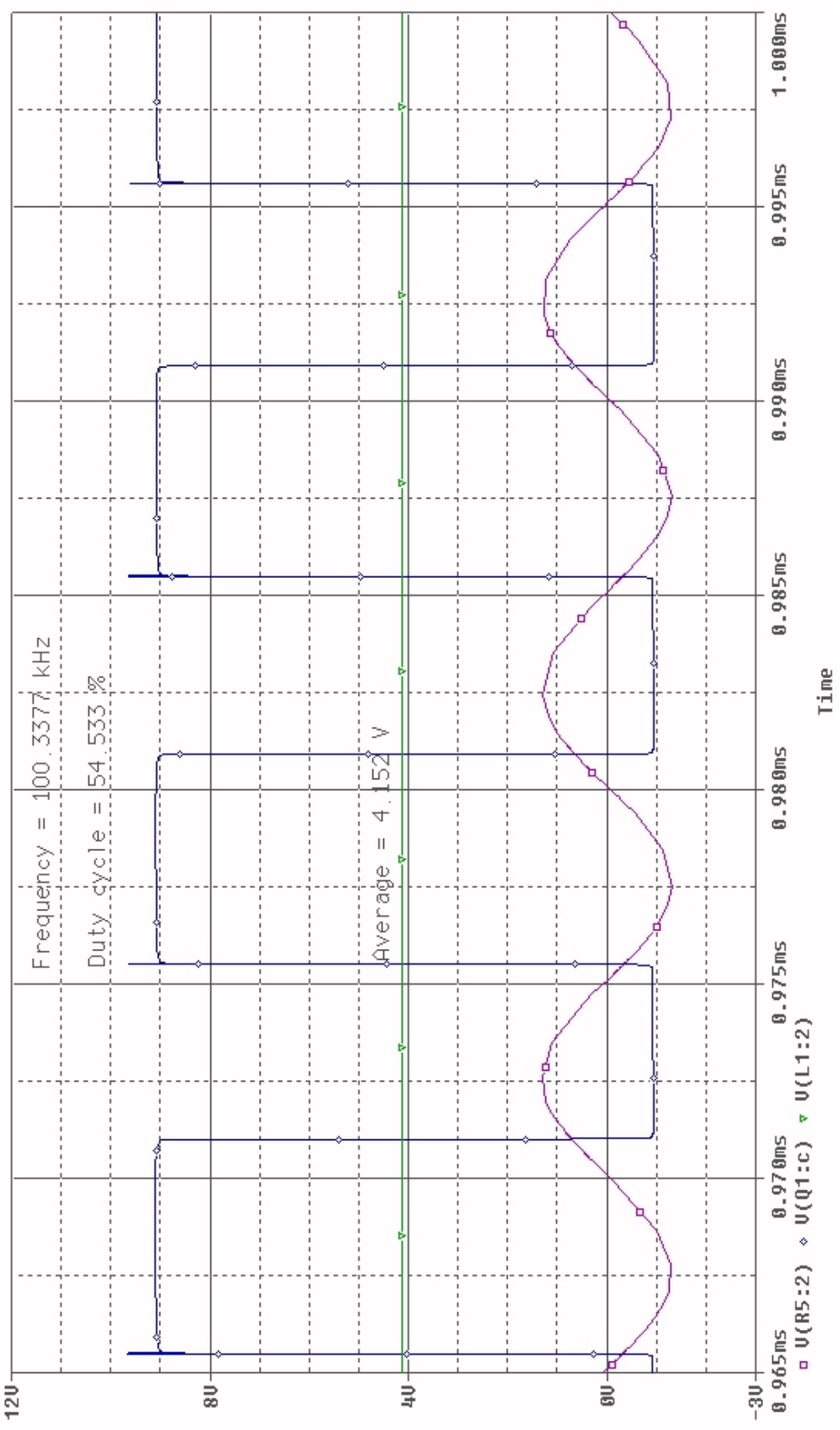

Simulated waveforms for a switching frequency of 100 kHz

PSPICE FILE: FM_STDW-SCHEMATIC1.NET

```
* source FM_STDW
C_C10         0 -5V  100n
V_V3         -5V 0 -5V
D_D1         0 N07143 BAS21
C_C11         0 -5V  100n
R_R2         N13994 N13986  1.2k
C_C7         N10516 N00160  47n
L_L1         N07143 N02846  350uH
V_V4         N13755 0 DC 0 AC 0
+SIN 0 0.5V 1000000 0 0 0
R_R9         N20511 N13986  3.9k
R_R4         0 N00063  51
R_R5         0 N00160  4700
C_C6         N00063 N097871  470n
R_R6         0 N10516  4700
R_R3         N10516 +5V  1000000
R_R8         0 N00174  1000
X_Q1         N07143 N13986 N05782 BST62/PLP
R_R7         N00160 N00174  4200
C_C4         0 +5V  100n
V_V2         +5V 0 5V
X_U6A         N10516 0 +5V -5V N20511 LM393
R_R10         0 N02846  20
V_V5         N13994 0 12V
C_C5         0 +5V  100n
R_R1         N097871 N13755  50
C_C1         0 N02846  44u
V_V1         N05782 0 10V
X_U11A         N00063 N00174 +5V -5V N00160 TL082
```

PSPICE LIBRARIES IN USE:

- BST62/PLP è PHIL_BJT.OLB
- BAS21 è EDIODE.OLB
- LM393 & TL082 è OPAMP.OLB
- PASSIVE COMPONENTS è ANALOG.OLB
- POWER SUPPLIES AND STIMULUS è SOURCE.OLB